Final Report:

Prosthetics & Orthotics Manufacturing Initiative (POMI)

Project #J2256

21 December 2012

Submitted to:

Office of Naval Research

One Liberty Center

875 North Randolph Street, Suite 283

Arlington, VA 22203

Contract No. N00014-11-D-0504

Submitted by:

SCRA Applied R&D

Composites Manufacturing Technology Center

81 Technology Drive, Suite 100

Clemson Research Park

Anderson, SC 29625

Report Documentation Page

Form Approved
OMB No. 0704-0188

1. REPORT DATE	2. REPORT TYPE	3. DATES COVERED
APR 2013	**N/A**	**-**

4. TITLE AND SUBTITLE	5a. CONTRACT NUMBER
Prosthetics & Orthotics Manufacturing Initiative	5b. GRANT NUMBER
	5c. PROGRAM ELEMENT NUMBER
6. AUTHOR(S)	5d. PROJECT NUMBER
	5e. TASK NUMBER
	5f. WORK UNIT NUMBER
7. PERFORMING ORGANIZATION NAME(S) AND ADDRESS(ES) **SCRA Applied R&D, 81 Technology Dr, Suite 100, Anderson, SC**	8. PERFORMING ORGANIZATION REPORT NUMBER
9. SPONSORING/MONITORING AGENCY NAME(S) AND ADDRESS(ES)	10. SPONSOR/MONITOR'S ACRONYM(S)
	11. SPONSOR/MONITOR'S REPORT NUMBER(S)

12. DISTRIBUTION/AVAILABILITY STATEMENT
Approved for public release, distribution unlimited

13. SUPPLEMENTARY NOTES

14. ABSTRACT

The Prosthetics & Orthotics Manufacturing Initiative (POMI) was an ambitious program designed to give tools to the practitioners providing patient care to the nations wounded warriors. The intent was to improve the design and manufacture of custom composite sockets. This was expected to improve the sockets produced, while at the same time reducing cost and labor input required from practitioners, allowing them to focus limited resources on patient care, including emerging best practices for the rehabilitation of those suffering from limb loss.

15. SUBJECT TERMS

16. SECURITY CLASSIFICATION OF:			17. LIMITATION OF ABSTRACT	18. NUMBER OF PAGES	19a. NAME OF RESPONSIBLE PERSON
a. REPORT	b. ABSTRACT	c. THIS PAGE			
unclassified	**unclassified**	**unclassified**	**SAR**	**188**	

Executive Summary

The Prosthetics & Orthotics Manufacturing Initiative (POMI) was an ambitious program designed to give tools to the practitioners providing patient care to the nation's wounded warriors. The intent was to improve the design and manufacture of custom composite sockets. This was expected to improve the sockets produced, while at the same time reducing cost and labor input required from practitioners, allowing them to focus limited resources on patient care, including emerging best practices for the rehabilitation of those suffering from limb loss.

Five major activities were pursued. They will be referred to by the following names and numbers throughout this report. Task 1: Reconfigurable Sockets pursued two competing technologies to allow composite sockets to be adjusted after they were fabricated. The goal was to allow sockets to be changed to adjust to changes in the patient's anatomy, thereby reducing the number of sockets that needed to be fabricated. Task 2: Medical Imaging and Modeling pursued a novel paradigm for designing sockets with full information of the patient's anatomy, gathered by Magnetic Resonance Imaging (MRI). Using the information from the MRI, and applying stress-strain properties generalized for each tissue type, this task sought to allow prediction of the loading paths for a given socket design, which would allow an assessment of the design's comfort prior to fabrication, and would allow great flexibility in implementing novel designs. Task 3: 3-D Pressure Mapping focused on implementing a pressure mapping system which could be deformed over the patient's residual limb, allowing for full, high-resolution information for the entire limb, informing design decisions. Task 4: Automated Fabrication translated a well-established composites manufacturing technique, braiding, to the manufacture of composite sockets. Task 6: Active Cooling Liner demonstrated a new system for providing cooling to the residual limb, to combat overheating issues, increase comfort, and aid in skin care. This technology had been previously commercialized for full body use, and it's efficacy for the prosthetic environment was demonstrated.

These various activities met with varying levels of success and transition. One of the two competing technologies pursued in Task 1: Reconfigurable Sockets was determined to have promise in allowing sockets to be adjusted after manufacture. The most likely configuration involves placing shape-memory foams, which are activated with heat, between layers of carbon fabric during socket fabrication. Prototypes were developed, and delivered to Walter Reed Army Medical Center (WRAMC), The Center for the Intrepid (CFI) at Brooks Army Medical Center (BAMC), and the Navy Medical Center at San Diego (NMCSD), and were well received. Task 2: Medical Imaging and Modeling encountered numerous difficulties in verifying the results of the finite element analysis (FEA), and were unable to overcome these difficulties. Task 3: 3-D Pressure Mapping was successful in developing a system which took pressure maps of the residual limb. There were issues in calibrating the system, and the temporal resolution was insufficient to measure events associated with activities such as walking. The system was commercially launched, and a small population of first adopters has purchased it. Since, the system has been extended into use for orthotics and measuring the pressure wave associated with blast events, for helping to diagnose traumatic brain injuries. Task 4: Automated Fabrication succeeded in proving out the use of braiding for production of prosthetic sockets. Using 3-year average numbers for the cost of a prosthetic socket from a central fabrication facility, braided

sockets save 34% of the cost of a traditional socket, offer approximately twice the strength-to-weight ratio, and require roughly half of the skilled labor input to create. As a result, two central fabrication facilities invested in the technology, purchasing, installing, and operating braiding units to supply sockets to active, veteran, Paralympian, and civilian populations. Task 6: Active Cooling Liner demonstrated that the liquid carbon dioxide-based system could provide cooling through the thermal resistances of the viscoelastic liner now commonly worn by prosthetic patients. This is the only known design capable of preventing overheating in the socket, and this concept may be suitable for commercialization efforts in the future.

Table of Contents

Introduction

The realities of the current engagement are that more warriors are surviving injuries and living with amputations. The capabilities of our care systems are strained by increased demands, not only in terms of sheer numbers, but also in the functional level that our young warriors want to be restored to. While the current care systems are providing excellent care, this project focused on opportunities to improve processing and manufacturing of prosthetic systems to increase durability and comfort, and on giving medical personnel tools to aid in the care of our most deserving. This will allow them to focus limited resources on patient care.

Background

The asymmetric nature of the conflicts in Iraq and Afghanistan has resulted in a high number of traumatic injuries. In addition, major improvements to battlefield medical logistics have resulted in greatly increased survival rates. These brave men and women returning from combat are facing multiple challenges in returning to life, either as a veteran or as part of the active military.

At the same time, these young warriors are demanding restoration to higher and higher functional levels. This is enabled by the advance of prosthetics technology, certainly, but the commitment of resources required to achieve it has increased as the complexity of the technology has increased.

In order to allow increased focus on patient care, and the restoration of function, this project sought to improve the most simple of the components of the prosthetic system, the socket. These are often fabricated based on a volumetric cast of the residual limb, without much insight into the underlying anatomy. They are then fabricated using a wet lay-up infusion, using for raw materials, braided fabric tubes for the reinforcing fabric. The fabrication method takes a large amount of skilled labor, which may be better invested in patient care and more intensive rehabilitation techniques. Further, the method fails to control several key variables which determine the strength of the socket. As a result, and in order to prevent catastrophic failure in the socket, the structure is commonly 'over-built,' increasing weight for the system.

The grand design of this project was to address the fabrication method, utilizing instead, braiding, which is well established in the composite industry. The technique is known to produce very good strength to weight ratios, by increasing the fiber volume fraction in the components produced. Braiding can be used to create a number of different properties, but in order to meet the requirements of a design, a key question must be first answered. What structural properties are required? If we can make a structure with gradient properties, where would stiff sections belong, and where would more compliant sections be positioned?

The answers from the prosthetic industry were lacking, which is to say, the community did not consider their fabrication methods to be an area of need, nor did they see the need for more understanding of the underlying anatomy, for one main reason; they are able to provide excellent patient care without such things. The state of the practice is to design the socket based upon patient feedback, and the use of transparent 'check' sockets, and on gait analysis.

This project envisioned a different way. The patient's anatomy can be studied through various medical imaging techniques. The exact positions of all of the various tissues (muscles, fat, bone, ligaments, vascular structures, neural structures, etc.) can be determined. This can be coupled with known stress-strain relationships for the tissues, allowing a complete model of the physical response of the residual limb. The goal was to use this tool to virtually design a socket for a patient, using finite element analysis to determine the load transfer paths that a given socket design would impose on the soft tissues, allowing a predictive analysis of the comfort of that

design. In addition to providing patient care, a tool such as this could also allow for 'virtual innovation,' the testing of very novel socket designs without ever risking a patient's well-being.

In order to inform such a model, an additional tool must be brought to the field. The model requires data for input and for assessment of its predictions. One of the few ways we can verify the predictions of the model is at the surface of the residual limb. This project sought to use a polymer-based pressure measuring material to supply a high-resolution, 3-dimensional map of the pressures experienced at the surface of the residual limb.

In the course of preparing the project, and discussing worthwhile activities with stakeholders, additional needs were brought up. One of these was the desire to change a socket's fit after fabrication. This commonly arises as a need, because the human body is a dynamic system, and the residual limb more dynamic than healthy limbs, which continues to change volume in response to muscle atrophy, or abnormal bone growth. The community has some techniques for allowing such changes to the socket shape, including grinding away the composite in local areas and the inclusion of non-structural features specifically for removal at later times. When viewed from the viewpoint of a composite structure, both of these techniques have negative consequences on the socket structure; the former requires the socket to be either overbuilt from the beginning, or fatally compromised structurally, by the reduction in the composite structure, and the later adds parasitic weight to the structure specifically to allow later modification. In order to investigate alternatives, materials which have demonstrated alterability after fabrication were investigated. These would allow adjustment to the socket fit at later points in time, using techniques familiar to practitioners, without adding parasitic weight to the system.

A second area of need that came to light was the need to address overheating issues in the residual limb. When a patient's residual limb is covered by the prosthetic system, including a viscoelastic liner, the limb is robbed of all natural mechanisms for regulating temperature. No air flow is permitted, and the evaporation of sweat is repressed. This results in overheating, which is itself a major comfort issue which can limit prosthetic system use. The problem is exacerbated by the effect it has on the socket fit caused through overheating. The accumulation of sweat in the prosthetic system affects the system by acting as a lubricant, allowing more movement than desirable between the residual limb and the socket. Further, the generation of sweat by the residual limb is accompanied by local decrease of tissue volume, which further affects fit. What is required is some method of increasing heat removal from the system. A demonstration of such a system is reported here.

Objectives

The objective of this project was to dramatically improve the quality and comfort of sockets for lower-extremity prosthetic systems by shifting away from the current experience-based design and production paradigm. This project intended to allow intelligent design decisions for the composite socket, informed by both load requirements and soft tissue reactions.

An accompanying objective was to produce sockets at reduced costs, reduced labor inputs, and increased strength, in order to allow resources to be focused on patient care, more advanced terminal devices, and the latest rehabilitation techniques.

Another objective of this project was to implement resins developed in other areas into the field of prosthetics to enable local modifications of the composite structure.

The final objective of this project was to demonstrate that an active cooling system could be added to the prosthetic system and provide relief to overheating of the residual limb.

Approach

Task 1: Reconfigurable Sockets pursued two competitive technologies. One was from Clemson University, and focused on Diels-Alder chemistry, and the formation of a resin with cross-link bonds which could be broken and reformed through the application of heat. The second was the application of shape memory composite resins from Composite Technologies Development (CTD). These two technologies were both shown to have promise in this area. The materials developed by Clemson, while able to meet most of the key metrics for the application, faced a long road to scale up sufficiently to impact the problem, and so were not pursued further. The materials from CTD are already mature from a manufacturing readiness level, and so prototypes of sockets which were capable of reconfiguring were fabricated and evaluated.

Task 2: Medical Imaging and Modeling made use of a small patient population to gather MRI data from. This required careful manipulation of the patient's residual limb, to insure that the gathered data represented the state of the limb when confined to a relevant socket shape, and not the state of the limb when subjected to unconstrained gravity effects in a prone position (the position of the patient during the MRI). This also required optimization of the MRI collection, in order to provide a coherent data set which could be easily segmented into various tissue types. Only after this can the modeling effort be started, allowing analysis of sockets during donning, static standing, and single limb support.

Task 3: 3D Pressure Mapping used a material previously developed which is based on a polymer with carbon black fillers which changes the surface resistivity (as opposed to the bulk resistivity) in response to changes in applied pressure. In order to allow measurement of discrete points, areas of filled polymer needed to be seamlessly integrated with areas of neat polymer in a way that would allow the combination to be thermally deformed without creating flaws. Further, the system needed a way to measure each of the points at high temporal resolution and with good calibration.

Task 4: Automated Fabrication started from a firm belief that braiding could easily produce sockets, and worked to prove that point. A large portion of the effort was invested in quickly and easily fabricating molds which can be used in conjunction with the braiding technique. Several methods and materials were pursued. In parallel, the team optimized the braiding unit for use in the prosthetic environment and investigated ways in infusing composites with appropriate resins and producing acceptable sockets.

Task 6: Active Cooling Liner started with a well-established technology which was based upon a regulated flow to provide a set amount of cooling for a user's torso. In order to demonstrate this technology in the prosthetic environment, the system was modified to provide a smaller flow rate of liquid carbon dioxide. This was tested on the bench top to determine if the cooling levels achieved would be able to provide cooling effect through the insulation provided by liners currently used as part of the prosthetic system.

Results and discussion

Task 1: Reconfigurable Sockets

Clemson University explored several chemistries with 'self-healing properties' which were based on Diels-Alder reactions. Diels-Alder reactions are a broad class of organic chemical reactions in which two compounds join together in such a way as to form a new cyclic compound at their joint. This requires that the reaction sites have certain functional groups which contain a great amount of electrons, which are also able to participate in the reaction to form the new bonds required to form the new cyclic group. This reaction was exploited to form self-healing polymers by allowing the cross linking between polymer chains to be formed by Diels-Alder reactions because this reaction is relatively easy to drive in the reverse direction by the application of temperature. This allows the cross-links to be broken by the application of temperature, which results in increased molecular movement, filling in scratches (self-healing), or allowing the repositioning of fibers within the polymer (reconfiguration).

Clemson investigated several plausible chemistries for this purpose. One was a modified epoxy containing a furan moiety which was combined with commercially available bismalimides and maleimides, which showed crosslinks formed at 55 ^{o}C and the breaking of crosslinks at 130 ^{o}C, a relevant temperature range. Composites made using carbon fiber and this resin system demonstrated a heat-activated state in which reconfiguration was possible, and that the 'new' state would be retained when the sample was cooled to room temperature.

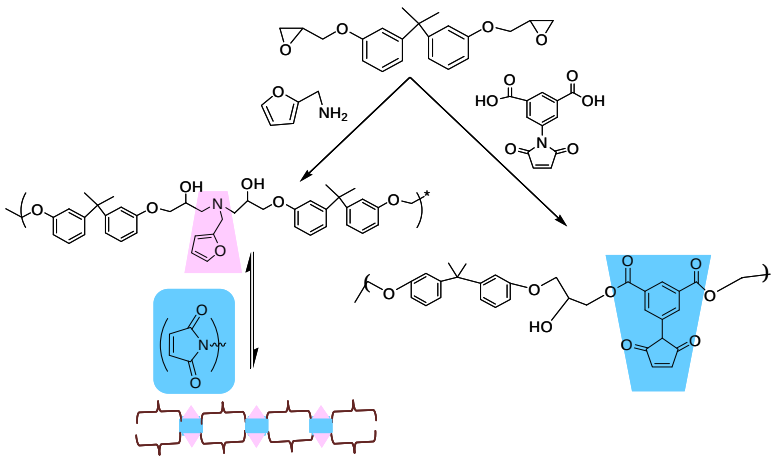

Figure 1: Reaction scheme for modifying commercially available epoxy with furan and maleimides.

The modification of commercially available epoxies achieved many of the program goals, but the resins had relatively high viscosity, making them difficult to process into high-quality composites. The system was therefore modified using various viscosity modifiers with epoxy end groups, such as aliphatic epoxies, and amine groups such as aniline and dodecyl amine.

These modifiers became part of the matrix upon curing, and decreased the viscosity of the resin during wet out, while maintaining the reversible crosslinking behavior.

In limited testing, the composites formed with the unmodified and modified resins showed remarkably stable mechanical properties after repeated healing cycles, meant to test the ability of the system to maintain strength through an adjustment of the socket. This is consistent with the findings of other researchers, where composites have shown 100% retention of mechanical properties after up to seven thermal cycles.

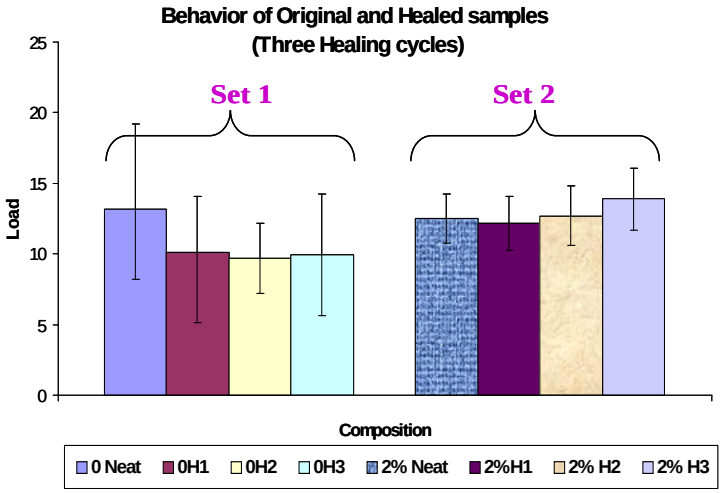

Figure 2: Epoxy Resin (Set-1), Modified Epoxy Resin (Set-2). Subset 1, Subset 2, 3 & 4 of each resin represents the original, first, second and third healing cycles of composite.

A third option explored was the use of terpolymers based on furfuryl methacrylate. Two options were successful in demonstrating the reversible cross linking behavior. These were polymerizations of furfuryl methacrylate, methylmethacrylate, and methacrylate, and polymerizations of acrylonitrile, furfurylmethacrylate, and styrene. These options were explored as lower cost alternatives to those discussed above.

Whereas Clemson University was focused primarily on the optimization of materials, Composite Technology Development (CTD) focused more on the application of their existing materials to the prosthetic socket. CTD's work to demonstrate the feasibility of applying TEMBO® Shape Memory Polymers showed that the resins and foams could allow a reconfigurable socket. The materials are well suited to this environment, having a glass transition temperature which allows a practitioner to fabricate a socket using familiar techniques and modify the socket with common tools (heat gun).

It was determined during the program that local reconfiguration requires more than the use of materials which can be reconfigured. This is simply because the woven nature of the composite fabric commonly used prevents changes in a local area; the fabric is 'locked' into place, and even full compliance in a local area may not be sufficient to allow the desired reconfiguration to be

accomplished. Because of this 'locked in' nature, other measures are required to allow sockets to be truly 'reconfigurable.'

CTD investigated several methods which would allow effective reconfiguration. These include localized thinning of the socket, localized slitting of the socket, and incorporation of foams at selected locations.

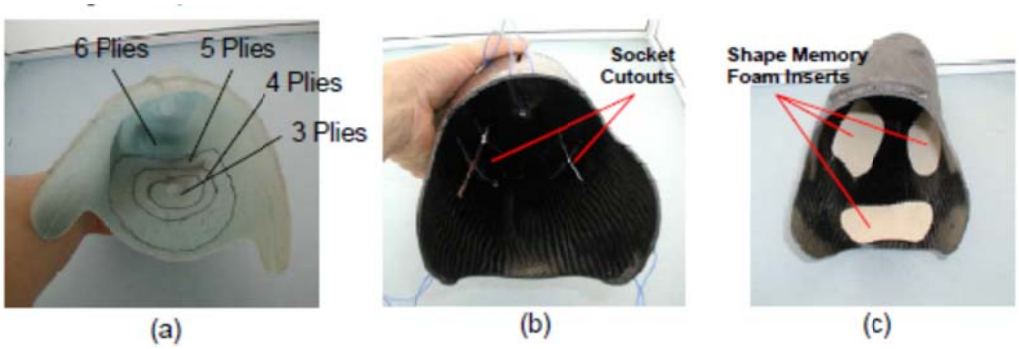

Because thinning and slitting of the socket both involve the compromise of the sockets mechanical properties, they were rejected as possible routes. Foams, on the other hand, do not compromise the structure of the socket, and can accommodate both positive and negative volume changes in the residual limb. This is possible because the foam can be inserted into the socket layup in either an expanded or compressed state. Upon heating, all foams will tend toward the expanded state, but are extremely pliable. Compressed foams will expand, altering the socket nearby to accommodate negative volume changes in the residual limb (which are most common); expanded foams can be compressed by the application of small forces, altering the socket nearby to accommodate positive volume changes. This approach provided the maximum socket reconfiguration (12mm of localized shape change).

Prototypes of reconfigurable sockets were fabricated and delivered to WRAMC, CFI, and NMCSD. They were well received.

For additional information on this task, please see Attachments A and B, the final program reports from Clemson University and Composite Technologies Development.

Task 2: Medical Imaging and Modeling

Collection of the MRI data from the patient population was accomplished first. In order to present the same anatomical configuration of the residual limb in the standing, loaded position to the MRI taken in the prone position. Previous researchers have accomplished this by using a plaster 'containment shell' to constrain the residual limb throughout the scanning process. This prevents the residual limb from conforming to the force of gravity acting in a new direction. In order to apply a similar load to the forces applied to the residual limb during use, a belt or strap attached to the torso was used.

Figure 3: Containment shell and belting system

MRI is a volumetric imaging technique based on the excitation of hydrogen in water bearing tissues. However, a single tissue type will not return a constant signal throughout the imaging volume. This greatly complicates the segmentation of the scan data into various tissue types. Further complications regarding the scanning parameters required to provide the most straightforward reconstruction of the data. The optimum protocol for trans-tibial amputations used a GE Medical Systems Sigma HDxt 3.0 Tesla MRI, conducted in the sagittal plane with a 28.0-30.0 cm field of view, and 1.6 mm slice thickness, with no overlap. An optimum set of conditions for the trans-femoral amputations was not found, and each patient was different. However, a recent innovation from GE, referred to as the IDEAL algorithm, provided the best images for modeling purposes.

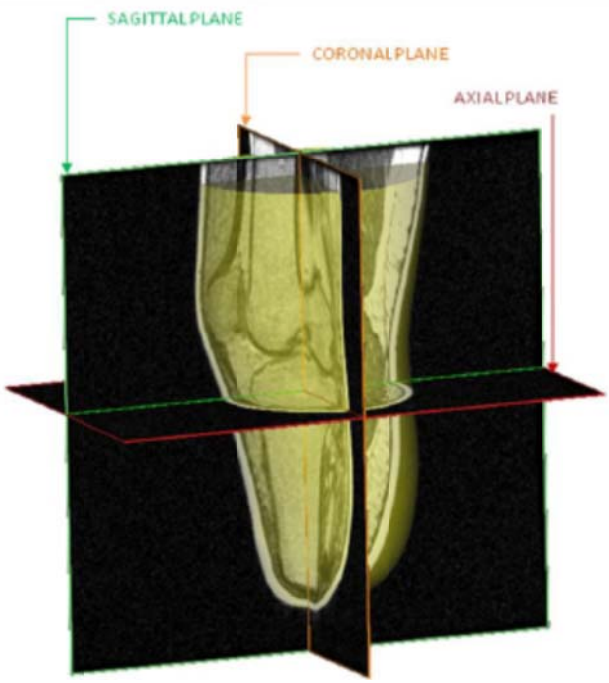

Figure 4: Representative MRI scan data

Segmentation of the MRI data is a difficult, laborious process, mainly due to two factors. First, adjacent tissue types are not easily distinguished by MRI in most cases, because adjacent tissue types commonly have similar water levels. Second, each tissue types will return a range of signal strengths (interpreted as gray-scale values by the MRI) throughout the imaging volume. In practice, the input of an experienced modeler cannot be removed from the process at this time.

The MRI data serves as the starting shape for the residual limb. Modifications are made to the model according to the state of the art practices of the prosthetics field; these are done to apply loads to areas which are best suited to carry it. With some accommodations made for the limitations of the various software packages which must be used, these can be done while visualizing the underlying anatomy of the patient.

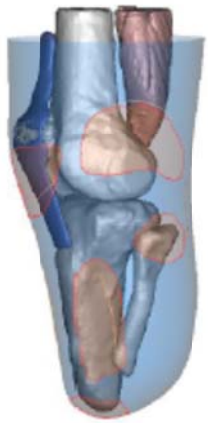

Figure 5: Highlighted areas to be modified for an effective socket design, with patient anatomy present to inform decisions

The modeler then assigns the relationships between the various anatomical tissues, as appropriate. Some tissues slide past each other at their interfaces, and some are fixed.

The various tissue types are then assigned properties, and are assumed to be isotropic and homogeneous. With further manipulation, the virtual socket can be applied to the model of the anatomy in a variety of loading states. Two were analyzed; donning, when the socket is only put on the limb and no load applied, and static standing, in which the body weight is applied to the residual limb. It was shown that the model can be used to analyze the pressure distribution on the residual limb, which demonstrates the major function of the gel liner. It also allows access to information never before seen. This includes the loading state of internal anatomical features, such as the external pressure distribution on the patella tendon, a feature which is considered capable of carrying load, and the internal tensile stresses of the same.

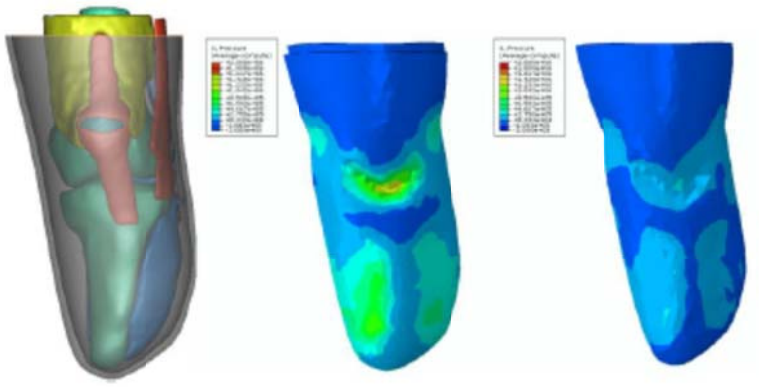

Figure 6: A visual demonstration of the function of the gel liner. The middle image shows the pressures on the surface of the gel liner, and the image on the right shows the pressures exerted on the skin, under static standing loads.

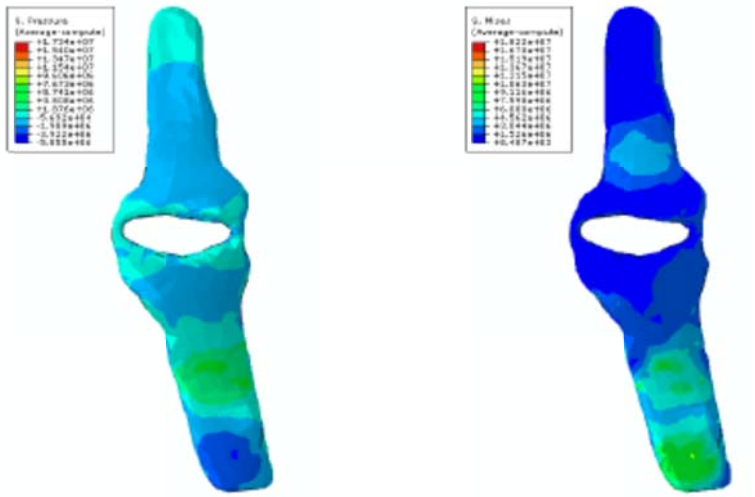

Figure 7: Comparison of the external pressure (left image) and the internal tensile load (right image) predicted for a patient wearing a patella tendon bearing socket design under static, standing loads.

In a way, this feature of the model perfectly illustrates the difficulty of this task. The model is capable of making predictions, but has no method of assessing the quality of these predictions. Without a method for assessing the output of these models, there is no way to improve them or determine their utility. This is the limitation at present. There is no method for assessing the accuracy of the predictions made, either on internal anatomy (illustrated by the images of the patella tendon above), or on the surface pressures (illustrated by the images of the residual limb).

In addition to the difficulty in confirming the predictions made by the models, there are a number of additional issues. One is that the tissue properties used by the model are garnered from healthy tissue. These may or may not be applicable to the tissues of a given patient, whose residual limb cannot be considered to be 'healthy' in the same way other limbs are. Finally, the skill sets required to accomplish this type of modeling rarely exist in the same individual, and it is unlikely that the modeling work will be able to replace the skill set that a trained prosthetist can bring to the process.

For additional information on this task, please see Attachments C, the final program report from the Georgia Institute of Technology.

Task 3: 3D Pressure Mapping

The filled material had been previously developed. In order to make a pressure map, areas of the filled material had to be combined with areas of unfilled material. This proved difficult. Pressure molding of various shapes proved ineffective; the active regions either smeared unacceptably or the joint between the disparate regions was unacceptably weak during thermoforming events. The solution was to form a solid rod, made up of alternating discs of neat and filled polymers. These were compressed under heat, forming a strong, durable bond between the two materials. The rod was then put onto a skiving machine, allowing a thin sheet, with stripes of alternating materials, to be cut from the rod. The thin sheets were able to survive the thermoforming process and function as sensors.

With that accomplished, the system development focused on computing algorithms to continually monitor each sensor site. With the striped sheets, the system relied on two such sheets, with stripes oriented perpendicularly. Each intersection formed a sensor site. However, measuring each of these sites would require separate measurements on each of the sheets. With roughly 250 individual sensor sites available, the number of electrical measurements was a challenge for the system. The measurement of the sites limits the temporal resolution of the system. Further, the calibration of the system formed a significant challenge during the program.

The system was commercially launched as the ZEBRATM system, with the following properties:

- Supports 16 x 16 Zebra stripes, for 256 total sensor data points.
- Provides a maximum data rate of 1 kHz
- Powered by AC adapter and rechargeable lition-ion battery
- Wi-fi enabled communication
- Short circuit and electrostatic discharge protection
- High-speed digital data averaging for noise reduction
- Real-time display of data
- Comma separated value file formats, compatible with common software packages
- Playback and display of data

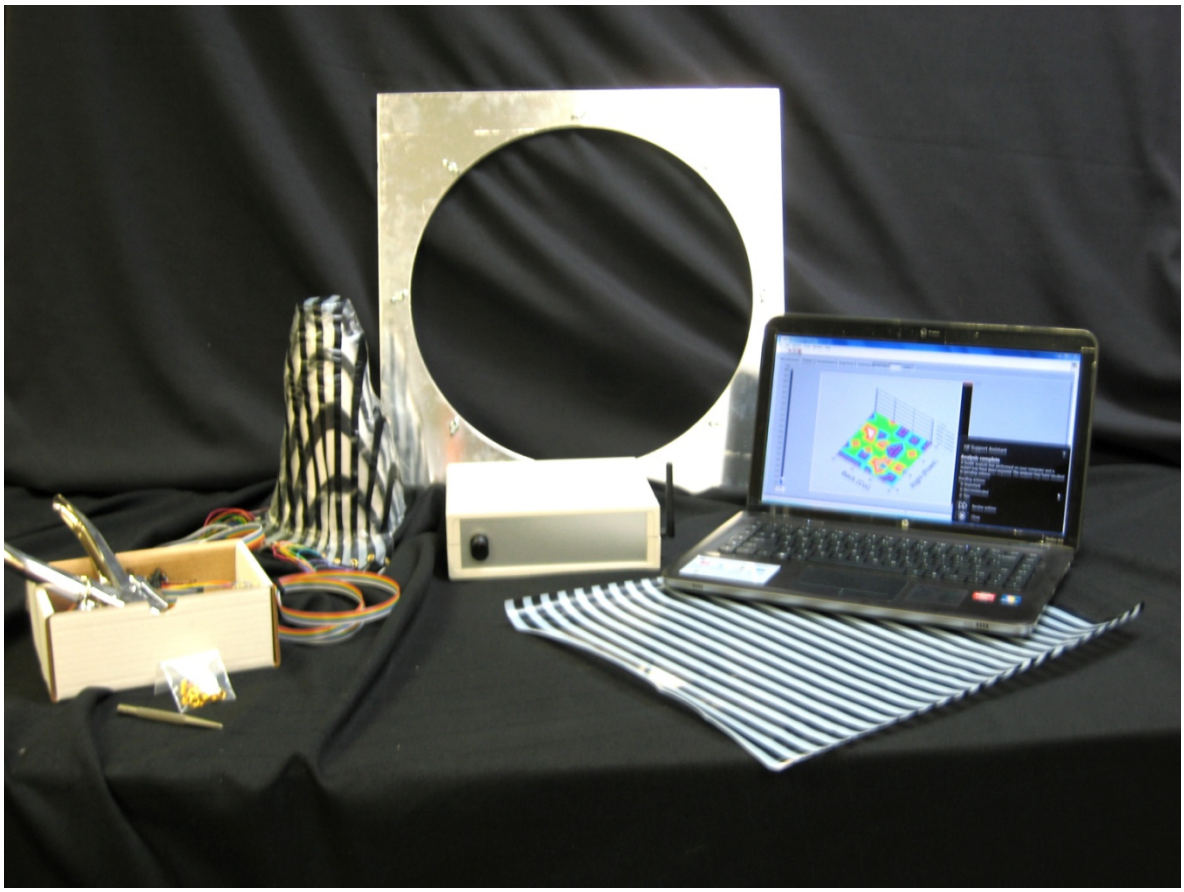

Figure 8: Picture of the system as developed during the program.

For additional information on this task, please see Attachment D, the final program report from SensorTech.

Task 4: Automated Fabrication

Mentis Sciences originally envisioned the use of braiding to create sockets, and they were convinced from the beginning that this was feasible. In order to have the maximum impact, not only were sockets to be fabricated, but they were to be superior products both mechanically and economically.

In order to accomplish this, one of the most important cost factors which needed addressing was the cost of the male mold. Prosthetists have been very comfortable over the years using plaster, but the use of plaster to make sockets efficiently and cost effectively would be implausible. Mentis investigated alternatives such as Aquacore, a washout material designed for the composites industry to make tooling from. Mentis determined a method to use Aquacore, which involved machining blanks via CNC, followed by coating the mold to prevent resin infusion into the mold. Mentis also attempted to use plaster combined with CNC machining, however, these molds did not survive the machining process, due to the brittle nature of the material. Finally, Mentis investigated a machinable wax. This brought many advantages; it was machinable easily

and quickly, was easily removed from the finished part, and could be collected and reused, addressing the cost of the material. The machinable wax proved to be a major cost savings over traditional methods. Others in the prosthetics industry use foam blocks; these may also be feasible, but were not investigated during this program.

In parallel, Mentis set about assembling a custom braider for use in the prosthetics environment. It was based on a commercially available, 64 carrier Wardwell braider, combined with a custom designed and built gantry system. The final design was a large actuator, which was chosen for its physical envelope and a minimization of pinch points, which was bolted to the braider to ensure proper alignment. The system also included a protective shroud, which made the system safer and contained dust from the system. The controls for the system, which allowed for user control over the process, were mounted to a swing arm, allowing quick and easy control over the speed of the braider and gantry. Although the program's original goal was for 'fully automated' braiding, it was determined that this was impractical given the wide variety of prosthetic shapes and the low repetition of individual parts. The cost of developing automated pathways for each socket would drive production costs unnecessarily high, and would require a more highly skilled workforce than is currently available. Instead, the controls were mounted such that a user can manually control the system during fabrication. The main controls are the speeds of the braider and the speed of the gantry, and the user can manipulate these controls as they observe the deposition of fiber onto the mandrel. In order to enable repeatability, the braider and gantry speeds can be recorded based on the position through the braid plane, and can be repeated numerous times. The manual controls make training quick and easy, and the training manual is attached as Attachment E.

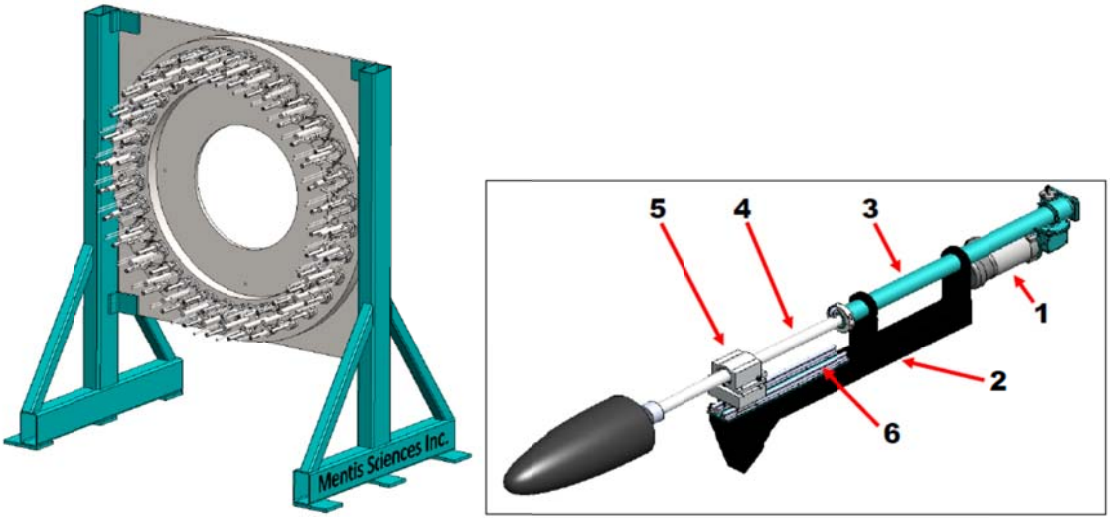

Figure 9: Wardwell braider and custom gantry

Figure 10: User Interface. Most important features include #1, Braider & Gantry Control Knob, #4, Braider Speed Control Know, and #5, Gantry Speed Control Knob.

In addition to the braiding process, socket fabrication demands the infusion of resin into the part. This can be accomplished in two ways. The first was to add the resin in between braiding of the fabric layers onto the mold. The second was to put all the fabric onto the mold and infuse the resin in the vertical position, as traditionally done. In either case, because the braider applies tension to the composite fabric as it is placed onto the mold, superior compression and compaction occurs between layers. This means the same amount of reinforcement fabric occupies less space, and then takes less resin to fill in the voids in that space. This in-situ debulking of the part reduces the resin required by approximately 50%. This has a huge impact on the strength-to-weight ratio of the socket, because the mechanical properties are mainly determined by the fibers, and the optimum strength is found when the resin content is kept to a minimum.

Figure 11: Socket braiding, the infusion process, and a completed socket

In the end, the second method of infusing the resin was chosen, because this results in the smoothest exterior surface for the composite. This was an appearance issue for the socket.

The braiding technique was transitioned to two central fabrication locations, which were trained on its use.

For additional information on this task, please see Attachment F, the final program report from Mentis.

Task 6: Active Cooling Liner

The first thing that must be done in repurposing the cooling system for use in the prosthetics environment is to determine the cooling level that is desired. After analyzing the literature in a number of different ways, it was determined that the goal would be 5-7 Watts of cooling. This was arrived by analyzing the temperature rise reported by amputees in their prosthetic system (1.7 ^{o}C after 10 minutes of walking), and the metabolic rate of the average body during similar activity levels, apportioned by the body area of the residual limb.

With this goal, additional requirements for the system were detailed. These included low noise generation, minimal comfort impact caused by the cooling lines, refillable coolant supply, to be mounted to the user's belt. It was determined that, for the needs of demonstrating the technology, the cooling lines would be sewn onto a sock, and that sock would be sandwiched in between two commercially available liners. The arrangement was required to allow radial and axial stretching, expected deformation directions for the liner during use, and survive 1200 bending cycles.

The majority of the effort was to determine a way of reducing the coolant flow rate to meet the relatively low cooling requirement. At the end of the period of performance, we were unable to achieve a flow low enough to supply only the desired 5-7 Watt cooling while maintaining stable flow.

Alternative methods for restricting the flow of liquid carbon dioxide may be required to provide a steady flow of liquid carbon dioxide and achieve the cooling rate projected. However, it may be worth noting that lower cooling levels may also be both clinically effective and perhaps even desirable; this must be optimized in the future, as the lower flows will make a given supply of liquid carbon dioxide last longer.

The major finding of the work was that the viscoelastic gel liner presented only a small barrier to the heat transfer of the system. The insulating effect of the liner is a primary driver of the overheating problem experienced by patients. However, the driving force for heat transfer present at room temperature is extremely small, on the order of 20 ^{o}F, compared to the driving force for the active cooling liner, which can be as high as 80 ^{o}F. With this larger driving force for heat exchange, a steady state temperature gradient can be established, which is certainly affected by the insulating effect of the liner, but is not rendered ineffective by its presence. This was tested using a bench top test in which water was used as a flowing medium for heat exchange, which measured the heat transfer from the cooling lines through the liner

accomplished by the system. The results show that relevant heat transfer rates can be achieved through the liner.

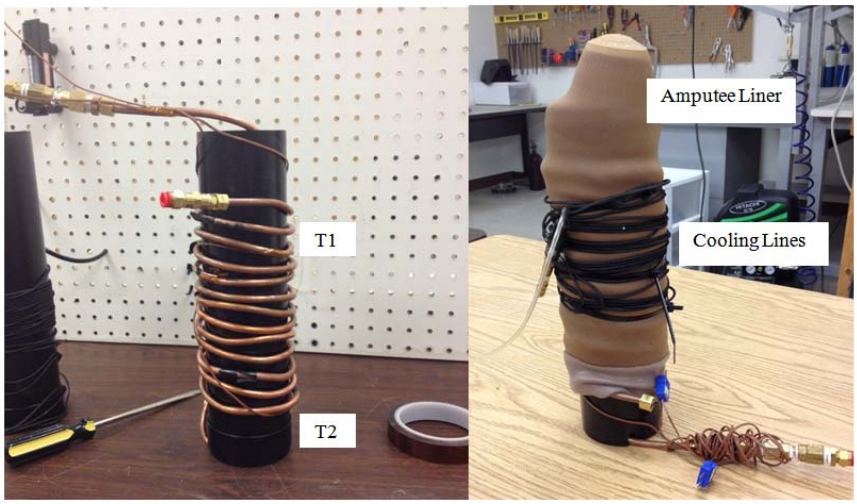

Figure 12: Water flow system used to establish the thermal resistance presented by the liner to the active cooling system.

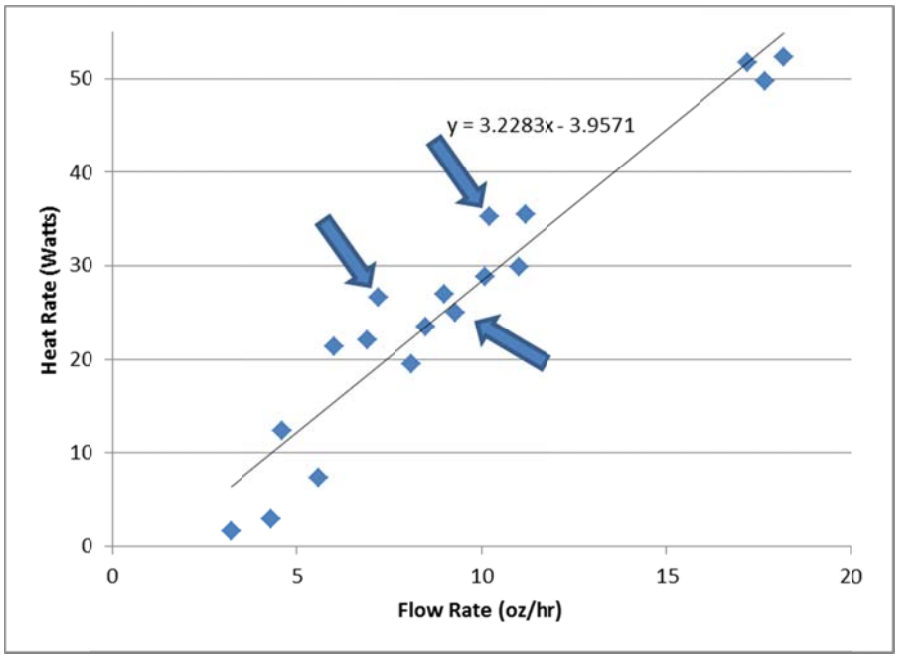

Figure 13: Measured heat exchange rate as a function of liquid carbon dioxide flow rate, when measured through the liner material.

For additional information on this task, please see Attachment G, the final program report from Porticos.

Benefits Analysis

The resins used in Task 1: Reconfigurable sockets displayed suitable amounts of adjustability and retained strength suitably through the adjustment cycles. However, these resins were considerably more expensive than the common prosthetics resins.

The 3D Pressure Mapping system developed in Task 3 brought a new capability to the field, and development has continued on it after the conclusion of the program's investment in it.

The braiding technology was successful in producing custom composite sockets at a reduced cost **(~34% reduced cost)**, and are capable of producing stronger and more consistent prosthetic sockets. The technology allows for the fabrication of a truly engineered product, and is expected to enable the development of standards on the fabrication of sockets. Further, this technique is expected to help facilitate the design and production of emerging paradigms for comfortable sockets. The skilled labor required for fabrication is reduced **(~50% reduced labor input)**, as is the waste in production. Finally, the produced sockets are roughly **50% lighter** for the same strength as traditionally fabricated products, while maintaining all other relevant criteria, including aesthetic. This will allow a focus of limited resources (both time and funding) on providing care directly to the wounded while delivering superior components for prosthetic and orthotic systems.

The active cooling system demonstrated that such a technology can provide cooling through the thermal barrier of the liner. Further development is required to build on this initial proof of concept.

Task 1: Conformable Resins									
Parameter	Baseline Value	Requirement Threshold Value	Requirement Objective Value	How to Measure	Date to be Achieved	Achievement Value	Achievement Date	How Demonstrated	How Demonstrated
Conformability	0	2 mm	4mm	Direct Measurement	March-09	4 mm	March-09	CTD Socket Deliverables	CTD Socket Deliverables
Retained Strength	0	90%	95%	Direct Measurement	August-09	95%	July-09	Clemson 3-pt bending test	Clemson 3-pt bending test
Resin Cost	$60.00	130%	120%	Project Estimates	August-09	~300%	August-10	Clemson Price Quote	Clemson Price Quote
Task 4: Automated Manufacturing									
Parameter	Baseline Value	Requirement Threshold Value	Requirement Objective Value	How to Measure	Date to be Achieved	Achievement Value	Achievement Date	How Demonstrated	How Demonstrated
Cost (excluding non-recurring costs)	$162.73	$155	$146	Project Estimates	Dec-10	$101.13	Nov-10	Cost Estimates	Cost Estimates
Labor Time	4	2	1	Project Estimates	Dec-11	2	Nov-10	Cost Estimates	Cost Estimates

Implementation Status

Task 3: 3D Pressure Mapping

The high resolution pressure mapping system was commercially launched (Zebra™ Sensors) in September 2010; this system allows for the measurement of the pressures that the residual limb experiences, and is capable of making detailed measurements during all major phases of a patient's activity (sitting, standing, walking, and running). This system has been purchased several early adopters for use in clinical and research settings.

Task 4: Automated Fabrication

This task has resulted in significant transition of the braiding technology to the industrial base serving the prosthetics community. This technology allows for fabrication of sockets at approximately **34% reduced costs**, and with approximately **half of the skilled labor input**. An industrial partner (Friddles Orthopedic Appliances, FOA) has agreed to serve as a distributer for the braider systems assembled by Mentis Sciences, and two central fabrication facilities (FOA; O & P 1) have already purchased braiders for producing components. These sites are now servicing all branches of the government, including both Defense and Veteran's Administration; further, these facilities are also servicing the civilian population and elite Paralympic athletes as well.

These technologies were proven out for prosthetic sockets, but have application to other components applicable to the field, including orthotics. Transition to the industrial base is allowing innovation utilizing these advanced techniques to develop new products for the field, including facilitating the design and production of emerging paradigms for comfortable sockets.

Task 1: Reconfigurable Sockets

The shape memory foams and resins are currently available for government purchase for use in fabricating sockets. Prototypes, which were positively received, were delivered to Walter Reed Army Medical Center, the Center for the Intrepid, and Navy Medical Center San Diego.

Task 6: Active Cooling Liner

The demonstration of this technology has only recently been accomplished. SCRA, in partnership with Porticos, is investigating transition opportunities, which are expected to be significant.

Attachment A

Annual Progress Report (2008-2009)

Orthotics and Prosthetics:
Thermally Reversible Cross-linked Composites Materials

Professor Dennis W Smith, Jr.

#

DEPARTMENT OF CHEMISTRY
CLEMSON UNIVERSITY, CLEMSON-29634

Orthotics and Prosthetics: Thermally Reversible Cross-linked Composite Materials

Annual Progress Report
(2008-2009)

Dr. Dennis W. Smith, Jr.
Department of Chemistry,
Clemson University, Clemson.

Technical Approach:

Inspired by the self-healing phenomenon in biological systems, self-healing polymeric materials have the capability of repairing and recovering themselves from the mechanically induced damage with the help of external stimuli (e.g. heat), once or multiple times. This valuable property can extend the lifetime use of various applications and may results in more comfortable prosthetics sockets capable of thermally reversible cross-linking. However, costly and complex synthetic route and loss of properties after remending has limited the use of various available technologies so far. Diels-Alder (DA) and retro Diels-Alder (r-DA) reaction represents a highly promising route to introduce this property into the polymeric systems without affecting their recyclability and refrabricability. We have tried to incorporate our novel and facile method of thermal reversibility by modifying commercially available monomers, furan compounds and bismalimides. This allows flexibility in the variety of polymer which allows controlling the resin's final properties (Scheme 1). For prosthetic socket resins, we have focused to apply our technology on two polymeric systems i.e. epoxy and acrylate, which are very commonly used in prosthetic industry.

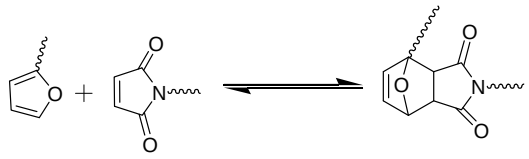

Scheme 1*. Thermally reversible cross-linked polymers with furan in the backbone and multi-functional maleimide as the cross-linker. These polymers cross-link at 45-60 ºC and uncross-links above 125º C.*

1. Thermally Reversible cross-linked epoxy with self healing properties:

We have developed and modified the traditional BP-epoxy resin with furan and mailimde units, (Scheme 2) which are capable of introducing reversible cross-linking based on DA reaction. These modified epoxy resins containing furan moiety, have successfully demonstrated the reversible cross-linking with commercially available bismalimides as well as with maleimide modified epoxy (Scheme 2). Thermally reversible cross-linking was visualized by solubility test at 55 ºC and 130 ºC, Fig.1. The high temperature promoted the retro diel-alder (RDA) reaction i.e. break down of cross-linked structures causing the swollen cross-linked polymer to revert to the solution.

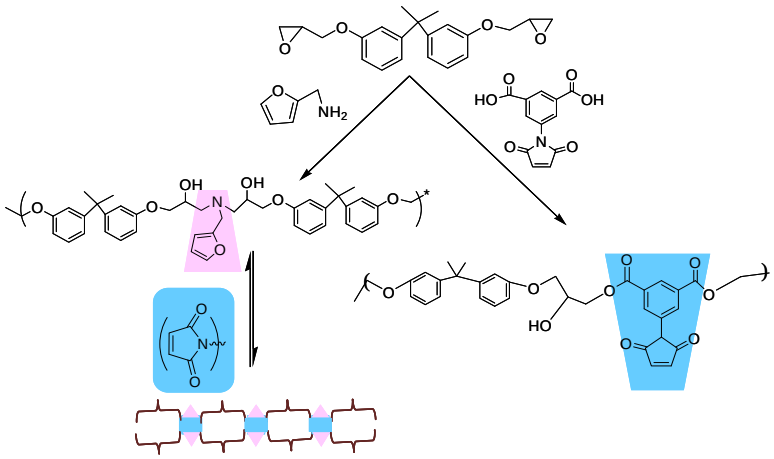

Cross-linked Epoxy

Scheme 2: Modification of commercially available epoxy with furan and mailimdes

Fig 1: Photographs taken to observe thermally reversible cross linking behavior of modified epoxy with BMI. The cross-linked polymer was insoluble in DMF at room temperature (a), soluble at 130 ºC and recross-linked at 45 ºC.

These DA and r-DA reactions were confirmed with the ATR-IR, Fig.2. The norbornene-like adduct has distinguishing vibrational peaks at 1043, 1124 and 1273 cm^{-1}. The broad peak present at 1720 cm^{-1} in the cross-linked and r-DA reaction is from the carbonyl (C=O) stretching in the maleimide cross-linker. The vibrational peaks from the distinctive norbornene-like adduct disappeared, thereby proving the reversibility of this DA reaction, and thus the thermal reversibility in the cross-linking. These transitions of DA and r-DA were also observed in thermal studies (Fig. 3). Initial degradation temperature in TGA and a new transition at 134 °C in DSC supported the r-DA transitions i.e. indication of dissociation of cross-linked network at elevated temperature.

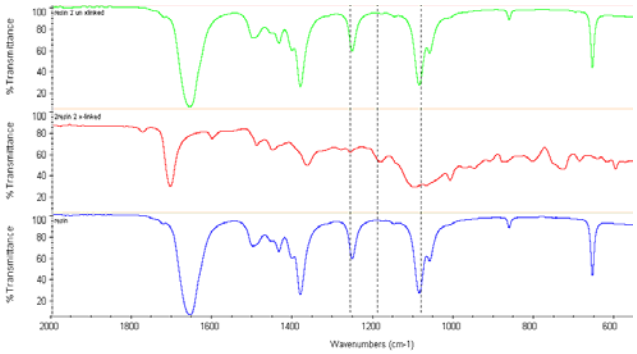

Fig 2: ATR IR of modified epoxy (bottom), x-linked resin (Middle) and uncross-linked resin (Top)

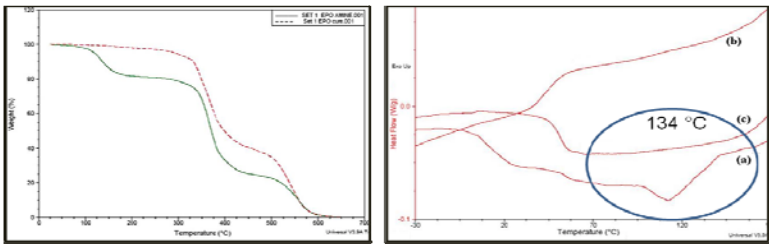

Fig. 3: TGA (left) and DSC (Right) thermogram of cross-linked modified epoxy and BMI. New endothermic transition at 134 °C in DSC thermogram of cross-linked epoxy indicated r-DA reaction

These sequences of cross-linking (DA), uncross-linking (RDA) and recross-linking (DA) reactions make the new modified epoxy system not only remendable but also reworkable. The C-fiber composites were prepared by using modified epoxy resin cross-linked with BMI as shown in Fig. 4. These composites were temporarily deformed at high temperature and cooled down at 25 °C, Fig. 4b. These composites regained their shape when exposed to 80-90 °C (*Video attached*). *Composites can be easily reshaped / reconfigured with heating gun as per patient's comfort.*

1.1 Additives for modified BP-Epoxy: These resins, however, showed promising results for the composite materials but they had very high viscosity. Such resins are considered to be the cause of occasional difficulty not only in casting of resin into the mold but also in the production of fiber reinforced composite materials by wet impregnation process usually by hand layup technique. Therefore, we have used various viscosity modifiers (Fig.

Fig: 4 Visual shape memory effect in thermally remandable epoxy composites

5), having epoxy end groups i.e. aliphatic epoxies (*hybrid resin*) and compounds with other amine groups such as aniline (*NTFA*) and dodecyl amine (*NTFD*) so that these modifiers can become a part of matrix after curing and this would help in preventing bleeding / blooming of additives, a major problem in composite industries. *The viscosity of the resulting resins was decreased with increase in BDGE content. Also, NTFA resin showed viscosity comparable to commercially available epoxy. Above all, these modified resins with e*poxy and amine *additives were successfully tested for thermally reversible cross-linking and were characterized by ATR-IR, TGA and DSC.*

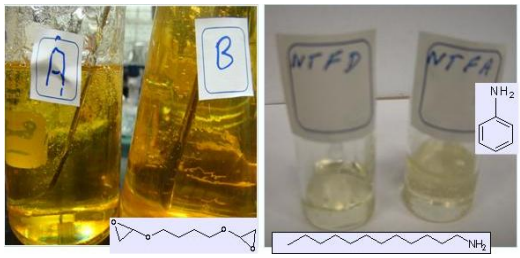

Sample	T_g
Set 1 (BP-epoxy)	59.9
Set 2 (BDGE epoxy)	-31.6
2 wt(%) Hybrid	54.1
5 wt(%) Hybrid	50.9
10 wt(%) Hybrid	45.7

Fig.5: Photographs of neat modified resin (A) hybrid resin (B) and amine modified resins: (Right), Table showing decrease in T_g of hybrid resin (Table).

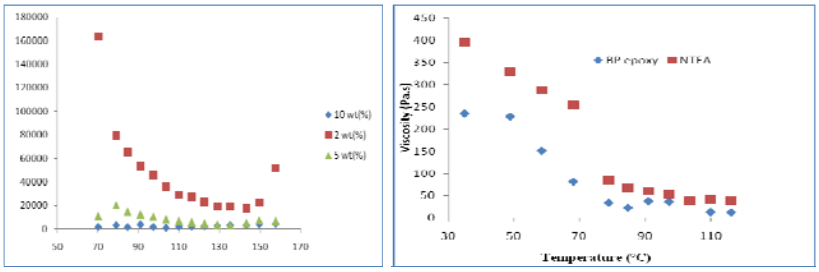

Fig. 6: BDGE modified hybrid resin (left) Viscosity of resin decreased with increase in BDGE content and viscosity of amine (Aniline) modified epoxy (Right) comparable with commercial epoxy.

The reduced viscosity of these hybrid epoxies as compared to neat modified BP-epoxy resulted in better and easy processing during composite fabrication. Both the appearance and T_g reduction (Fig. 5) with addition of modifier strongly indicated that the modified resin was homogenous. This effect can be seen on mechanical properties and energy at break of the composites based on these resins.

Three Point Bending Test: The ability of the thermally reversible cross-linked epoxy to function as a self-healing resin was evaluated by measuring the load taken by C-fiber composites in three point bending tests at Instron testing machine (Fig 7). These composite panels are 4 layers and ± 45 orientations. In Fig 7, neat modified BP epoxy (0) & 2 wt (%) hybrid resin with three healing cycles is shown. The compressive

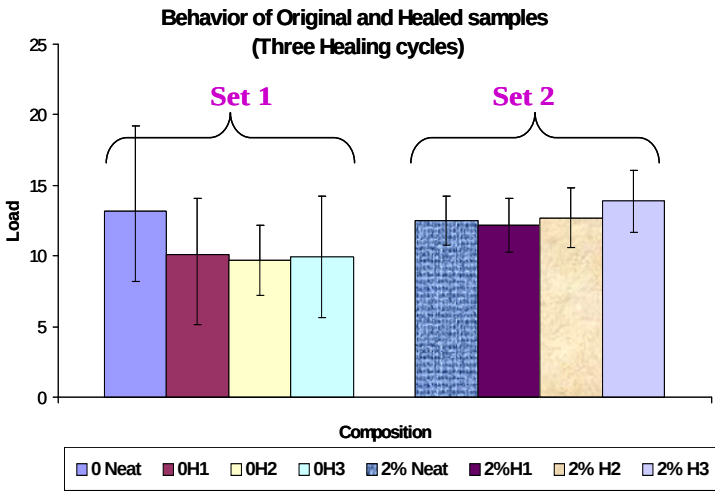

Fig 7: Neat modified BP epoxy Resin (Set-1), 2 wt (%) hybrid epoxy (Set-2). Subset 1, Subset 2, 3 & 4 of each resin represents the original, first, second and third healing cycles of composite.

load was marginally decreased with increase in BDGE modifier while after healing it was observed that the healing was higher in case of hybrid epoxy as compared to neat resin. However neat resin showed a decrease after first testing but after that up to three healing cycles the performance was consistent while hybrid resin showed better performance even after four testing cycles. The appearance of modified resin before and after curing was transparent and no phase separation was found with the naked eye. *Our results are in consistence with other DA and r-DA based composite systems where composites have shown 100 % recovery up to seven testing cycles*. The standard deviation (SD) in the samples showed more uniformity in the hybrid samples indicating better wetting between C-fiber and resin. It was also observed that the *energy required at break* was higher in case of hybrid epoxy (0.075J; SD 0.01) as compared to neat BP epoxy (0.065J; SD 0.01) and even after three healing cycles it was higher in case of hybrid epoxy which is in support of the compressive load data.

1.2 Shape Memory Epoxy (SME) Resin: Transparent SME were prepared by varying compositions of diglycidyl ether of bisphenol-A epoxy and butandiol diglycidyl ether epoxy (BDGE) cured with hexamethylene diamine. These SME were tough at room temperature and exhibited shape memory (SMP) effect at around 70 ºC, Fig 8. (*Video Attached*). The thermal stability of all these compositions was ~ 350 ºC.

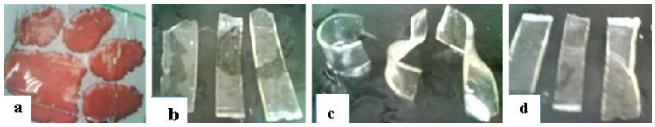

Fig: 8 Visual Shape memory effect of Epoxy resin, a) Transparent epoxy sheet; b) original shape; c) temporary shape; d) recovered shape

2. ACRYLATE Terpolymers:

Two different sets of terpolymers, based on furfuryl methacrylate (FMA) were prepared by solution polymerization. These FMA based terpolymers were prepared from commercially available monomers and successfully tested for thermal remendability and can be another cost effective substitute for prosthetic sockets.

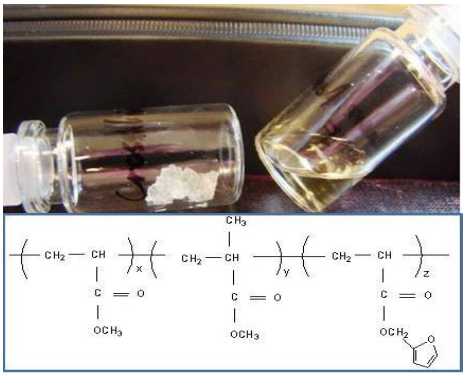
Fig 9: Photographs taken to observe thermally reversible cross linking behavior of MA/MMA/FMA terpolymer

a) MA/MMA/FMA Terpolymer: Free radical polymerization of furfuryl methacrylate (FMA), methylmethacrylate (MMA) and methacrylate (MA) in different molar ratio were prepared (Fig 9). This terpolymer with Tg ~ 55 °C, having molecular weight (M_w) ~ 44,000 and PDI~ 4, were successfully tested for thermally reversible cross-linking which was confirmed and characterized by ATR-IR, DSC and TGA.

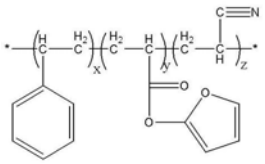
Fig 10: Photographs taken to observe thermally reversible cross linking behavior of AFS terpolymer

b) **ASA (AFS) Terpolymer:** Acrylonitrile (AN) – furfurylmethacrylate (FMA) – styrene (S) terpolymers (AFS) terpolymers were prepared by free radical polymerization. These polymers after cross-linking have shown good solvent resistance in THF, DMF, acetone and other common solvents at room

temperature while their commercially available analogues shows poor solvent resistance. These terpolymers were also successfully demonstrated the thermally reversible cross-linking.

As per submitted schedule, we have achieved the project deliverables in time. The results of hybrid epoxy resins arebetter than our initial neat BP epoxy resin and composites showed recovery up to four testing cycles. Therefore scale up of these hybrid resins is in progress for further optimization of composites properties. The mechanical properties of our acrylate and ASA terpolymers are currently underway.

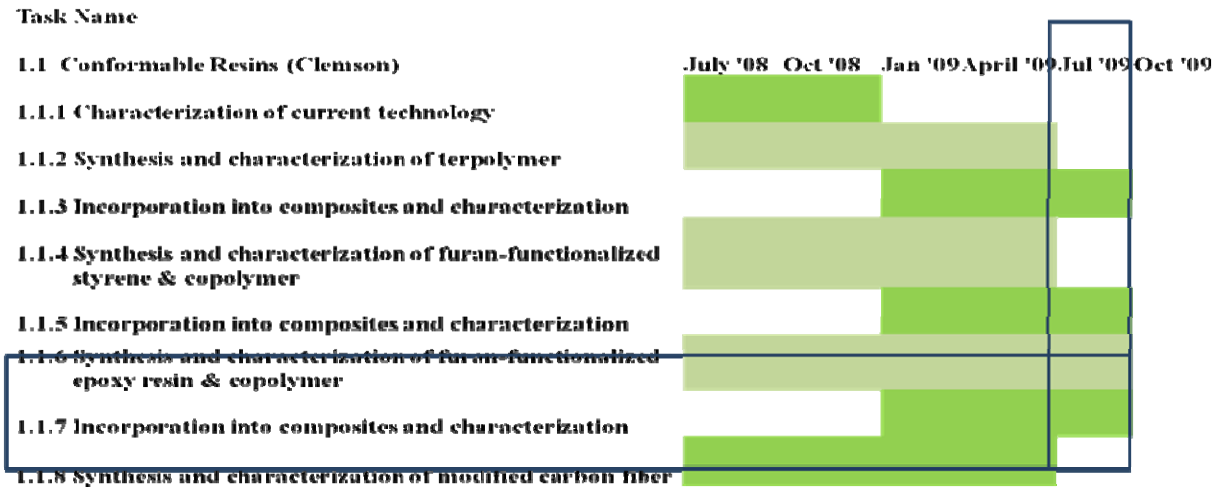

Publications:

1. Sharma B, Tomar N, Norfolk CW, Smith Jr. DW, "*Thermally remendable ASA terpolymers*" Southern Rubber Group Summer Meeting, July 12th-16th 2009, Charleston, SC.
2. Deng W, Tomar N, Sharma B, Norfolk CW, Smith Jr. DW, "*Thermally reversible cross-linked terpolymers*", Proceedings of 238th National Meeting of the ACS Poly Div, Washington DC, August 16, 2009.

Manuscripts under preparation:

1. Tomar N, Deng W, Sharma B, Norfolk CW, Smith Jr. DW, " *Mechanical Properties of Recyclable Epoxy and C-Fiber Composites"*
2. Deng W, Tomar N, Sharma B, Norfolk CW, Smith Jr. DW, "*Terpolymerization of Methyl Acrylate / Furfuryl methacrylate/ Methyl methacrylate"*.
3. Sharma B, Tomar N, Deng W, Norfolk CW, Smith Jr. DW, "*Terpolymerization of Acrylonitrile/ Furfuryl methacrylate/ Styrene"*.
4. Tomar N, Deng W, Sharma B, Norfolk CW, Smith Jr. DW, "*Influence of Reactive Diluents on Cure Kinetics of Thermally Self-healing Epoxy*".
5. Tomar N, Deng W, Sharma B, Norfolk CW, Smith Jr. DW, "*Effect of Thermally reversible cross-linked gels as healing agent for Conventional Epoxy/Amine Systems*".
6. Tomar N, Deng W, Sharma B, Norfolk CW, Smith Jr. DW, "*Properties of Network obtained by internal Plasticization of Thermally Remediable Epoxy Resin with Aliphatic Glycidyl Compounds"*
7. Tomar N, Deng W, Sharma B, Norfolk CW, Smith Jr. DW, "*Miscibility and Morphology of Thermally Reversible Gels and Epoxy Blends."*

Attachment B

COMPOSITE TECHNOLOGY DEVELOPMENT, INC.
ENGINEERED MATERIAL SOLUTIONS

Development and Demonstration of a TEMBO® Shape Memory Prosthetic Socket

Prosthetics and Orthotics Manufacturing Initiative (POMI)

Task Order No. 0001

Subcontract No. 2008-546

Prime Contract No. N00014-06-D-0045, DO 0007

Final Report

Reporting Period August 11, 2008- February 11, 2009

Prepared By:

Composite Technology Development

Douglas Campbell, Technical Representative

303-664-0394 x125

2600 Campus Drive, Suite D

Lafayette, CO 80026

Prepared For:

SCRA Applied Research and Development Institute

91 Technology Drive, Suite 200

Clemson Research Park

Anderson, SC 29625

TABLE OF CONTENTS

1.0 Program Summary

The overall goal of the program was to evaluate the feasibility of reconfigurable prosthetic sockets enabled via the use of TEMBO® shape memory polymer (SMP) technology. In particular, the present program was focused on demonstrating the feasibility of using existing TEMBO® SMP chemistries in a composite prosthetic socket to enable local modifications to the socket's shape. TEMBO® SMP's are a family of fully cured, thermoset epoxy resins that can be processed using industry standard composite processing techniques (e..g, wet layup, resin infusion, pre-impregnation, etc.). The materials can be processed as neat resins, fiber-reinforced composites and as open- and closed-cell foams of variable relative density. TEMBO® SMP materials possess the unique capability of "freezing" and recovering mechanically-induced strains via a specific thermo-mechanical cycle that consists of: 1) elevate the temperature above the polymer's glass transition temperature, T_g, (via ovens, heat guns, etc.), 2) deform the material while in a compliant state at temperatures above T_g, 3) while maintaining the deformed shape, remove the heat source and allow to cool to room temperature, 4) once cooled below T_g, remove the constraint after which the "frozen" shape will be maintained indefinitely and 5) reheat the material back above T_g to self-recover the as-manufactured shape. Using this cycle, it is envisioned that the use of TEMBO® SMP resins for socket construction and/or foam liners would enable socket reconfiguration to account for short- and long-term changes in the volume and shape of an amputee's residual limb thereby improving socket fit and comfort.

Sockets developed under the present program utilized existing TEMBO® SMP resin chemistries and braided carbon fiber fabric and were manufactured using industry-standard techniques including hand-layup and/or resin-transfer-molding. Focus was placed on simple socket reconfiguration methods using a combination of ovens or heat guns for temperature source and hand pressure or simple mechanical systems for inducing desired socket reconfiguration. Existing TEMBO® SMP resins were chosen with reconfiguration temperatures (i.e., approximately equivalent to the polymer's T_g) that are sufficiently low to allow for comfortable handling by a gloved practitioner and/or technician while also being sufficiently high to eliminate undesired reconfigurations (i.e., softening) in the presence of naturally occurring elevated temperatures. CTD chose three overarching approaches or, design features for optimal socket reconfiguration. These include: 1) localized thinning of the socket, 2) localized socket cutouts (i.e., slitting) and, 3) incorporation of CTD's TEMBO® SMP foam at select locations (i.e., as pads). All three design approaches maximized socket reconfiguration while maintaining adequate socket structural properties. A video-demonstration of the reconfiguration of a TEMBO® SMP sockets was produced. Furthermore, a total of ten (10) sockets of CTD-defined shape and form were manufactured incorporating one or more of the three methods adopted for optimal socket reconfiguration. Both the video demonstration and sockets were delivered to SCRA at the conclusion of the program.

2.0 Program Accomplishments

The principal achievements of this program was the demonstrated use of CTD's TEMBO® SMP resin and SMP foam to enable the reconfiguration of prosthetic sockets. CTD has identified three simple design features for optimal socket reconfiguration. These include: 1) localized thinning of the socket, 2) localized socket cutouts (i.e., slitting) and, 3) incorporation of CTD's TEMBO® SMP foam at select locations (i.e., as pads). Figure 1 illustrates these three

approaches. In all cases, CTD's TEMBO® SMP resin is used as the matrix material in the composite construction. Socket thinning is achieved by cutting the dry, braided reinforcement in a leafed pattern to achieve the desired thickness reduction prior to resin introduction. The reduced socket thickness allows the socket shell to achieve higher displacements (both in and out) due to local reductions in stiffness. Socket slitting is achieved by cutting slits into the fully cured socket thereby locally increasing socket compliance. Finally, incorporating CTD's TEMBO® SMP foam as pad inserts can provide significant reductions in effective socket volume. This was achieved by adhering the shaped foam pads to matching recesses in the socket shell. When fully compressed, the surface of the foam and inner socket shell are coincident. Thus, heat-cycling the TEMBO® SMP foam results in foam recovery thereby accommodating local reductions in residual limb volume. It should be noted that for all three cases, the use of TEMBO® SMP material technology in combination with these design features uniquely provides a socket that is highly stiff when in use (i.e., at ambient temperature) and highly compliant for socket reconfiguration (i.e., at elevated temperature).

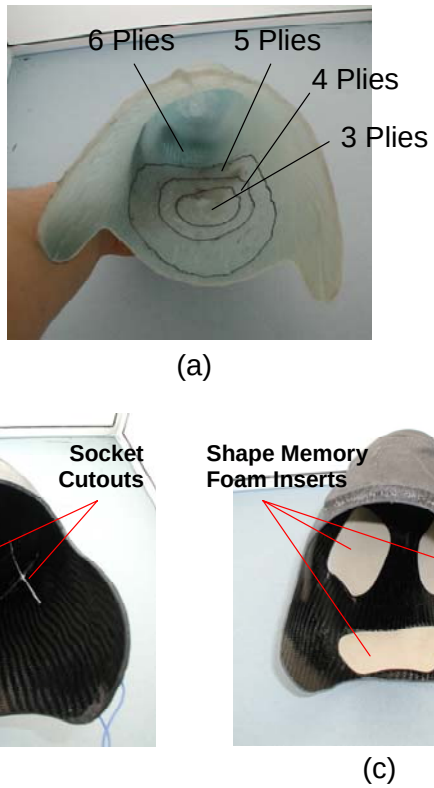

Figure 1. CTD's thinning (a), slotting (b) and foam padding (c) methods for optimizing socket reconfiguration.

2.1 Socket Manufacturing

The major characteristic that enables socket reconfiguration is the unique chemistry of CTD's TEMBO® SMP resins and foams. CTD possesses a family of TEMBO® SMP materials each uniquely developed to meet performance, manufacturing and cost goals for target applications. It should be noted that no material development efforts were undertaken during the present

program; rather existing TEMBO® SMP resins were evaluated to assess general feasibility. Table 1 summarizes the TEMBO® SMP resin chemistries either used for socket production or investigated for use under the present program. Relevant mechanical properties, processing characteristics, and reconfiguration temperatures are provided for reference. Reconfiguration temperature is loosely consistent with polymer glass transition temperature, T_g. Both the glassy- and rubbery-state Young's modulus is provided illustrating the dramatic reduction in polymer and hence, composite, stiffness (i.e., increased socket compliance) that occurs across the transition (i.e., above polymer T_g). Relevant processing data is also provided in Table 1 including initial viscosity and working time. All resins considered were highly flow-able at room temperature (i.e., wet) to allow socket processing using the Vacuum Assisted Resin Transfer Mold (VARTM) technique.

Table 1: Summary of CTD's TEMBO® SMP resin chemistries evaluated in the present program.

SMP Resin	Processing Types	E-Glassy (Msi)	E-Rubbery (Msi)	Viscosity (cP)	Working Time (hr)	Reconfigure Temp (C^o)
CTD-DP5.1	Wet, Foam	261	1.45	4000	2	70
CTD-DP5.4	Wet, VARTM	--	--	1600	4	60
CTD-7.1	Wet	218	2.9	1600	4	70
CTD-7.1B	Wet, VARTM	72	0.4	450	12+	35
CTD-7.1HT3	Wet, VARTM	--	--	1200	12+	90

Figure 2 provides a photograph illustrating the VARTM process used to manufacture the sockets produced during the present program. This process consists of drawing resin into the dry, braided reinforcement using vacuum pressure (see Figure 2). The dry reinforcement is applied to the mold and the entire assembly is sealed in a vacuum bag. Vacuum is applied to the assembly via an outlet port drawing resin into the reinforcement via the inlet port. The process is continued until resin is drawn into the outlet indicating complete wet-out has occurred. The entire assembly is then placed in an oven and the appropriate cure schedule is followed. Slight vacuum is maintained during initial cure (i.e., past the gel-point) to ensure adequate consolidation. Following cure, the part is de-molded, trimmed and evaluated for reconfiguration (see Figure 3).

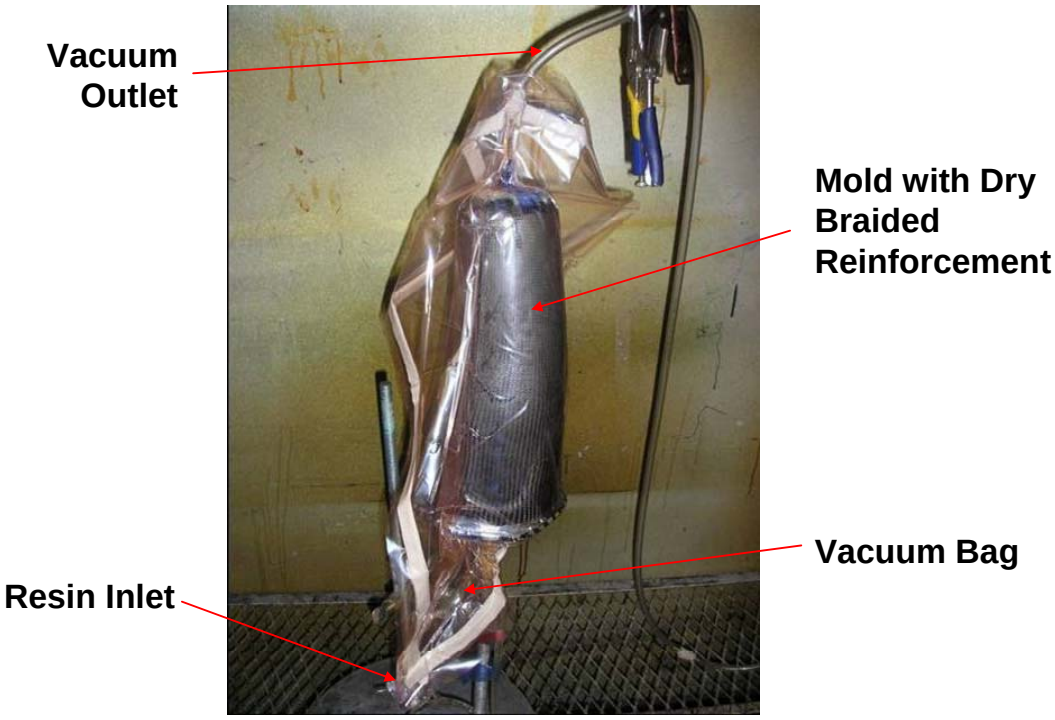

Figure 2: VARTM process assembly.

Figure 3: Completed sockets.

2.2 Socket Reconfiguration

As earlier stated, CTD identified several design features to provide a varying balance of socket reconfiguration, stiffness and functionality. The socket thinning approach provided for a seamless socket construction but provided the smallest magnitude of socket reconfiguration. Through testing it was found that the maximum amount of shape change was approximately 1-2 mm of either inward or outward deflection. It is noted that this degree of socket deflection is

directly dependent both on the extent of socket thinning and shape of the thinned area, thus being highly customize-able. For example, as shown in Figure 4 CTD locally thinned the socket of the present deliverables in circular pattern symmetric about the socket's anterior face. Naturally, this area would yield the greatest extent of socket reconfiguration.

Figure 4: Area of socket thinning.

The socket slitting approach provides a much greater magnitude of socket reconfiguration as compared to the socket thinning approach. Several patterns of slitting were explored to provide maximum socket reconfiguration while minimizing socket compliance at room temperature. As shown in Figure 5, single- and double-cross patterns were used for the posterior and anterior socket locations. Reconfigurations trials revealed that this method provides approximately 6-8mm of socket deflection. Figure 6 provides a series of photographs illustrating the extent of socket reconfiguration achievable via the socket slitting methods.

Figure 5: The anterior slotting of the socket (left), posterior slotting of the socket (right)

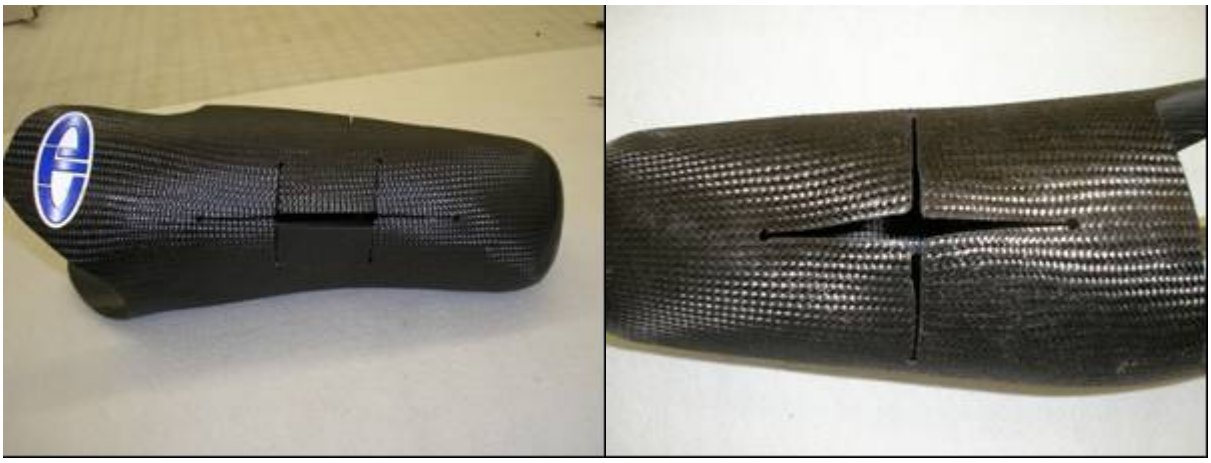

Figure 6: The maximum deformation of the slotting reconfiguration mechanism

Finally, the inclusion of SMP foam pads was considered to enable the maximum extent of socket reconfiguration. When fully compressed, the surface of the foam pads is coincident with the socket's inner surface. Thus by shape recovering the foam pads, an effective reduction in socket volume is achieved. As shown by the photographs in Figure 7, several patterns of foam pad placement were considered. The extent of volume reduction is dependent of the relative density of the SMP foam pads. Under the present program, 15-percent relative density SMP foam was used. As shown in Figure 8, this allowed for a maximum 12mm local deflection (i.e., volume reduction) with the foam in the fully recovered state. This enables the socket to accommodate highly localized changes in socket volume through locally deforming anywhere from 0 to 12mm. Furthermore, the high compliance and conformability of the SMP foam can accommodate substantial variations in surface topography thereby locally conforming to the highly variable shape of a residual limb. Ultimately this approach provides true custom fit capability.

Figure 7: Foam pad placement patterns.

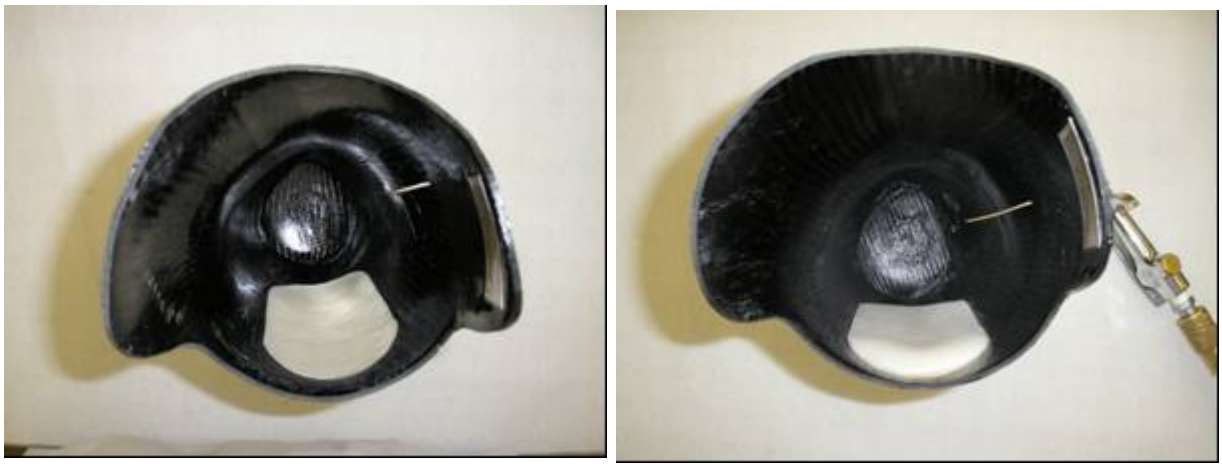

Figure 8: SMP foam pad fully compressed (left) and recovered (right).

Figure 10: Left foam in the original none deformed state, center, foam heated and deformed locally, right, foam rigid in its locally deformed state.

Table 3 provides a summary of the maximum shape change achieved via the socket design features explored under the present program. As discussed and reflected in Table 3, the three design features provide a varying degree of socket reconfiguration characteristics and functionality. The socket thinning approach provides highly localized shape change, while the slitting and foam pads approaches offer a larger area and greater extent of socket reconfiguration. In addition, both the socket thinning and slitting approaches require only modest changes in socket manufacturing relative to current industry practice. In contrast, it is acknowledged that the method of including SMP foam pads as explored under the present program would require modest changes in the socket manufacturing process. However, the SMP foam pads approach provides a highly unique solution due to the material's ability for highly localized reconfiguration. Finally, while each design feature was explored individually, it is likely that these features may be incorporated together into a single socket design for maximum functionality. Ultimately, the unique attributes of a reconfigurable, fully-cured prosthetic socket is enabled only through the use of TEMBO® SMP material technology that provides a multifunctional behavior of compliance, shape storage and shape memory for a unique combination of socket reconfiguration and structural integrity for in-use operation.

Table 3: Summary of maximum shape change among the different reconfiguration mechanisms

Reconfigure Mechanism / Socket Design Feature	Maximum Shape Change in Delivered Socket Designs
Thinning	2 mm
Slitting	8 mm
SMP Foam Pads	12 mm

2.3 Program Deliverables Summary

A total of 10 representative sockets were delivered to SCRA at the conclusion of the program to satisfy program deliverable requirements. The sockets were of a relevant, representative shape but did not incorporate additional prostheses hardware (e.g., suspension system, socket-ankle/knee interface, etc.) associated with a complete prosthetic system. More specific, the purpose of these deliverables was to provide a method for hands-on demonstration of the functionality of a reconfigurable prosthetic socket enabled via the use of TEMBO® SMP material technology. To that end, the sockets incorporated the various design features discussed in the present report based on CTD-derived, qualitative socket functional requirements. In summary, these sockets are not intended to represent a final, functional design, but merely to provide a means of conveying the general capabilities of a truly reconfigurable, custom-fit prosthetic socket.

All but one of the sockets manufactured and delivered under the present program utilized the same positive mold. Additionally, all sockets were manufactured using the same braided carbon fiber perform reinforcement. Finally, each socket incorporated one or more of the design features previously identified for optimizing local socket reconfiguration. Table 2 provides a summary of the prototype reconfigurable sockets that were provided to SCRA as program deliverables at the completion of the present program. Sockets labeled 8, 9, and 10 in Table 2 incorporate all three socket reconfiguration design features identified in Figure 1. Sockets labeled 5 and 6 incorporate both the foam inserts and socket slitting design features, while the remaining four sockets feature either the socket slitting or thinning design feature in multiple socket locations. As shown by the example in Figure 4, all sockets included tags identifying the hardware as government property and listing the relevant government contract and CTD part number.

Table 2: Summary of the delivered reconfigured prototype sockets

Socket	Part Number	Reconfiguration Mechanism	Location of Reconfiguration	TEMBO® SMP Resin
1	216010	Socket Slitting	Anterior and Posterior	7.1, 7.1B
2	216011	Socket Slitting	Anterior and Posterior	7.1, 7.1B
3	216008	Socket Thinning	Anterior Only	7.1, 7.1B
4	216009	Socket Thinning	Anterior Only	7.1, 7.1B
5	216015	Foam inserts/Socket Slitting	Knee and Posterior	DP5.1 Foam, 7.1, 7.1B
6	216016	Foam inserts/Socket Slitting	Knee and Posterior	DP5.1 Foam, 7.1, 7.1B
7*	216002	Foam Inserts	Anterior and Posterior	DP5.1 Foam, 7.1, 7.1B
8	216012	All Three	Anterior and Posterior	DP5.1 Foam, 7.1, 7.1B

9	216013	All Three	Anterior and Posterior	DP5.1 Foam, 7.1, 7.1B
10	216014	All Three	Anterior and Posterior	DP5.1 Foam, 7.1, 7.1B

*Different positive mold than the rest of the sockets

Figure 4: Example of part identification tag.

3.0 Program Conclusions

The present program was executed to assess the feasibility of a reconfigurable prosthetic sockets enabled via the use of TEMBO® shape memory polymer (SMP) technology. It is envisioned that the use of TEMBO® SMP resins for socket construction and/or foam liners would enable socket reconfiguration to account for short- and long-term changes in the volume and shape of an amputee's residual limb thereby improving socket fit and comfort. TEMBO® SMP's are a family of fully cured, thermoset epoxy resins that can be processed using industry standard composite processing techniques (e..g, wet layup, resin infusion, pre-impregnation, etc.). They can be processed as neat resins, fiber-reinforced composites and open- and closed-cell foams of variable relative density. As a shape memory material, TEMBO® SMP materials possess the unique capability of "freezing" and recovering mechanically-induced strains via a specific thermo-mechanical cycle. Under the present program, existing chemistries of TEMBO® SMP materials were used in constructing numerous prosthetic sockets. Furthermore, several socket design features were explored to provide an optimal balance in socket reconfiguration and structural integrity. These features included: 1) localized thinning of the socket, 2) localized socket cutouts (i.e., slitting) and, 3) incorporation of CTD's TEMBO® SMP foam at select

locations (i.e., as pads). These design features in combination with CTD's TEMBO® SMP material technologies uniquely provides a socket that is highly stiff when in use (i.e., at ambient temperature) and highly compliant for socket reconfiguration (i.e., at elevated temperature).

The present program concluded in the manufacture, demonstration and delivery to SCRA of a set of 10 prototype reconfigurable prosthetic sockets. The sockets were manufactured in a representative form using an existing CTD positive mold and an intermediate modulus carbon fiber, braided reinforcement. The industry standard Vacuum Assisted Resin Transfer (VARTM) composite processing technique was used to manufacture all deliverables. The purpose of these deliverables was to provide a method for hands-on demonstration of the functionality of a reconfigurable prosthetic socket enabled via the use of TEMBO® SMP material technology.

The conclusions of the present program include:

- Utilizing TEMBO® SMP resin chemistries provides a modest degree of socket reconfiguration capabilities. Locally thinning the reinforcement laminas in key areas greatly increases the extent of socket reconfiguration (i.e., deformation) achievable.
- Socket deformation can be achieved both inward and outward corresponding to local reductions and increases in residual limb volume, respectively.
- Slitting of the socket in a pre-determined pattern greatly increases the extent of socket reconfiguration achievable as compared to socket thinning.
- The use of recessed, TEMBO® SMP foam pads provides the greatest extent of socket reconfiguration variability thereby accommodating maximum variations in residual limb volume. Furthermore, the high compliance of this material at elevated temperatures allows for the greatest extent of conformance to a variably shape residual limb.
- *A reconfigurable prosthetic socket enabled via TEMBO® SMP material technology is greatly feasible.* The numerous design features explored under the present program provides a high degree of customization based on amputee needs.

Attachment C

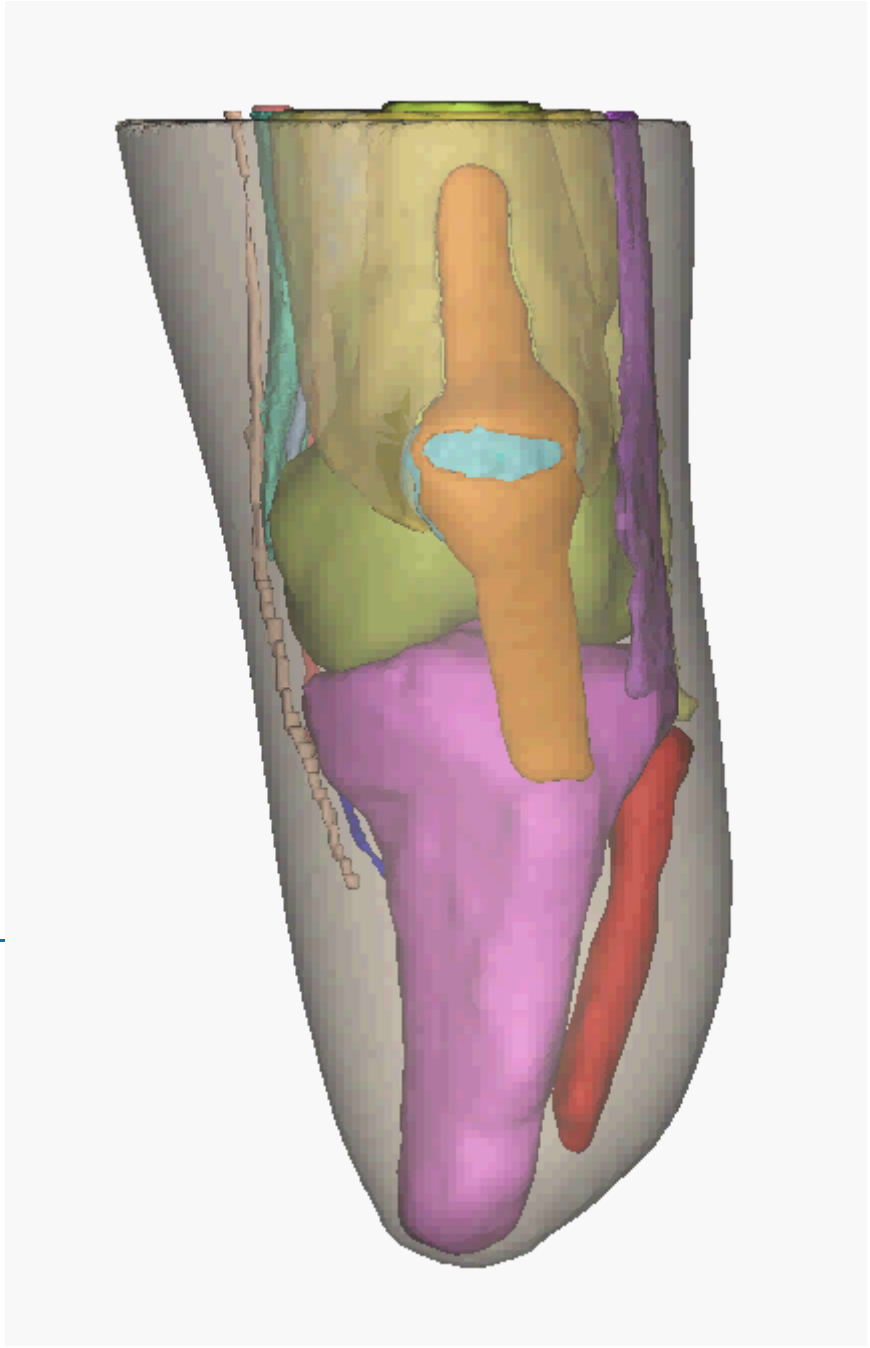

Medical Imaging Generated Dynamic Prosthetic Sockets

FINAL REPORT

CNTS 2008-00059

May 31, 2011

Robert S. Kistenberg, PI
Shayne Kondor, Co-PI
Samer Tawfik, PhD, Co-Investigator
Michael Terk, M.D., Co-Investigator

Georgia Institute of Technology

MSPO

Acknowledgements

This Project was sponsored by the Office of Naval Research through the South Carolina Research Authorities' Prosthetic Orthotic Manufacturing Initiative. Special recognition is also given to Dr. Chris Norfolk for his support and guidance through this project.

Executive Summary

The Medical Imaging Generate Dynamic Prosthetic Socket project was an ambitious 2 year effort which aimed to develop a system that would allow for direct MRI scanning of residual limbs to generate prosthetic sockets that were based upon the underlying anatomical structures whilst assessing the pressures these sockets would impose upon the residual limbs through finite element analysis.

The process was divided up into specific tasks including the Non-Deformational Shell, MRI Scanning, Segmenting and Modeling the Residual Limb, Fabrication of the Prosthetic Socket, Finite Element Analysis and Socket Iterations. Completion of the final tasks was entirely dependent on completion of the earlier tasks.

Processes were established and tested for the Non-Deformation Shell, MRI Scanning, Segmenting and Modeling the Residual Limb, Fabrication of the Prosthetic Socket and Finite Element Analysis. Validation of the finite element analysis required that the assumptions made for pressure in the socket be tested and confirmed. This step proved to be the most challenging due to the absence of an accurate and consistent pressure measurement system. Because we were ultimately unable to obtain in-socket pressure measurement data, the socket iteration task was not completed.

This project, however, was successful in a number ways. The fabrication method of the non-deformational shell was completed and tested. Many protocols for RL scanning were investigated and settings were optimized for obtaining scans for both transtibial amputations and transfemoral amputations which then facilitated residual limb segmentation. The process for segmentation proved to be cumbersome and difficult to achieve without significant experience on the part of the person performing this task. Automated segmentation is still not developed to the point where this process if feasible in clinical practice.

Once the arduous process of segmentation was completed, the residual limb modeling allowed for the prosthetist to “look into” a residual limb for the first time ever. This allowed for precise modifications of the anatomical structures but emphasized how little we know about how to load and relieve these anatomical structures. The process

of transferring the residual limb data between multiple software programs (MIMICS, 3-MATIC, ABAQUS & CANFIT) was cumbersome and required creative work around solutions in order to maintain data fidelity while allowing the job of each software program to be completed.

Once the rectified model was completed, the answer to how the anatomical structures could be loaded and relieved was to be solved by the finite element modeling (FEA). The FEA process also required an extensive amount of time and expertise on the part of the research however in the end; the process was established and refined, resulting in a straight forward method to perform FEA on sockets including donning, static standing and single limb support. We were not able to establish the ability to generate residual limb pressures and stresses in a dynamic state.

It was at this point that the project stalled. We made multiple attempts to obtain valid and reliable socket pressure measurements in order to validate the FEA assumptions. While each of the three transtibial and three transfemoral subjects' sockets were being moved through the process concurrently, the process needed to be completed for the first of each subject type to its conclusion before we progressed with the other two of each subject type. The lessons learned from the first transtibial and first transfemoral subject needed to be applied to the subsequent subjects so that process enhancements could be implemented.

In the end, the first transtibial subject, TT01, was fit with three iterations of sockets and then tested for socket pressure repeatedly over the course of the project however the pressure measurements, even with continued system refinements, proved inaccurate. Two iterations of each of the transtibial subjects were completed. Sockets were fabricated for the first and third transfemoral subjects and the first socket was fit to transfemoral subject TF01.

In summary, this project significantly enhanced our understanding about residual limb anatomy, the processes for obtaining residual anatomy through MRI scanning as well as the processes for performing finite element analysis on a residual limb/socket interface. It also identified a number of limitations that persist making automatic socket generation from MRI scanning impractical until these limitations are overcome.

Table of Contents

Table of Figures

Table of Tables

Introduction

This report details the activities of the two-year Medical Image Generated Dynamic Prosthetic Socket Project undertaken collaboratively by the Georgia Institute of Technology, Emory University and the Georgia Tech Research Institute. The overall goal was to investigate the methods by which prosthetic sockets are fabricated in order to ascertain methods to improve the process for fabrication as well as the ultimate fit of the sockets to the residual limbs.

This report has been formatted to communicate the lessons learned during this project while also serving as a user's manual to some extent so that those interested in investigating, recreating or refining any aspect of this project will be readily able to so. As such, many of the sections contain tables and figures that walk the reader step by step through the processes.

Background/Problem Statement

It has been long recognized that the most significant and critical aspect of any artificial limb is the socket—that part into which the residual limb is inserted in order to create an intimate connection between the human and the artificial limb designed to replace his/her missing anatomy. While the sophistication of prosthetic components has been rapidly improving over the last two decades, the fact remains that if the socket does not fit comfortably, the wearer will reject the prosthesis regardless of the components attached thereto.

When reduced to basic elements, the process for constructing artificial limb prostheses consists of four steps: residual limb model acquisition, positive model rectification, prosthetic socket fabrication & fitting. The current practice behind each of these steps is heavily dependent on practitioner and technician experience with little scientific or evidentiary support.[3]

The subjective nature of socket design is based upon prosthetists' experience and feedback from the wearer. Current methods for acquisition of residual limb models only take into account surface topography and, if hand casting is employed, surface palpation of the underlying structures. The exact location of the anatomy, the quantity

and quality of skeletal and soft tissue structures cannot be ascertained through current residual limb model acquisition techniques. Furthermore, a method to quantify socket fit is lacking.

Because of the reasons mentioned above, a scientific approach to socket synthesis does not exist. This project aimed to explore currently available diagnostic imaging techniques, modeling software, computer aided design/computer aided manufacturing software and finite element analysis software packages. Our overall goal was to create a fast and automated prosthetic socket design tool utilizing MRI data for shape acquisition, RL modeling and FEA for model rectification, which will ultimately generate the quantitative properties of a dynamic prosthetic socket.

Objectives

Specifically, this project aimed to:

1. Develop a model acquisition protocol utilizing a Magnetic Resonance Image (MRI) of a person's residual limb (RL) for the initial model. This included both transfemoral (above the knee) and transtibial (below the knee) amputations.

2. Develop a protocol that would rectify the MRI acquired model by applying tissue density properties to the unique soft tissue structures of that RL so that a computer aided design (CAD) socket can be fabricated for that individual.

3. Test the fit of the CAD socket through instrumented gait analysis (IGA) and RL/socket interface pressure mapping.

4. Utilize the MRI model, CAD socket model and data gathered from the IGA and pressure interface mapping to generate a Finite Element Analysis (FEA) model of a dynamic prosthetic socket.

This project was conducted through collaboration between The School of Applied Physiology (AP) at the Georgia Institute of Technology, The School of Aerospace (AE) Engineering at the Georgia Institute of Technology, The Georgia Tech Research Institute (GTRI), and the Division of Musculoskeletal Imaging (MI) in the Department of Radiology at the Emory University School of Medicine

Approach

Non-Deformation Shell

Based upon the procedure outlined by Douglas, *et al[4]*, and Buis, *et al[5]*, a plaster containment shell was fabricated in order to retain natural, non-deformed shape of the residual limb throughout the scan as the subjects would be required to lie on a gantry during their scans. The plaster cast was formed over the residual limb with the subject wearing the gel liner used with their normal prosthesis. A waist belt (for transtibial applications) or shoulder strap (for transfemoral applications) was attached to secure the plaster cast and to simulate minimal loading the limb during the scan. A trans-tibial subject is shown wearing the cast in Figures 1 & 2.

Figure 2: Lateral view of Subject TT1 in the non-deformational shell

Figure 1: Anterior view of Subject TT1 in non-deformational shell

Fabrication of the non-deformational shell

A description of the fabrication process for a transfemoral non-deformational shell follows in Table 1. The process for fabrication of a transtibial shell is identical with the exception of utilizing a waist belt instead of a shoulder strap. The waist belt consists of an adjustable belt utilizing polypropylene buckles and a 2" elastic suspension strap which descends to the anchor strap. The descending elastic strap also has Velcro® to allow for a secure attachment.

		
Step 1: A liner is selected for the subject based upon their current system or the type of liner anticipated to be utilized during the subjects' fitting and walking trials.	Step 2: The liner is protected with a plastic parting agent. The plastic is wrapped around the waist in order to provide anchorage of the wrap and to protect clothing.	Step 3: Plaster bandage is applied distally to proximal. In this example, the Ossur X5 Seal-In Liner™ is being utilized. Care is being paid to identify these rings in the shell.
		
Step 4: Plaster bandage continues to be applied proximally.	Step 5: Once all the plaster is applied, the ischial tuberosity is palpated so that it can be identified in the shell. Lateral View.	Step 6: Once all the plaster is applied, the ischial tuberosity is palpated so that it can be identified in the shell. Posterior View.

		
Step 7: The shell is removed from the subject. Marks must be placed on the shell to include their ID number, date and a reference line for directly anterior which will be used for the belt installation. Superior View.	Step 8: The suspension component consists of a 1' anchor strap with a buckle and a 5' – 6' long shoulder strap with hook and loop Velcro® to allow for secure fastening. With the shell on its posterior side, the shoulder strap is wrapped into the shell. Anterior View.	Step 9: On the posterior side, the anchor strap is wrapped into the shell. A custom polypropylene buckle was fabricated to allow for MRI compatibility and strap adjustability.
		
Step 10: The completed non-deformational shell.	The buckle measures 2 ¾" wide and 3" high. It has two ¼" x 2 ¼" slits cut into it to accommodate the 2" webbing.	

Table 1: Fabrication of the non-deformational shell

The shell was designed to prevent RL distortion while lying on the gantry of an MRI scanner. In the event a stand-up MRI scanner is utilized, this process will need to be tested in order to determine the necessity of the shell or if modifications or refinements are needed.

MRI Scanning

Residual Limb Scanning Background

Various modalities of medical imaging have been used to derive anatomical models of a lower extremity amputee's residual limb. Volumetric imaging modalities such as Computed Tomography (CT), Magnetic Resonance Imaging (MRI), or ultrasound, allow for the generation of a patient specific three dimensional (3-D) digital models of limb anatomy. These models capture a snapshot of both the residual limb shape and the structure of the underlying tissues. This information about residual limb specific anatomy, such as bone structure or fat/muscle distribution, facilitates improved custom prosthetic limb socket design using CAD/CAM tools and FEA simulation[1].

A number of previous studies have employed X-ray CT scans of the residual limb to obtain models of the limb shape and underlying bone structure. Smith and Vannier performed CT scans on a sectioned human cadaver leg to assess the viability of patient specific modeling of limbs[6]. Zachariah, Sanders, and Turkiyyah assessed the feasibility of CT based patient specific limb modeling using existing CT datasets (from previously scanned amputees) to avoid exposing human subjects to ionizing radiation[7]. Shuxian, Wahhua, and Bingheng utilized CT scans of volunteer subjects to develop 3-D digital models of the residual limb shape and underlying bony structure. In the latter study, the resulting digital model was limited to bony structure contained within undifferentiated soft tissue[8]. Peery, et al, generated a CT based model of a trans-tibial residual limb in a prosthetic socket and attempted to differentiate soft tissue structures[9]. The resulting soft tissue structures were as greatly simplified, to nearly cylindrical, concentric, layers of muscle, fat and skin encompassing the bone. Although CT scans generally produce adequate image quality for simplified limb modeling, one major drawback is the radiation hazard from X-rays. Because of this hazard, the patient generally cannot (or should not) be rescanned if the CT images do not possess adequate soft tissue differentiation for more detailed modeling.

Ultrasound and MRI offer the possibility to obtain models with improved differentiation of soft tissues while not exposing the subject to ionizing radiation. Douglas et al, demonstrated a custom ultrasound scanning device for residual limbs as

an inexpensive scanning option [10]; however, this custom equipment is not universally available. MRI is a commonly available, albeit expensive, imaging modality offering similar benefits. MRI has been successfully employed to generate detailed models of residual limb anatomy in several previous studies [4, 5, 11] and is known to produce excellent soft tissue differentiation.

MRI is a volumetric imaging modality based on excitation of hydrogen nuclei in water bearing tissues to a high energy state using a strong magnetic field. When the magnetic field oscillates, the nuclei alternate between high and low energy states, emitting radio waves in the process. These radio emissions are received by the scanner and spatially reconstructed into an image of the internal tissue structures. Planar images are reconstructed at regular intervals, from slices of within a volume encompassing the anatomy. Signal intensity detected at a point in space is encoded as a grayscale value, ranging from black for an absence of signal to white for the most intense return.

Each pixel records the detected radio emission at the corresponding point in the scan volume. Tissue at any spatial location can be differentiated by the encoded grayscale intensity. However, unlike CT images, the tissue types cannot be readily calibrated to specific grayscale values in the image sets. Different excitation profiles and different methods of image reconstruction result in different grayscale intensities for a tissue types. Furthermore, the grayscale intensity of a tissue type can change with location in the scan volume. Local contrast in gray values denotes a difference in tissue type.

The full set of image slices comprises a tomographic dataset of the scanned volume. This is a discrete approximation of a 3-D volume, consisting of a stack of slice images constructed in the axial, sagittal or coronal planes of the anatomy. This tomographic dataset is typically stored as a stack of digital images in the DICOM 3.0 format. A 3-D model is generated from the image set by interpolating surfaces through selected pixels in adjacent image slices. An example 3-D reconstruction is shown against the typical image planes in Figure 3.

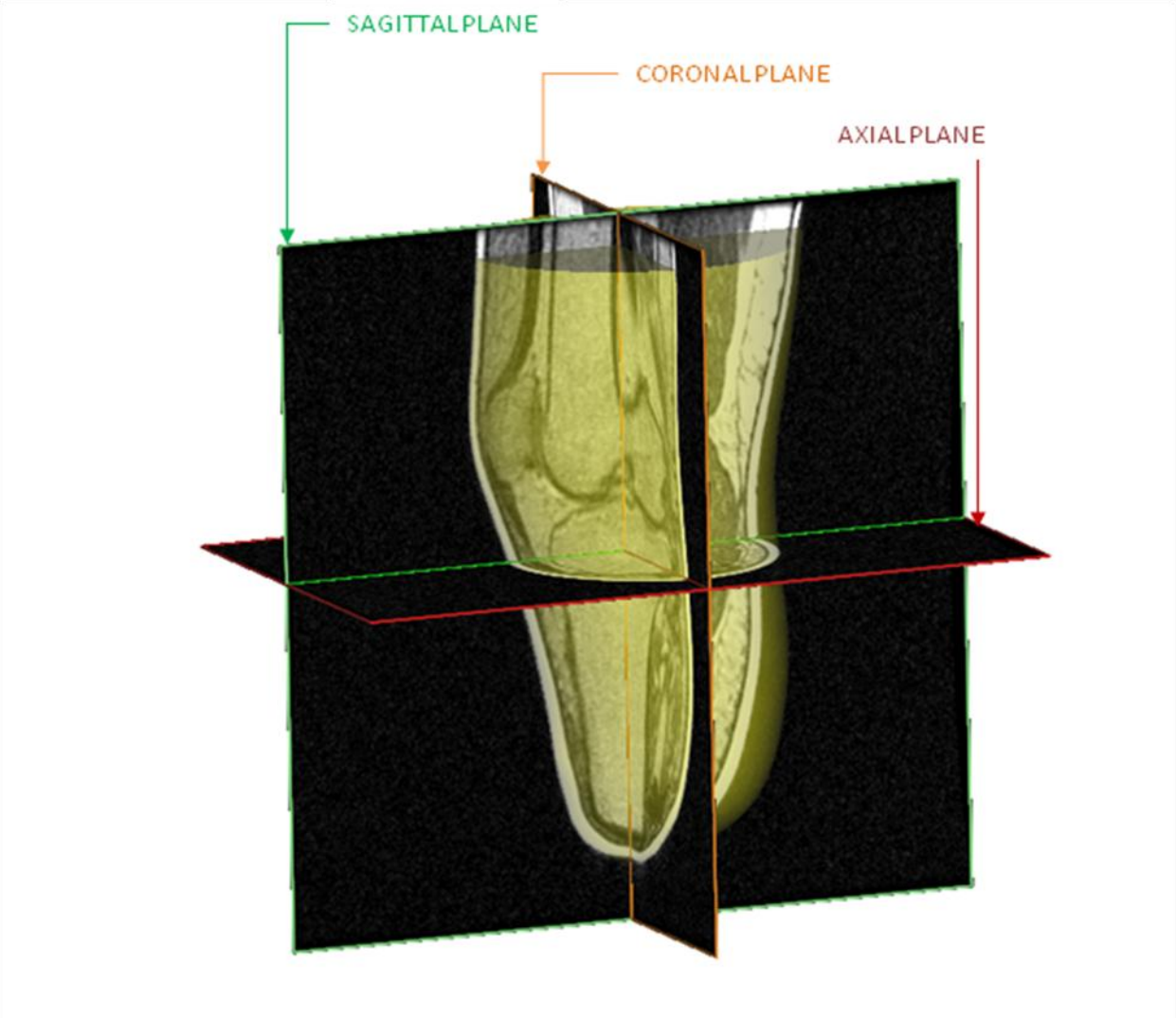

Figure 3: Orientation of planes with representative scan for TT01

Overview of Scan Series

A research protocol involving MRI imaging of multiple trans-tibial and trans-femoral residual limbs on volunteer subjects was approved by the Gerogia Tech and Emory University Institutional Review Boards (IRB). Residual limbs of six adult patient subjects were scanned by MRI. Three patient subjects were scanned for each class of lower extremity amputation, trans-tibial (below knee) and trans-femoral (above knee). Each scan provided a tomographic image set of limb shape and internal anatomy, from which the limb was reconstructed in 3-D.

Patient positioning and MRI imaging parameters were optimized during the sequence of patient scans, resulting in the recommended procedure in the subsequent

sections. Each class of amputee required a different set of scan parameters to obtain an image set suitable for modeling. Two scanning sessions were required to obtain suitable images of the first patient subject in each class. A series of scans were conducted with different coils, fields of view, and reconstruction parameters to find the optimal imaging parameters. Scans with subsequent patient subjects bracketed these parameters values to find an optimal image. All MRI scans were conducted at Emory Healthcare facilities under the direction of Dr. Michel Terk, Department of Musculoskeletal Radiology, Emory University School of Medicine.

MRI scans were conducted on GE Signa HDx 1.5T and Signa HDxt 3.0T scanners. Pilot scans of the first patient subject (TT-01) were conducted on a GE Signa HDx 1.5T scanner; these were deemed to have insufficient contrast for modeling purposes. All subsequent scans were performed on GE Signa HDxt 3.0T scanner proved, and proved suitable for modeling. Scans of all six patient subjects were scheduled and conducted on the GE Signa HDxt 3.0T scanner.

Figure 4: GE Sigma HDxt 3.0T scanner

Trans-tibial Scanning Protocol

Two sessions of pilot scans were performed with first amputee subject (TT-01) to explore various MRI scanning options. The objective was to determine the approach which would yield the best image contrast and resolution. For all scans, the subject was

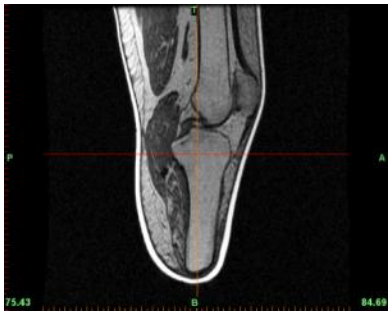

SAGITTAL PLANE SLICE (VIEWED FROM LEFT)

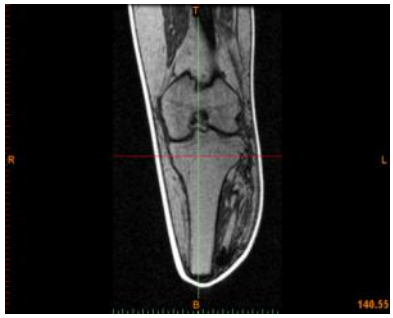

CORONAL PLANE SLICE (VIEWED FROM FRONT)

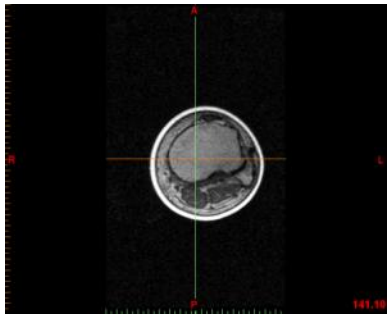

AXIAL PLANE SLICE (VIEWED FROM BOTTOM)

Figure 5: Sagittal, Coronal and Axial view of Subject TT01

supine on the gantry, with no gantry tilt, with the residual limb extended. The gel liner and plaster non-deformation cast were worn on the residual limb. The patient was instructed to remain still, while pressing the residual limb into the containment cast to contact the distal end of the limb to the cast thought the duration of the scan. Imaging slice distance, overlap and reconstruction resolution were varied to find the combination producing the best image quality. Generally, the longer scan times generated better image quality. High resolution scans with excellent contrast were obtained using scanning protocols requiring in excess of 10 minutes; however, during these long scans patient motion generated in mechanical shift artifacts rendering the scans useless. The final scanning protocol was developed as a compromise between image quality (resolution and contrast) and scan time. Reduction of scan time was sought in an effort to mitigate mechanical shift artifacts. Scan acquisition in the sagittal plane, as opposed to the axial plane, significantly reduced scan time significantly by reducing the number of image slices necessary to capture the extents of the residual limb. Albeit lower resolution, this approach still provided adequate image quality for detailed reconstruction of the internal tissue structures of the residual limb.

In the final protocol, the anterior to posterior extents of the scan were, nonetheless, affected by chemical shift, or a change in the MRI return values for a given tissue. Examples of MRI image artifacts encountered in the pilot scan sessions include mechanical shift artifact and chemical shift artifact.

A *Mechanical Shift Artifact* results from patient motion during the scan. The artifact is manifest as a serrated edge along the limb. This is due to patient motion combined with interleaved slice acquisition. This type of artifact was minimized by restraining the patients' residual limb and minimizing scan time. See Figure 6.

A *Chemical Shift Artifact* is a change in the grayscale value of a tissue type depending on spatial position in the scan. This is evident at the extreme ends of the scan value, due to loss of signal at the edges of the coil; significant differences in the grayscale value of bone marrow in the tibia and fibula are noted, as well as a general loss of return at the top of the scan. This type of artifact is minimized by increasing the field of view. See Figure 7.

Figure 6: Mechanical Shift Artifact in TT subject

Figure 7: Chemical Shift Artifact in TT Subject

The final trans-tibial residual limb scan protocol employed a GE Medical Systems Signa HDxt 3.0 Tesla MRI at the Emory Orthopedics and Spine Center facility in Atlanta, GA. The scanning protocol captured the extent of the residual limb, from >10 cm above the femoral epicondyles, to beyond the distal end of the limb. The scan was conducted in the sagittal plane with a 28.0 -30.0 cm field of view, and 1.6 mm slice thickness, and no overlap. Images were reconstructed with 3-D inversion, fast spoiled gradient pulse sequence (FSPGR), with a 256 x 256 matrix. The scan was exported as a DICOM 3.0 image set.

An example slice image from the data set of each trans-tibial subject is shown in the following table. Different soft tissue can be clearly differentiated; fat is denoted by a bright return, muscle denoted by a medium gray return. Cortical bone and tendons provide little to no return, thus appear black in the image. Outlines of the cortical bone are contrasted buy the bright return of the bone marrow contained within the cortical bone outline. The gel liner is easily differentiated from the skin, having a bright return like fat, while the skin return is similar to muscle. A chemical shift artifact can be noted brightening at the extreme anterior or posterior of the limb. The plaster non-deformation shell cannot be detected in the scan.

	**Subject TT-01** Imaging Mode: 3D Pulse Sequence: 3D FSPGR Imaging Plane: Sagittal Acquisition Matrix: 256 freq, 256 phase Body Coil 28 cm Field of View 1.6mm slice thickness 0.547 mm pixel pitch
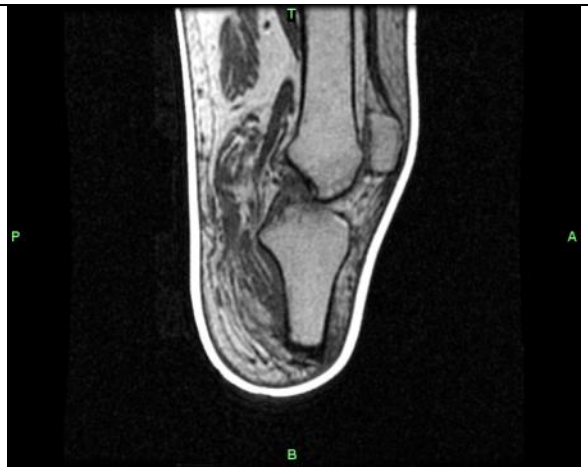	**Subject TT-01** Imaging Mode: 3D Pulse Sequence: 3D FSPGR Imaging Plane: Sagittal Acquisition Matrix: 256 freq, 256 phase Body Coil 28 cm Field of View 1.6mm slice thickness 0.547 mm pixel pitch
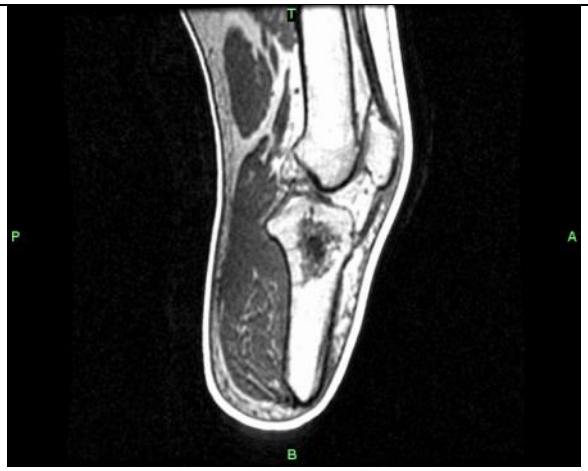	**Subject TT-03** Imaging Mode: 3D Pulse Sequence: 3D FSPGR Imaging Plane: Sagittal Acquisition Matrix: 256 freq, 256 phase Body Coil 30 cm Field of View 1.6mm slice thickness 0.586 mm pixel pitch

Table 2: Examples of MRI scans of the Transtibial Subjects

Trans-femoral Scanning Protocol

Two scanning sessions were conducted with the first trans-femoral subject (TF-01) to determine a scanning protocol which would provide suitable image quality. In the first scanning session the patient was positioned both supine and on the side of the intact limb. The first set of images was affected by wrap artifacts, appearing as a reflection of adjacent anatomy into the field of view. An example of the wrap artifact is shown in Figure 8. The wrap artifact was addressed by modifying patient position and increasing field of view. All three trans-femoral subject scans proved to be unique cases. Ultimately, a different scanning approach was employed for each trans-femoral subject however the position that was preferred was side lying on the unaffected side. The objective in each scanning session was to capture the full volume of the limb with good contrast to noise ratio, while minimizing artifacts.

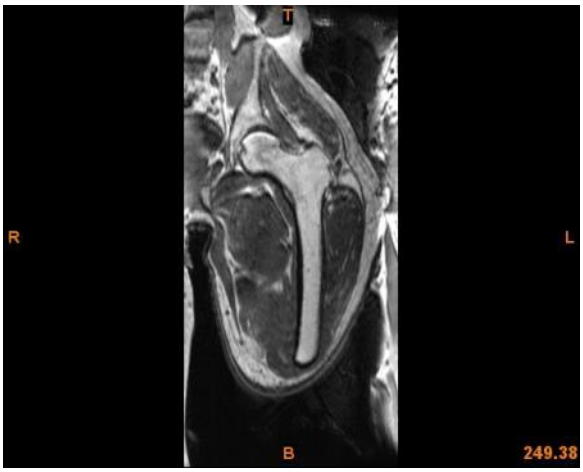

Figure 8: Example of a wrap artifact on a transfemoral subject scan

Chemical shift artifacts can be noted in the example images from the selected studies subjects TF-01 and TF-02 (See Table 3). The chemical shift presents a significant challenge in differentiating and segmenting tissues. Of note for both of these cases is the fact that they have very long residual limbs.

Figure 9: Example of TF01 Subject lying on his unaffected side with his legs strapped to assist with keeping them still

Figure 10: Example of TF01 subject lying on affected side for scan. This produced a wrap artifact.

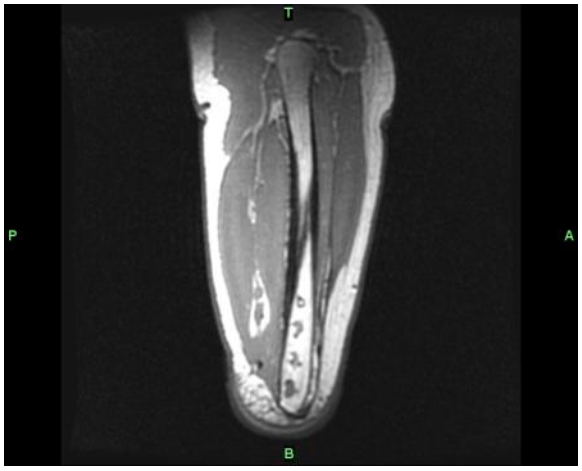

Subject TF-01

Imaging Mode: 2D, T1
Pulse Sequence: FSE-XL
Imaging Plane: Sagittal
Acquisition Matrix: 192 freq, 192 phase

Body Coil
48 cm Field of View

2 mm slice thickness, 0.5 mm spacing
0.938 mm pixel pitch

Subject TF-02

Imaging Mode: 3D
Pulse Sequence: FSPGR
Imaging Plane: Sagittal
Acquisition Matrix: 192 freq, 192 phase

Body Coil
42 cm Field of View

1.8 mm slice thickness
0.820 mm pixel pitch

Table 3: Representative scans of the TF 01 and TF 02 subjects

The IDEAL MRI Algorithm

An optimal protocol may have been found when scanning the last trans-femoral subject (TF-03), the GE IDEAL algorithm. IDEAL is an MRI algorithm released in 2007 for use on the General Electric Signa HDxt3.0T MRI scanner. This algorithm provides four image sets from a single acquisition; these image sets provide multiple contrasts: fat-only, water-only and combined fat/water in-phase and out-of-phase images. Furthermore, this imaging algorithm is less susceptible to chemical shift artifacts. This image set proved ideal for modeling purposes. Images from Subject TF03 using the IDEAL algorithm are found in Table 4. Chemical shift artifacts are not evident in the image sets generated using the IDEAL algorithm.

Subject TF-03

Imaging Mode: 3D
Pulse Sequence: SPGR
Imaging Plane: Coronal
Acquisition Matrix: 320 freq, 192 phase

Body Coil
48 cm Field of View
4.0 mm slice thickness

TT-03 Image A: Fat Only

TT-03 Image B: Water Only

TT-03 Image C: Fat/Water In Phase

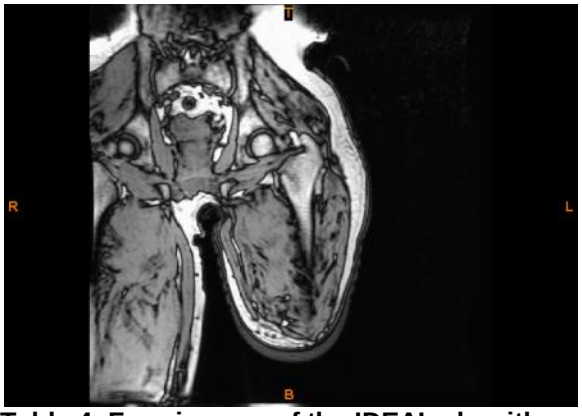

TT-03 Image D: Fat/Water Out-of Phase

Table 4: Four images of the IDEAL algorithm which was used to scan subject TF03

Segmentation & Modeling

Patient specific three dimensional digital models of residual limb anatomy were reconstructed from the DICOM datasets using Materialise MIMICS. MIMICS is a medical image viewing, manipulation package, and model reconstruction software application for Windows based workstations. Over the duration of the project several versions of MIMICS were employed, starting with V12.1 and ending with Version 14.0. The MIMICS graphic user interface is depicted in the following figure, showing the modeling of a residual limb gel liner from an MRI data set.

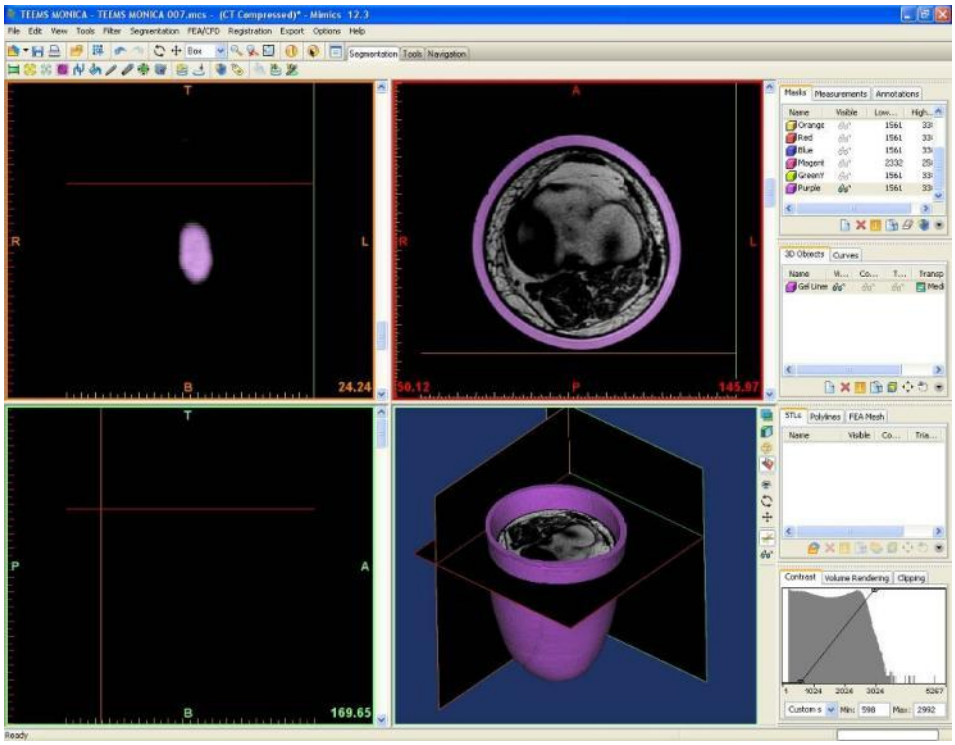

Figure 11: MIMICs user interface showing a TT residual limb

Using one or more specialized utilities in MIMICS, the medical image data is segmented into subsets, or masks, encompassing a tissue structure of interest. Each mask is a selected subset of voxels, or slice image pixels thickened to the distance between slices. With the mask defined, MIMICS interpolates surfaces between outer contours of the voxels. Surfaces are interpolated using an implementation of the Marching Cubes Algorithm [12]. In this implementation of the algorithm, local gray value is used to weight the interpolation between the slices to account for partial volume effects in voxels along the boundaries of tissue structure. A triangular patch is

generated which locally approximates the true surface contour. An entire surface of triangles encompasses a volume, defining a three dimensional model of the anatomy segmented in the mask.

The quality and resolution of the image data influence the final accuracy of the derived model. Independent assessments of MIMICS accuracy modeling anatomical structures appears in published literature. For example, Jamali, et al [13], investigated the accuracy MIMICS computer model reproduction of a pelvis by comparison of physical measurements of anatomical landmarks on a standard to software based measurements on the MIMICS model; measurements on the computer model deviated from the standard by a mean of 1.5 mm. Gelaude, VanderSloten and Lauwers concluded that 3-D model of a human femur generated by MIMICS deviates by half the maximum voxel dimension, or the defining resolution of the medical image set [14].

The volumetric model generated by MIMICS is structurally equivalent to the STL model universal STL 3-D model format. The STL model is an efficient format to represent complex three dimensional forms. Furthermore the STL model is defined, explicitly, in three dimensional space; thus, the geometric relationship of anatomical STL models, generated from the same medical image set, is inherently defined and maintained. MIMICS provides several utilities to refine and optimize the 3-D model for simulation and manufacturing purposes. Furthermore, starting with MIMCS V14.0, a direct link is provided to the Materialise 3matic STL manipulation application. Within 3matic, the STL models can be used as the basis for computer aided design or prepared for Finite Element simulation.

The following section outlines the modeling of a residual limb from MRI images using MIMICS. The section is broken into five distinct tasks. The first task is **Mask Segmentation based on Gray values** and it is detailed in Table 5. The second task is to **Create a 3-D model from the Mask.** This task is detailed in Table 6. The third task related to segmentation and modeling the residual limb is to **Create STL Models for Export** the details for which are found in Table 7. The fourth task is **Modeling Internal Anatomy** (Table 8) and finally **Assembly of the Residual Limb** (Table 9).

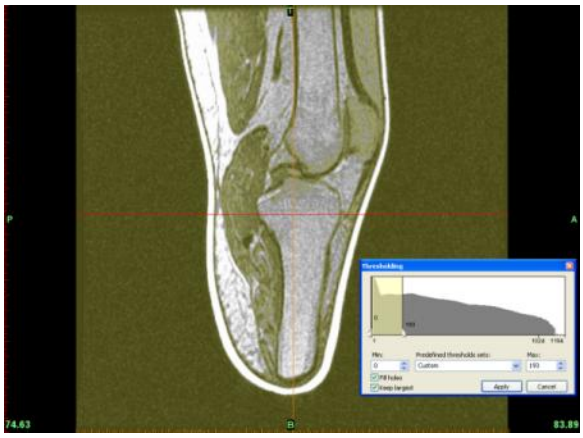

Step 1: Pixels in a slice image are segmented into subsets using the "Segementation" tool in MIMICS. The mask encompasses all pixels of a selected gray value range in the dataset, selected pixels are shown in yellow. Successful modeling requires sufficient contrast to isolate the tissue of interest.

In the case of MRI images created by an SPRG algorithm, air, cortical bone, muscle and tendons will generally be captured in the lower gray value range, as shown in the figure to the left.

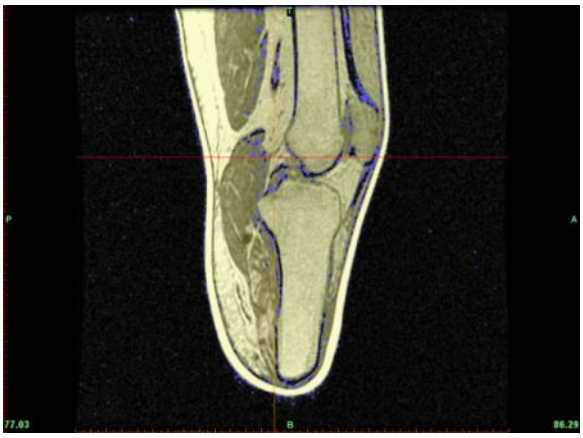

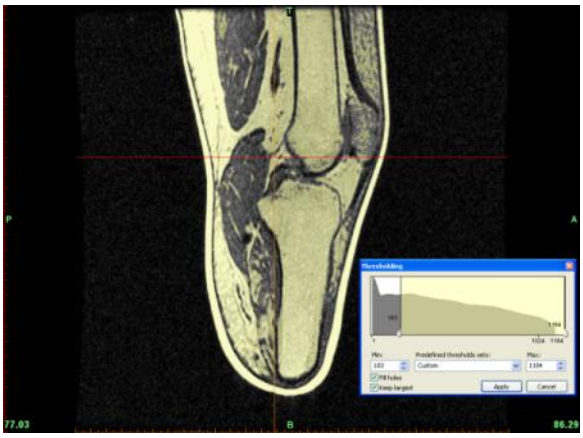

Step 2: Higher gray values typically capture issues with greater lipid content, such as fat or bone marrow; as shown in the figure to the left. The subject's mineral gel liner comprises the highest return values, seen as the bright ribbon around the limb.
In most scans the gray values for a given tissue type or anatomical structure are not consistent across the entire image slice. As shift in the intensity of gray values in the fat can be seen where the posterior values are aft structures lighter than the anterior. Likewise, a general loss of contrast from muscle to bone is noted.

Step 3: This example will produce a model of the entire limb volume, which will serve as the limb shape for socket design. The MIMICS "Segmentation" tool is used to select a gray value range that captures the majority of the pixels comprising the leg, while excluding noise in the airspace. The blue pixels highlight that external noise can be picked up if the gray value range is set too low in an attempt to capture tendons and bone within the limb. The proper gray value range is a judgment call for the modeler. This mask is segmented globally from the entire image set. If necessary, overall image contrast to noise ratio can be improved by applying digital image filters from the "Filter" menu in MIMICS.

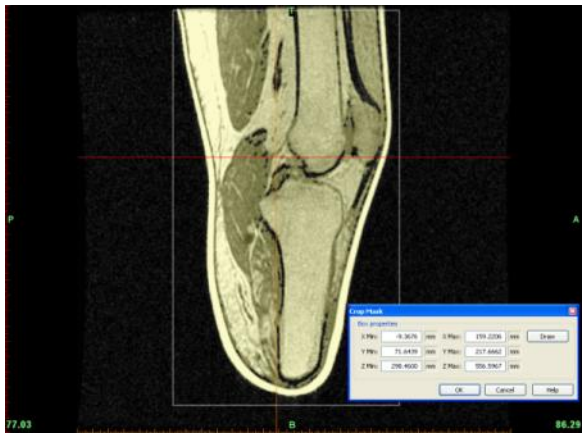

Step 4: A basic approach to eliminating noise or unwanted tissue structures in the mask (pixel subset) is to limit the region of the mask in the image dataset using the "Crop Mask" tool in MIMICS. The range of interest can be limited to a three dimensional region defined by a bounding box. The bounding box is adjustable in all three slice views (coronal, sagittal, and axial). Once set, the mask will be limited to the defined region; however, the global segmentation range cannot be modified. The mask is now named and saved.

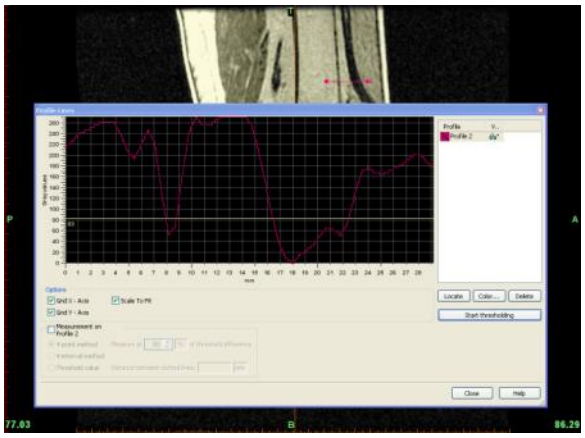

Step 5: The saved mask can be filtered in a number of ways to insure that the pixel subset encompasses only the tissues of interest. First, using the "Region Growing" tool, the mask can be further filtered to only the pixels connected to a region of interest. This can be done in a single slice, or globally across all slices, where connection of adjacent pixels can be detected.

Measurements of distances and grayscale variations in an image are useful in deciding how two further filter the mask. The image to the left is a measurement of grayscales and distance across a gap in the mask.

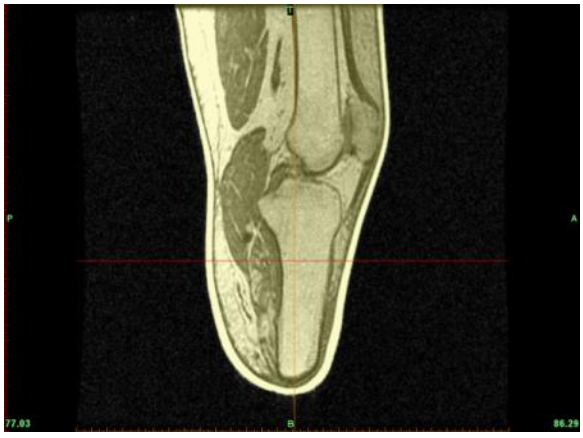

Step 6: Filters which can be applied to the mask set include:

- Morphology filters based on digital 3-D topography
- Region growing combined with image morphology
- Localized gray value segmentation
- Manual pixel editing on the slice level

Gaps in the mask, shown to the left, were eliminated using the "Close" morphology operation. The filter first dilates the mask subset by adding pixels to the edges in each slice, then only retains the added pixels which touch each other along multiple edges. The effect of this filter is to close three dimensional gaps in the mask, without changing the overall shape.

Table 5: Mask Segmentation based on Gray values

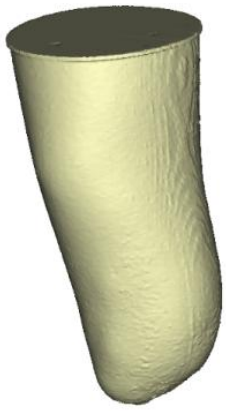

Step 1: A three dimensional surface model can be generated from any mask (pixel subset) spanning two or more contiguous image slices. The surface is computed in MIMICS using the "Calculate 3D" tool. This tool interpolates between the contours of the mask in each image slice using the Marching Cubes Algorithm[##]. The result is a tessellated 3-D model, using many triangular surface panels to approximate the shape. The image to the left is a rendering of the limb external shape from the mask set in the previous section. Some defects related to the interpolation algorithm are evident as bumps and scalloping on the surface.

Step 2: Quality of the 3-D model and accuracy to the contours of the medical image slices can be assessed by displaying the 3-D surface contours over the original images. Yellow surface contours in the figure to the left show an internal void and some slight deviation of the 3-D surface from the limb shape. These problems can be addressed either by editing the mask and re-computing the 3-D surfaces or refining the 3-D surface using the "Wrap" or "Smoothing" tools.

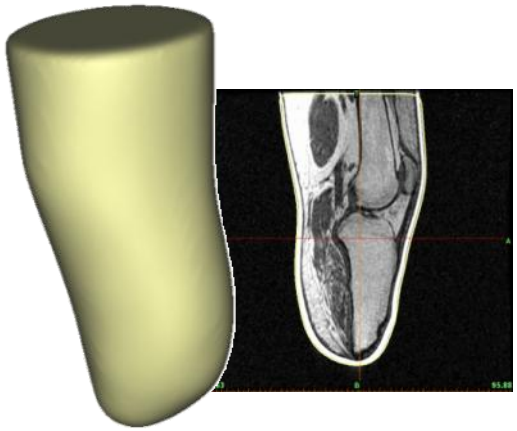

Step 3: The "Wrap" tool smoothes and closes surface gaps in the 3-D model, but at the same time reducing detail and dilating the model. The "Smoothing" tool acts similar to a noise filter, averaging away small asperities in the surface. Smoothing generally gives in a more accurate and realistic surface contour, but may lead to a minor volumetric shrinkage of the model or hole.

As shown in the figure to the left, the rough surface of the original 3-D model of the limb was eliminated using a combination "Wrap" set to a smallest detail level of 2mm. This was followed by "Smoothing" (2nd Order Laplacian, factor = 0.9, 10 iterations) until the surface contours closely match the limb outline in the slice images.

Table 6: Create a 3-D model from the Mask

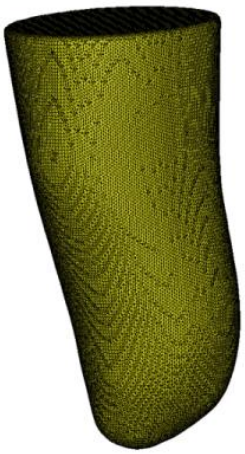

Step 1: The end product of the modeling procedure is generation of an STL digital model for use in simulation, socket design, and automated manufacture. The 3-D model produced by MIMICS is in the tessellated structure of an STL model, and need only be exported in the explicit STL file format. However, the triangulated structure of this model is generally not suitable for use in simulation without additional processing. A typical STL triangle surface structure of a MIMICS model is shown in the figure to the left, this is the smoothed and wrapped model of the limb with the triangulated structure displayed. The surface structure still retains artifacts of the noise present before the smoothing operations, and is comprised of thousands of triangles.

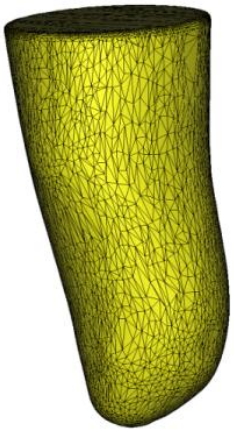

Step 2: The triangulated surface approximation can be optimized using the “Triangle Reduction” and “Remesh” tools in MIMICS. In the Figure to the left, “Triangle Reduction” was applied using the advancing edge algorithm. Ten iterations were run at a tolerance of 0.1mm and edge angle of 2. The new triangle structure is nearly free of all scalloping from previous surface artifacts. Furthermore, the number of triangles was reduced by an order of magnitude, while maintaining a surface fidelity to within 1/5 of the minimum pixel dimension. However, the surface is comprised of a number of narrow, high aspect ratio triangles, which are not suitable for simulation.

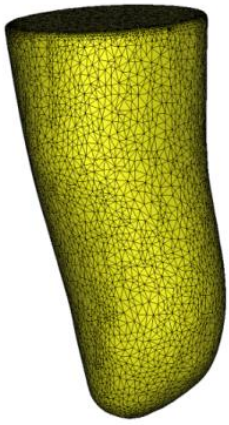

Step 3: As a final step, a re-meshing of the surface is performed, using the “Remesh” tool; this utility is launched in 3matic directly by MIMICS. The “Remesh” utility optimizes the triangulated surface, eliminating the high aspect ratio triangles, while maintaining a specified tolerance to the original surface. The optimized triangle mesh is shown in the figure to the left. This optimized version of the limb was exported in binary STL format using the “STL+” utility in MIMICS. This version is of the limb shape is suitable for use in socket design and for to support detailed modeling of the of the limb’s internal anatomy.

Table 7: Create STL Models for Export

Modeling the internal tissue structure of the limb follows the same general procedure as outlined for obtaining an STL model of the limb shape. The major difference is that more sophisticated mask segmentation techniques are often required to obtain an accurate model. Most tissue structures are composed of several distinct ranges of gray values, which are not easily distinguished from adjacent tissues, especially in cases of low image contrast or contrast to noise ratio. More sophisticated segmentation approaches are required to generate these models. The following is a general outline of a modeling approach; however, in practice each model required some unique steps based on the experience of the modeling engineer.

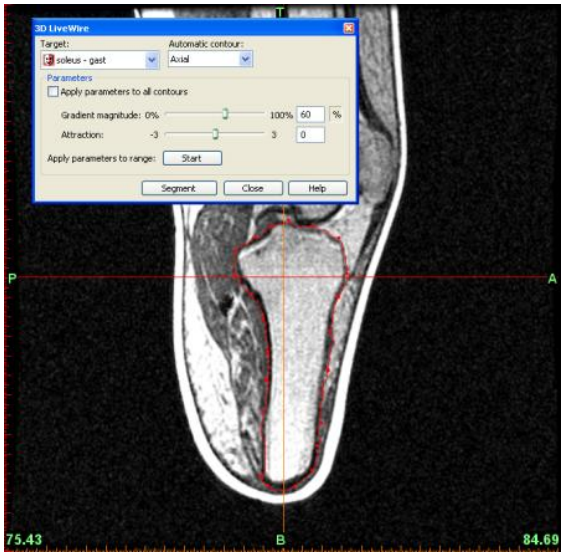

Step 1: Boundaries of internal anatomical structures were often defined by the gradient in grayscale values from adjacent anatomy, as opposed to a narrowly defined band of grayscale values. Often it was not possible to define a mask by conventional segmentation. However, the mask could be defined in a number of other ways. A powerful approach, introduced in MIMICS 13.0, is the ***"Live Wire"*** tool. This tool provides semi automatic detection of contours based on gradient in grayscale values. A contour is formed around the region of interest by tracing the contour and adding anchor points as shown above. Contours are traced in a number of slices on two orthogonal planes, and a guiding wireframe is automatically computed.

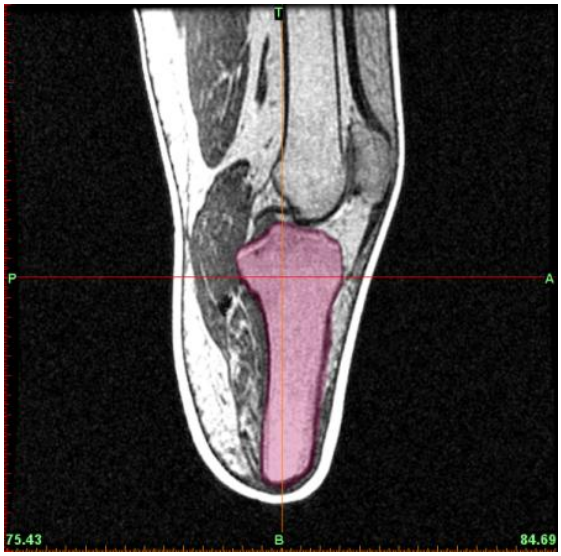

Step 2: The resulting mask spans all of the slices contained between the boundaries of the wireframe. Manual editing of the mask is necessary to capture any areas that are excluded, or erroneously included in mask region.

The resulting mask is depicted in the single sagittal slice image to the left, the pink highlighted pixels show the mask selection. Here the masked pixels cover a wide range of gray values, from nearly 0 in the cortical bone of the tibia, to over 300 in the marrow. Gray values in adjacent muscles and fat overlap these values, precluding a simple segmentation.

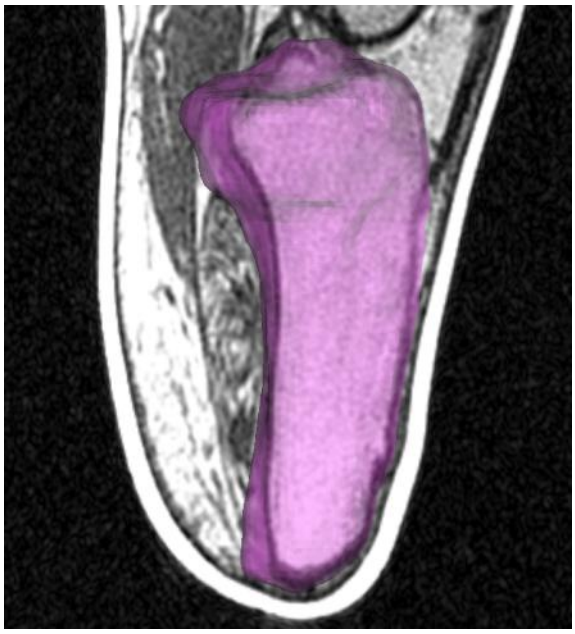

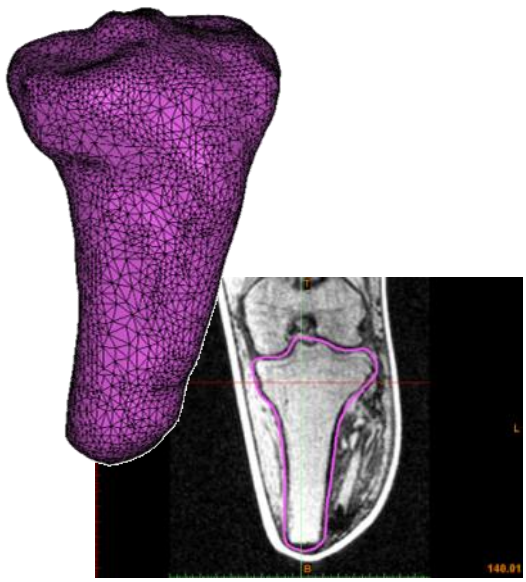

Step 3: A 3-D model is computed from the mask following the sme procedure outlined in the previouos example. The 3-D model is superimposed on the sagittal slice image in the figure to the left using the “Toggle Reference Planes” viewing mode and solid transparency. It is often useful to use this visualization mode as a quality control check to insure that all of the anatomy has been captured in the 3-D model. In addition, the contours of the 3-D model can be compared to the slice images, as decribed in the case of the external limb model.

The “Optimal” setting is recommended for intial generation of a 3-D model from the mask. Smoothing and wrapping can be applied as a secondary step. If the contrours do not match the slice images, a custom 3-D interoplation can be generated. In the latter case it is recommended to switch the interpolation algorithm to “Contour” before adjusting any other settings.

Step 4: The resulting 3-D model must be wrapped and/or smoothed as previously described for the limb. These procedures must be followed by a triangle reduction and remeshing, as necessary to obtain a suitable surface. In general, the surface should be comprised of primarily equilateral or near equilateral triangles, with the minimum density required to maintain a maximum tolerance of 20% of the smallest pixel dimension. In the example case, the smallest pixel dimension in the image set was 0.57mm; therefore, a tolerance of 0.11 mm, or better, is desired for the 3-D surface. As a final quality control check the contours of the 3-D model should be compared to the original slice images.

Table 8: Modeling Internal Anatomy

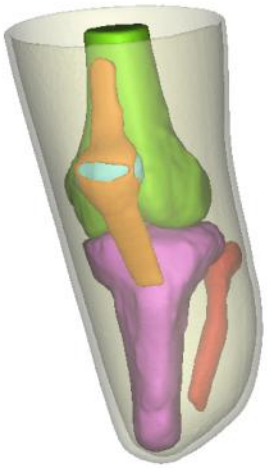

Step 1: Modeling of the residual limb generally proceeds are follows:

- STL Models of the bones and major ligaments are produced using the procedures previously outlined.
- An STL model of the subjects' gel liner (if present) is generated.

These are generally the least complex geometry and easiest structures to segment and model from the MRI dataset.

Table 9: Assembly of the Residual Limb

Step 2: Next, models of the muscles are generated by advanced mask segmentation techniques, including:

- Live Wire
- Morphology Region Growing
- Local Thresholding
- Manual mask editing

3-D models are created from the masks. The 3-D model surfaces are generally crude and require extensive application of Wrap and Smoothing before export as an STL. The STL models of the muscles are matched to the bone models by a Boolean subtraction of the bone model from the muscle models, eliminating overlapping regions.

Step 3: The skin and fat are generally the most complicated geometry to extract. As opposed to the normal segmentation, this model is obtained by Boolean subtraction of the other STL models from the original STL model of the entire limb. The result of the described Boolean subtraction is shown in the figure to the left.

The resulting geometry is often quite complicated and contains geometric features unsuitable for FEA simulation. Further manipulation is thus required before generating the FEA mesh. The details are provided in the section on FEA simulation.

CAD Socket Design

The anatomical model of the residual limb and gel liner, generated in MIMICS, is used as the basis for design of prosthetic socket variants. STL models of the tissue structures and the gel liner are exported from MIMICS, retaining spatial relationship. Design of prosthetic limb socket is performed using the modeled internal anatomy for guidance. Multiple variants of the prosthetic socket design can be generated in the digital CAD environment. These designs can then be evaluated by FEA simulation or, if deemed a satisfactory, used to manufacture of a socket mold pattern.

A starting surface shape definition of the residual limb is extracted from the gel liner STL model, as described in the previous section, this starting shape model is analogous to the plaster casting of the limb made by the prosthetist in traditional fitting procedures. Modifications, or *rectifications,* are made to the starting shape in software. Two CAD approaches were explored:

- Direct manipulation of the limb shape STL in 3matic
- Export of a the limb shape STL to a standard prosthetics design application

Using 3matic allowed for direct manipulation of the external limb shape STL, referencing the internal anatomy as a guide to perform rectifications. This approach, while ideal for modifications proved extremely difficult to implement due to limitations in the software to allow for the modifications to be completed, thus an alternative approach was pursued using CANFIT (Vorum Research Company, Vancouver, Canada) prosthetics software. The major drawback to using CANFIT was the inability to import more than one STL model into CANFIT, making it impossible to directly reference the internal anatomy.

A work around solution was developed to solve this problem by applying anatomical landmarks on the limb surface shape with small indentations (using 3matic) which related to the underlying anatomy of interest. Thus the marked STL file could be exported for manipulation to CANFIT software with the relevant anatomy identified and the orientation maintained. Once the file was rectified in CANFIT, it would then be converted into an STL for export. An outline of each approach is provided in the following sections.

Socket Design using 3matic

A Patella Tendon Bearing Below-Knee Prosthesis, or PTB, socket design was generated for subject TT-01 using solely using 3matic. The rectifications are applied to the external shape of the limb, generating the inner surface shape of the PTB socket. The typical PTB design and rectifications are detailed in a classic reference report by Radcliffe and Foort [15]; these include reliefs and protrusions necessary to suspend the socket on the residual limb, or to relive pressure points in sensitive areas on the limb.

To obtain the starting shape for the socket, the outer surface of the gel liner STL model is copied to a new part. Next, the part is smoothed and refined to eliminate surface imperfections, using smoothing and remeshing tools in 3-matic. Finally, the triangle density of the surface increased to facilitate surface morphing operations. Shape modifications, or rectifications, are applied to this prepared model of the limb shape.

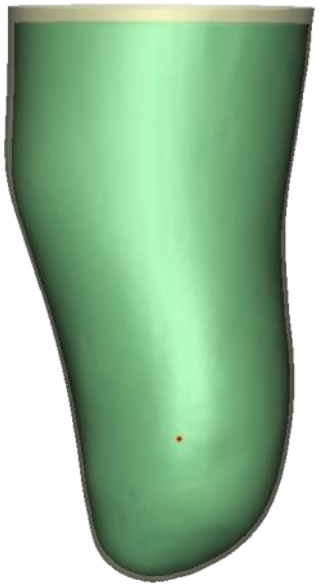

Step 1: The first morphing operation is a *ply reduction*, or volumetric reduction of the starting limb shape. To perform this operation, a suitable center point for a uniform scaling operation is necessary. A centerline spline through the residual limb shape is generated and 3-D points are placed along the centerline spline. Trial ply reductions are performed using these points as center points for uniform scaling, until a nearly uniform offset of the original surface was obtained, as shown in the figure to the left. Typical ply reductions are on the order of 10% of the original limb volume, and are necessary for comfortable fit and proper walking gait.

In the model to the left, the original is shown in tan, the modified model in green.

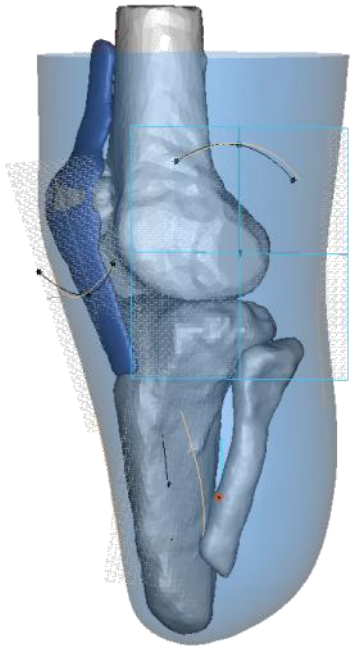

Step 2: The hard tissue anatomy of the residual limb and the patella tendon STL models are imported in the original spatial relationship to the gel liner model. These structures are visualized under the underlying reduced surface shape using the transparency renderings in 3-matic. Next, sketch planes are positioned on the anatomical structures at the locations normally identified by palpitation of the patient; the origin of each plane is positioned at the exact anatomical landmark location, parallel to the local surface. Rectification guide markings, as outlined in Radcliffe and Foort [15] are drawn on these planes, as shown in the accompanying figure above.

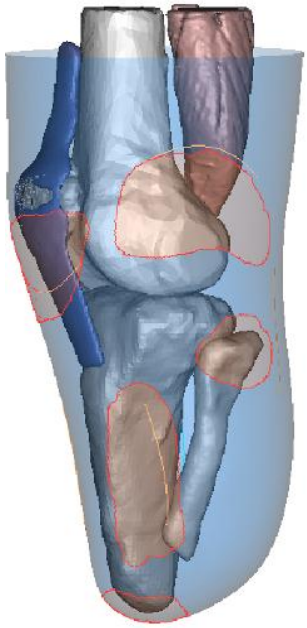

Step 3: The rectification guide markings are projected to the surface of the reduced starting shape as attached curves. The length of each curve is tailored as necessary for a particular socket design variant. Next, surface regions to be modified are selected using the marking tools (shown in orange).

Unnecessary anatomy can be temporarily hidden in order to simplify the review of the rectifications.

Additional rectifications include loading above the medial and lateral condyles of the femur (on the upper sides of the socket), loading either side of the tibial crest (on the lower anterior of the socket) and loading the patellar tendon.

Reliefs, or build ups are added over the distal tibial end and the fibular head.

It is necessary for these rectifications to be smooth for the comfort of the wearer, so smoothing operations are performed on the rectified socket and checked with curvature analysis tools in 3matic.

Step 4: Surface morphing tools are employed to create reliefs and protrusions on the surface. Most apparent rectification is the deep groove under the patella, or the Patella Tendon Bar (ref. the figure to the left). The position and extents of this groove are governed by the shape of the patella and the length of the patellar tendon, easily identified in the 3-D model.

The biggest unknown here is the extent to which each modification should be made.

Of note here is that the tendon appears to protrude through the rectified socket. This is the result of the patella bar which will ultimately be loading the patellar tendon.

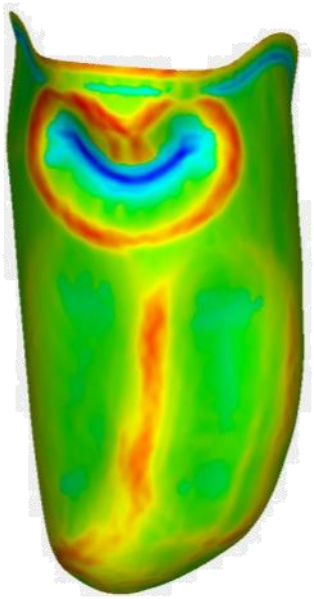

Step 5: The figure to the left shows a curvature analysis on the surface of a completed socket design, indicating some additional smoothing around the Patella Tendon Bar rectification may be necessary before the design is finalized.

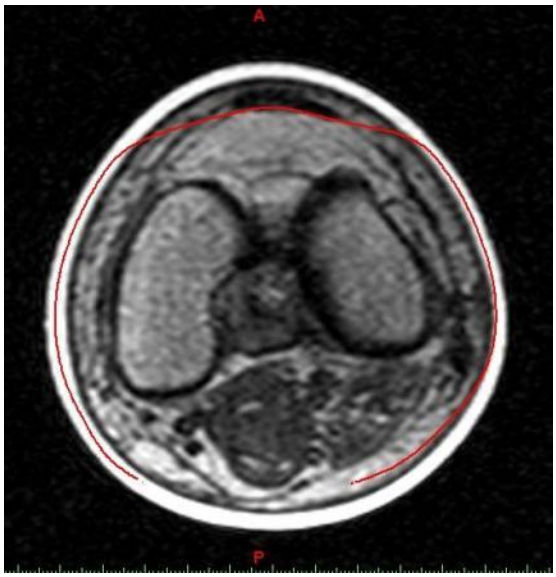

Step 6: Comparison of the rectified socket geometry to the internal anatomy can reveal possible areas where additional rectification is necessary. This assessment can be performed on the 3-D geometry in 3-matic, or an STL of the rectified socket shape can exported for comparison to the reformatted MRI slices using MIMICS, as shown to the left. The red outline of the socket shape is superimposed over an axial reconstruction of the MRI dataset.

Herein lays the beauty of having digital access of underlying anatomy.

Step 7: An example of a rectified socket design is compared to the original starting socket shape in the figure to the left. Once the rectifications are considered satisfactory, the resulting surface is exported as an IGES surface patch set using 3-matic CAD Link. This surface model is then used as the socket inner surface definition in FEA simulation and as a positive mold shape definition for manufacturing the socket. Positive mold patterns manufactured from the digital socket design can be used to produce thermoformed polymer trial sockets for patient fit checks, or can ultimately be used as mandrels for carbon fiber lay-up of a final, definitive socket for delivery to the patient.

Socket Design using CANFIT – Transtibial Models

The CANFIT prosthetics design software was used as the design environment to produce PTB diagnostic sockets for all three trans-tibial subjects. This approach provided the prosthetist with a familiar design environment, dedicated to the design and modification of prosthetic sockets. However, only the external shape of the limb could be imported into the CANFIT design software. CANFIT did not allow for the import and display of multiple STL files; thus the internal anatomy of the limb could not be directly referenced to guide the socket design. 3-matic was still necessary to perform initial STL

preparation, file conversion, and specific steps necessary for check socket pattern manufacture. All Diagnostic sockets tested on subjects were produced by this process. The process is summarized in Table 10:

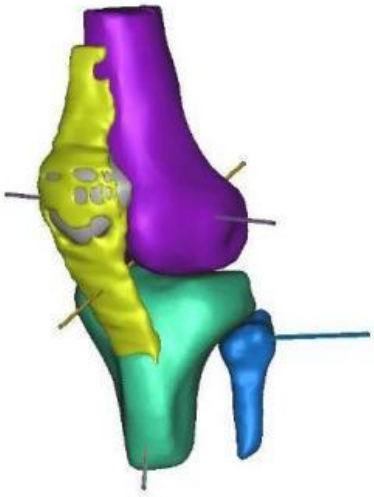

Step 1: The positions of internal anatomy of interest are marked by normal projections from the anatomical landmarks. This function is performed in 3-matic, using the STL models of the internal anatomy of the limb (bones and tendons). The markings projected from the anatomy are saved as a single STL file.

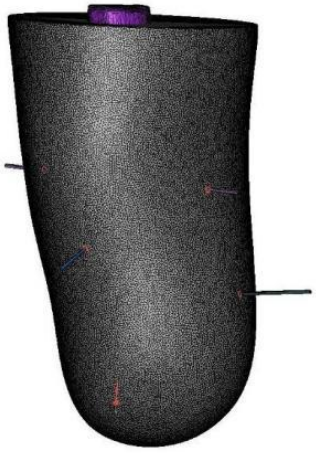

Step 2: The STL model of the residual limb shape is superimposed over the internal anatomy in 3-matic. The projections of anatomical landmarks to the gel liner surface are marked with surface points. Next, 2-4mm deep dimples are inscribed into the surface of the gel liner model at the marked points, using the carve tool in 3-matic.

Step 3: Resolution of the residual limb surface STL model is optimized for modification. Next, the STL model is rotated from the supine orientation of the MRI scan into the standing coordinates (this orientation is expected by the CANFIT design template, and necessary for proper import). The rotation consists of a 90º rotation about the transverse axis of the limb, followed by a 90º rotation about the centerline of the limb. The marked and rotated model of the gel liner was exported from 3-matic as an STL file, and imported into CANFIT.

Step 4: Modifications to the limb shape (rectifications) are performed in CANFIT according to the template for a PTB prosthetic socket. The prepared design is a surface shell representing the inner surface of the intended prosthetic socket. This can include the intended trim lines for the socket (as shown in the figure to the left). The final shape is exported as an STL file from CANFIT.

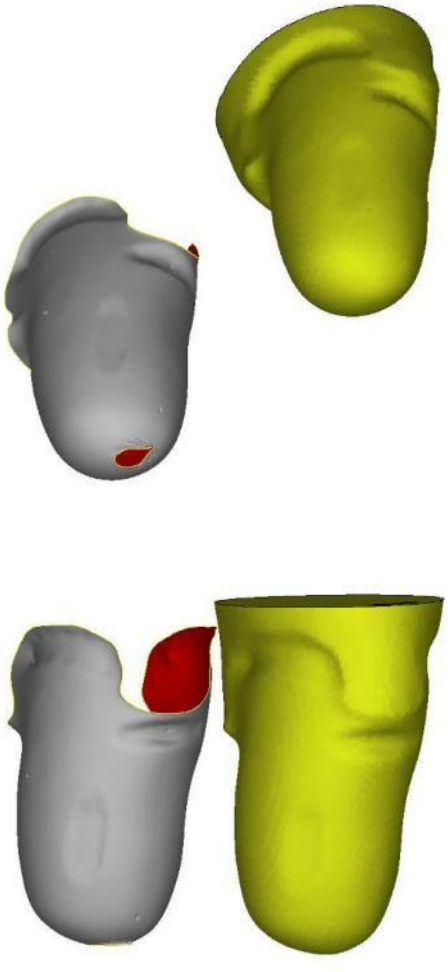

Step 5: The CANFIT socket design (gray) is imported back into 3-matic in order to correct surface flaws (holes, surface ripples) and refine the mesh structure of the socket surface. The corrected socket surface shell is exported as in IGES or STEP file for use in FEA analysis. For manufacturing purposes the open shell is closed into a watertight solid, by extending the free edges and lofting the superior edge of the socket shape to a circular or oval termination 20-50 mm above the most superior point on the trim line. Closing the surface in this manner provides a mandrel shape for casting a thermoformed check socket or braiding a final socket. The final socket mandrel shape is shown in yellow. This shape is exported as an IGES file for mandrel carving.

Table 10: Design method of transferring landmarks to CANFIT for transtibial model rectification

Socket Design using CANFIT – Transfemoral Models

Process of modification for the transfemoral models followed a similar route. This process is detailed in Table 11.

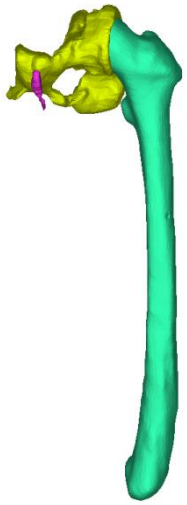

Step 1: For the transfemoral models, the initial landmarks are identified through the femur, the adductor longus tendon and the pelvis as captured from the MRI scan.

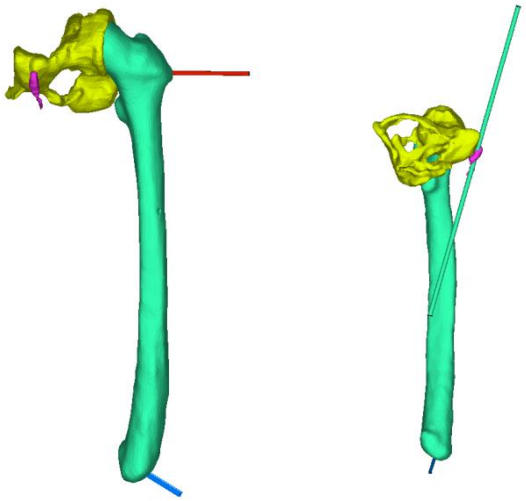

Step 2:.Pins are added to identify the location of the greater trochanter and the distal femur. The image to the right identifies the adductor longus.

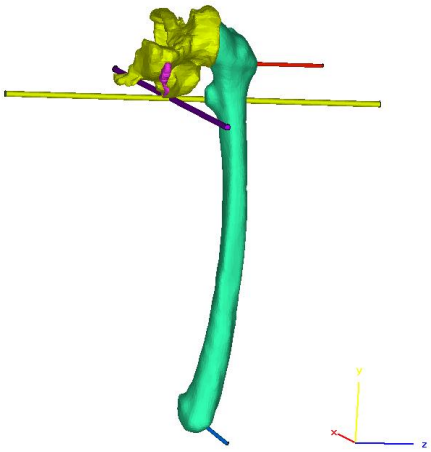

Step 3: Pins are added to identify the Ischial level in both the sagittal and coronal planes.

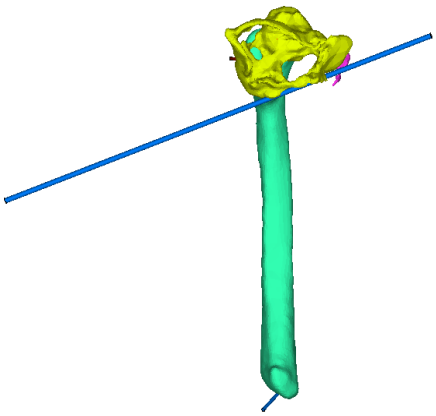

Step 4: The last pin identifies the Ischial ramal axis.

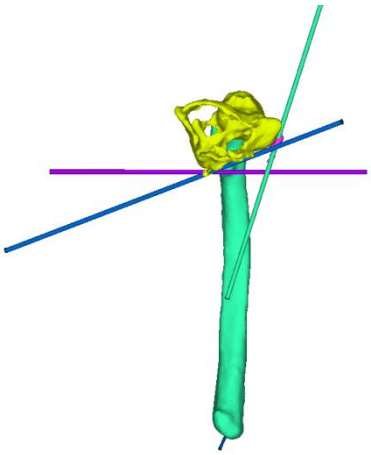

Step 5: The image above shows the transfemoral skeletal anatomy with the pins projecting towards the surface of the model.

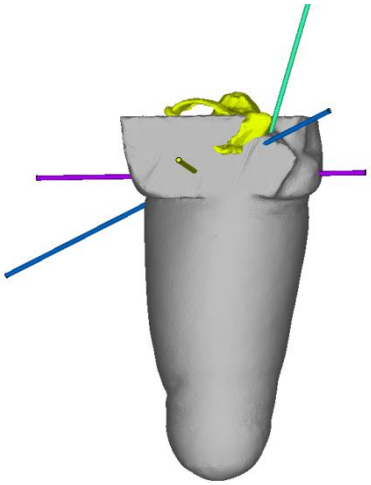

Step 6: Outer surface of the liner is shown with the relevant pins protruding through its surfaces. Hence the planes and anatomical landmarks of interest are precisely communicated to the model. This entire surface, complete with pins is saved as an STL file can is then imported into CANFIT in order to allow for model rectifications.

While the planes create artifacts as part of the importation process, these are easily rectified out and then used accordingly as landmarks.

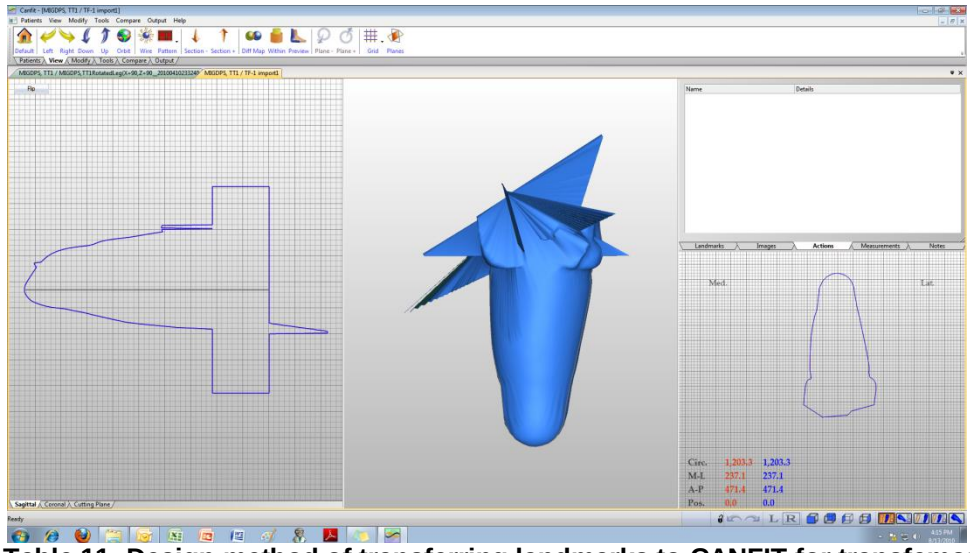

Table 11: Design method of transferring landmarks to CANFIT for transfemoral model rectification

FEA Analysis

FEA Introduction

Optimized Magnetic Resonance Imaging (MRI) protocol is identified and successfully used to obtain the shape of the residual-limb. In a subsequent step MRI data of the residual limb are imported into *Mimics* medical imaging software. Utilizing Mimics digital CAD capabilities MRI slices are transformed into three-dimensional volumetric geometry representing major tissues, i.e. bone, tendon, muscle and fat. This manual provides the detailed steps required to perform Finite Element Analysis (FEA) to simulate prosthetic socket interaction with the residual limb. Patient-specific requirement of the analysis entailed two major challenges, namely, its repeatability and general applicability. Therefore, the FEA is designed based on the principals of computational anatomy in order to attain these requirements. First, repeatability is required to eliminate the need to rebuild the Residual Limb (RL) FEA model every time an analysis iteration is required upon socket model rectification. A simple rule is used at attain the repeatability, a *model developer* (person with advanced knowledge of FEA) will import the anatomical entities “only once” to *ABAQUS* and prepare the analysis, while a *user* (person with minimal knowledge of FEA) will import rectified socket geometry into *ABAQUS* and run the analysis as many times as required to converge to the final design. Second, general applicability is required to guarantee the FEA steps are universal and independent of the specific patient anatomy or amputation location and history.

The outline of these steps is provided in Table I. Only model preparation is performed in *3-matic* (by Materialise) while all other steps are performed in *ABAQUS*. Model preparation starts at importing the three-dimensional volumetric geometry of major tissues (obtained from MRI segmentation) into *3-matic* to obtain CAD representative models in STEP format (ISO 10303) or Initial Graphics Exchange Specification (IGES). *ABAQUS* FEA software is capable of importing TEP or IGES data of major tissue structures as individual parts of the residual limb assembly. Subsequent steps to importing geometries into *ABAQUS* involve meshing, material assignment, assembly, interactions and loading.

Table 12: Overview of creating the FE model options

Software	Task
Mimics	***MRI to 3D volumetric geometry***
	Segmentation
Finite Element Model Development	
3-matic	***Model Preparation***
	Individual anatomical entities
	– Wrap function
	– Smooth function
	– Auto Remesh
	– Quality Preserving Reduce Triangles
	Interaction of anatomical entities
	– Boolean CAD operations
	CAD Link export to STEP or IGES
ABAQUS	***Finite Element Analysis***
	Import parts
	Generate optimized FEA mesh
	Assign material models
	Assemble model
	Create contact behavior (interaction)
	Assign loading
	Run analysis checks

For demonstration purposes this guide will use example cases independent of the patient case under study to guarantee the generality of discussion. Meanwhile, all FEA steps will be applied to a single patient model (example) to provide a comprehensive discussion.

FEA Model preparation

Model preparation, Individual anatomical entities

Segmentation procedures of MRI data performed in *Mimics* results in three-dimensional (3D) volumetric geometries of tissue structures. Figure 1a provides the muscle community above the knee all lumped in one 3D entity as obtained from MRI data segmentation. This 3D volumetric geometry lacks surface smoothness including holes and/or small inclusions as shown in Figure 12-A. These imperfections are filtered out using the Wrap and Smooth functions provided in the *remeshing* module. As these details are filtered out, smooth 3D volumetric geometries of reasonable accuracy are obtained as shown in Figure 12-B. The purpose of filtering out these imperfections is to obtain optimized geometry suitable for numerical analysis. Existing or remaining imperfections in the model may render any FEA impossible since imperfections are major cause for numerical singularities in the mathematical models associated to the analysis. Irregular yet smooth surfaces will result in less than optimal interaction or contact identification between different tissues, and hence drastically increase analysis cost in terms of run time.

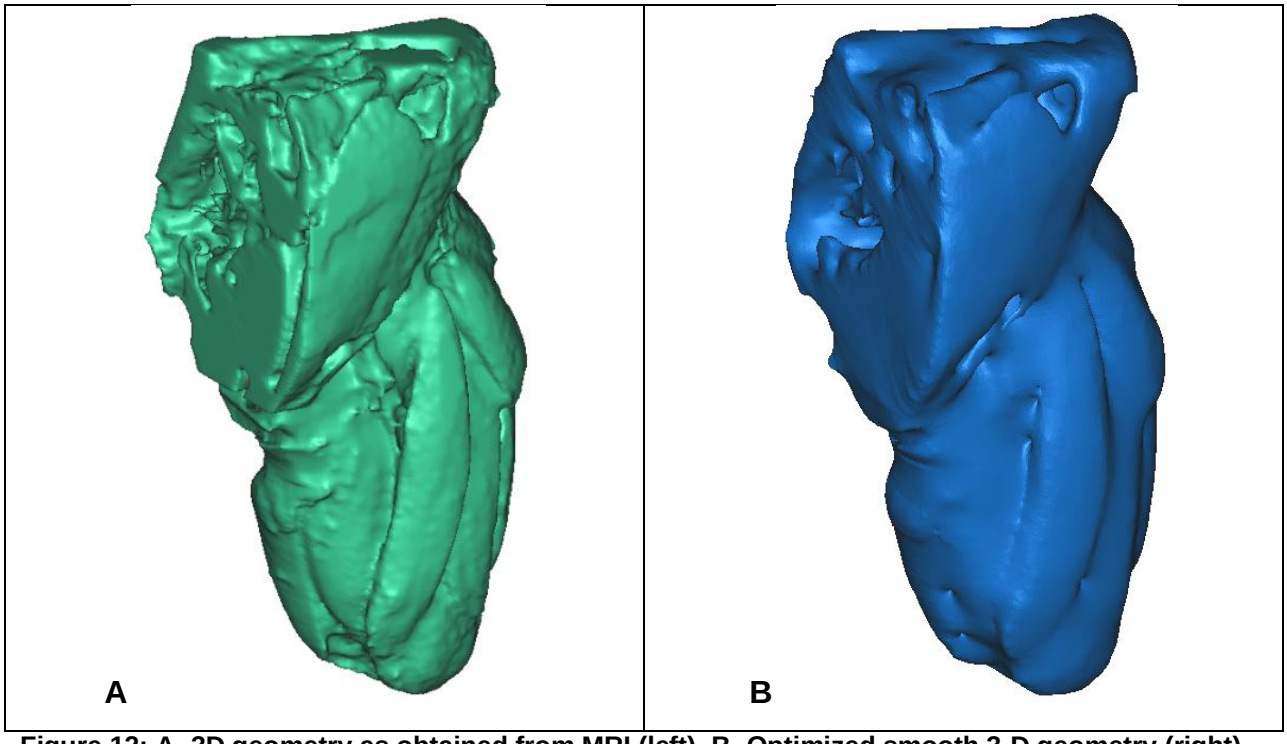

Figure 12: A- 3D geometry as obtained from MRI (left), B- Optimized smooth 3-D geometry (right)

In order to filter out imperfections two *3-matic* functions are used, namely, *Wrap* and *Smooth*. *Wrap* function as described in *3-matic* user manual *"The wrap operation will create a wrapping surface of the selected entities. The wrap function is useful for medical parts, to filter small inclusions or close small holes. Furthermore the function is a useful tool towards Finite Element Analysis, where an enveloping surface is needed"*. Also *Smooth* function will result in enhanced surface geometry in terms of better triangulation of the surfaces by *reducing the noise in the triangulation*. In order to guarantee that a 3D geometric entity will be exported in an optimal size CAD data file two more operations are performed. *Auto Remesh* and *Quality Preserving Reduce Triangles* are designed to optimize the volumetric triangular mesh while maintaining the 3D model accuracy.

Model preparation, Interaction of anatomical entities

In this section the guide utilizes an example of a trans-tibial case in order to illustrate the necessity of the suggested step. Performing MRI segmentation in *Mimics* different tissue types are constructed and their associated surface imperfections and/or inclusions are filtered out. A critical aspect in preparing a computational model is to eliminate overlaps and/or gaps between matching surfaces of adjacent tissues. These gaps and overlaps result from numerical anomalies when *Mimics* is constructing the surfaces through interpolation of sectional and intersectional points. Figures 13 and 14 provide an example of such overlaps between different entities of fat, tendons, bones and muscles. Meanwhile, the Finite Element model requires minimum flaws (gaps and overlaps) of mating surfaces. Therefore, the assembly of the FEA model is prepared in *3-matic* by creating identical mating surfaces of neighboring anatomical entities.

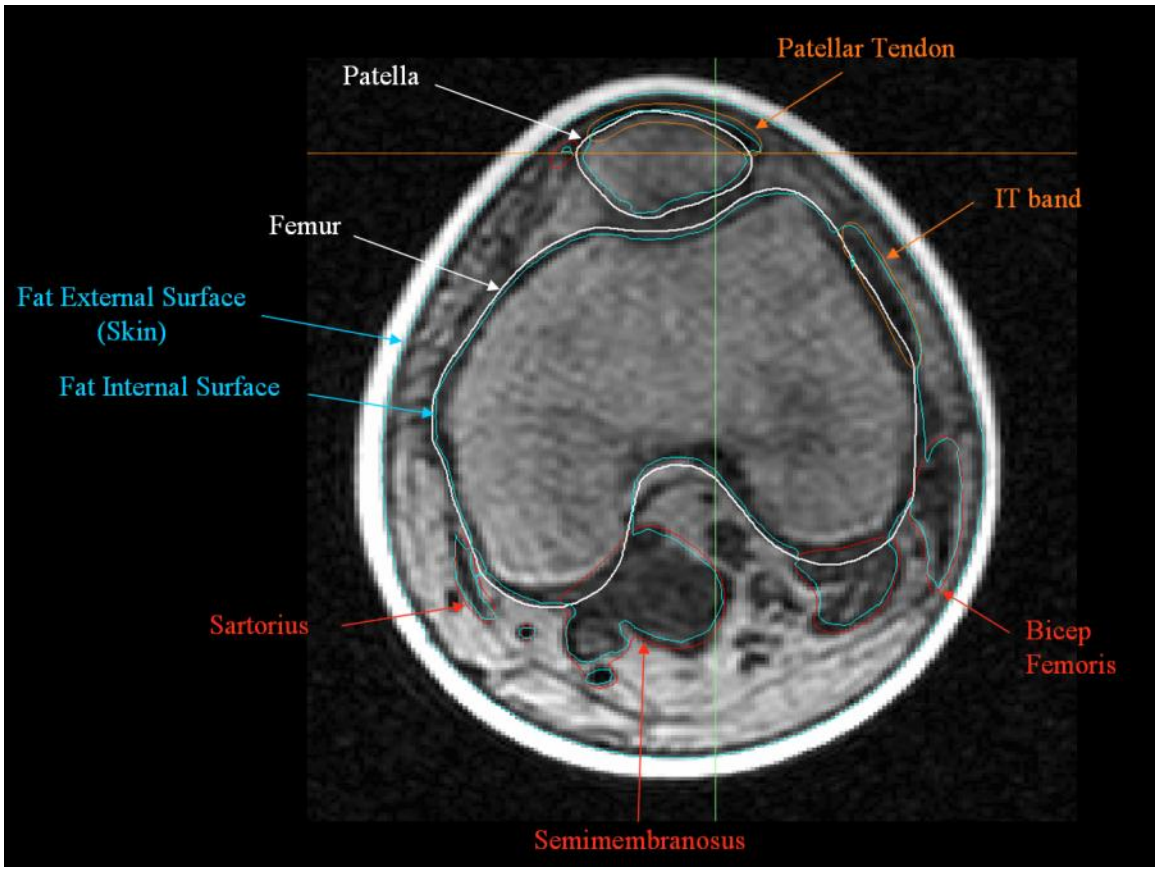

Figure 13: Overlapping boundaries of tissues (section above the knee in a trans-tibial case)

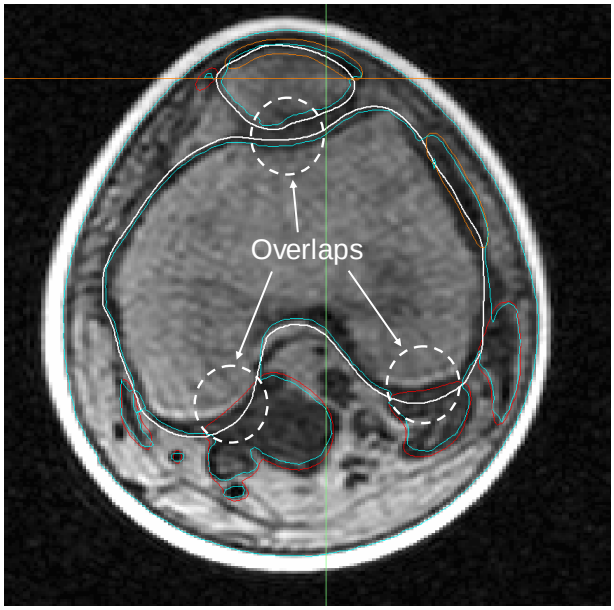

Figure 14: Overlaps between different tissue types

A first step to resolve mating surfaces flaws is to identify major anatomical parts of the model. For the example of a trans-tibial patient analysis major bones are Femur, Tibia,

Patella, and Fibula. Major muscles are Quadriceps femoris, Biceps femoris, Sartorius, Semimembranosus and the Triceps surae. Finally major tendons are the Patellar tendon and the Iliotibial band. Table 13 provides the interaction or contact among the formerly mentioned major anatomical parts

Table 13: Major anatomical tissue interaction (contact) matrix

Item	Femur	Tibia	Patella	Fibula	Quads	Biceps	Sartorius	Semimem	Gastroc	Pat Ten	IT band
Bones											
Femur					✓	✓	✓		✓		
Tibia				✓				✓	✓	✓	✓
Patella										✓	
Fibula		✓							✓		
Muscles											
Quads	✓					✓				✓	
Biceps	✓				✓				✓		
Sartorius	✓										
Semimem		✓							✓		
Gastroc	✓	✓		✓		✓		✓			
Tendons											
Pat Ten		✓	✓		✓						
IT band		✓									

Fat tissue in a trans-tibial amputee's case represents further contacts or interactions with all formerly mentioned anatomical parts. Meanwhile, fat as a major tissue type is not mentioned in Table 12 as its geometric model, and consequently its computational model, is constructed through Boolean operation.

The Triceps Surae is used as an example to demonstrate eliminating interaction flaws. Figure 15 provides the original shape of the Triceps obtained from segmentation (in *Mimics*) together with the modified shape at its interface surfaces with mating tissues. These modifications are obtained in *3-matic* using Boolean subtract operations of surrounding tissues from the Triceps.

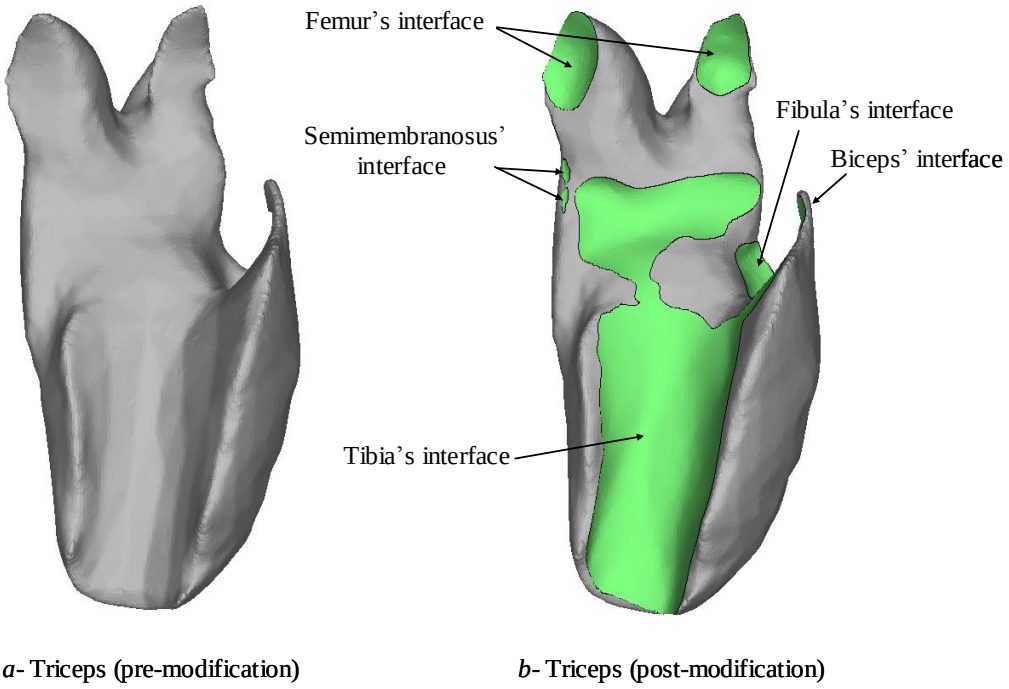

a- Triceps (pre-modification) *b*- Triceps (post-modification)

Figure 15: Modified surface of the Triceps muscle at the interface

Interaction flaws are removed in each anatomical entity according to the interaction matrix provided in Table II. Afterwards, all major tissue structures are assembled into one object using Boolean union operation as shown in Figure 16. This assembled object is consequently subtracted from the internal surface of the gel liner using a Boolean subtract operation and resulting in the three dimensional geometry of the fat. Figure 17 provides the fat geometry obtained from direct segmentation of the MRI, while Figure 18 provides the product of the Boolean operation to construct the fat. It can be seen in Figure 17 that surface construction is poor consisting of fragments, ridges small inclusions due to the interpolation numerical anomalies discussed earlier. On the other hand Figure 18 provides higher quality surfaces, precise boundaries and most importantly optimum interface with major tissues of the model.

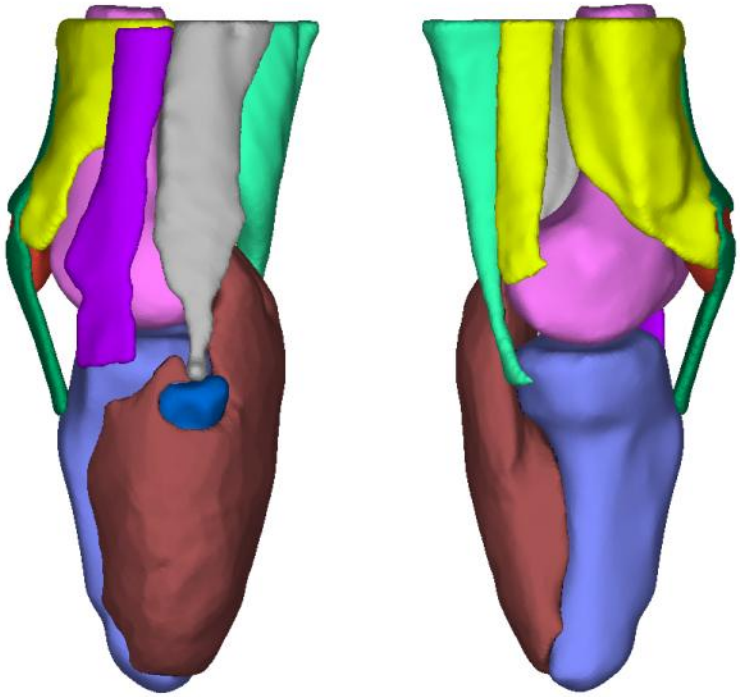

Figure 16: Assembled bones, tendons and muscles (left leg – lateral and medial views)

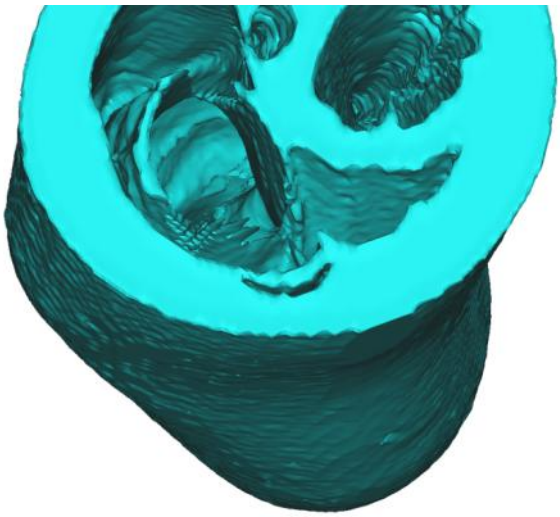

Figure 17: The 3D geometry of fat tissue as obtained directly from segmentation

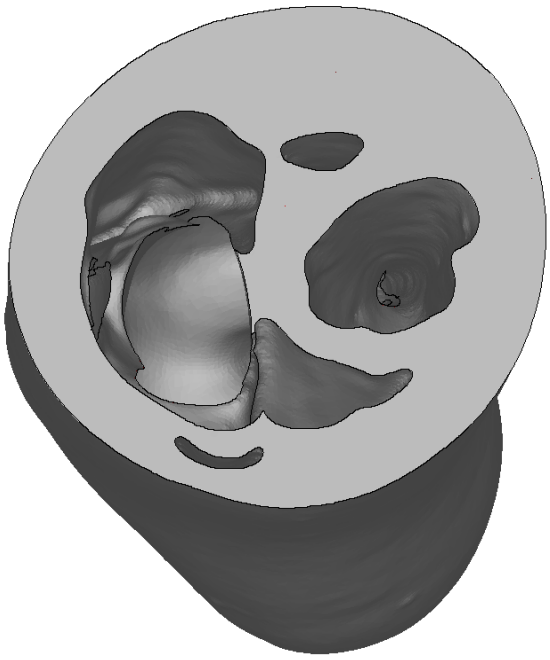

Figure 18: The final 3D geometry of fat tissue as obtained via Boolean operations

Model preparation, *CAD Link* export into STEP or IGES

CAD Link module in *3-matic* facilitates converting 3D triangular based model description into an analytical representation recognizable by any CAD or FEA software. Resulting analytical representation of the surface are transformed into planes, tabulated cylinders, general surface of revolutions and/or NURBS surfaces (Non-uniform rational b-spline, i.e. freeform). Analytical representation of 3D geometries are exported via the *CAD Link* tool into either STEP or IGES format, both CAD format are readable by ABAQUS FEA software. Figure 19 illustrates the analytical representation of the muscles community above the knee which is to be imported into the FEA software. Different color (red) lines show the boundaries of analytical surface patches in the new analytical representation of the muscle community.

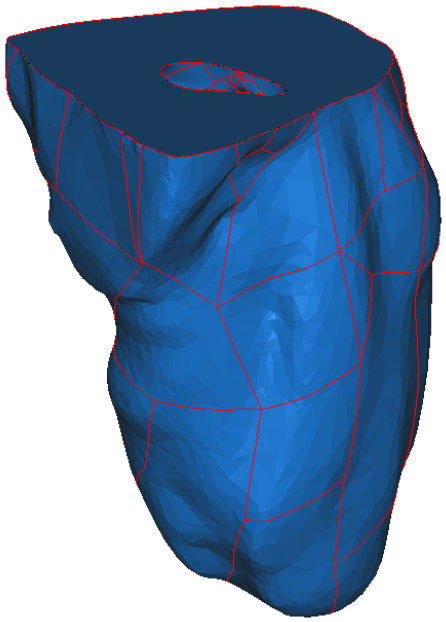

Figure 19: Analytical geometry of the muscle community as obtained from CAD Link

When performing the *CAD Link* operation to export analytical representations, *3-matic* provides a feedback report regarding the quality of the export process. In order to guarantee error proof export/import process this feedback should include “zero” errors as shown in Figure 20.

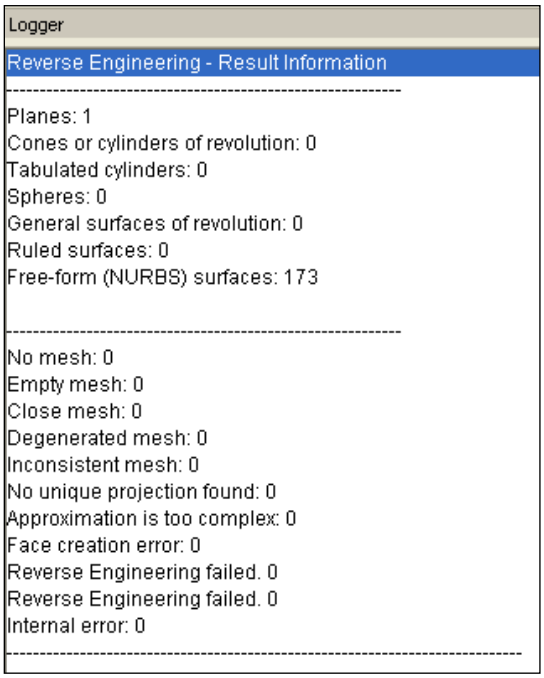

Figure 20: 3-matic Logger feedback report providing the export process quality

This process of model preparation in *3-matic* is essential for successful FEA of socket interaction with the RL. The process should be performed by an advanced user of the medical CAD software *3-martic*, preferably the same FEA *model developer* or at least with perfect coordination with. This requirement of perfect coordination is implied by the practical flow of tasks and clear understanding of the *3-matic* user of FEA requirements.

FEA Process

In this section, for demonstration purposes, a trans-femoral model (TF03) is used. The steps were tested in the cases of trans-femoral (TF), trans-tibial (TT) amputation alike and proven both repeatability and general applicability. An FEA *model developer* is to follow the demonstrated steps here within to establish the FEA model for the first time. The FEA model is to be built only once for any specific patient.

The TF03 example model used contains the following major anatomical entities, bones, muscle and fat together with other entities or parts of the gel liner and the socket. All parts belong to 3D geometries SOLID except for the prosthetic socket which belongs to 3D SHELL geometry. The interaction matrix for a TF case is given in Table 14 and obtained by combining all bones into one structure and similarly treating the muscles and the fat. The extended interaction matrix provided in Table III includes non-anatomical entities or parts such as the gel liner and the socket. It must be noted that the skin is not considered in the FEA model. Therefore an interaction between the gel liner and the muscle implies that it takes place across the skin. The assumption of neglecting the skin is justified by the fact that the skin possesses very low strength and hence does not contribute to the load carrying capacity of the RL.

Table 14: Extended contact matrix – TF03 case

Item	Bones	Muscles	Fat	Gel liner	Socket
Bones		✓			
Muscles	✓		✓	✓	
Fat		✓		✓	✓
Gel liner		✓	✓		✓
Socket			✓	✓	

Importing part (individual successive operations)

Important note: *Mimics* and *3-matic* represent the 3D geometry in the same units as the MRI data, i.e. in millimeters. Meanwhile *ABAQUS* FEA software requires the user to employ a consistent set of units across all variables, i.e. length dimensions in meter, forces in Newton and mechanical properties such as Young's modulus in Newton/m^2. Therefore, while importing parts into *ABAQUS* the user will scale the part dimension to one hundredth to be in meters instead of millimeters. Erroneous outcomes associated to relative location in space will result in case the user attempts to import the parts in millimeters and scale them down at later step.

*Importing the **bones** as SOLID 3D geometry* is shown in Figure 21.

Import process: File menu → Import Part

Options: Solid – Stitch edges using tolerance (2 *mm*)

3D –Deformable

Multiply length by 0.001 (from *mm* to *m*)

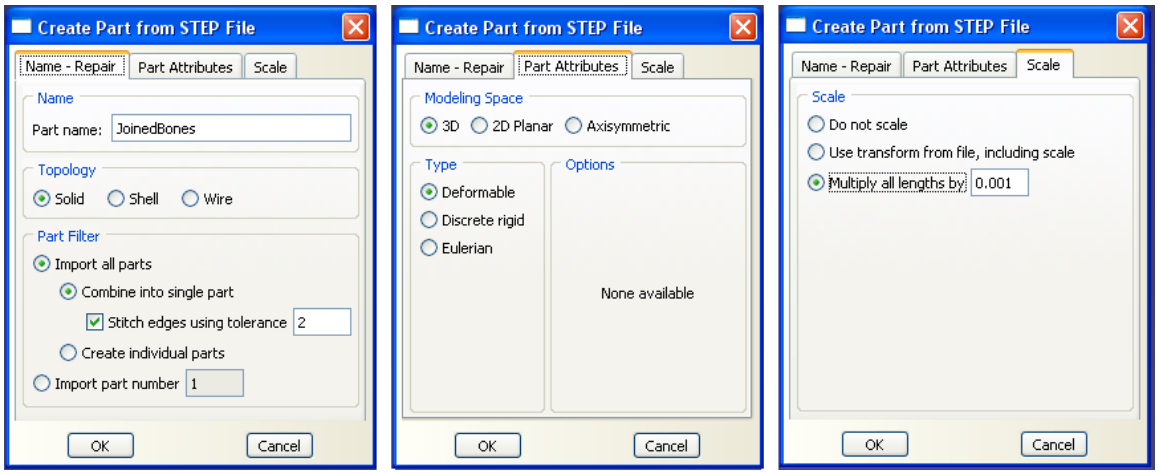

Figure 21: Solid import options

The imported object of the 3D solid analytical geometry of bones is shown in Figure 22 with warnings associated to, imprecise geometry (stitched edges) and partitioning or quad/hex meshing may fail (no need for partitioning and a tetrahedron mesh will be used instead of quad/hex mesh)

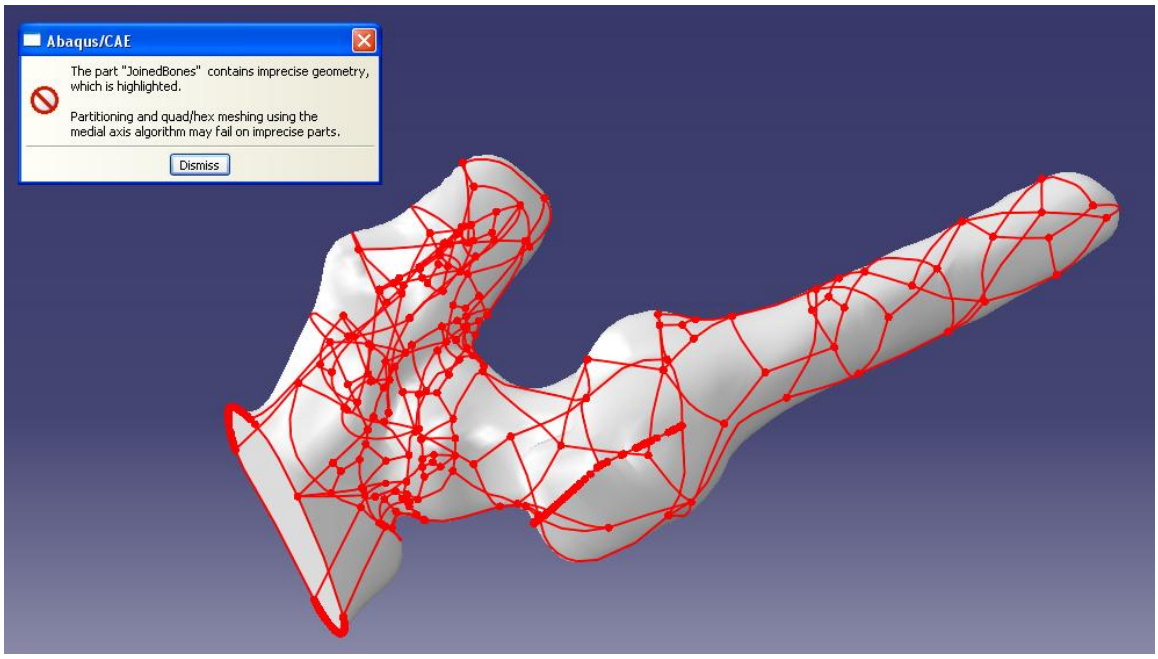

Figure 22: Imported 3D solid analytical geometry of bones

The user has to verify that the part import was successful as a 3D solid by updating part validity from the part manager. When updating the validity for the 3D solid analytical geometry of bones, the user should obtain a similar message

Part 'JoinedBones' contains valid geometry and topology.
Part 'JoinedBones' is a solid part (1 cell, 136 solid faces, 442 edges, 306 vertices).

A message reporting invalid geometry or a shell part (not solid with 1 cell), the user has to repeat the CAD export from *3-matic* using the *CAD Link* tool with refined parameters.

*Importing the **socket** as 3D SHELL geometry* is identical to importing a solid part except for using the option SHELL instead of SOLID (Figure 21)

Meshing part (individual successive operations)

The FEA mesh of a part obtained in *ABAQUS* is more efficient than the one obtained in medical CAD software such as *Mimics*. An external or surface mesh of similar element size in both options, *Mimics* and *ABAQUS*, results in reduced number of

volume mesh when *ABAQUS* adaptive mesh rules by allowing size growth of the interior elements. Consequently, the total number of degrees of freedom of the *Mimics* mesh is many times higher than the corresponding *ABAQUS* mesh. Also obtaining a FEA mesh in *ABAQUS* is used as a verification step for the imported 3D geometries. In other words, successful mesh is obtained for a solid part, e.g. bones, provides further verification of correct imported geometries.

Mesh module:

Seed part: Figure 23

Assign seed size (this is the element side length in meters, e.g. 0.008 *m*)

Accept defaults in terms of curvature control and minimum size factor

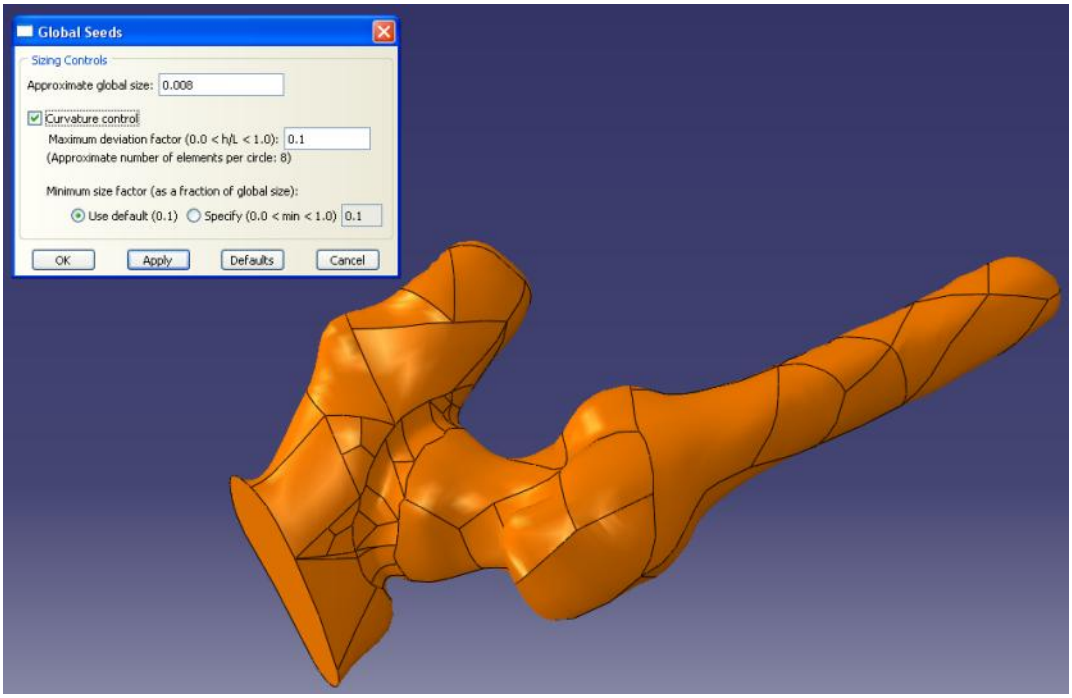

Figure 23: Mesh module, seed part

Mesh Controls: Figure 24

Select **Tet**rahedron mesh (since 3D geometry was developed using triangulation)

Accept defaults algorithm with increasing size of interior elements

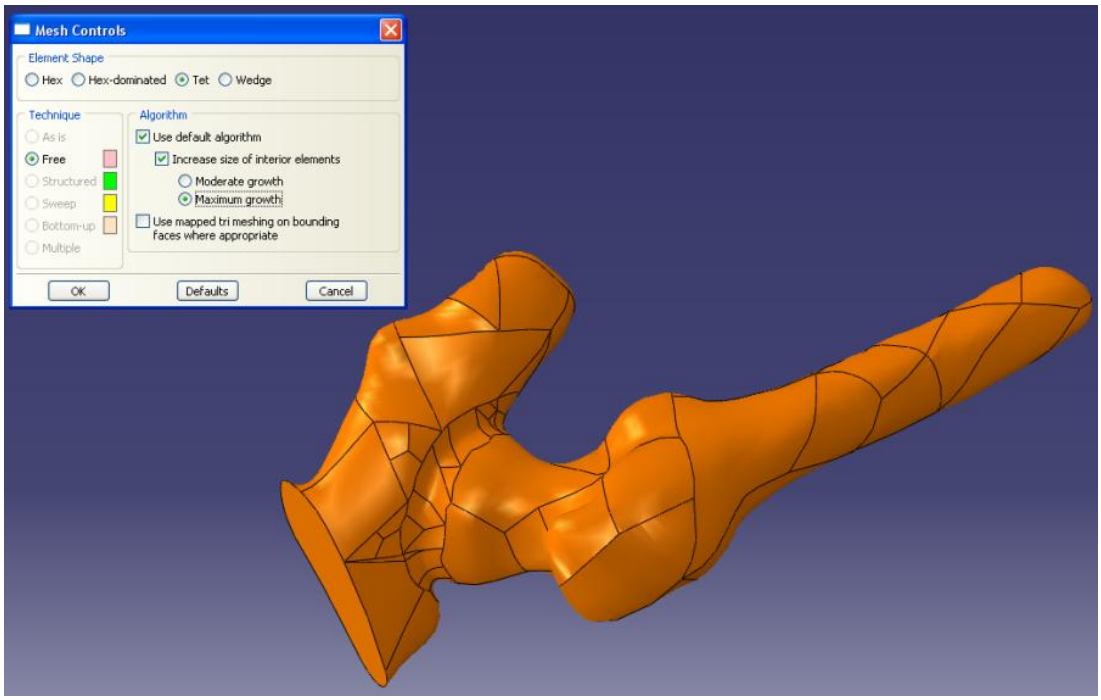

Figure 24: Mesh module, mesh controls

Element Type: Figure 25

Element library Standard, *Geometric Order* Linear, *Family* 3D stress

Tet element controls: accept defaults, element is C3D4: 4-node linear tetrahedron

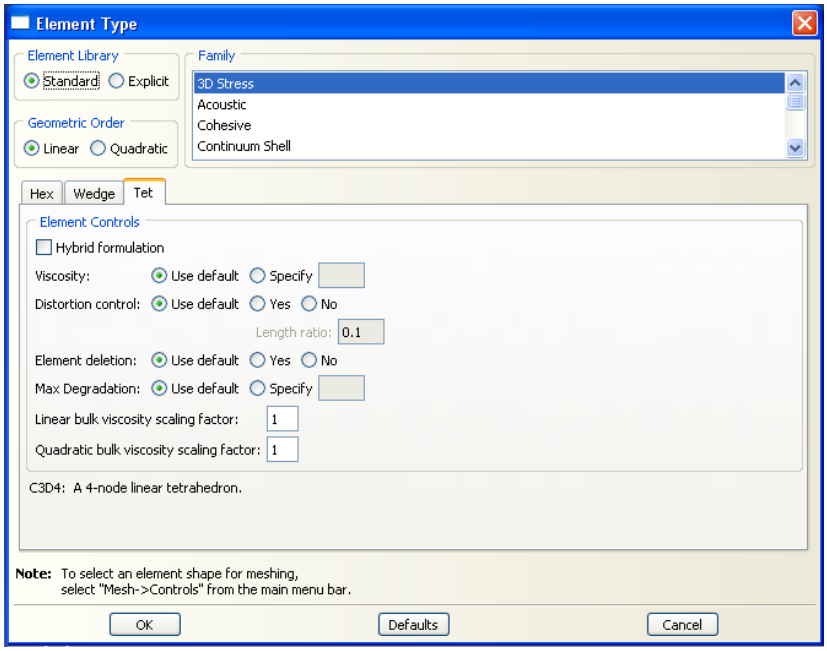

Figure 25: Mesh module, element type

Mesh part: Figure 26

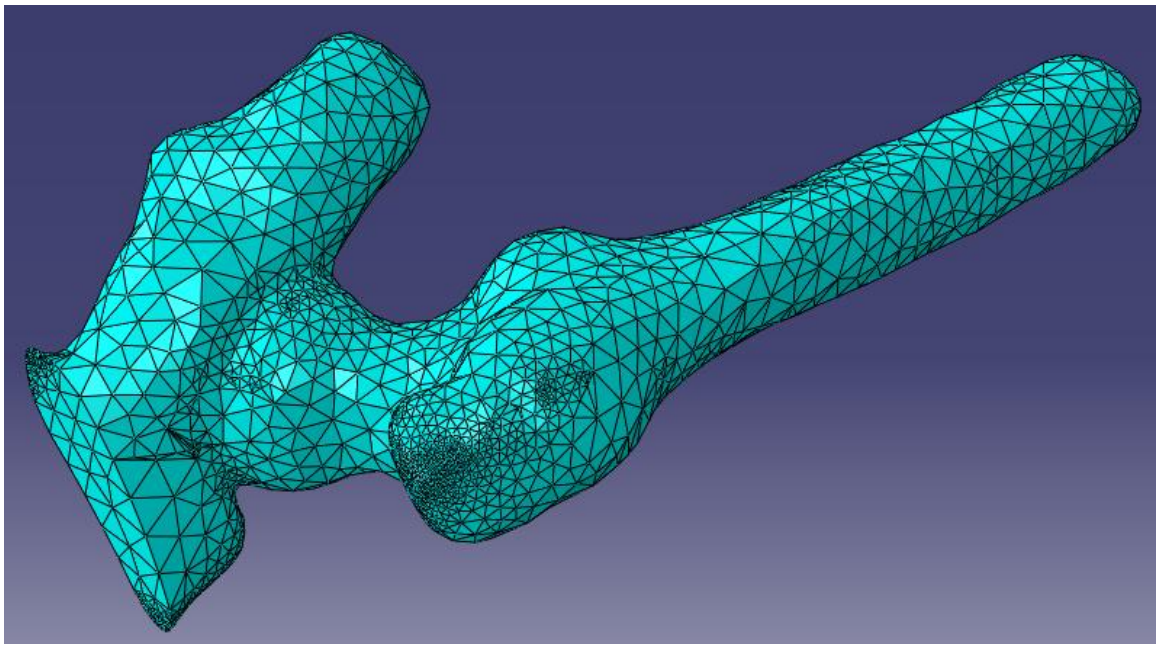

Figure 26: Mesh module, final mesh

Property Module (Material assignment)

All anatomical entities, bones, muscles and tendons, are assumed to be isotropic and homogeneous. Meanwhile, the material nonlinearities are associated to the rubbery like nature of the soft tissue, i.e. fat and muscle. Hyper-elastic models are used to represent such rubbery behavior in terms of first and second order expressions describing the strain energy function of the muscle and fat tissue, respectively. The Mooney-Rivlin material model assigned to the muscle is expressed in terms of it strain energy *W* as

$$W = C_{10}\left(\bar{I}_1 - 3\right) + C_{01}\left(\bar{I}_2 - 3\right) + \frac{1}{d}\left(J - 1\right)^2$$

Where $\bar{I}_1$ and, $\bar{I}_2$ are the first and second deviatoric strain invariants and *J* is the determinant of the deformation gradient. The strain energy parameters C_{10}, C_{01} and *d* take the values, C_{10} = 30 kPa, C_{01} = 10 kPa and $d = 1.667\times10^{-5}$ Pa^{-1}. See Figure 27.

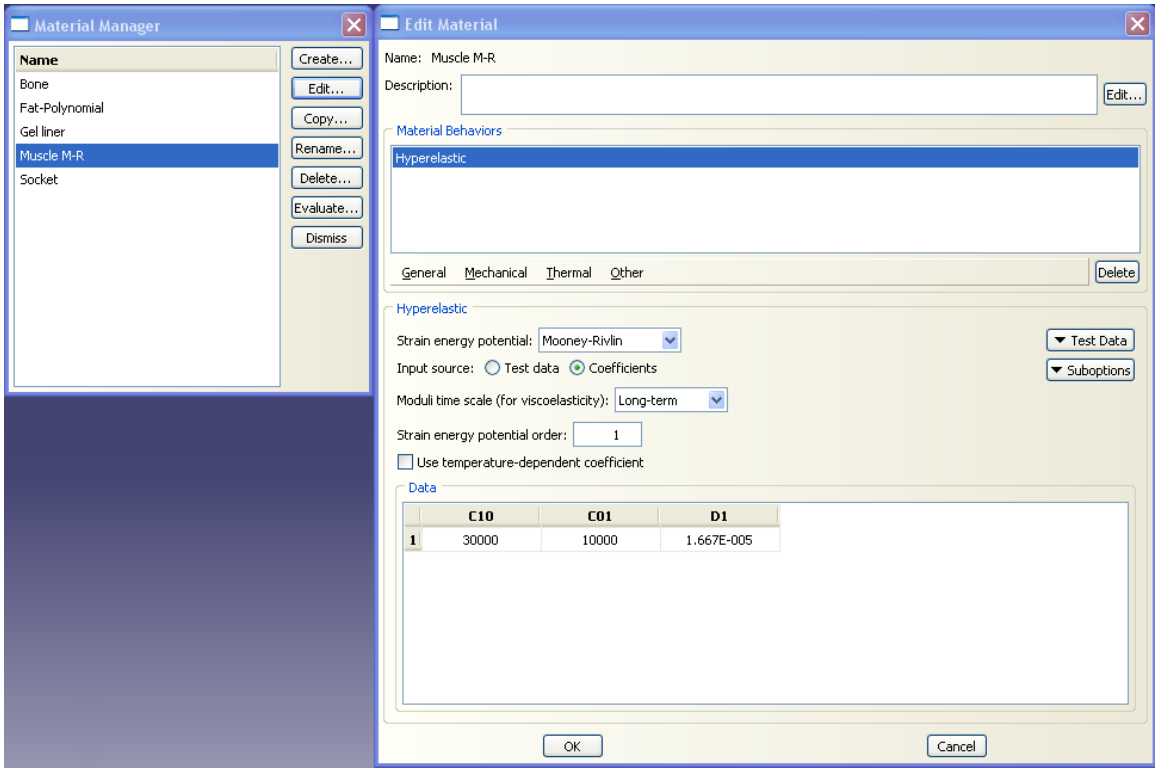

Figure 27: The Mooney-Rivlin material model assigned to the muscle

While a second order polynomial strain energy *W* utilized to describe the hyper-elastic fat tissue behavior is

$$W = \sum_{i+j=1}^{2} C_{ij}\left(\bar{I}_1 - 3\right)^i \left(\bar{I}_2 - 3\right)^j + \sum_{i=1}^{2} \frac{1}{D_i}\left(J - 1\right)^{2i}$$

Where $\bar{I}_1$ and, $\bar{I}_2$ are the first and second deviatoric strain invariants and *J* is the determinant of the deformation gradient. The strain energy parameters assume the values C_{10} = 85.56 kPa, C_{01}= –58.41 kPa, C_{20}= 39 kPa, C_{11}= –23.19 kPa, C_{02}= 85.1 kPa, D_1= 3.653×10^{-6} Pa^{-1} and D_2= 0.0 Pa^{-1} See Figure 28.

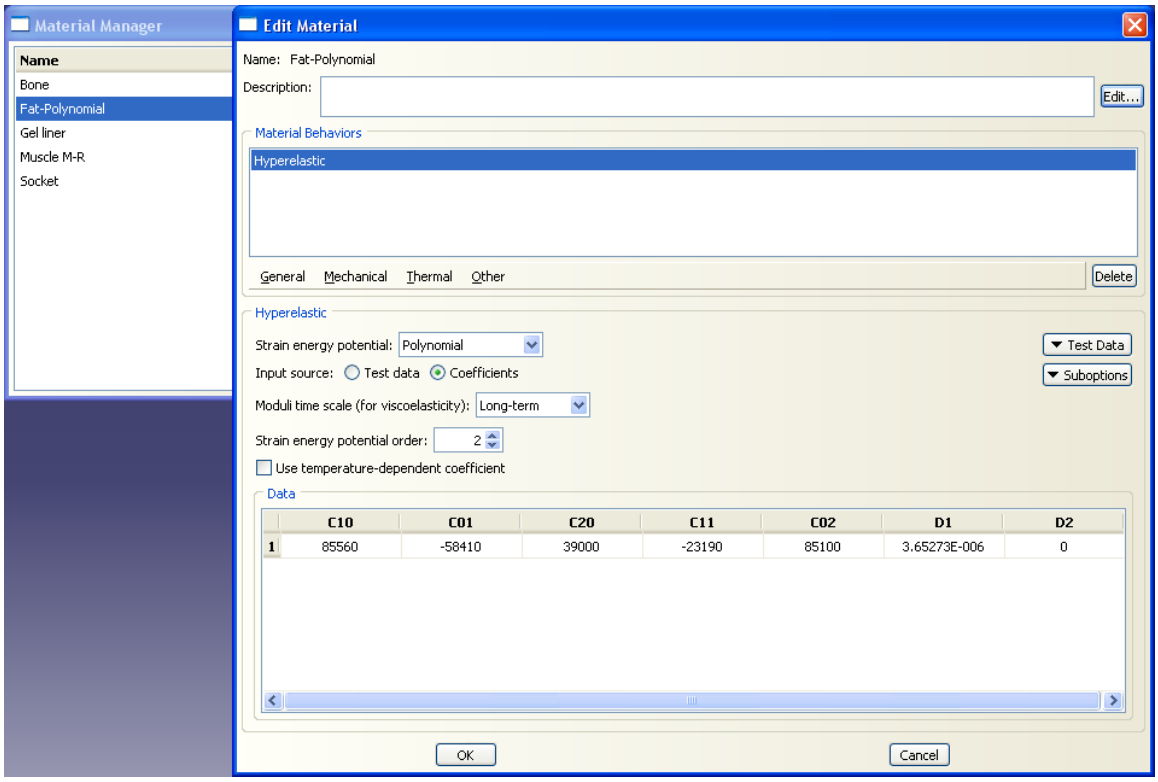

Figure 28: A second order polynomial strain energy assigned to the fat

Other anatomical entities or parts such as bones and tendons are assigned linear elastic material models according to literature. Also non-anatomical parts such as the gel liner and the socket are assigned linear elastic material properties. Table 15 provides the linear elastic material properties used in the analysis.

Table 15: Linear Isotropic material properties

Material	Young's Modulus (*Pa*)	Poisson's Ratio	Thermal expansion coefficient ($^{o}C^{-1}$)
Bone	7.3×10^{9}	0.3	
Tendon	2.0×10^{8}	0.3	
Gel Liner	5.17×10^{6}	0.3	
Socket (polypropylene)	1.5×10^{9}	0.3	8.6×10^{-5}

Assembly Module

The user creates instances associated to all imported parts. Figure 18 includes all the instances created for the TT case (from left to right, Muscles, Bones, Gel liner, Socket and Fat). Figure 29 is obtained in exploded view, while correct parts import demonstrated identical reference or global coordinates as shown in Figure 30.

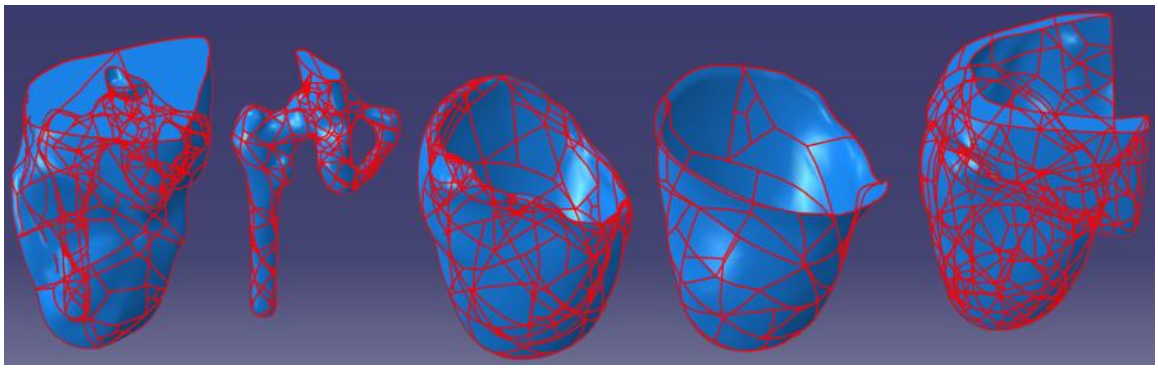

Figure 29: Exploded view of parts import

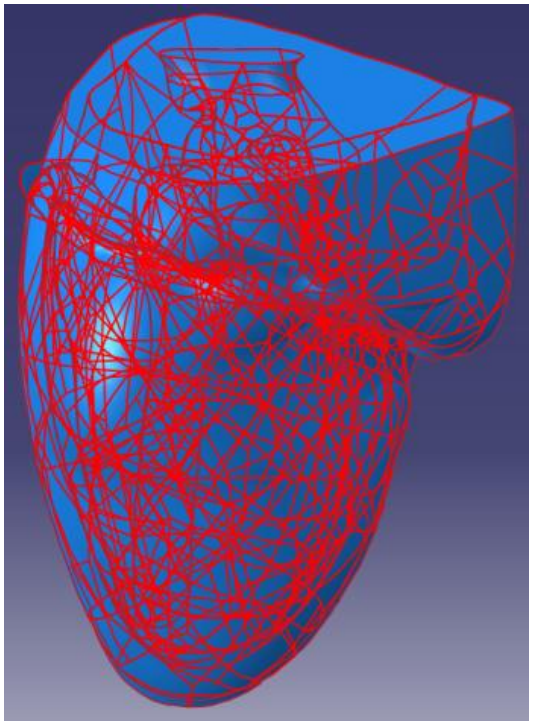

Figure 30: Identical global coordinate system for imported parts

Step Module

The *model developer* creates a number of analysis steps starting Socket Donning performed followed by a number of load cases associated to standing and motion kinetics. Socket donning as the initial step of analysis represented a challenge in terms of its dynamic nature to simulate sliding the socket up onto the RL. Dynamic analysis in any FEA software is time consuming and of high complexity being associated to many convergence iterations of nonlinear deformation steps and utilizing nonlinear material models.

The socket donning simulation challenge was overcome by replacing the dynamic analysis of sliding the socket up and onto the RL by a thermal shrinking the socket over the RL. In the initial step of the analysis the socket is aligned at the distal end of the RL. Socket donning is performed in two analysis steps, the first step is to thermally expand the socket beyond the external boundaries of the RL while the in the second step the socket undergoes thermal shrinkage to its original dimensions and hence shrinks over the RL.

The standing and walking simulations are simulated each in a separate analysis with a loading applied at the distal end of the socket corresponding to half the body weight, full body weight or the forces and moments associated to phases of gait. Load application method will be introduced in the section dedicated to “Load Module”.

The *model developer* creates all analysis steps as static general steps accepting all defaults except for setting “convert severe discontinuity iteration” set to ON. Figure 31 provides a screen capture of the options in the step module.

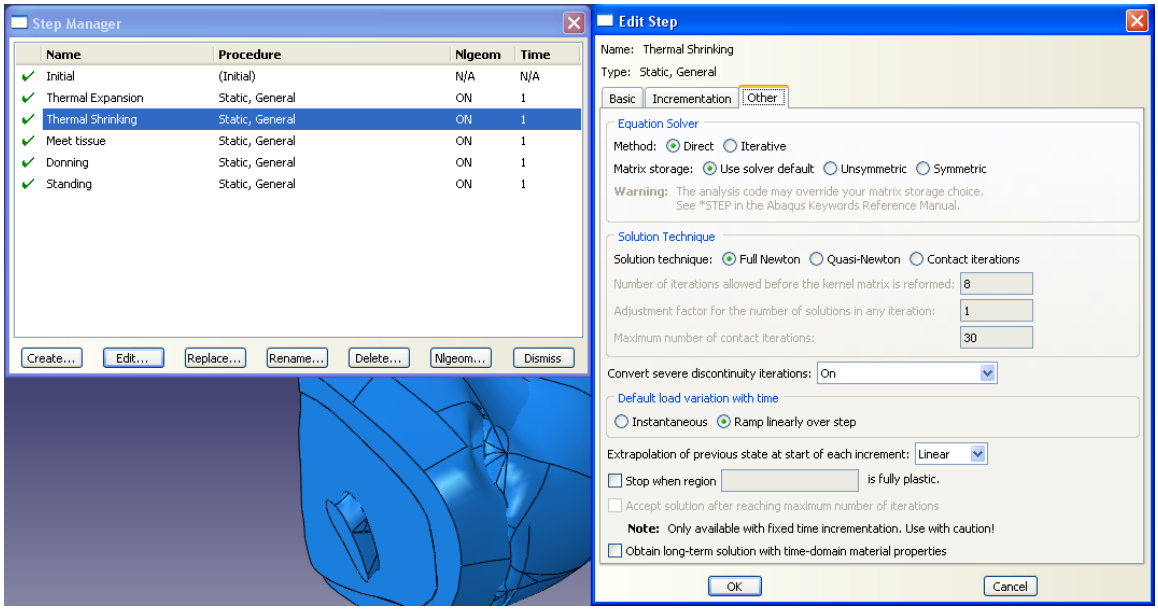

Figure 31: Step Module

Interaction Module

One of the major advantages of *ABAQUS* FEA software is its well developed interaction module ranking it superior to all other commercial FEA software. *ABAQUS* provides contact and constraint detection tool that will detect contact surfaces between any two or more entities (parts) selected by *model developer*. Also ABAQUS has an automated contact subroutine that provides a variety of automated contact properties for realistic normal or tangential surface to surface behavior.

Two major types of contact are used. Among all anatomical entities contact “tie” constraint is established in which matched displacements are enforced along the contact interface. Whereas, the socket/gel liner and socket/tissue contact interaction is identified as hard contact normal behavior (no penetration) and a frictional tangential behavior with coefficient of friction μ = 0.3. Figure 32 provides all identified contact surfaces in the TT model as per the extended contact matrix provided in Table III. Figure 33 provides the parameters chosen for the contact interaction.

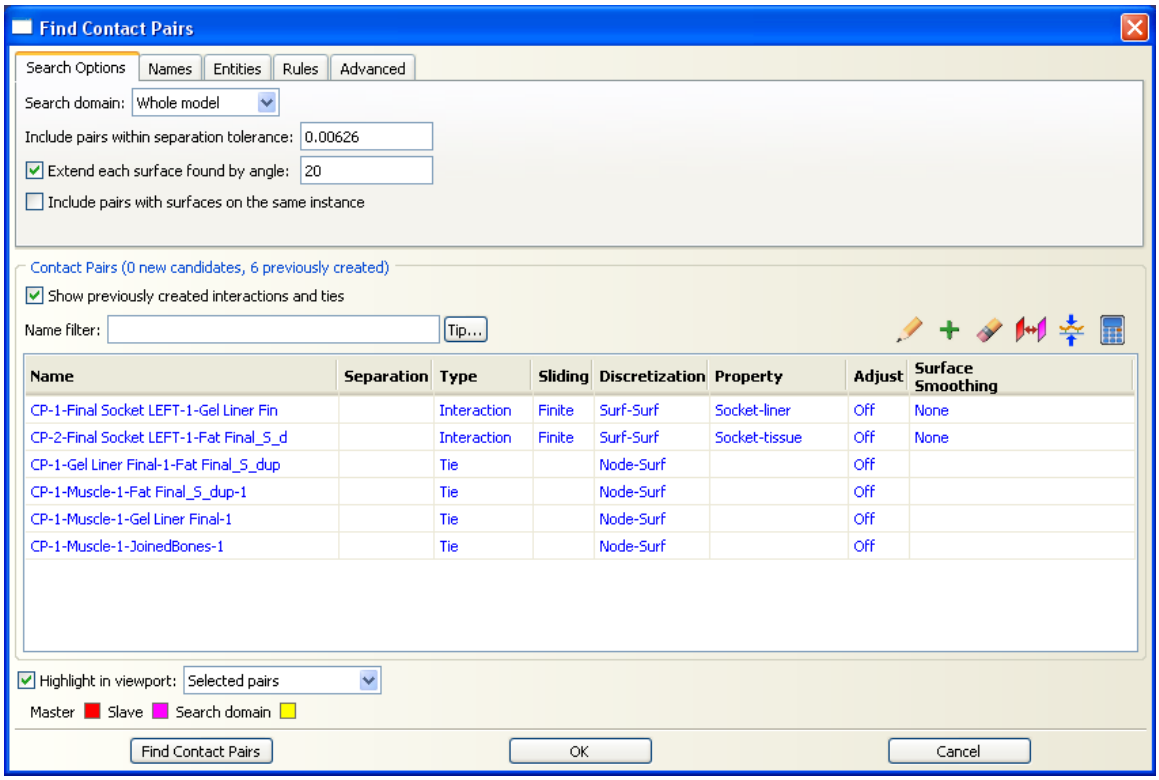

Figure 32: Extended contact matrix applied through ABAQUS detection tool

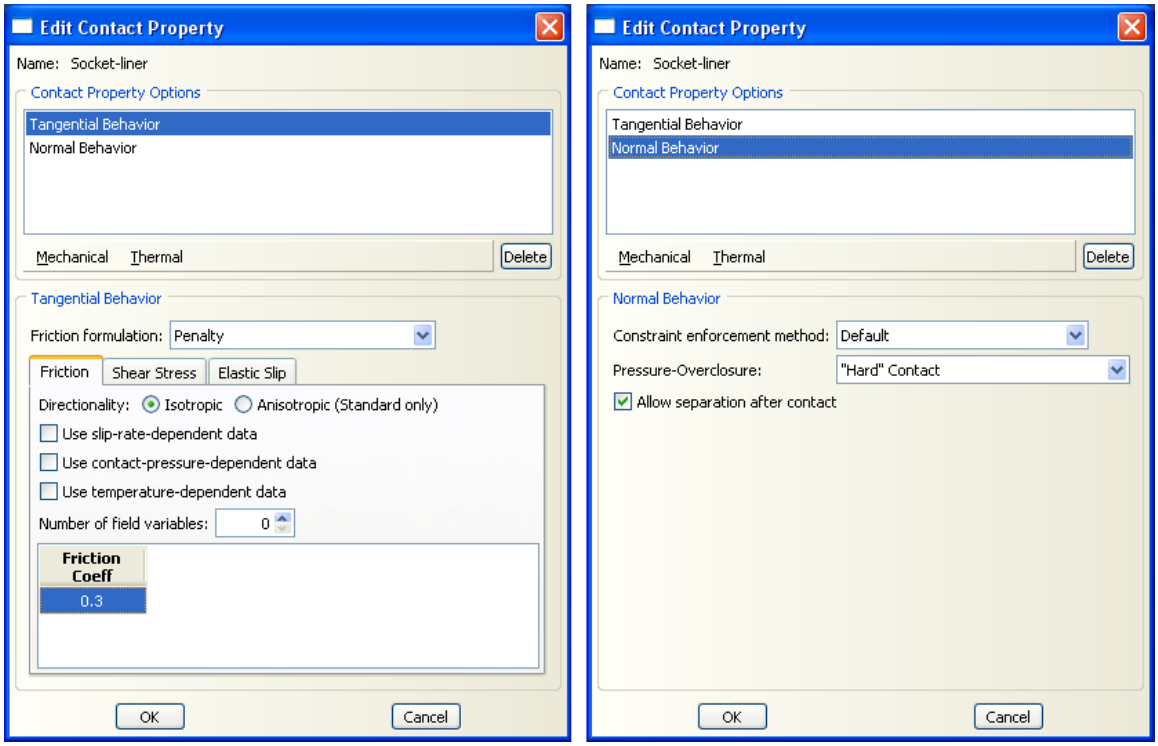

Figure 33: Socket interaction property with the gel liner

Load Module

In the load module the model developer will identify the Boundary Conditions (BCs), predefined field, and applied loads. In contact problems involving nonlinear geometric deformation identifying the BCs correctly and accurately is essential for analysis completion. If the BCs are not sufficient to prevent rigid body motion/rotation, severe discontinuity iteration arise signifying separation of contact surfaces and preventing the analysis from completion.

Boundary conditions: The femur is fixed in space along the top and bottom points as shown in Figure 34. All six degrees of freedom, translation and rotation, are constrained at the top and bottom points of the femur.

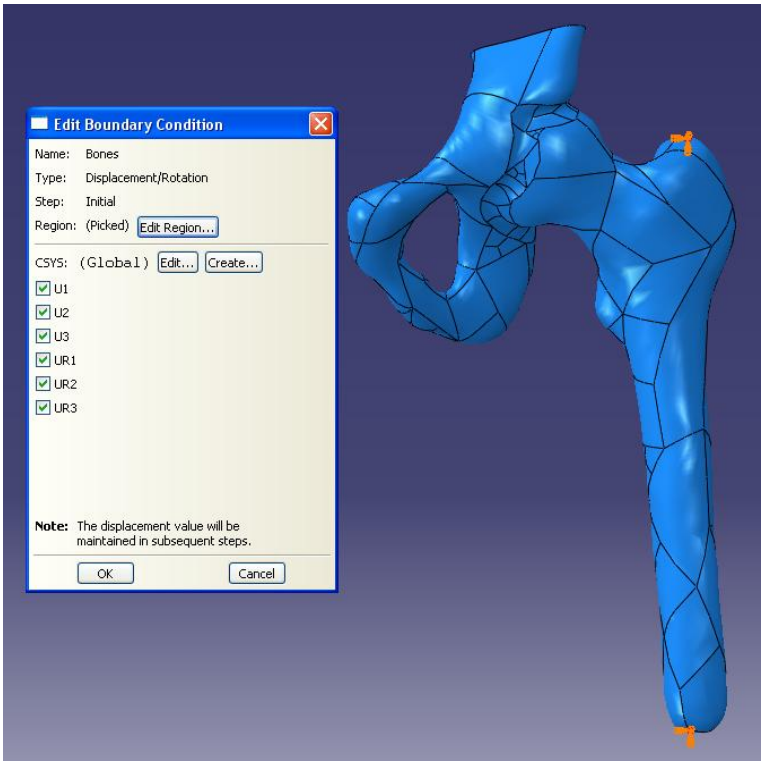

Figure 34: Boundary conditions applied to the RL

Predefined field: a temperature field constant through the thickness is applied to the socket in the expansion step. The predefined field is set to initial or zero value in the socket shrinkage step. During both thermal expansion and shrinkage a distal point on the socket is constrained in all six degrees of freedom. Figure 35 shows a predefined

thermal field of 5000 ºC applied to the prosthetic socket in the thermal expansion step and reset to initial in the thermal shrinkage step\

Loading: standing example, full body weight is applied vertically to the distal point of the socket (same point was previously constrained during the donning simulation). Figure 36 shows the load application point at the distal end with concentrated force of 800 *N* (equivalent to the patient's full weight of 180 *lb*).

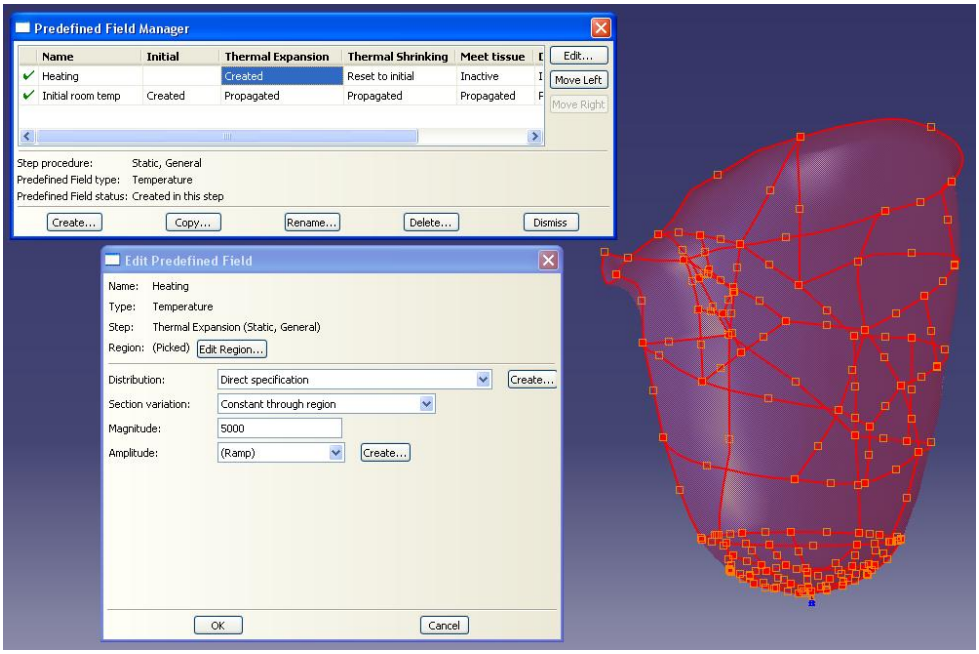

Figure 35: Predefined thermal field

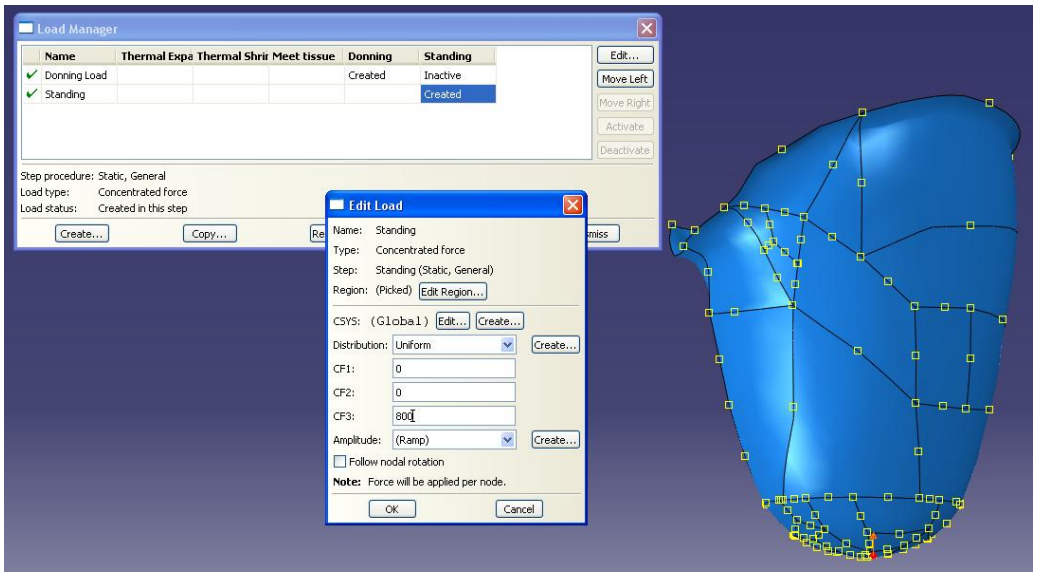

Figure 36: Applied load for standing load case

Job Module

The Job module is used to Data Check or to submit the developed FEA. The module defaults are accepted throughout. The analysis requires parallelization in order to become cost effective. Therefore 8 parallel processors are used to allow the simulation in general run under 30 minutes.

FEA Analysis Results

FEA being conducted according to computational anatomy principals facilitated extracting important information such as the function of gel liner in minimizing the pressure distribution over the RL, stress distribution versus pressure distribution over individual anatomical entities or undeformed versus deformed shape comparison.

Analysis results, a transtibial case

A transtibial case corresponding to TT01 is used to demonstrate the variety of information that can be extracted from the FEA. The FEA model specifics are obtained utilizing a mesh with 112600 C3D4 linear tetrahedrons elements for the anatomy and 1115 elements S4R shell elements for the socket, a total of 28409 Nodes with 114327 Degrees of Freedom. The analysis is performed in 25 minutes including standing or motion kinetics.

The pressure distribution, identifying the major function of the gel liner

At dual limb support pressure distribution over the gel liner is compared to the pressure distribution over the skin, i.e. on the RL. This comparison shows the function of the gel liner in terms of protecting the RL from excessive pressure. Figures 37 to 40 show pressure distribution comparison in the four different views, namely, anterior, posterior, lateral and medial views.

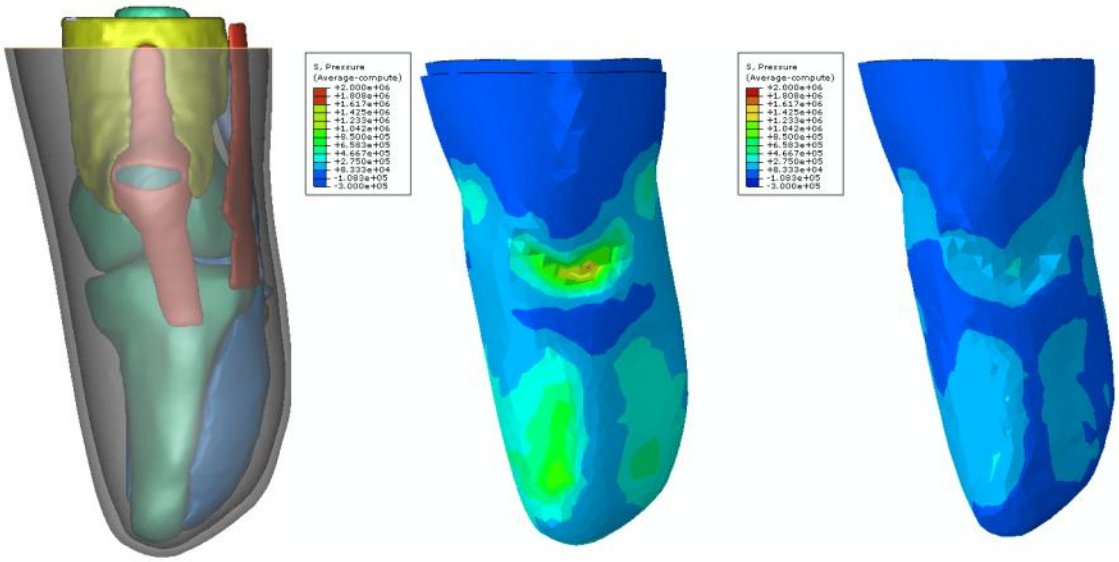

Figure 37: Pressure comparison over gel liner vs. skin – anterior view

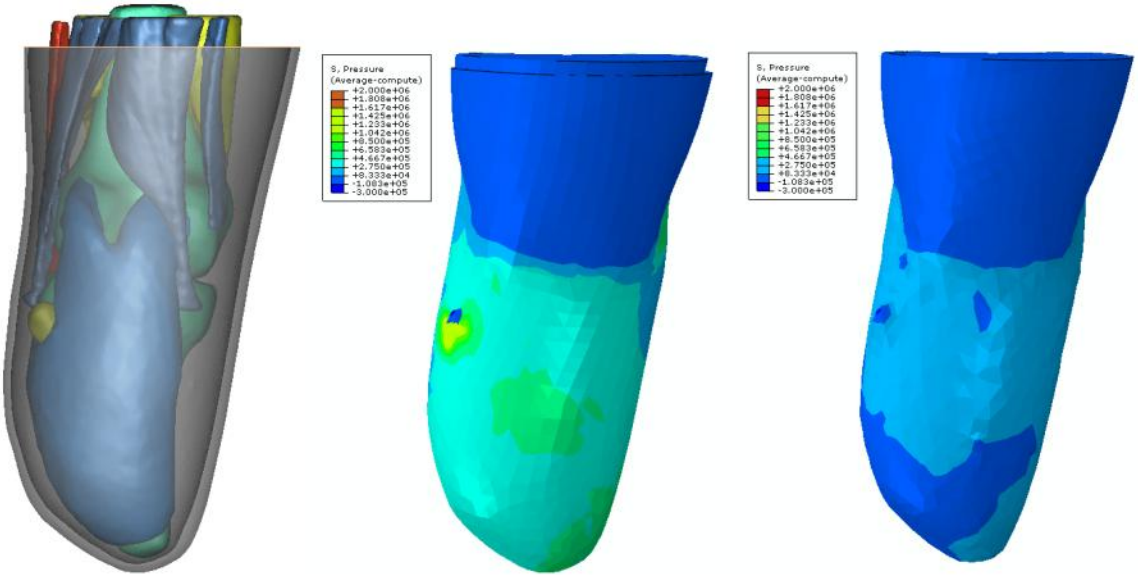

Figure 38: Pressure comparison over gel liner vs. skin – posterior view

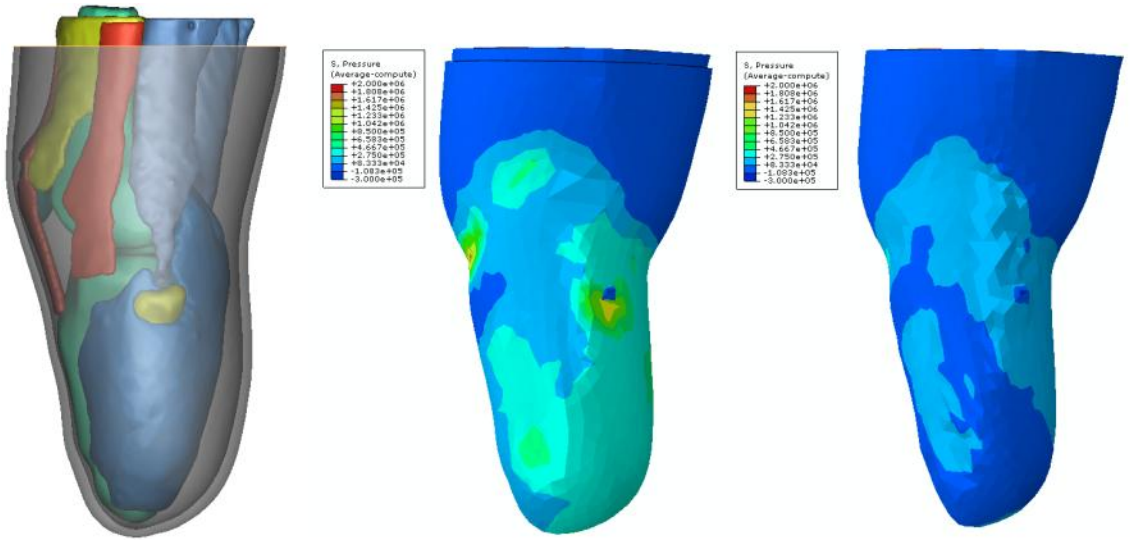

Figure 39: Pressure comparison over gel liner vs. skin – lateral view

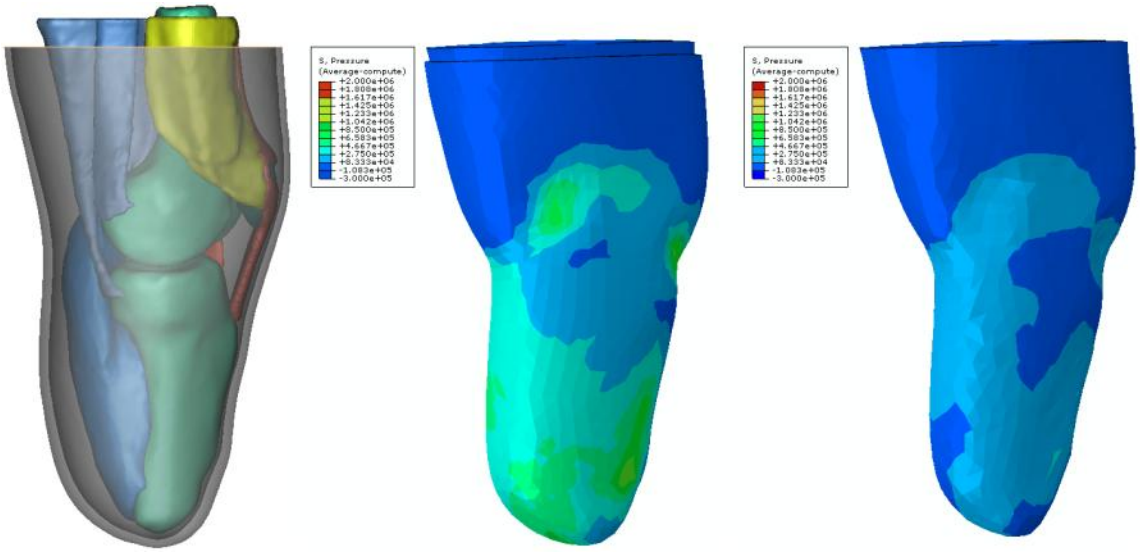

Figure 40: Pressure comparison over gel liner vs. skin – medial view

Also socket rectification efficiency can be seen in, for example, Figure 39 when noticing a pressure relief area around the fibula's head.

External versus internal load comparison, i.e. pressure versus stress

The patellar tendon/bar is studied by comparing the pressure (external load) versus the stress (internal load) at dual limb support. It can be noticed in Figure 41 that the pressure distribution at the tendon's attachment point to the tibia is very low. Meanwhile, this very low pressure corresponds to a high tensile stresses at the same

location. Will this tensile stress cause future complication to the patient, will it cause the tendon to adapt to its load requirements.

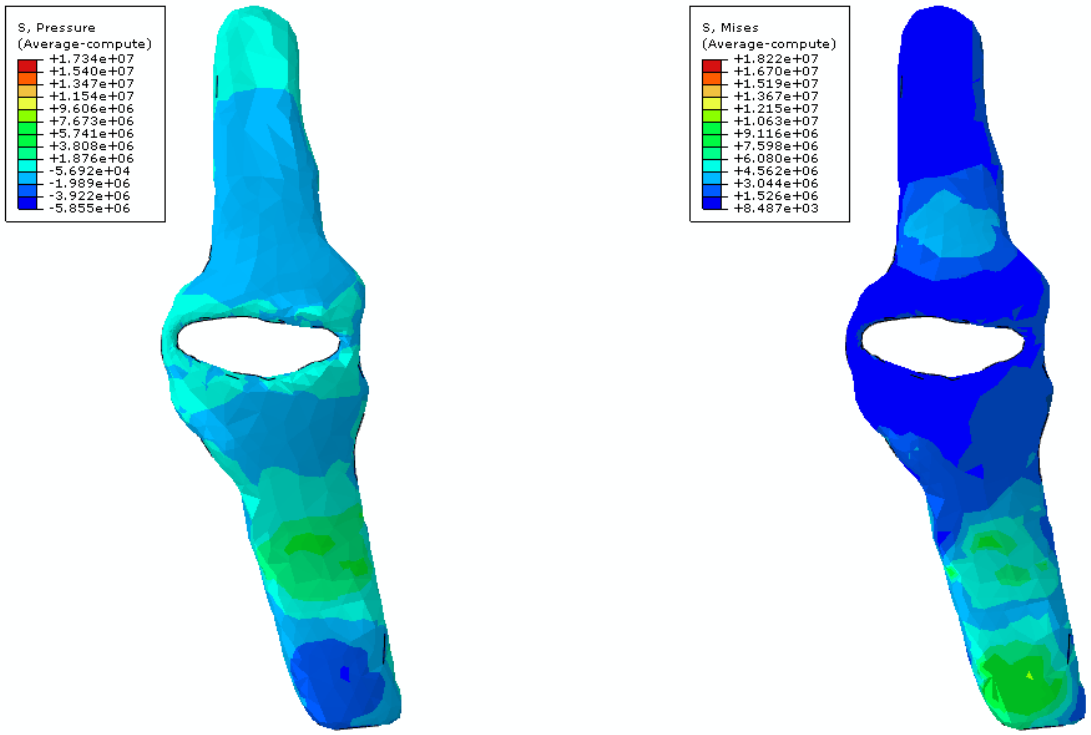

Figure 41: External vs. internal loads within the patellar tendon/bar

Undeformed vs. deformed shape comparison,

The gastroc shape is compared over stages of analysis, namely, deformed, after socket donning and at dual limb support. The deformed shape of a muscle (when compared in terms of volume reduction) determines the compressibility of the muscle and hence may become an important parameter used to identify muscle atrophy state. Figure 42 provides the undeformed versus deformed shapes of the gastroc together with the pressure distribution in loaded cases.

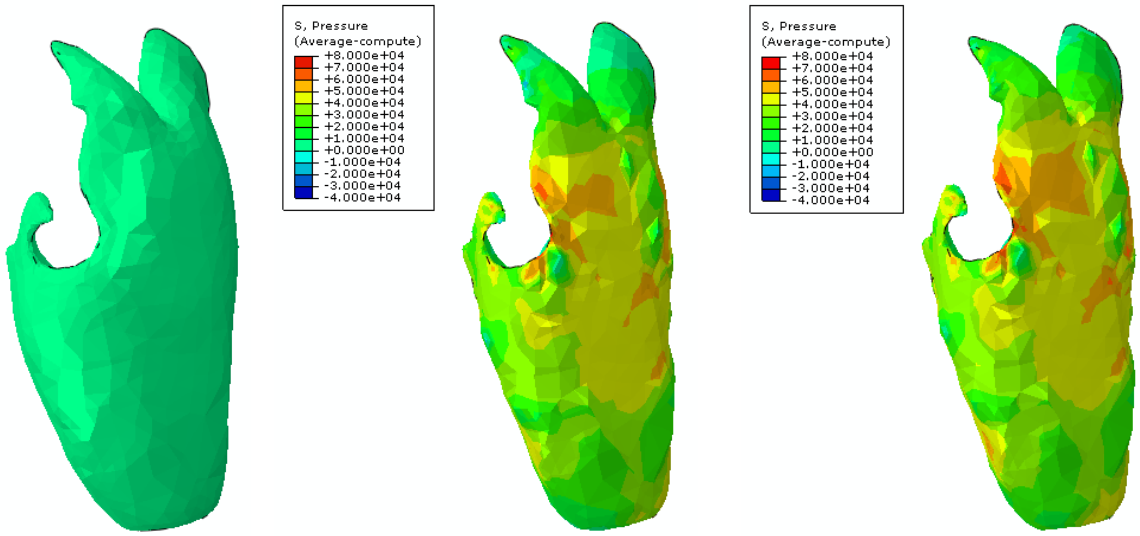

Figure 42: Undeformed shape vs. deformed shapes, associated to socket donning and dual limb support

Multiple data can be extracted from the FEA analysis. Meanwhile for the socket design purpose the pressure distribution over the skin is of specific importance. This pressure distribution should be compared with a reference value corresponding to the threshold of pain in order to optimize the socket shape. An animated simulation (video file) is attached to the manual to visually demonstrate the entire analysis)

A final illustration is depicted in Figure 43 showing a sectional view of the deformed shape in the case of dual limb support.

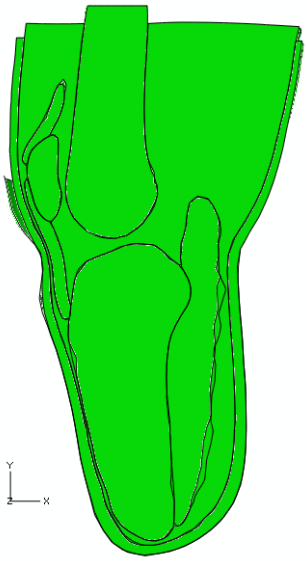

Figure 43: Sectional view in the deformed shape at dual limb support

Analysis results, a transfemoral case

A transfemoral case represents less challenge in modeling when compared to transtibial cases. Arriving at much simplified anatomy by merging anatomical features of the same family, e.g. all muscles, into one muscle community of simple shape is reason to the inherent simplicity of transfemoral case.

The pressure distribution, identifying the major function of the gel liner

The pressure distribution over the gel liner in this case is about one order of magnitude higher than the corresponding values over the fat tissue (i.e. skin). Figure 44 shows the efficient pressure reduction gained by using the gel liner. The function of the gel liner is well known and documented in literature meanwhile the current FEA present a quantitative tool rather than qualitative assessments of the gel liner. Figure 45 repeats the same results in Figure 44 using a different scale for the pressure distribution in the fat tissue. The pressure limits in this scale is about one order of magnitude less than the ones used for the pressure distribution in the gel liner.

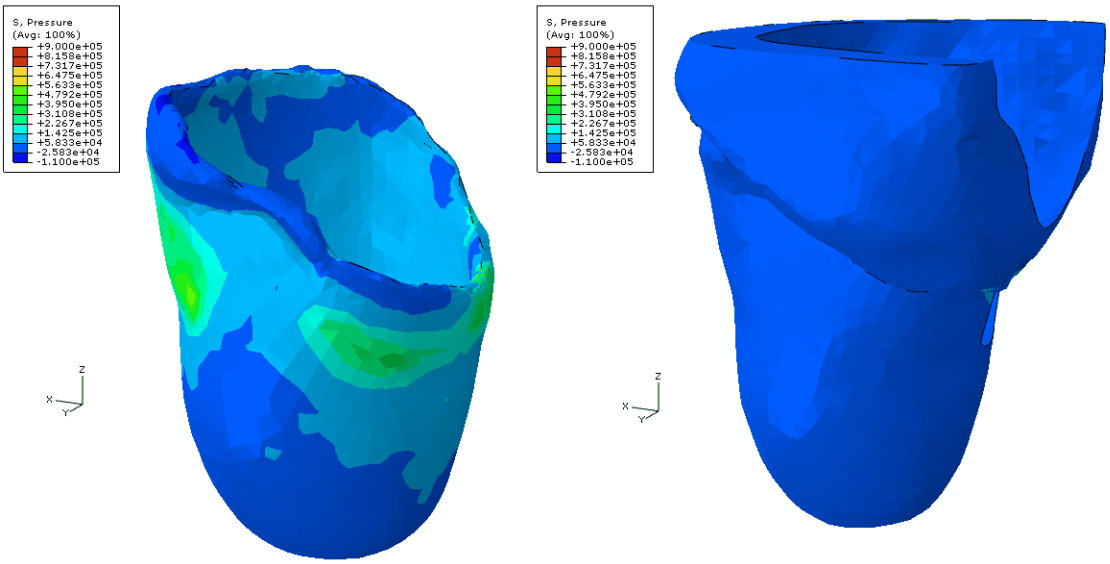

Figure 44: Pressure distribution over gel liner vs. skin – single limb support. Same pressure range or scale.

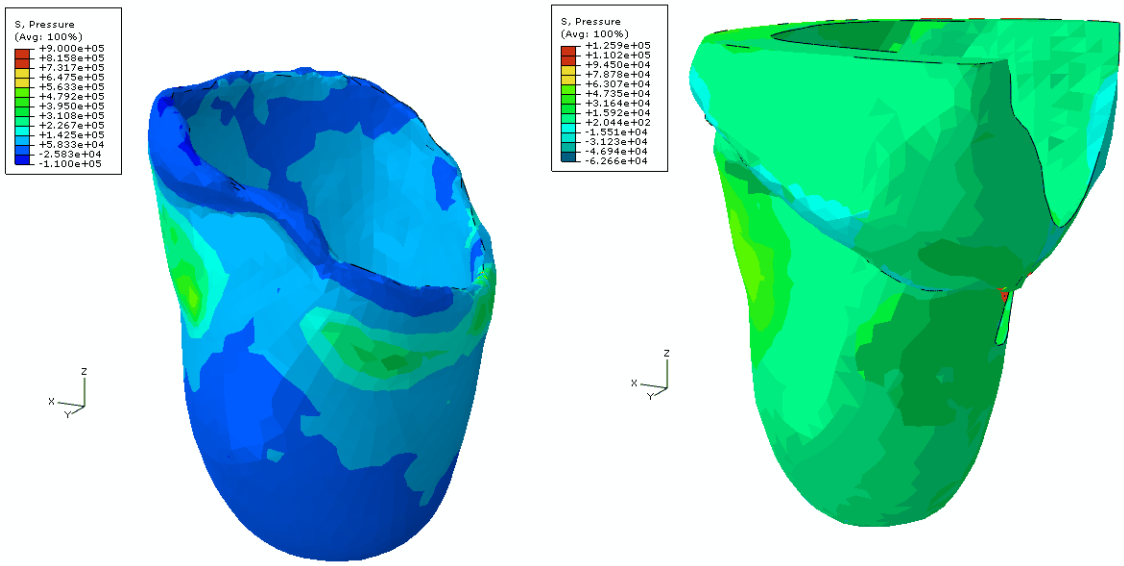

Figure 45: Pressure distribution over gel liner vs. skin – single limb support. Different pressure range or scale

The stress distribution, in the bones community

The stress distribution in the bones, Figure 46, shows very low stress distribution in the ischium. Figure 47 provides the stress distribution the bones with the socket in view.

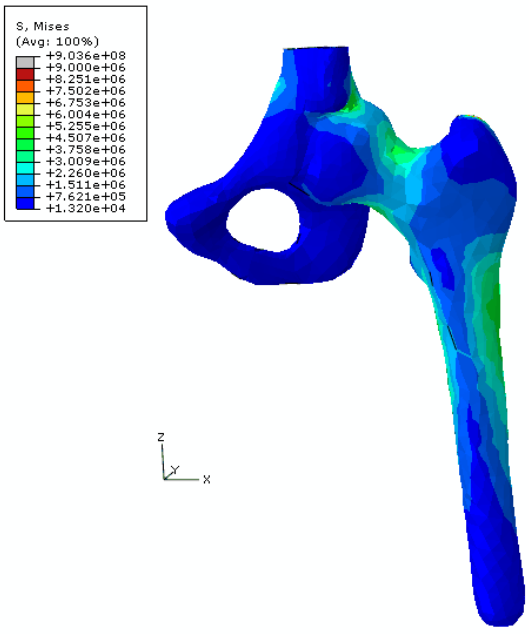

Figure 46: Stress distribution in the ischium

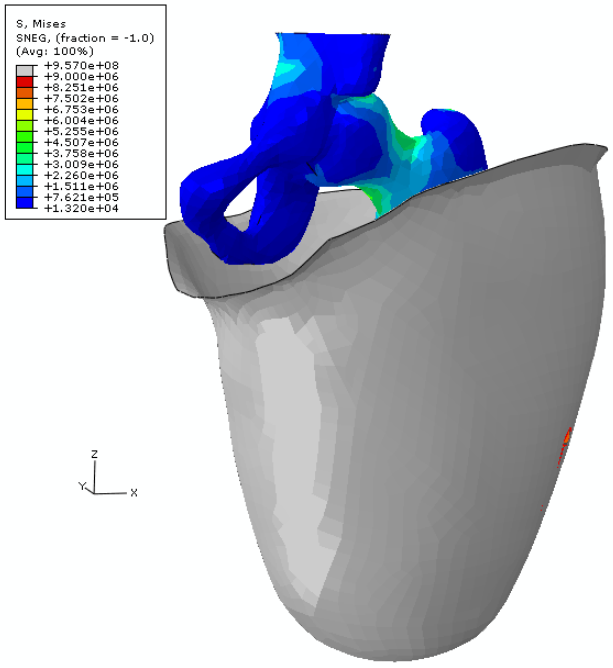

Figure 47: Stress distribution in the ischium with the socket in view

A section is performed in the deformed shape for single limb support loading case and shown in Figure 48.

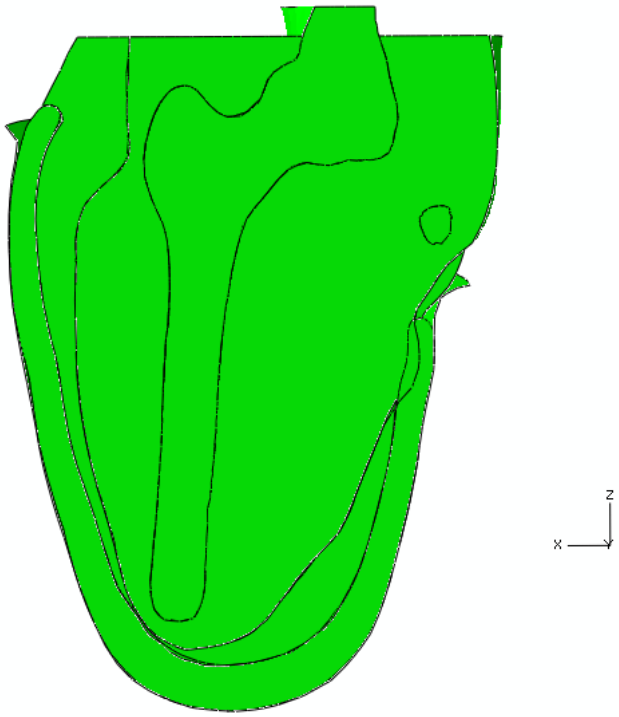

Figure 48: Sectional view for single limb support

FEA Challenges

Pressure measurements and verification

The pressure distribution over the RL limb is predicted using FEA. This pressure distribution is to be used to optimize the socket shape. Therefore the accuracy of the predicted values is of great importance. Hence verification of the predicted pressure by comparison to measured values is essential. The Zebra sensor system (SensorTech) was suggested as reliable pressure sensor that can conform to irregular geometry and is not associated with any size penalty being introduced as very thin sheets. Meanwhile the software that controls the data sampling process remains under continuous modifications and development to provide the intended versatility of data sampling. Also the sensor measurement system calibration process is still under developed. Therefore the data obtained from the Zebra sensors are not accurate. Consequently these data could not be used for the purpose of verification of the FEA predictions.

The Georgia Tech team MGDPS exhausted a multiple number of iterations in cooperation with SensorTech in order to extract accurate pressure measurements. Meanwhile all these attempts lead to no success. Pressure measurement as a validation step consumed good percentage of the time planned for further development and application of the FEA. Hence a major challenge is to measure the pressure within the socket in order to provide accurate verification of the FEA.

Figure 49: Sample of one of the Zebra Sensor sockets fabricated for TT01

Material models

The current material models used for soft tissue are obtained from open literature and optioned for healthy tissue. Meanwhile the mechanical properties of the soft tissue within the RL are dependent on the amputation history and the level of activity of the patient. FEA method can be used to predict or characterize the material properties of soft tissue combined with simple experiments.

FEA prosthetist

The FEA technique can be automated to perform the socket fitting trials on a patient to attain better socket fit. Meanwhile, the FEA cannot replace a prosthetist being licensed to work with human subjects as licensing issues will arise.

FEA Conclusions

Anatomically correct analysis

Anatomically correct FEA of prosthetic socket interaction with the RL is proposed and developed. The method proved repeatability and general applicability in the case of transfemoral, transtibial amputation alike. The current FEA allowed utilizing identifiable anatomical entities to construct the RL model. Therefore realistic conclusions were obtained regarding the socket fit in terms of inspecting the pressure/stress at critical sites of the RL. This allows the greatest understanding of sockets fit and rectifications and consequently provides a good foundation for enhancing their design.

Incorporating the history of RL health into the FEA (documenting deterioration or atrophy of muscle) will lower the cost of socket maintenance and also provide an insight for further development in the field. Predictive capabilities of the FEA can be utilized by assigning material models associated to less strength to tissues expected to atrophy and hence a better socket shape change/needs and future predictions.

Alternative accurate load measurements

The loading cases of FEA are mainly associated to simulating the socket donning, dual limb support, single limb support (prosthetic side) and walking gait. For the donning simulation there is no significant value for the applied load. While for the standing and walking exercises the iPECs system is used to measure the forces and moments applied to the distal end of the prosthetic socket (See Figures 50 - 52). Simple relationships are used to translate the measured loads to the proximal end of the socket and align the local axes of iPECS measurements with the socket's global system of

Figure 50: Subject TT01 on Diagnostic socket instrumented with ZEBRA socket pressure sensors and with an IPECs unit distal to the socket

axes. A sample data of standing exercise is provided within. In the standing exercise the patient is in dual limb support, and then lifts the sound side to attain single limb support (the prosthetic side). All forces and moments (kinetics data) are collected by the iPECS during this exercise. These loads are transferred at the distal end of the socket to be used in the FEA for standing simulation.

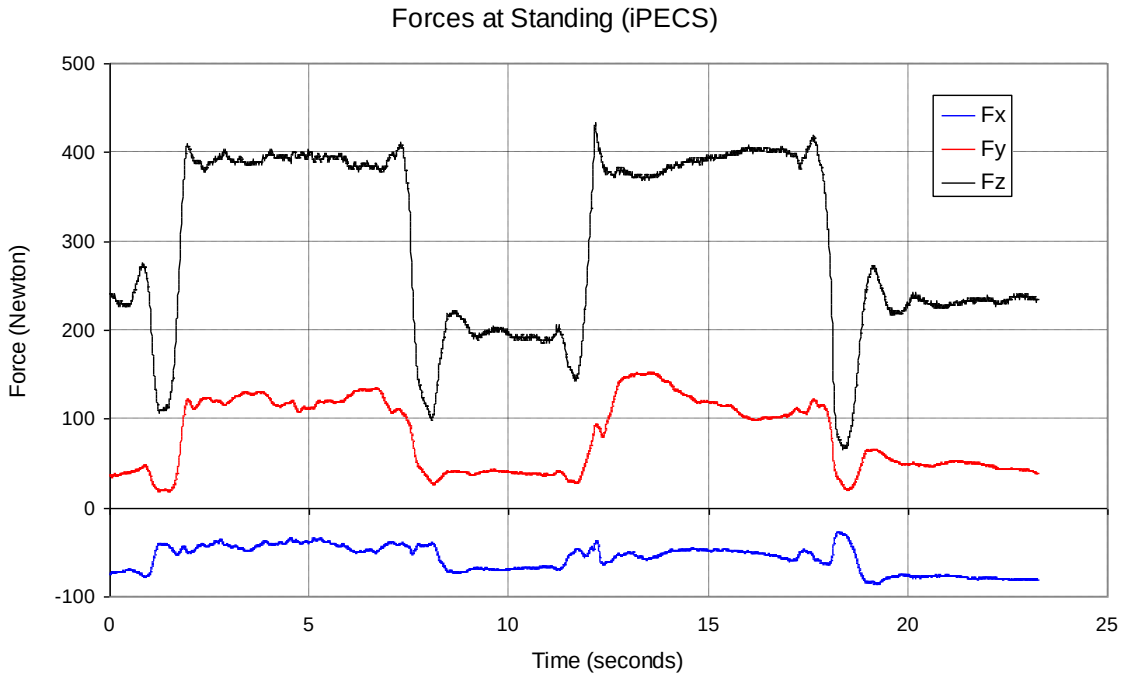

Figure 51: Standing exercise – force values

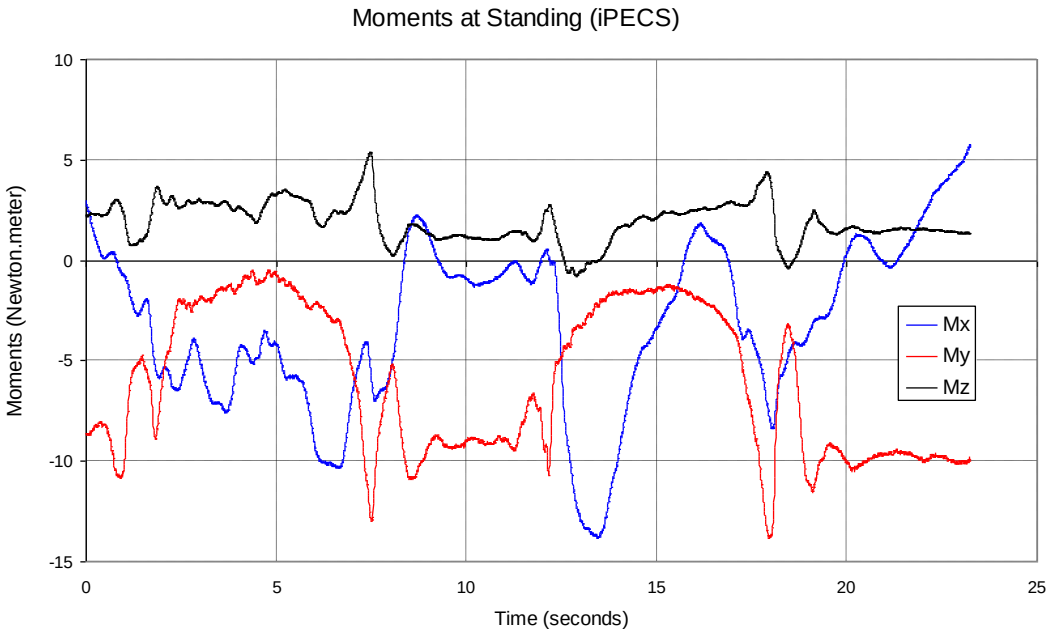

Figure 52: Standing exercise – moment values

FEA Suggested future work

The developed FEA methodology represents a first step towards a unified design environment of an adaptive socket. This claim is supported by the used software capabilities and the proven optimal communication. Shape changes of the RL during the course of the day and heat transfer simulations can be performed in *ABAQUS* simulation. Instrumented socket with sensors and actuators can also be modeled in *ABAQUS*. A great advantage is gained by utilizing Mimics Innovation Suite in the current tool by providing the modularity of medical image processing and geometry design and optimization.

Results and Discussion

This project endeavored to meet the following aims:

1. Develop a model acquisition protocol utilizing a Magnetic Resonance Image (MRI) of a person's residual limb (RL) for the initial model. This included both transfemoral (above the knee) and transtibial (below the knee) amputations.

2. Develop a protocol that would rectify the MRI acquired model by applying tissue density properties to the unique soft tissue structures of that RL so that a computer aided design (CAD) socket can be fabricated for that individual.

3. Test the fit of the CAD socket through instrumented gait analysis (IGA) and RL/socket interface pressure mapping.

4. Utilize the MRI model, CAD socket model and data gathered from the IGA and pressure interface mapping to generate a Finite Element Analysis (FEA) model of a dynamic prosthetic socket.

Aim #1: *Develop a model acquisition protocol utilizing a Magnetic Resonance Image (MRI) of a person's residual limb (RL) for the initial model. This included both transfemoral (above the knee) and transtibial (below the knee) amputations.*

This aim was met. The protocol is detailed in the non-deformational shell section and the MRI Scanning sections above.

Aim #2: *Develop a protocol that would rectify the MRI acquired model by applying tissue density properties to the unique soft tissue structures of that RL so that a computer aided design (CAD) socket can be fabricated for that individual.*

This aim was partially met. We did investigate and develop a process to rectify the MRI model so that CAD sockets could be fabricated for the subjects at both the transtibial

and transfemoral levels. The process, however, was not tied to unique tissue density properties of the residual limbs. These properties were estimated from the available literature however we were not able to validate these properties in our model without socket pressure measurements.

Aim #3: *Test the fit of the CAD socket through instrumented gait analysis (IGA) and RL/socket interface pressure mapping.*

This aim was partially met. The sockets that were fabricated for TT01 Subject were tested through instrumented gait analysis as well as force/moment analysis through the use of the IPECs component by College Park. We attempted to quantify the RL/socket interface through multiple iterations of sockets and Zebra sensor systems however this critical component was not successful. We did not have additional subjects ambulate in the gait lab.

Aim #4: *Utilize the MRI model, CAD socket model and data gathered from the IGA and pressure interface mapping to generate a Finite Element Analysis (FEA) model of a dynamic prosthetic socket.*

This aim was met. Finite element analysis was performed on the modified sockets generated from the processes above. A novel solution to virtual socket donning was established using thermal expansion to shrink the virtual socket onto the residual limb rather than push the socket up onto the limb as is done in reality.

Benefits Analysis (including final metrics tables)

The benefits from this project at its conclusion are the establishment of processes that will be beneficial to utilizing this approach to fabricating prosthetic sockets once the expressed limitations are overcome. The specific beneficial processes developed through this project include:

- **Process 1:** Fabrication of a non-deformational shell for either transfemoral or transtibial residual limbs utilized to simulate the residual limb anatomy.
- **Process 2:** MRI Scanning protocols. Through the collaboration with Dr. Terk at Emory and the research team at Georgia Tech, protocols for positioning as well as for scanning were established for both transtibial and transfemoral subjects.
- **Process 3:** Transferring MRI DICOM files and Segmentation of the residual limb tissue components and liner could be performed.
- **Process 4:** The residual limb modeling process was established and refined through the six socket iterations.
- **Process 5:** CAD Socket rectification. This process was established taking the STL files from 3 Matic and transferring them to CANFIT for rectification. Once rectified, the socket was converted back to a STL file with the orientation maintained thereby allowing comparison of the socket to the underlying anatomy in 3-Matic as well as to facilitate the finite element analysis in ABAQUS.
- **Process 6:** Refining the residual limb anatomical structures in preparation for finite element analysis.
- **Process 7:** Finite element analysis of donning a socket onto a residual limb as well as loading the residual limb in single and double limb standing.

Implementation Status

In order for this project to transition to a clinical feasible platform, a number of limitations will need to be overcome. First of all, the outcome from this process must be significantly better than the existing “sockets by experience” methods being utilized today as the costs will greater. Outcomes that would justify the increased cost would be:

- The ability to predict the sockets a wearer will need over time as the process of edema reduction and residual limb atrophy is quantifiable. In theory, one scan could be completed and the sockets the wearer will need over the next 6 months to a year could be fabricated and ready for them in advance.
- The ability to custom fabricate sockets that are optimized for pressure distribution thereby creating and “ideal” socket for that wearer.
- The ability to optimize the socket configuration so that instead of a static socket, a dynamic, multi property socket could be road mapped through FEA and then fabricated through advanced socket fabrication techniques.

The greatest limitation to the projects’ implementation was a method to obtain accurate and reliable socket pressure information. Multiple iterations of the Zebra Socket system by SensorTech were applied but in the end the results were not reliable. Without pressure data, the FEA assumptions cannot be validated and hence, there is no means to optimize the socket fitting process in the virtual world.

Other limitations to implementation include tissue segmentation from the MRI scans. This process needs to be automated. While Materialise was quite responsive to the feedback we provided them and they released multiple versions during the course of the project, the segmentation still leaves much to be desired. The time required to complete the segmentation process is highly dependent upon the experience of the person performing the segmentation process.

Once the segmentation is complete, the prosthetists’ input is required in order to rectify the residual limb socket model. Here again, the experience of the prosthetist plays a role in the rectification process. Ideally this process could be driven automatically depending on the quantity and quality of the underlying soft tissues but at this time, the rectifications must be done manually in order to have a jumping off point. Once we have enough data from residual limb/socket interfacing through finite element analysis, an algorithm could be created to automatically rectify residual limb models. Given that we do not yet have a means to obtain pressure information in order to validate the finite element analysis, we are still a ways off from automatic socket rectifications based on a segmented residual limb from and MRI scan alone.

In Summary, while this project was not able to meet all if its ambitious aims, it did make significant progress in developing processes towards meeting these aims. Automated prosthetic socket fabrication from MRI scanning is possible at this time, however not necessarily cost effective. As the software continues to improve and the costs associated with scanning decline, it is conceivable that MRI scanning will be not only feasible but will eliminate much of the guess work from prosthetic socket fabrication.

This project demonstrated that is possible to utilize of Finite Element Analysis for prosthetic socket fit assessment. We were not able to take the analysis to its full capacity for lack of accurate and reliable socket pressure measurements. Technology in this realm also continues to improve and it is likely that the ability to identify socket pressures in real time will be a reality in the next few years.

Given the progress made on this project, it will be feasible for prosthetic socket fabrication and optimization to be made from MRI scans in the near future. Critical steps towards this reality have been made as a result of this Medical Image Generated Dynamic Prosthetic Socket project.

References

1. Zhang, M., A.F. Mak, and V.C. Roberts, *Finite element modelling of a residual lower-limb in a prosthetic socket: a survey of the development in the first decade.* Medical Engineering & Physics, 1998. **20**(5): p. 360-373.
2. Zheng, Y.P., A.F. Mak, and A.K. Leung, *State-of-the-art methods for geometric and biomechanical assessments of residual limbs: a review.* Journal Of Rehabilitation Research And Development, 2001. **38**(5): p. 487-504.
3. Portnoy, S., et al., *Real-time patient-specific finite element analysis of internal stresses in the soft tissues of a residual limb: a new tool for prosthetic fitting.* Annals Of Biomedical Engineering, 2007. **35**(1): p. 120-135.
4. Douglas, T.S., et al., *Automatic segmentation of magnetic resonance images of the trans-femoral residual limb.* Medical Engineering & Physics, 1998. **20**(10): p. 756-763.
5. Buis, A.W.P., et al., *Magnetic resonance imaging technology in transtibial socket research: a pilot study.* Journal Of Rehabilitation Research And Development, 2006. **43**(7): p. 883-890.
6. Smith, K.E., et al., *Validation of spiral CT and optical surface scanning for lower limb stump volumetry.* Prosthetics and Orthotics International, 1995. **19**(2): p. 97-107.
7. Zachariah, S.G., J.E. Sanders, and G.M. Turkiyyah, *Automated hexahedral mesh generation from biomedical image data: applications in limb prosthetics.* Rehabilitation Engineering, IEEE Transactions on, 1996. **4**(2): p. 91-102.
8. Shuxian, Z., Z. Wanhua, and L. Bingheng, *3D reconstruction of the structure of a residual limb for customising the design of a prosthetic socket.* Medical Engineering & Physics, 2005. **27**(1): p. 67-74.
9. Peery, J.T., et al., *A Three-Dimensional Finite Element Model of the Transibial Residual Limb and Prosthetic Socket to Predict Skin Temperatures.* Neural Systems and Rehabilitation Engineering, IEEE Transactions on, 2006. **14**(3): p. 336-343.
10. Douglas, T., et al., *Ultrasound imaging in lower limb prosthetics.* Neural Systems and Rehabilitation Engineering, IEEE Transactions on, 2002. **10**(1): p. 11-21.
11. Lee, W.C.C., et al., *Finite element modeling of the contact interface between trans-tibial residual limb and prosthetic socket.* Medical Engineering & Physics, 2004. **26**(8): p. 655-662.
12. *MIMICS Accuracy*. [cited 2009 October]; Available from: www.materialise.com.
13. Jamali, A.A., et al., *Linear and angular measurements of computer-generated models: Are they accurate, valid, and reliable?* Computer Aided Surgery, 2007. **12**(5): p. 278-285.
14. Gelaude, F., J.V. Sloten, and B. Lauwers, *Accuracy assessment of CT-based outer surface femur meshes.* Computer Aided Surgery, 2008. **13**(4): p. 188-199.
15. Radcliffe C.W., F.J., *The patellar-Tendon Bearing Below Knee Prosthesis*. 1961: University of California Biomechanics Laboratory.

Attachment D

POMI Technical *Final* Report from SensorTech

November 2010

The smart socket system is complete. Specifically, SensorTech has completed the design of the sensor materials, data acquisition system, customized computer, software, and accessories as it pertains to Task Order 005 Subcontract No. 2008-547 (Note: the Task Order, however, has been completed in 2010 using SensorTech self-funded resources).

The system is now called ZEBRA™ 3D Pressure Mapping System. Detailed specification information and photos are available for downloading at the following three Internet links:
http://www.sensortechcorp.com/pdfs/Zebra_Brochure.pdf
http://www.sensortechcorp.com/pdfs/Zebra_Prosthetics_Brochure.pdf
http://www.sensortechcorp.com/pdfs/Zebra_Orthotic_Brochure.pdf

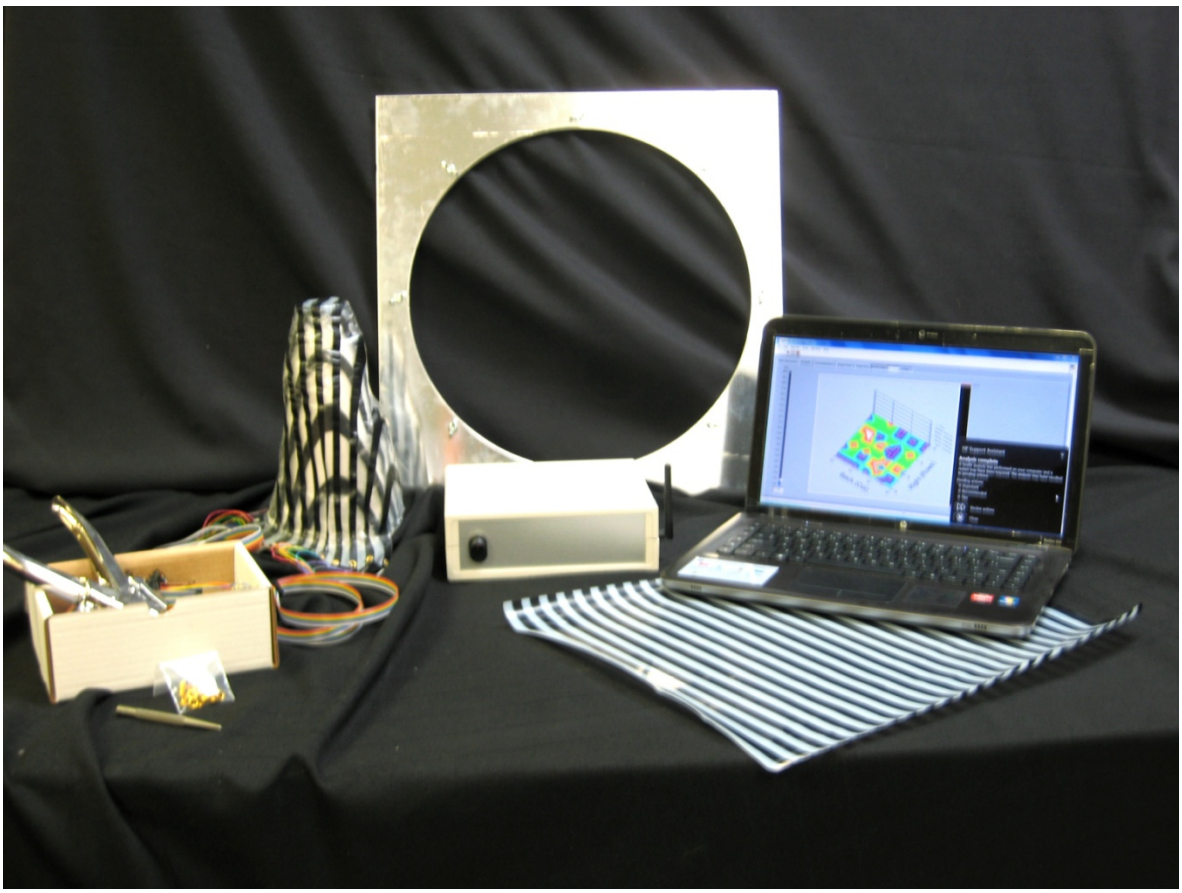

The ZEBRA™ System consists of thermoformable multi-point sensors wired to a data acquisition system that sends data messages via an ad hoc Wi-Fi wireless network to a custom computer with custom software that enables data recording and display.

For Report purposes some of the key technical data includes:

- Supports up to 16 x 16 Zebra stripes (horizontal “rows” and vertical “columns”), i.e. 256 sensor data points
- Provides a maximum data rate of 1,000 measurements per second (1 kHz).

The scan rate is determined by the scan delay, which is the time after the channel is selected before the measurement is taken, to allow for settling of the signal. Currently, firmware Release 1.0 has a 1 millisecond scan delay.

- The number of frames per second is determined by the number of rows and columns.

  A "frame" is one group of readings of all the intersecting points of the Zebra Sheets. For example an 8 x 8 array has frames of 64 data points.

  The number of frames per second is calculated by dividing the scan rate (1,000 per second) by the number of data points. For example an 8 x 8 array can be scanned at a rate of 1,000 / 64 = 15.6 frames per second.

- Powered by an AC adaptor and/or a Li-ion rechargeable battery
- The Wi-Fi wireless network communication is configured as an "ad-hoc" local network, between a Zebra Data Acquisition System and a customized laptop PC with the Zebra 3D Pressure Mapping Software, installed at SensorTech.
- All inputs and outputs have built-in short circuit protection and electrostatic discharge protection
- Noise reduction is achieved by high-speed digital averaging of measurement data.
- Excitation voltage for columns is 12 Volts DC.

Model 1.0 of the Zebra Data Acquisition System and Release 1.0 of the Zebra firmware works with Release 1.0 of the Zebra 3D Pressure Mapping Software. The features include:

- Real-time display of Zebra Pressure Mapping Sensor data in the form of graphs, and a table of PSI values.
- Calibration of Zebra Pressure Mapping Sensor data
- Storage of readings in standard comma-separated value file format, with the .CSV file extension.
- Playback and display of saved readings at a variable frame rate or one frame at a time.

The ZEBRA™ Sensors themselves have been modified extensively since the previous report in March 2010. The use of UHMWPE and carbon black in composite form are still the primary material components. However, the formulation and fabrication methodology have been significantly altered and improved. Changes include:

- Conductivity levels
- Type of UHMWPE
- Molding process
- Alternating "stripe" fabrication
- ~~Scything~~ Skiving process
- Lamination process
- Thermoforming process
- Calibration process

If there are any questions about the above information please contact:

Andrew Clark, PhD, Chief Technology Officer
aclark@sensortechcorp.com
864-298-0684

A ZEBRA™ System and 10 ZEBRA™ Sensor Sheets are ready to be delivered to Walter Reed Hospital once delivery details are provided. WE STRONGLY RECOMMEND THAT A TIME AND VENUE BE SET-UP FOR SENSORTECH PERSONNEL TO TRAIN WALTER REED PERSONNEL IN THE USE OF THE ZEBRA™ SYSTEM.

Final report prepared by: David Myers, CEO

David Myers
CEO, SensorTech Corporation
dmyers@sensortechcorp.com
www.sensortechcorp.com (updated 28Sep10)
Mobile 864-985-3334

sensortech™
SMART POLYMER SENSOR SOLUTIONS
100 Industrial Drive
Greenville, SC 29607
864-298-0684

Attachment E

MENTIS SCIENCES, INC.

Instruction Manual for 64 Carrier Braider Manufacturing Cell for Prosthetics Production

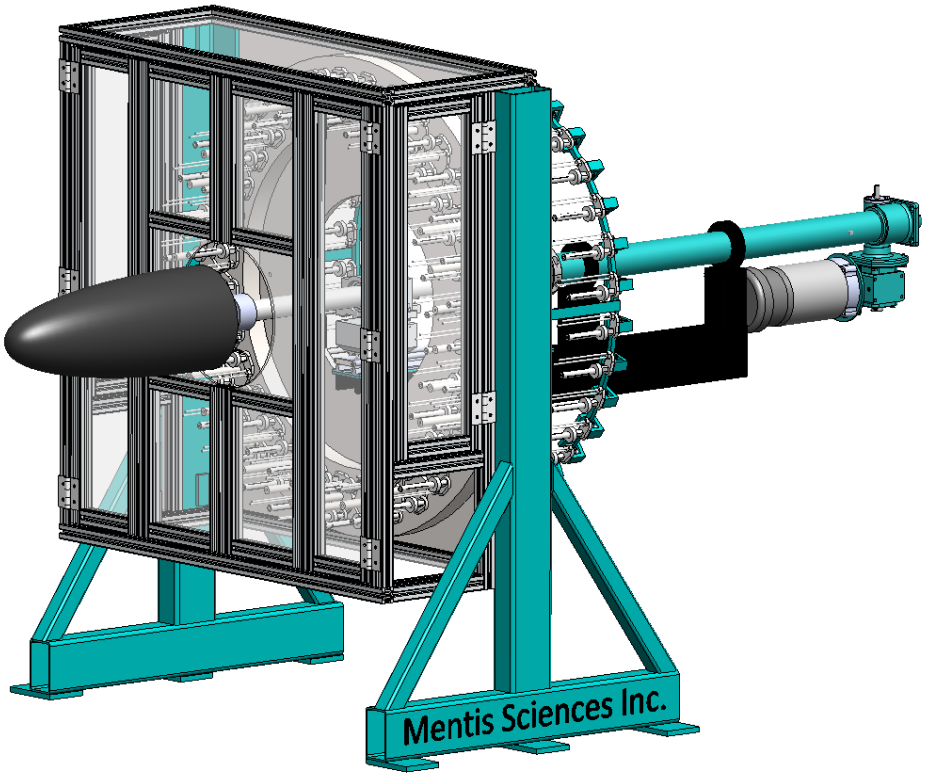

MENTIS SCIENCES, INC.

Contents

Introduction

This method of manufacture of prosthetic sockets and possibly other Prosthetic and Orthotic Appliances utilizes textile braiding manufacturing processes with aerospace fibers such as graphite or Kevlar, along with high performance resins, to create sockets that are stronger and lighter weight than conventionally manufactured sockets. The process generates a very accurate negative replica of the patient's residual limb, thus adding to the comfort of the patient.

The braiding process is flexible allowing incorporation of woven cloth into the braiding process for added reinforcement at selected areas, for example, where cut outs may be desired. The method also dramatically decreases the production time and cost of the prosthetic relative to conventional methods, which are very labor intensive.

The Integrated Braider Manufacturing Cell (BMC) consisting of a Braider, a Gantry that holds a mandrel for shaping the braided product, the control box with associated software and cabling, which regulates the speed of the Braider and Gantry, finally an environmental enclosure system to protect the operator.

This Manual covers the operation and maintenance of a 64 carrier Braider system with Gantry, control box, and environmental enclosure.

Braider Diagram

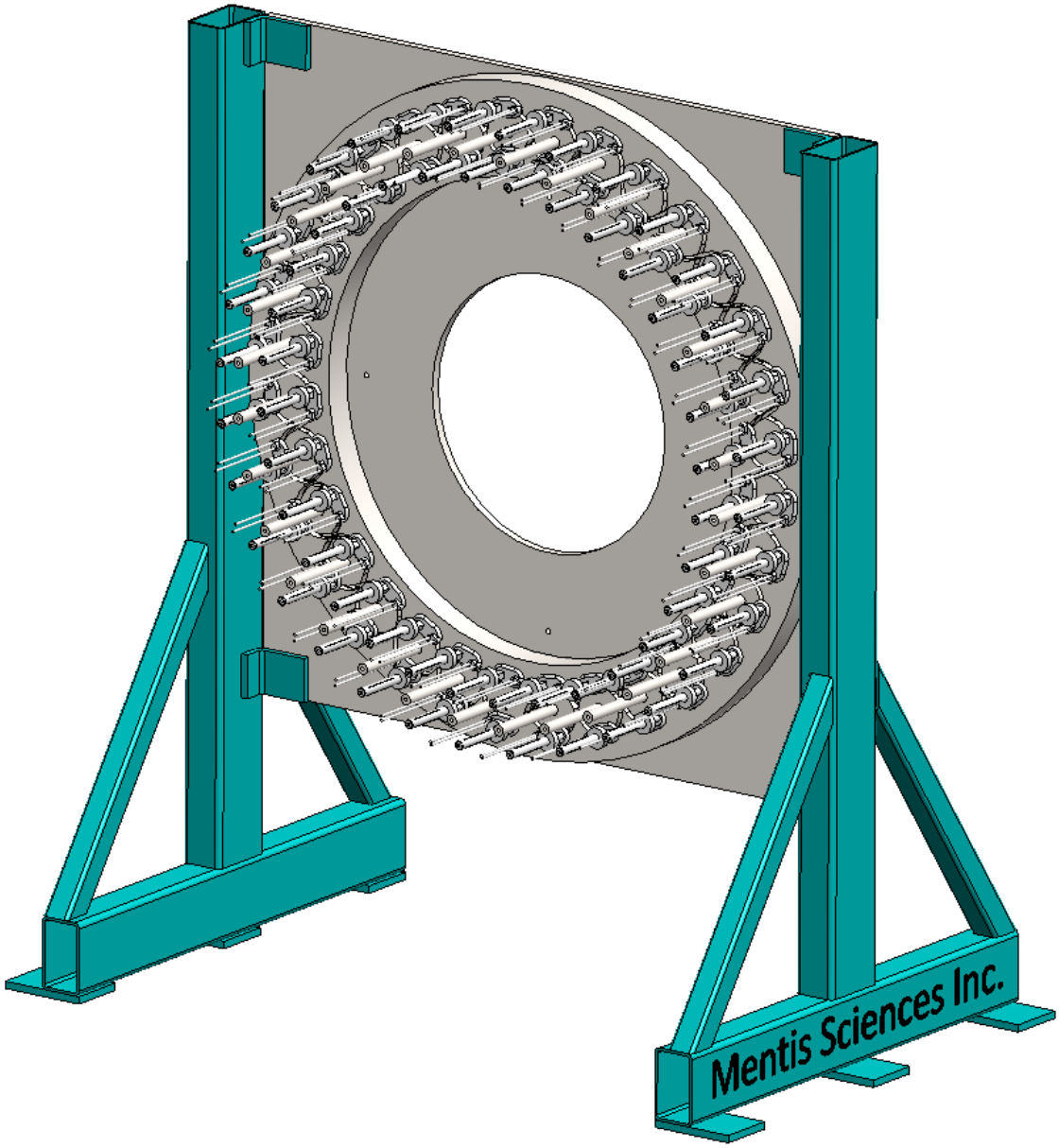

Figure 1

Description of braider:

1. 64 carrier composite braider (figure 1)
    a. Two A/C drive motors 480Vac 3 phase (not pictured)
    b. Qty. 64 of 2BX carriers
    c. 12” braid ring (not pictured)
2. For complete braider diagram refer to parts breakdown manual located in control box

Braider Components

Carrier

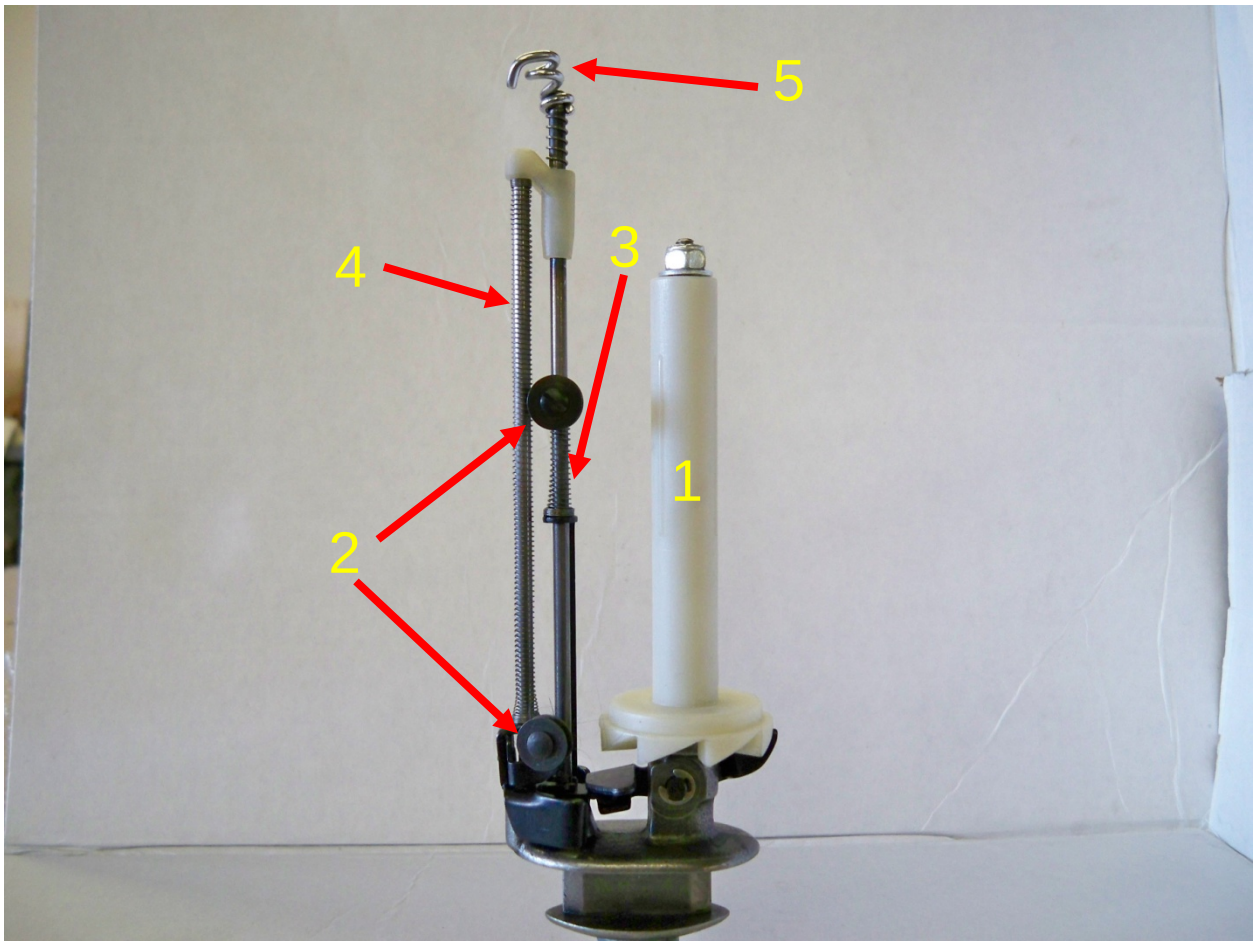

Figure 2

Description of carrier: (figure 2)

1. Cop Holder
    a. Holds the bobbin on the carrier
2. Sheave Wheels
    a. Transmits the fiber through the carrier
3. Pawl Spring
    a. Controls the payout of fiber from the bobbin
4. Tension Spring
    a. Controls the amount of tension on the fiber
5. Threaded Eyelet
    a. Holds the fiber upon exit of the carrier

Braider Components

Bobbins

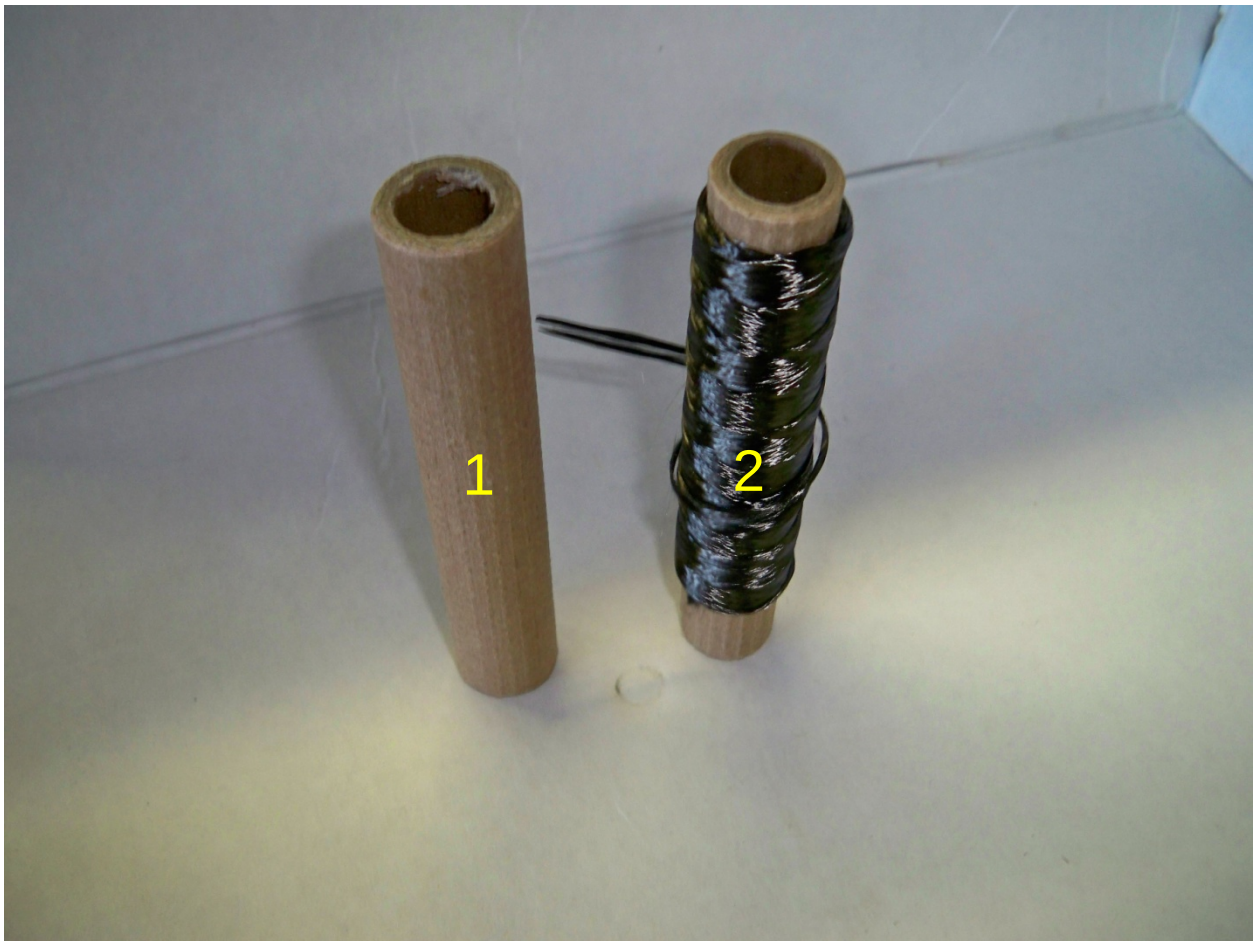

Figure 3

Description of bobbin: (figure 3)

1. Card Board Bobbin
    a. 5.25” L x 0.90” OD x 0.65” ID
2. Card Board Bobbin with Wound Fiber
    a. Amount of wound fiber depends on material

Braider Components

Carrier and Bobbin Assembly

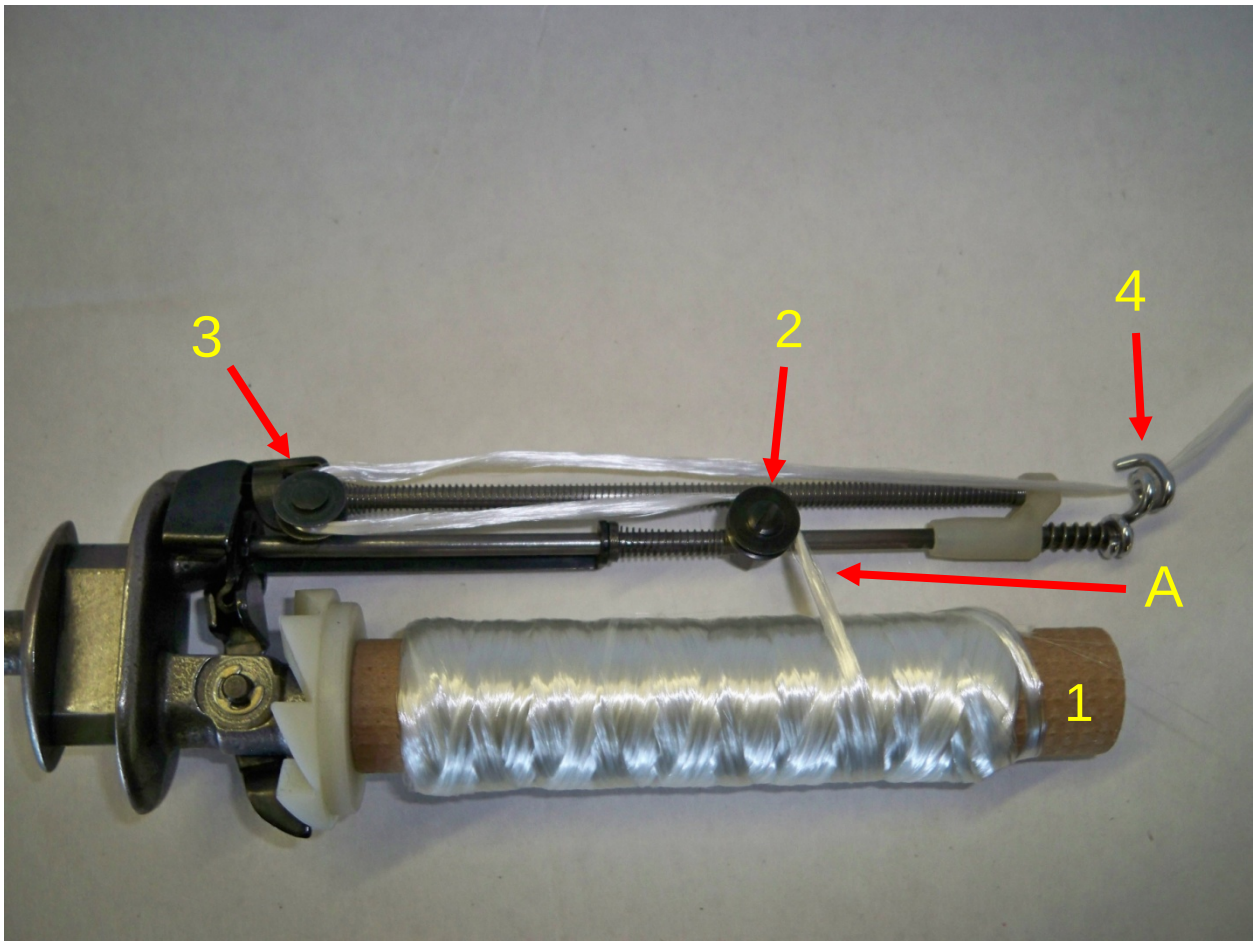

Figure 4

Description of assembly: (figure 4)

1. Place bobbin with wound fiber onto cop holder
    a. The direction of the bobbin must have the fiber coming over the top as shown in the assembly picture labeled as A
2. String fiber over top of the middle sheave wheel heading towards rear sheave wheel
3. Continue fiber under rear sheave wheel and pull towards threaded eyelet
4. Run fiber through threaded eyelet

Braider Usage

Unloading Bobbins

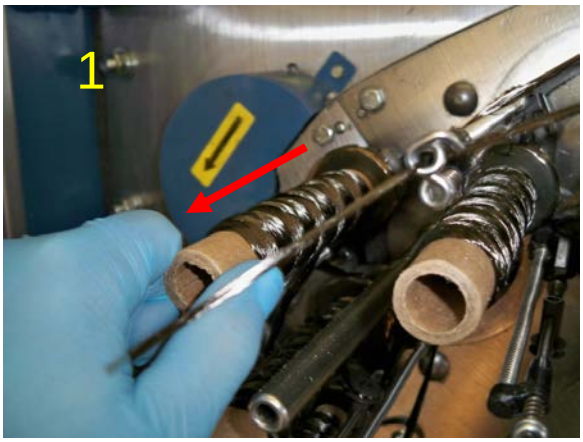

Figure 5

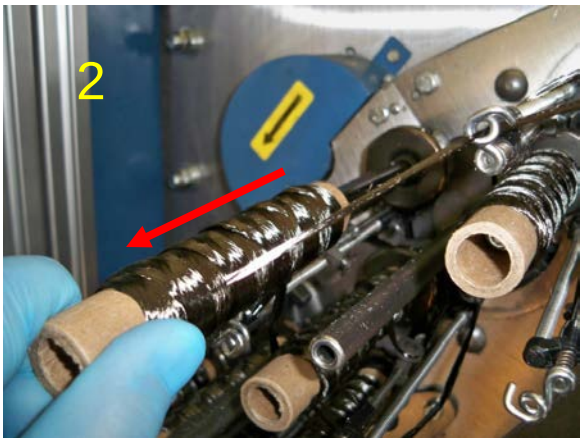

Figure 6

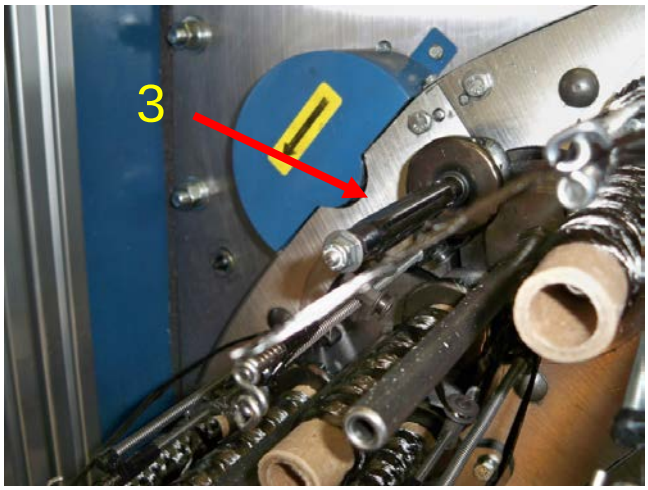

Figure 7

Description of Unloading Bobbins:

1. Firmly grab cardboard bobbin (figure 5)
2. Pull cardboard bobbin towards yourself removing it from the carrier (figure 6)
3. Carrier is now empty (figure 7)
    a. Repeat steps 1 and 2 until all bobbins are removed

Braider Usage

Unloading Carriers

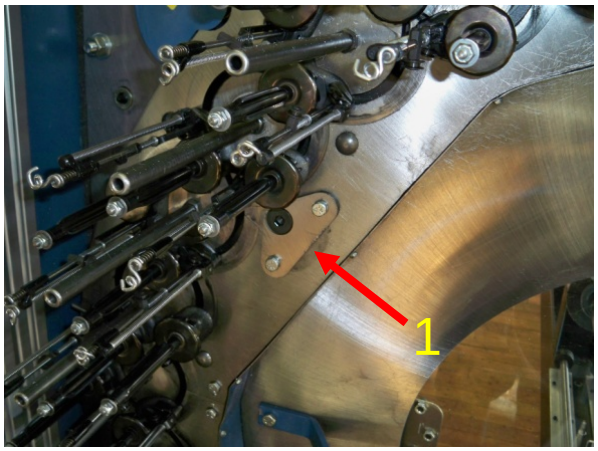

Figure 8

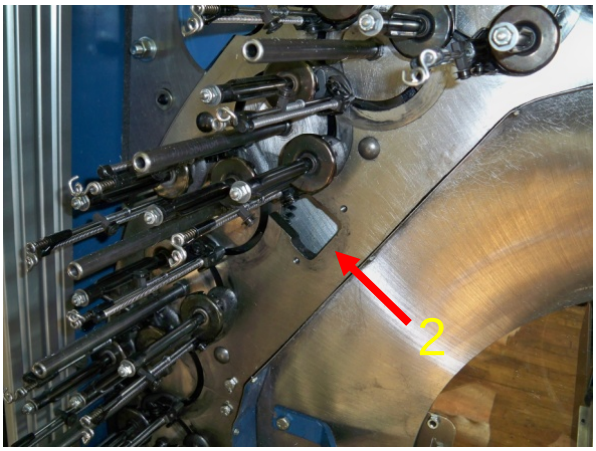

Figure 9

Description of Unloading Carriers:

1. Remove the two 7/16 bolts holding the deck key in place (figure 8)
2. Remove the deck key to access carrier removal slot in braider (figure 9)

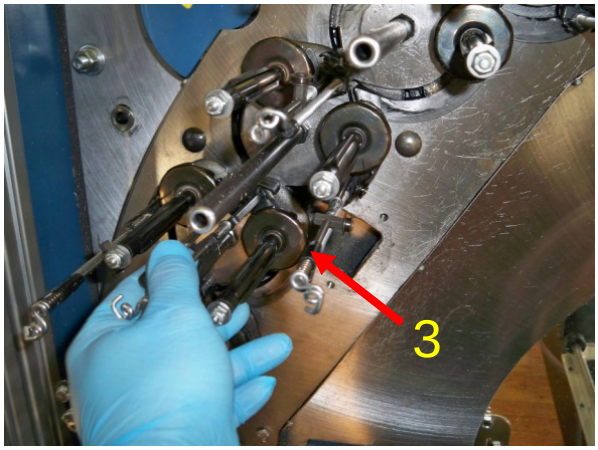

Figure 10

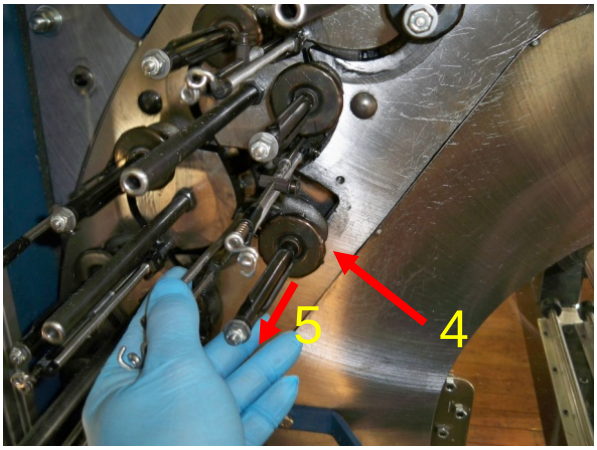

Figure 11

3. By using the jog button on the control box (refer to figure 68), jog the braider only to move carrier into carrier slot (figure 10)
4. With your hand, guide carrier into slot
5. Remove carrier by pulling carrier towards yourself (figure 11)
    a. Repeat steps 3, 4, and 5 until all carriers are removed

Braider Usage

Unloading Carriers

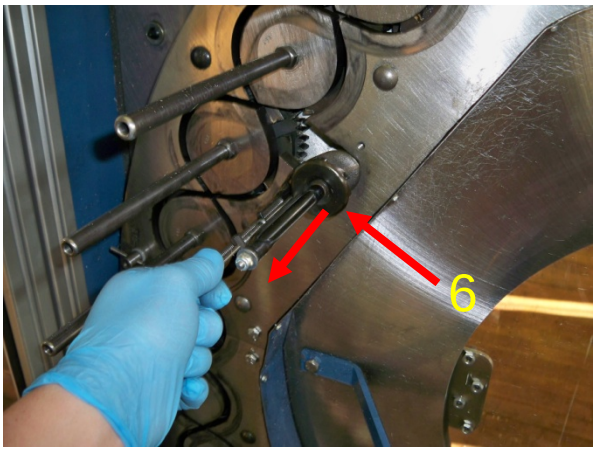

Figure 12

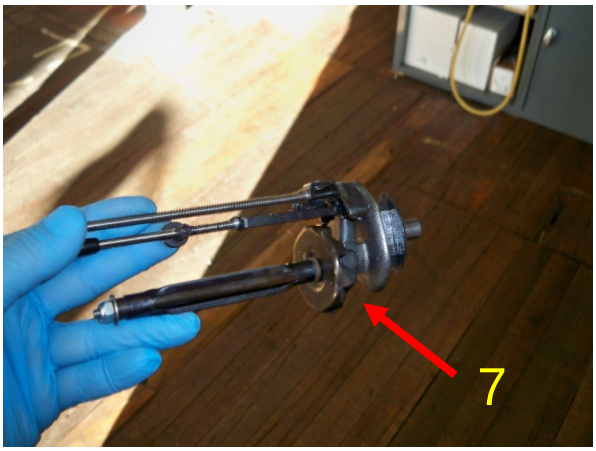

Figure 13

6. Remove last carrier as in steps 3, 4, and 5 (figure 12)
7. Take removed carrier and place into carrier holder (figure 14)

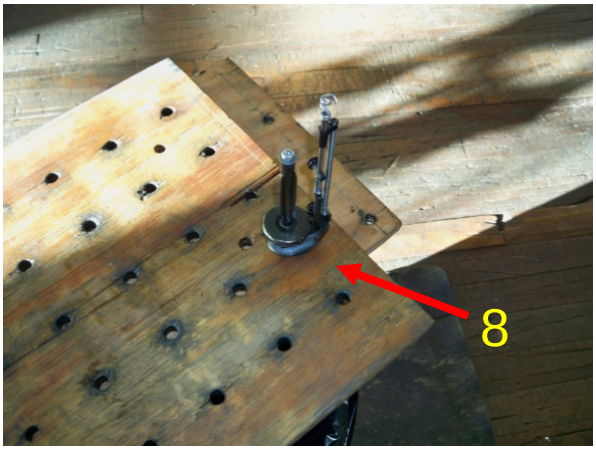

Figure 14

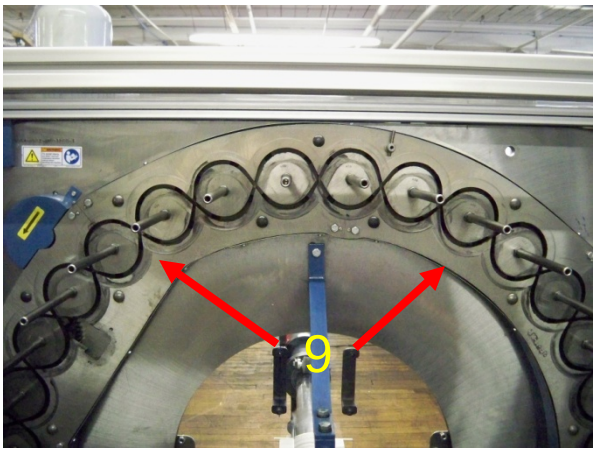

Figure 15

8. Carrier holder made of wood with 7/16 holes drilled to support carriers (figure 14)
9. Braider with all carriers removed (figure 15)

Braider Usage

Loading Carriers

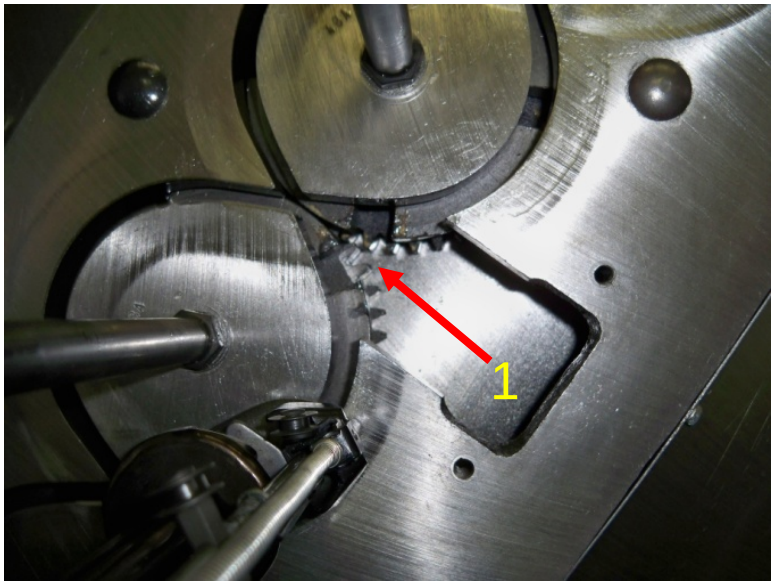

Figure 16

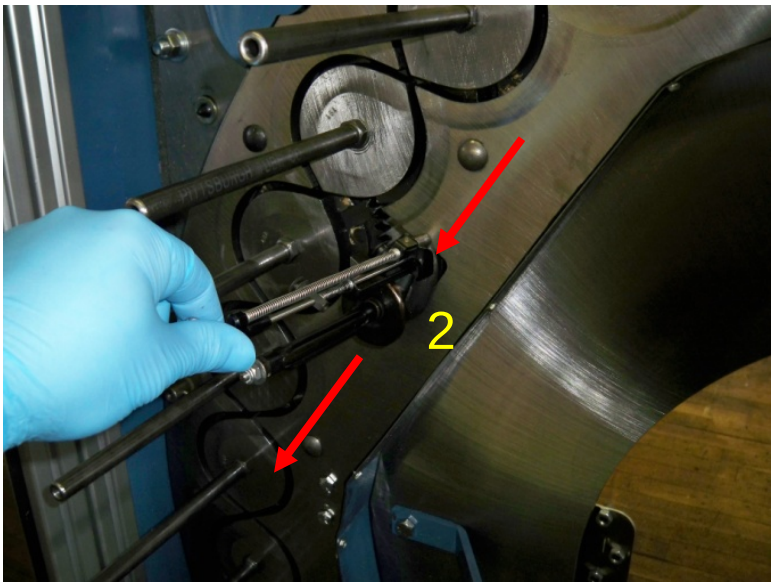

Figure 17

Description of loading carriers:

1. Using the Jog button on the control box (figure 68), line up the gear openings with the carrier loading slot on the braider (figure 16)
2. Insert carrier into carrier slot with cop holder facing down (figure 17)
    a. Carriers are load in a **"one down – one up"** sequence

Braider Usage

Loading Carriers

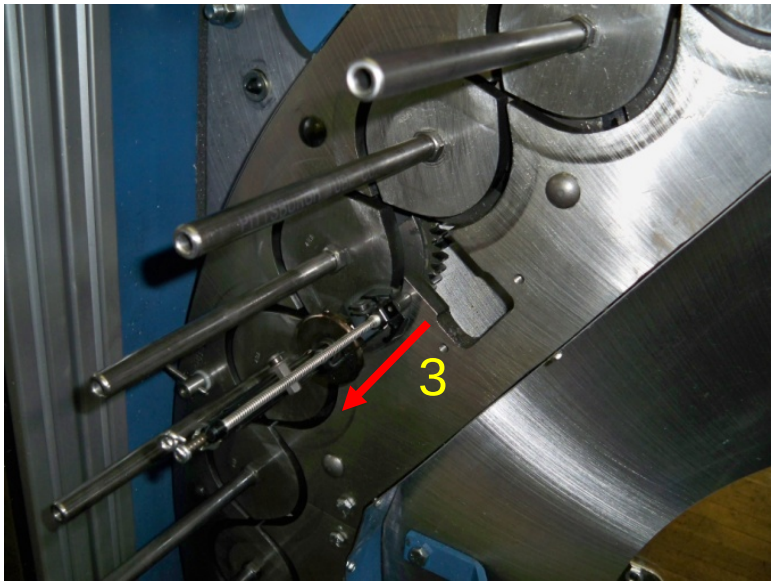

Figure 18

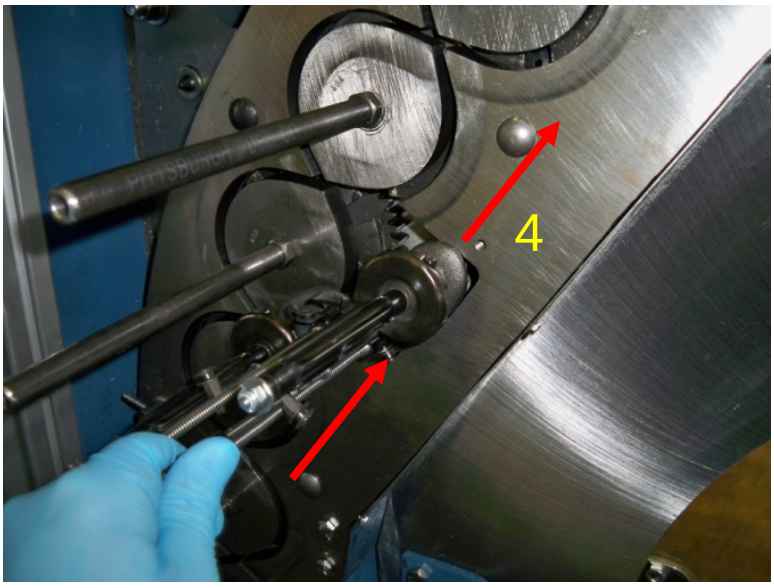

Figure 19

Description of loading carriers:

3. Simultaneously jog the braider while inserting carrier into gear opening heading down (figure 18)
    a. Continue jogging braider until next gear opening lines up with loading slot
4. Insert next carrier with cop holder facing up. Repeat step 3, however insert carrier into gear opening heading up (figure 19)

Braider Usage

Loading Carriers

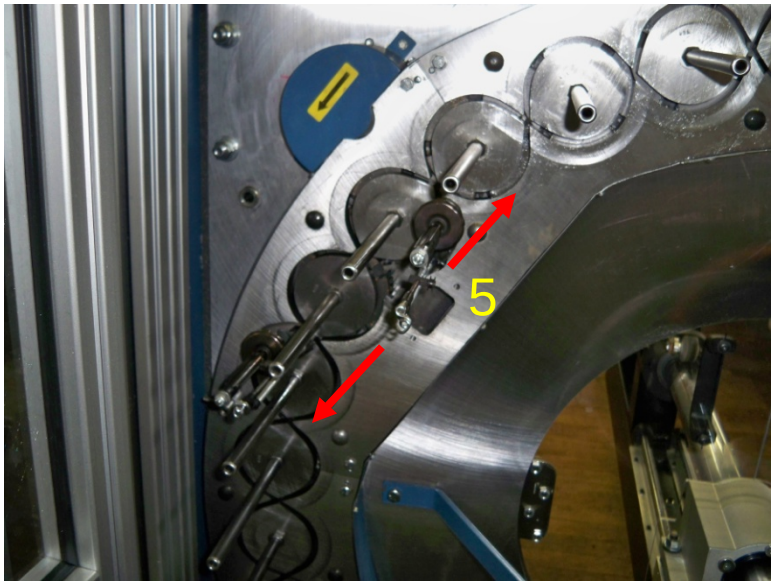

Figure 20

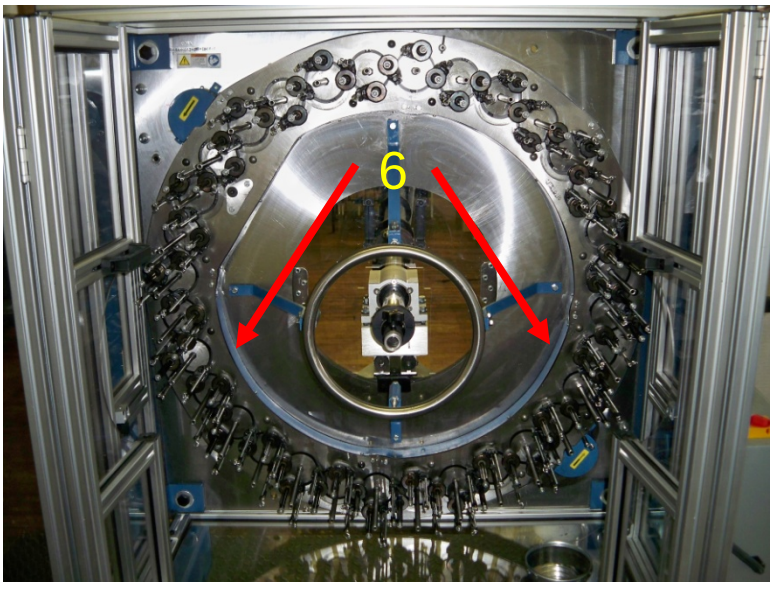

Figure 21

Description of loading carriers:

5. Repeat steps 1 thru 4 keeping in mind the **"one down – one up"** sequence until all 64 carriers are loaded (figure 20)
6. All 64 carriers loaded. Re-insert deck key and secure with two 7/16 bolts (figure 21)
    a. Slowly run braider only to check for correct carrier loading. If loading is correct, slowly increase braider speed to work in deck oil with carriers

Braider Usage

Loading Carriers

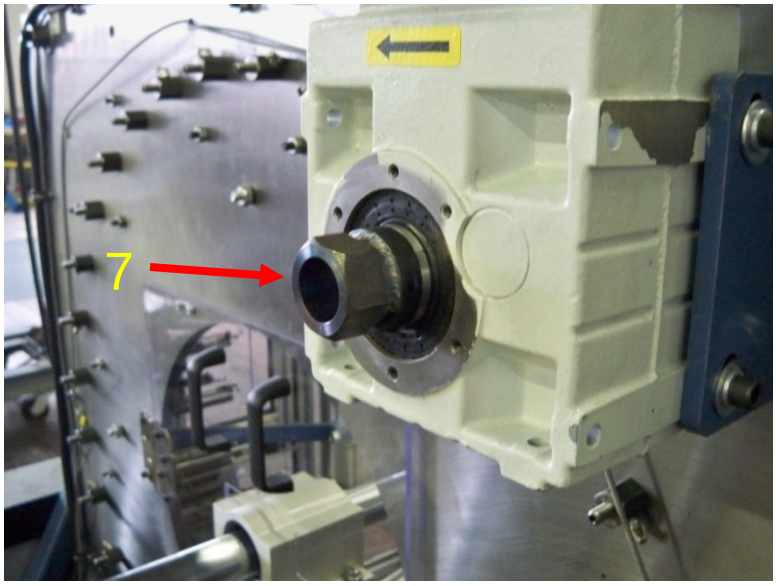

Figure 22

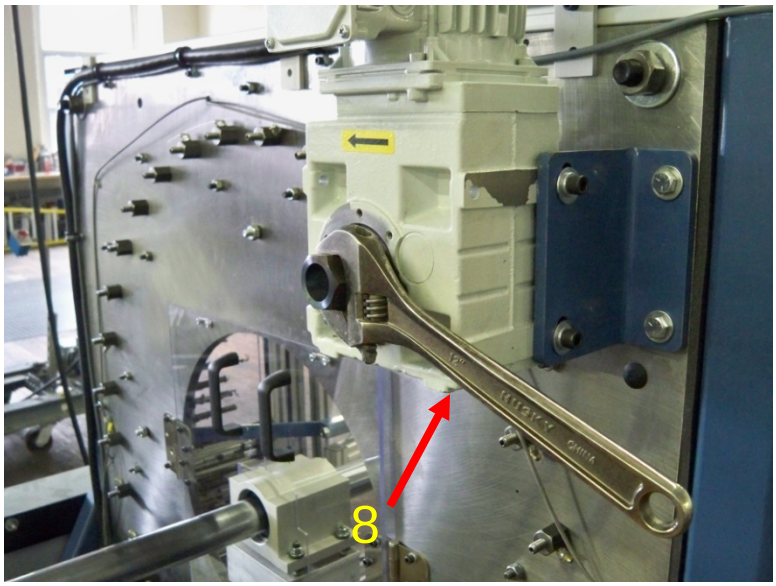

Figure 23

Description of loading carriers:

7. Hex nut on motor shaft used to rotate braider in reverse (figure 22)
    a. While loading carriers and gear slot is missed, braider can be manually turned in reverse to realign gear slot
8. Use adjustable wrench on hex nut to manually turn braider in reverse (figure 23)

Braider Usage

Loading Bobbins

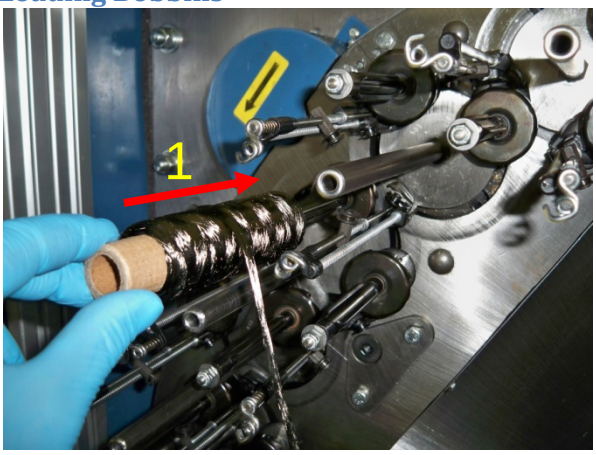

Figure 24

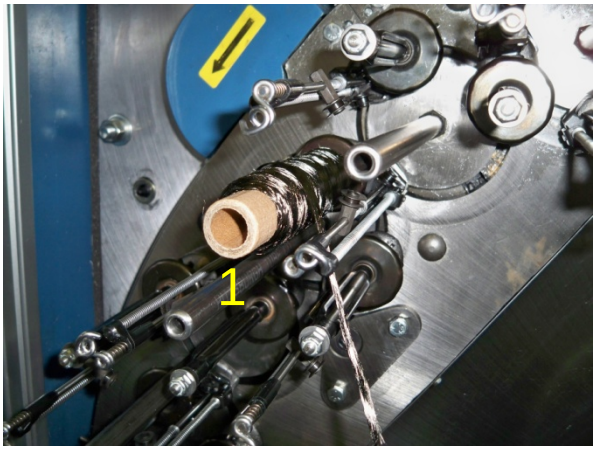

Figure 25

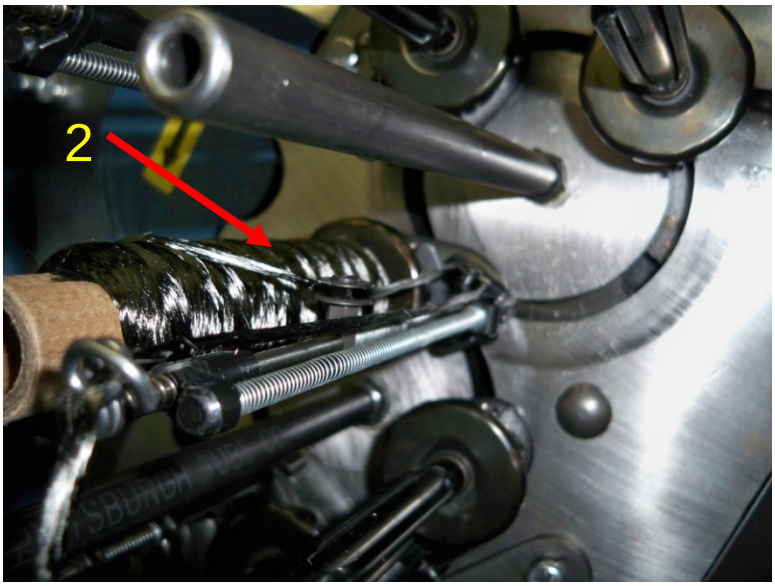

Figure 26

Description of loading bobbins:

1. Insert bobbin onto cop holder (figure 24)
    a. Bobbin is directional
2. String fiber onto carrier (figure 25)
    a. Payout of fiber must be over the top of the wound spool onto the middle sheave wheel as discussed in Carrier/Bobbin Assembly

Braider Usage

Loading Bobbins

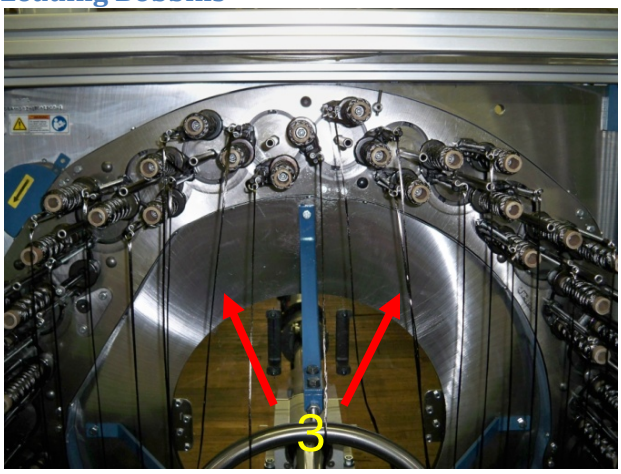

Figure 27

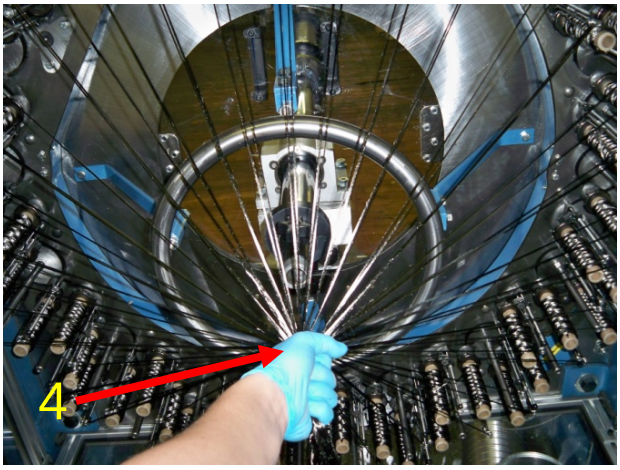

Figure 28

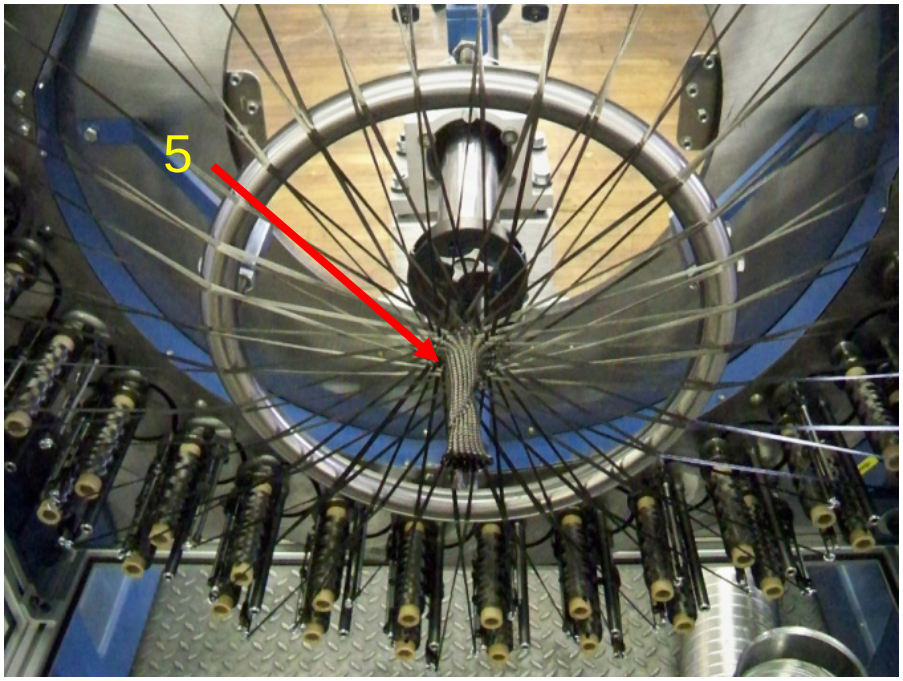

Figure 29

Description of loading bobbins:

3. Pull fiber through threaded eyelet roughly 12” to 16” after bobbin is installed on carrier
    a. Repeat steps 1 thru 3 until all bobbins are loaded (figure 27)
4. Grab all strands of fiber and pull into a tight gathering (figure 28)
5. Using the jog button (figure 68) run braider only and braid loose fiber into a 3” minimum fiber tube(figure 29)

Braider Usage

Braiding

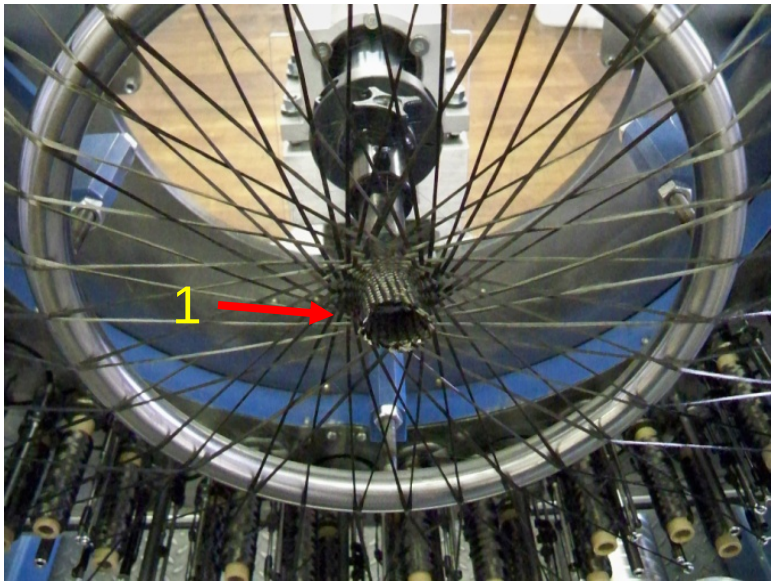

Figure 30

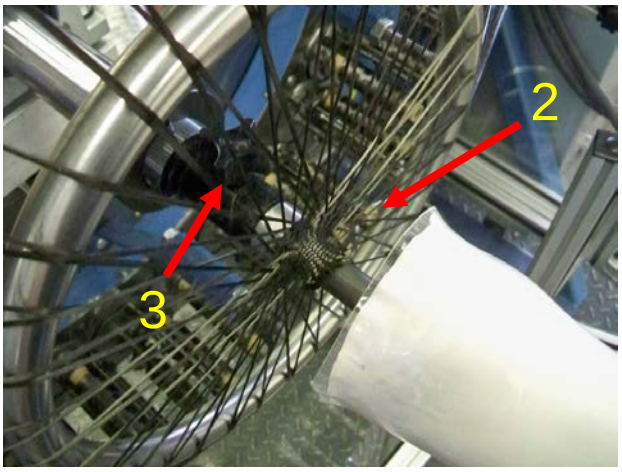

Figure 31

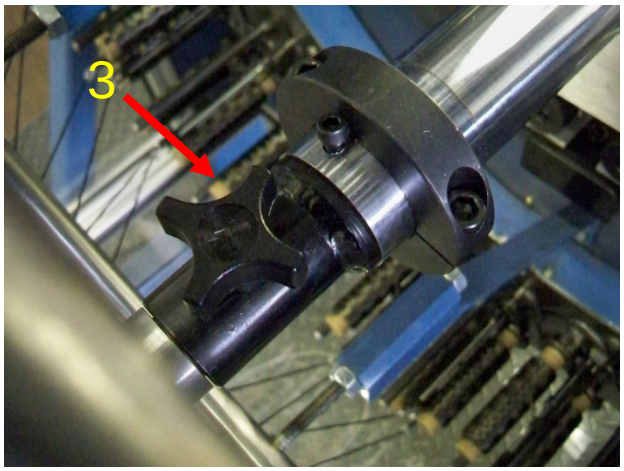

Figure 32

Description of braiding:

1. Braided fiber in tube shape with hole for entry of shaft on mold blank into gantry (figure 30)
2. Insert shaft of mold blank thru braided tube and into gantry (figure 31)
3. Once shaft is inserted into gantry tighten gantry knob to secure mold shaft into place (figure 32)

Braider Usage

Braiding

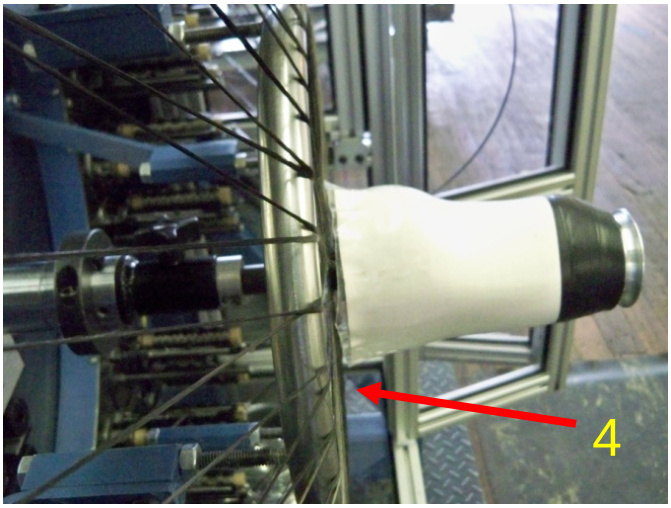

Figure 33

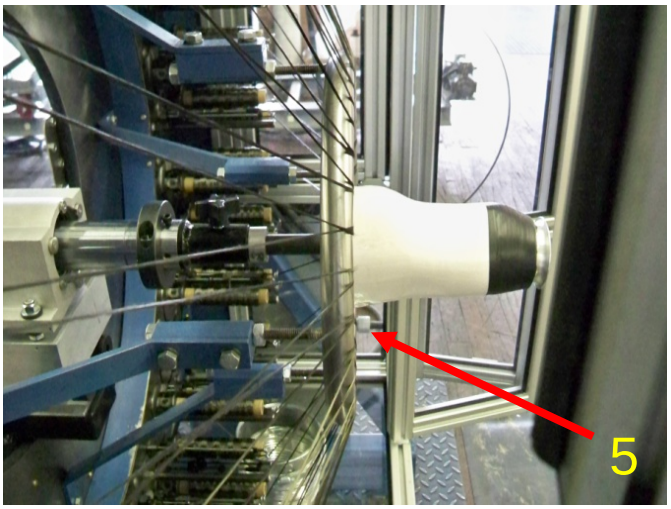

Figure 34

Description of braiding:

4. Using the control box, move gantry only in reverse until rear of mold is flush with braid ring (figure 33)
5. Once rear of mold is flush with braid ring continue to move gantry only in reverse until mold is roughly 1 to 1.25” behind ring (figure 34)
    a. This will put an attack angle on the braid to set a starting tension.
    b. Braid angle should be kept consistent for uniform braid
        i. A small attack angle will cause a tighter braid, less gapping
        ii. A large attack angle will cause a loose braid, more gapping

Braider Usage

Braiding

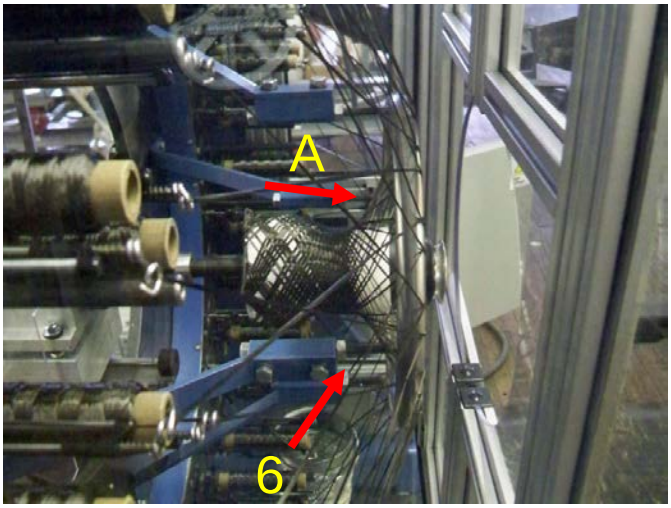

Figure 35

Figure 36

Figure 37

Description of braiding:

6. First layer braid (half way complete) (figure 35)
    a. Starting from rear of mold turn braider on at low speed and gantry at fast speed in reverse. Allow braider and gantry to braid complete part
    b. Adjust gantry speeds as shape of mold changes
        i. Leaving braider speed constant and increased gantry speed will cause fiber to gap more causing a loose braid (figure 36)
        ii. Leaving braider speed constant and decreased gantry speed will cause fiber to gap less causing a tight braid (figure 37)

Braider Usage

Braiding

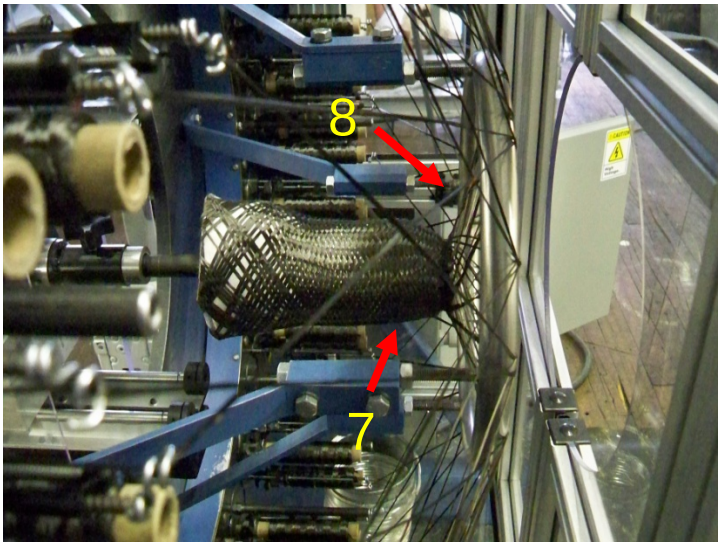

Figure 38

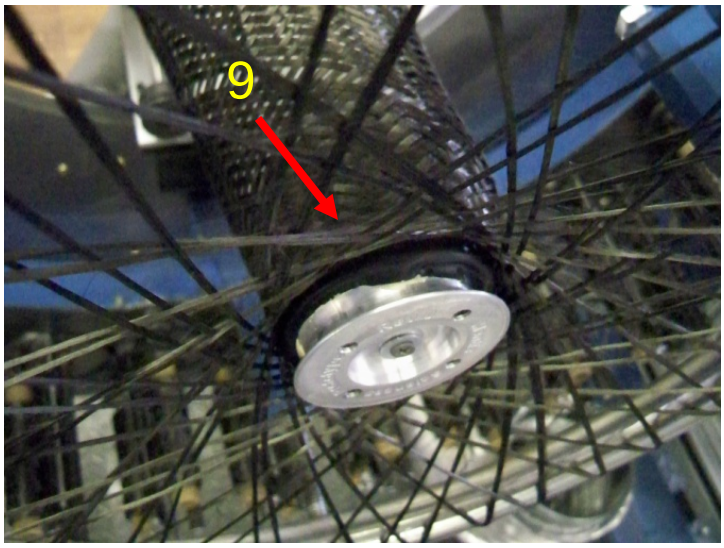

Figure 39

Description of braiding:

7. First complete braid layer with loose braid to achieve axial strength (figure 38)
8. Consistent attack angle to maintain desired fiber gap
9. Stopping point for gantry only (figure 39)
    a. Continue to run braider only to allow braid to fill in attachment plate groove to desired thickness
    b. Different attachment plates will require different stop points and braid angles

Braider Usage

Braiding

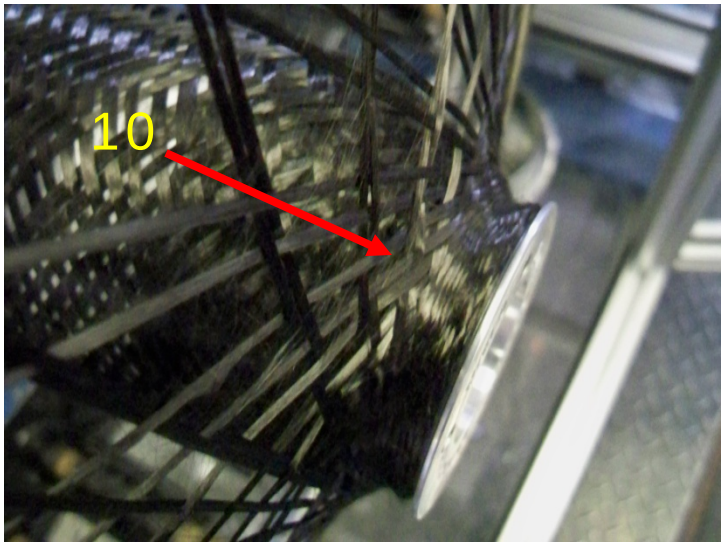

Figure 40

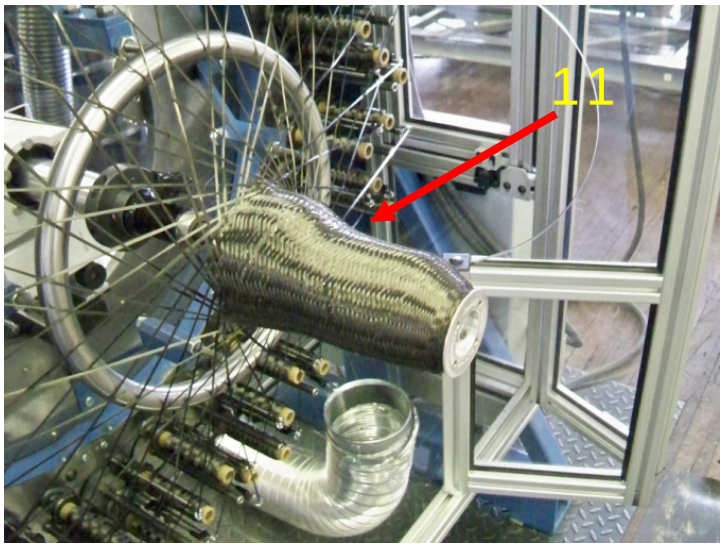

Figure 41

Description of braiding:

10. Attachment plate filled in with fiber (figure 40)
    a. Once attachment plate is filled to desired thickness start gantry into forward position and allow braider and gantry combo to apply second braid layer
11. Second completed braid layer (figure 41)

Braider Usage

Braiding

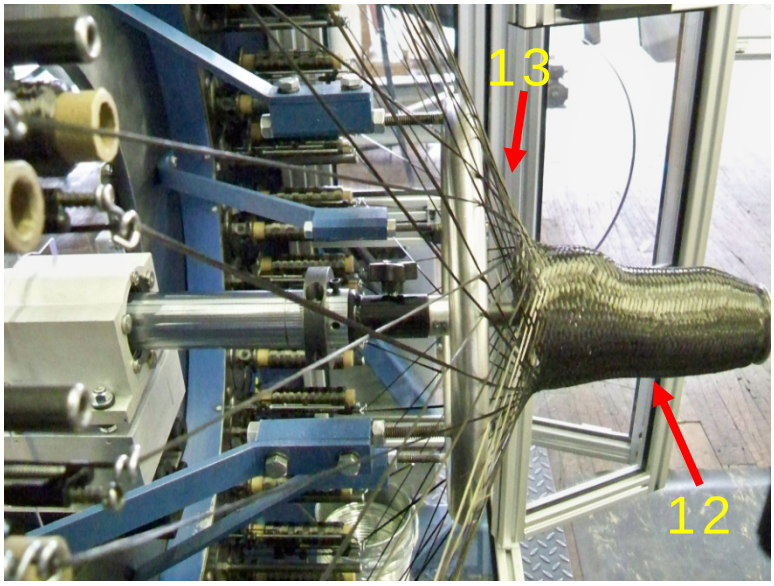

Figure 42

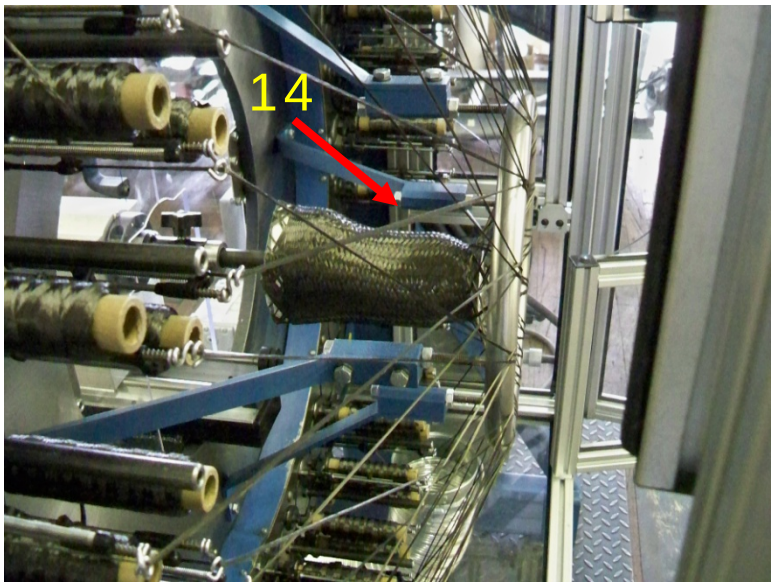

Figure 43

Description of braiding:

12. Second complete braid layer (figure 42)
13. Attack angle to maintain desired fiber gap
    a. Once braid layer is complete stop both braider and gantry.
    b. Put gantry into reverse and move mold behind braid ring to prepare for third braid layer
14. Third complete braid layer (figure 43)

Braider Usage

Braiding

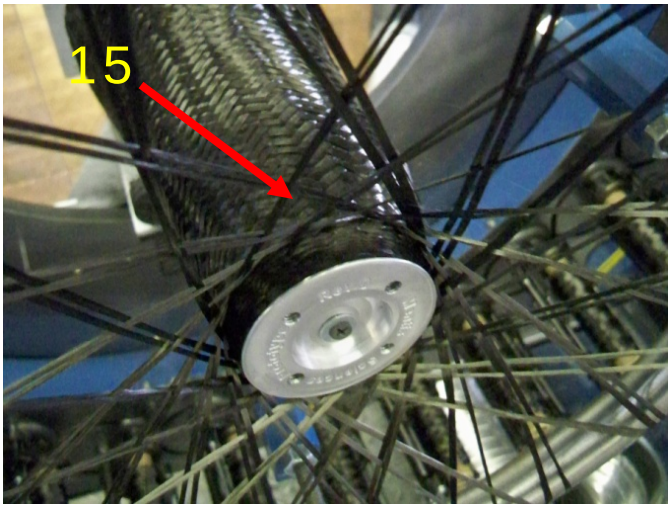

Figure 44

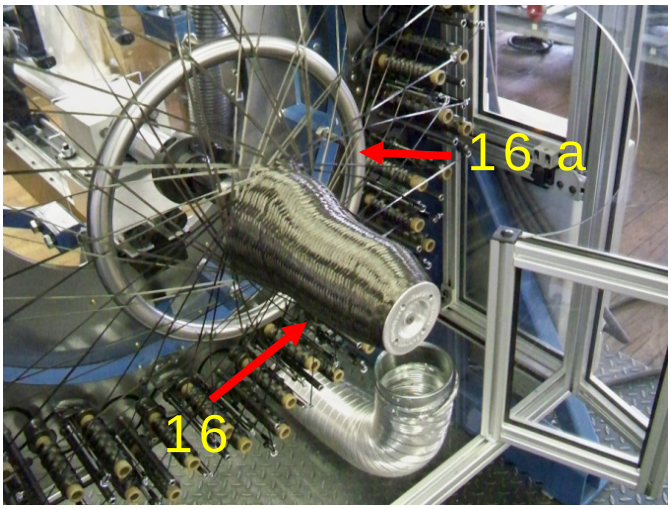

Figure 45

Description of braiding:

15. Stopping point for gantry only (figure 44)
    a. Continue to run braider only to allow braid to fill in attachment plate groove until braid is flush with attachment plate face
    b. Different attachment plates will require different stop points and braid angles
    c. Once attachment plate is filled to desired thickness start gantry into forward position and allow braider and gantry combo to apply final braid layer
16. Fourth and final complete braid layer(figure 45)
    a. Once final braid layer is complete stop braider and gantry at back of mold. If needed move gantry so fiber angle is flush with braid ring to allow for mold removal

Braider Usage

Braiding

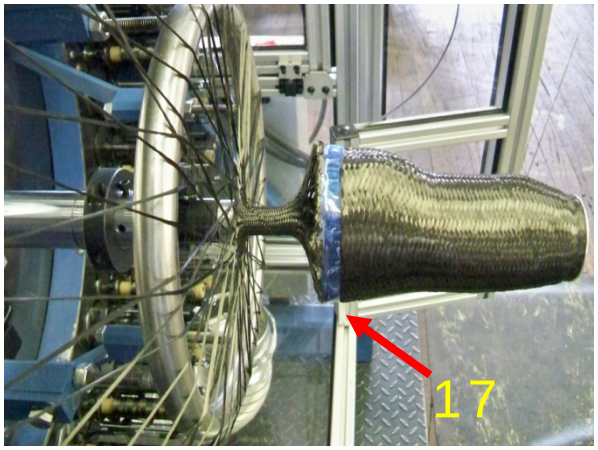

Figure 46

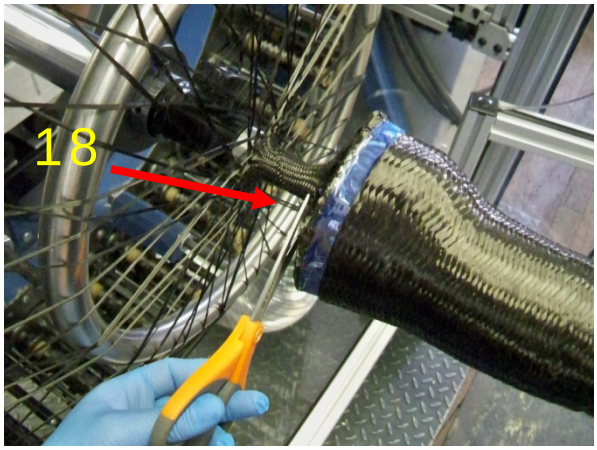

Figure 47

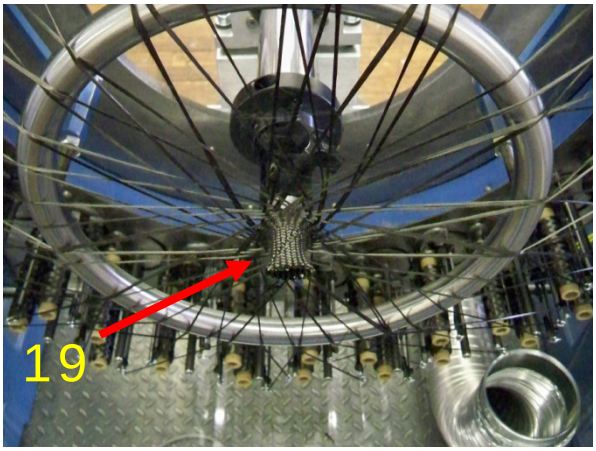

Figure 48

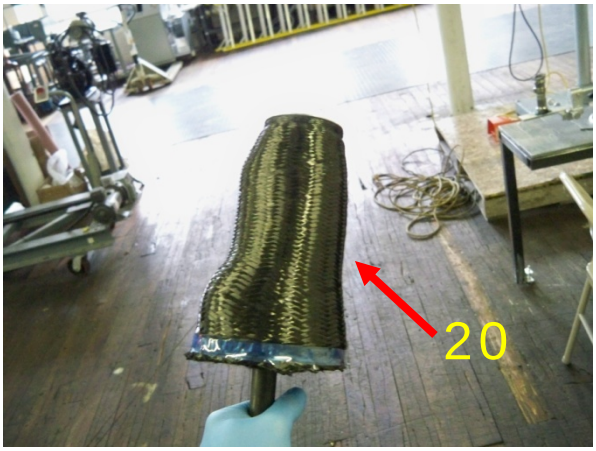

Figure 49

Description of braiding:

Option one

17. Secure final braid layer by applying tape fully around rear of mold(figure 46)
    a. Once tape is secure run braider only to braid a fiber tube over exposed mold shaft
18. Cut carbon at back of mold between tape and fiber tube(figure 47)
    a. Tape will secure final braid layer on mold
    b. Braided tube will secure fiber
19. Braided tube ready for next mold blank(figure 48)
20. Final braided part ready for resin(figure 49)

Braider Usage

Braiding

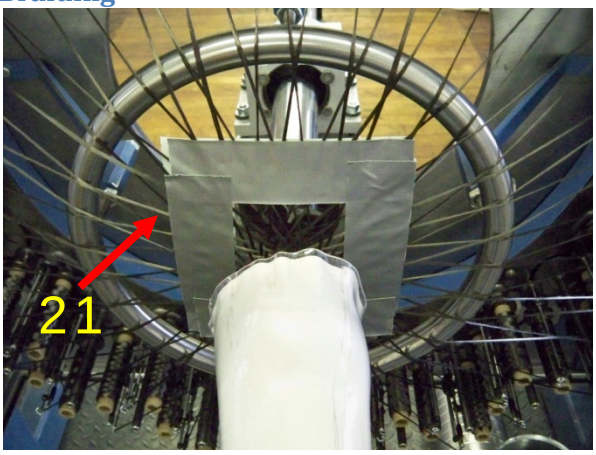

Figure 50

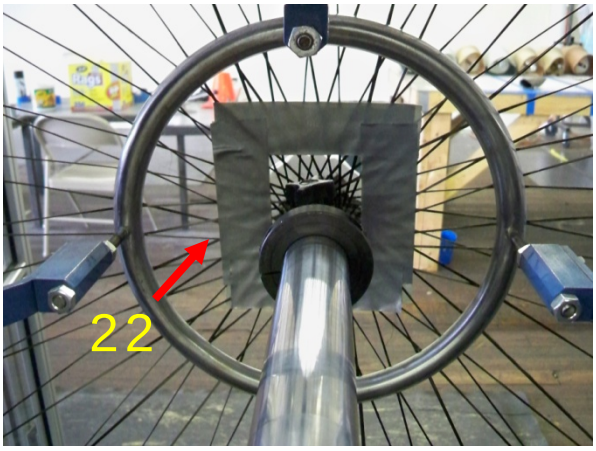

Figure 51

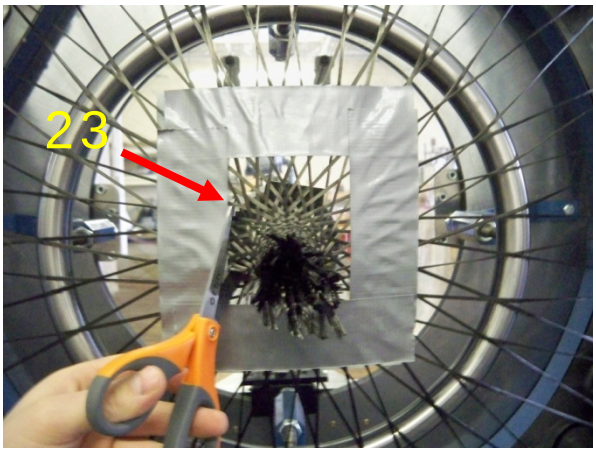

Figure 52

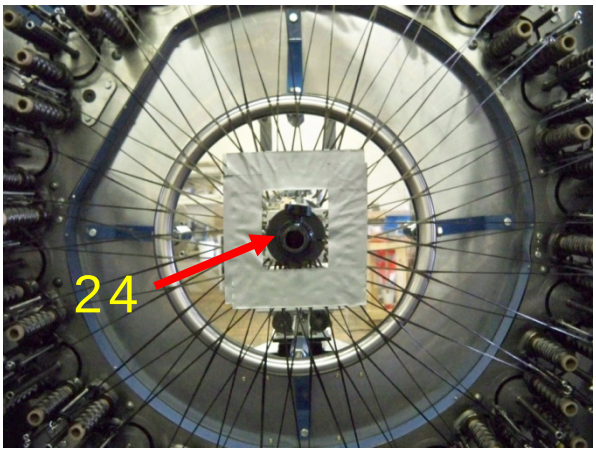

Figure 53

Description of braiding:

Option two

21. Apply duct tape to fiber making a square box around mold shaft (figure 50)
22. Repeat step 21 to back of fiber to secure fiber between tape(figure 51)
23. Cut excess fiber between duct tape to remove mold(figure 52)
24. Allow duct tape to hold fiber in place(figure 53)

Braider Usage

Braiding

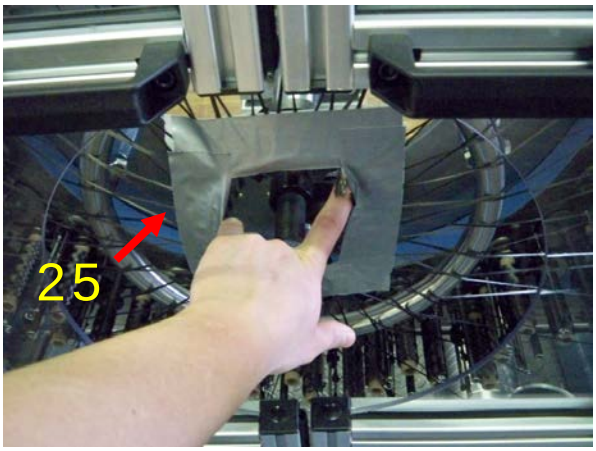

Figure 54

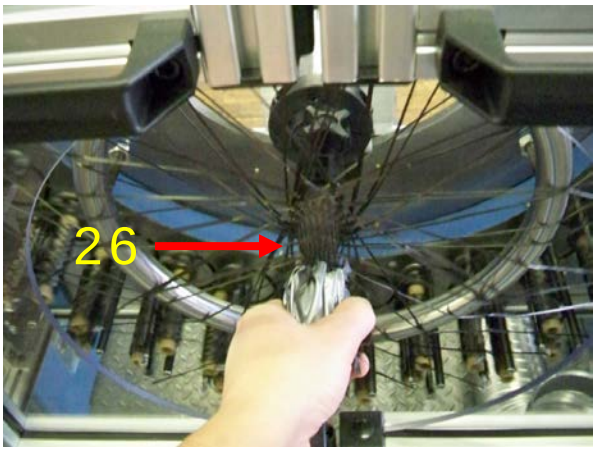

Figure 55

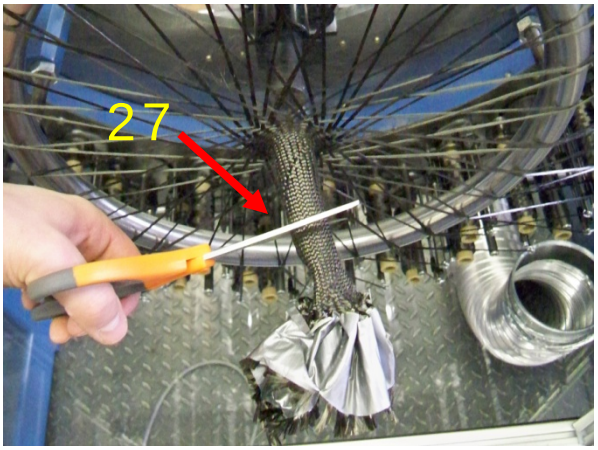

Figure 56

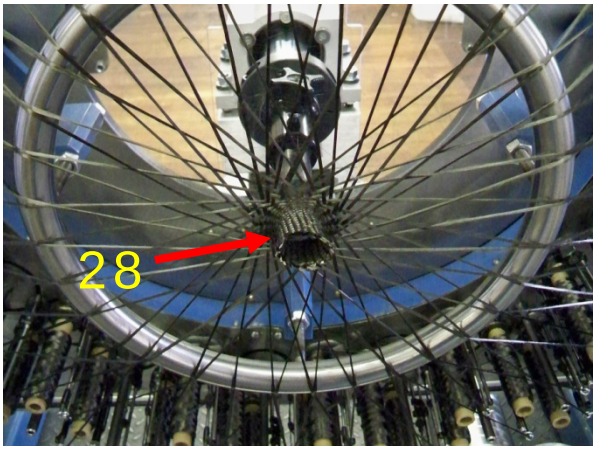

Figure 57

Description of braiding:

Option two

25. Using your hand run braider only while pulling tape square towards yourself(figure 54)
26. Once tape collapses on itself keep tension on fiber to braid tube(figure 55)
27. After tube is braided, use sissors and remove tape and excess tube(figure 56)
28. Braided tube ready for next mold blank(figure 57)

Braider Maintenance

Carrier Cleaning

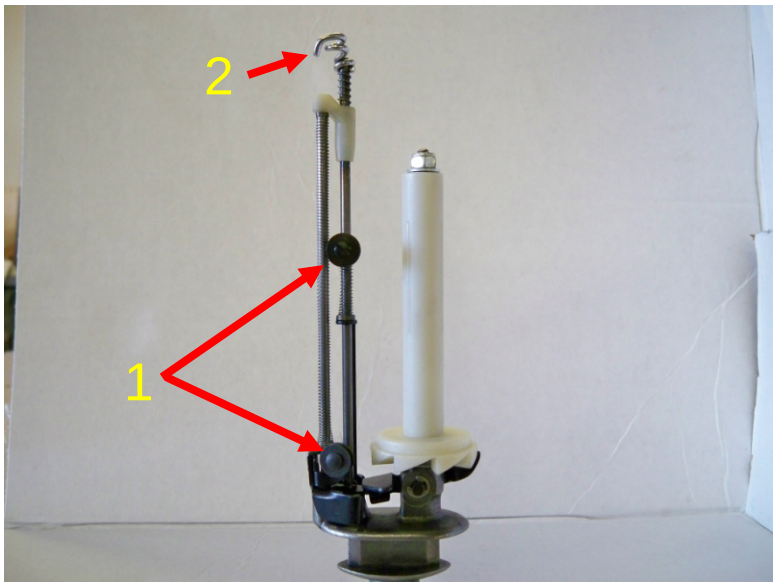

Figure 58

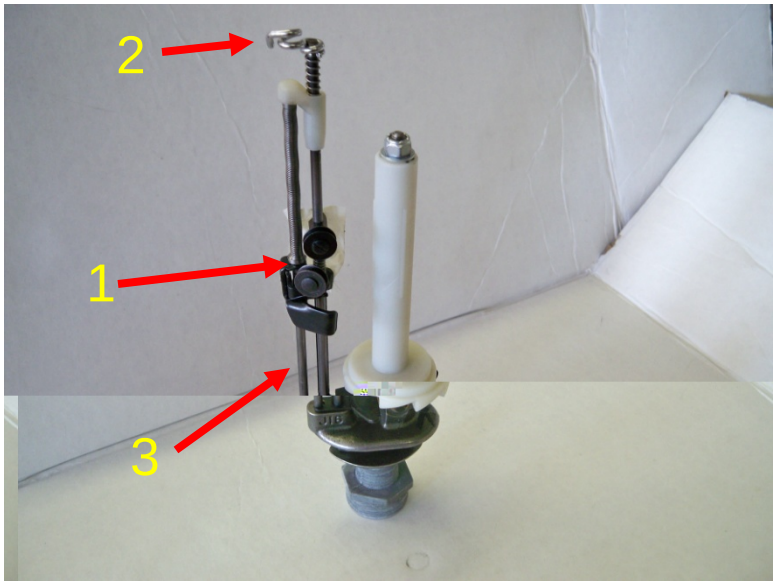

Figure 59

Description of carrier cleaning:

1. Used compressed air and blow off any debris from carrier. Use a razor blade and remove any debris wrapped around the sheave wheels.(figure 58)
2. Remove any debris from the treaded eyelet
3. Slide braid stop, attached to rear sheave wheel up towards middle sheave wheel. Wipe clean both rods and re-lubricate with 3-IN-ONE multipurpose oil or equivalent. (figure 59)

Braider Maintenance

Braider Cleaning

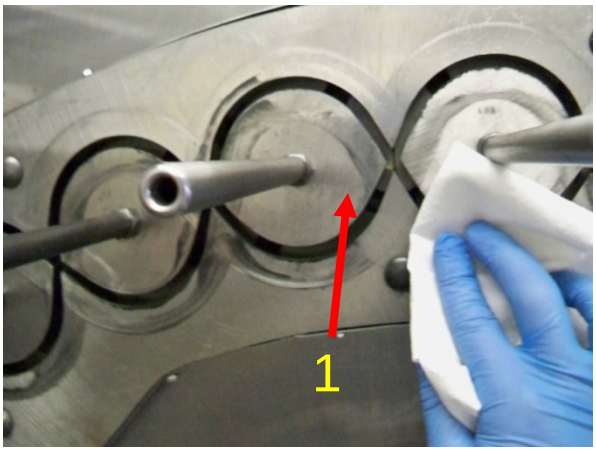

Figure 60

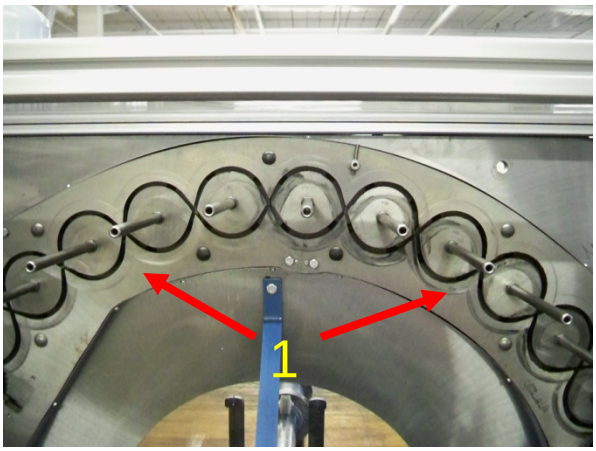

Figure 61

Description of braider cleaning:

1. Wipe complete braider deck with Acetone saturated rag to remove oil and debris(figure 60,61)

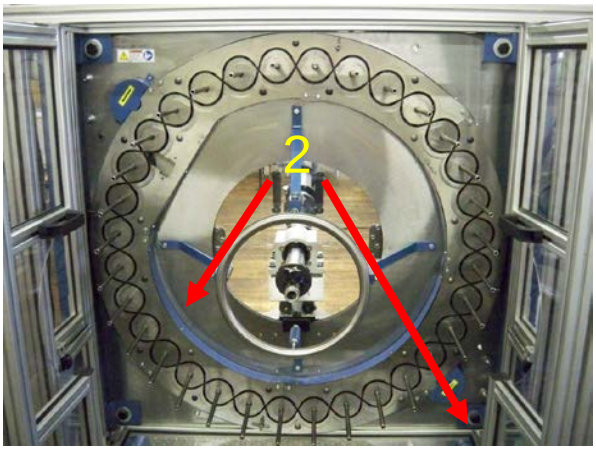

Figure 62

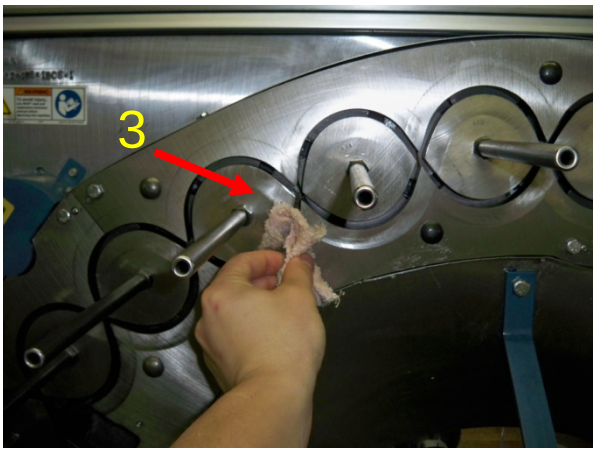

Figure 63

2. Wipe down all parts of braider with clean cloth to remove debris. Use vacuum to pick up excess fiber debris. Use dry rag or Windex to clean enclosure. (Acetone will etch the polycarbonate panels)(figure 62)
3. After cleaning is complete, braider deck must be thinly coated with 60W – 90W oil. Apply oil to cloth rag and slowly wipe braider applying a thin layer of oil for lubrication(figure 63)

Gantry

Diagram

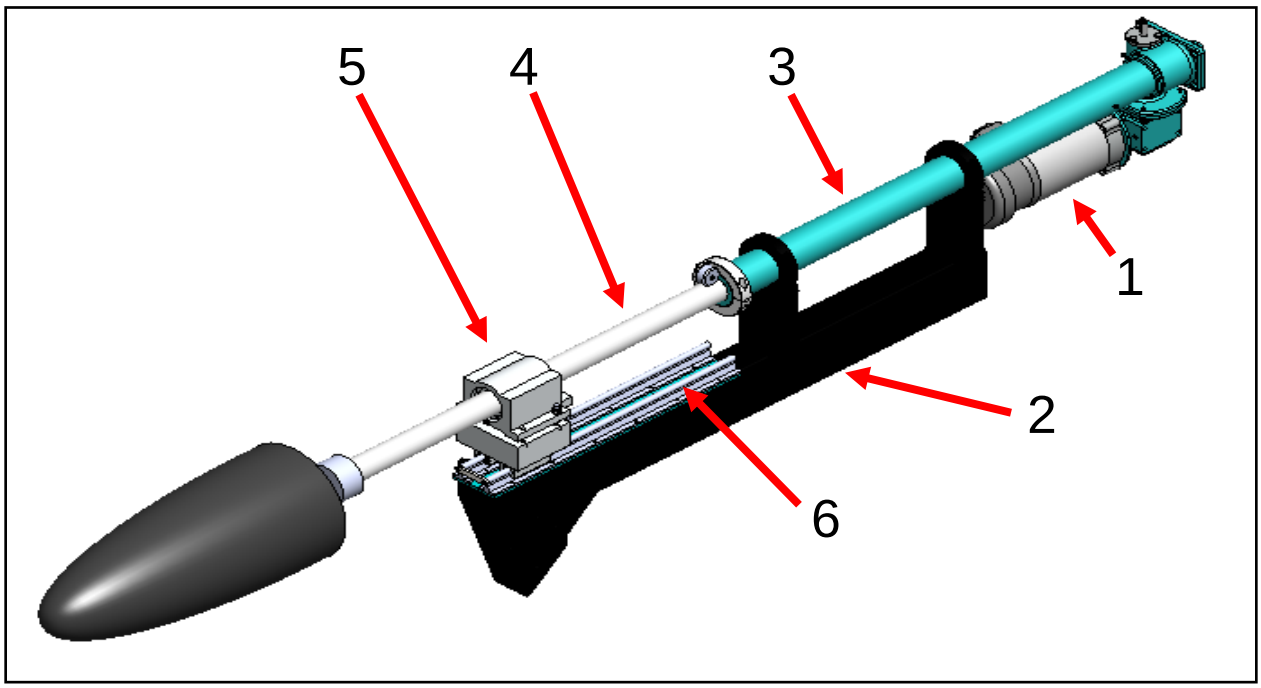

Figure 64

Description of gantry: (figure 64)

1. Gantry drive motor 480Vac 3ph 1Hp
2. Steel tube support beam that supports actuator and attaches to braider
3. Integrated linear actuator
4. Linear actuator piston
5. Pillow-Block self-align bearing to support load
6. Shaft and rail assembly, 0.5" x 24" long

Gantry

Usage

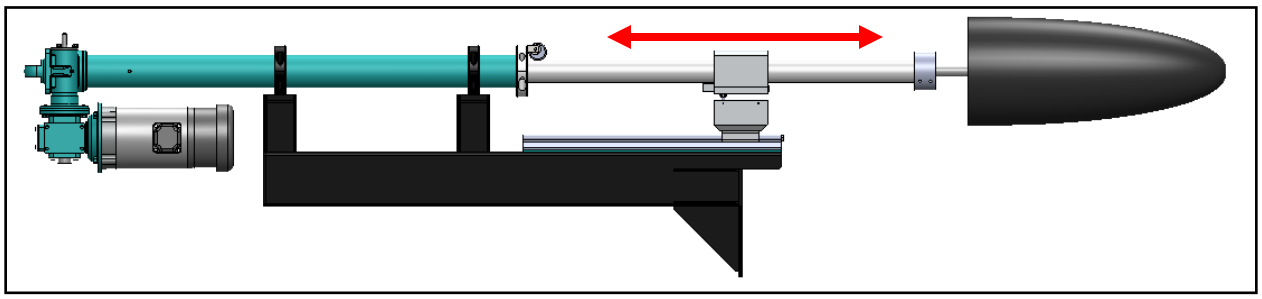

Figure 65

Description of usage: (figure 65)

1. Control box contains switches to activate gantry (refer to figure 68/69)
    a. Forward motion will extend actuator piston out
    b. Reverse motion will retract actuator piston in
    c. Actuator has adjustable limit switches to limit forward/reverse positions

Gantry

Maintenance

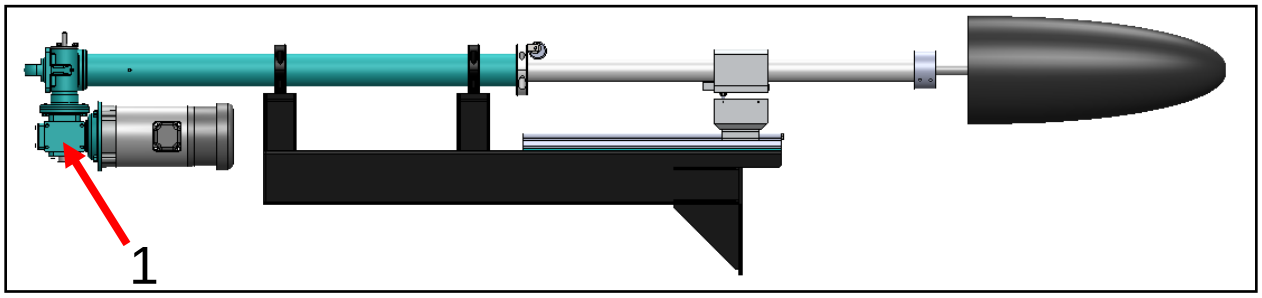

Figure 66

Description of maintenance: (figure 66)

1. Grease fitting
    a. Lubricate monthly using multipurpose grease

Controls

Control Box /Usage

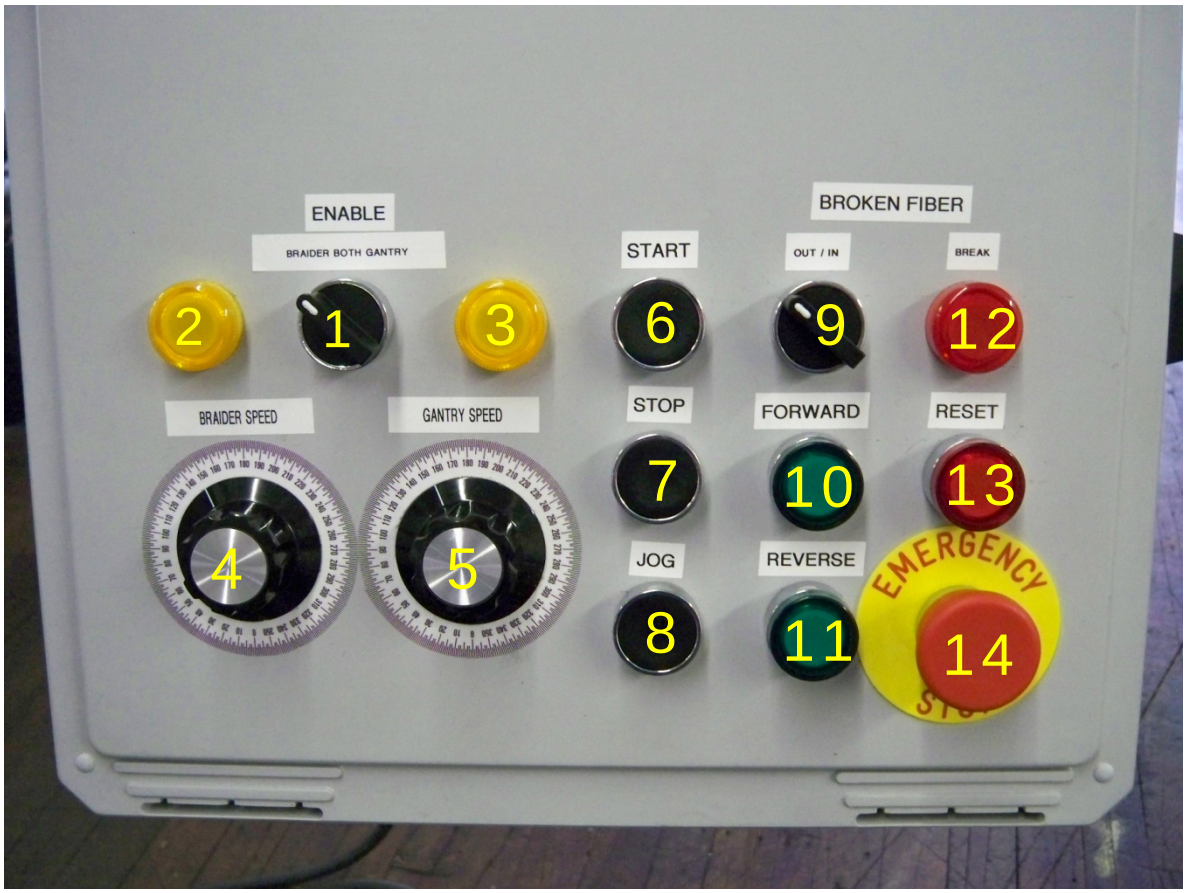

Figure 67

Description of controls: (figure 67)

1. Braider and Gantry (slide) Control Knob.
    a. Three different positions
        i. Middle – Allows both braider and gantry to run
        ii. Left – Allows braider only to run
        iii. Right – Allows gantry only to run
2. Yellow Indicator Light
    a. Illuminates when braider only is selected
3. Yellow Indicator Light
    a. Illuminates when gantry only is selected
4. Braider Speed Control Knob
    a. Turned completely left is off
    b. Turned completely right is full speed
5. Gantry Speed Control Knob
    a. Turned completely left is off
    b. Turned completely right is full speed

Controls

Control Box /Usage

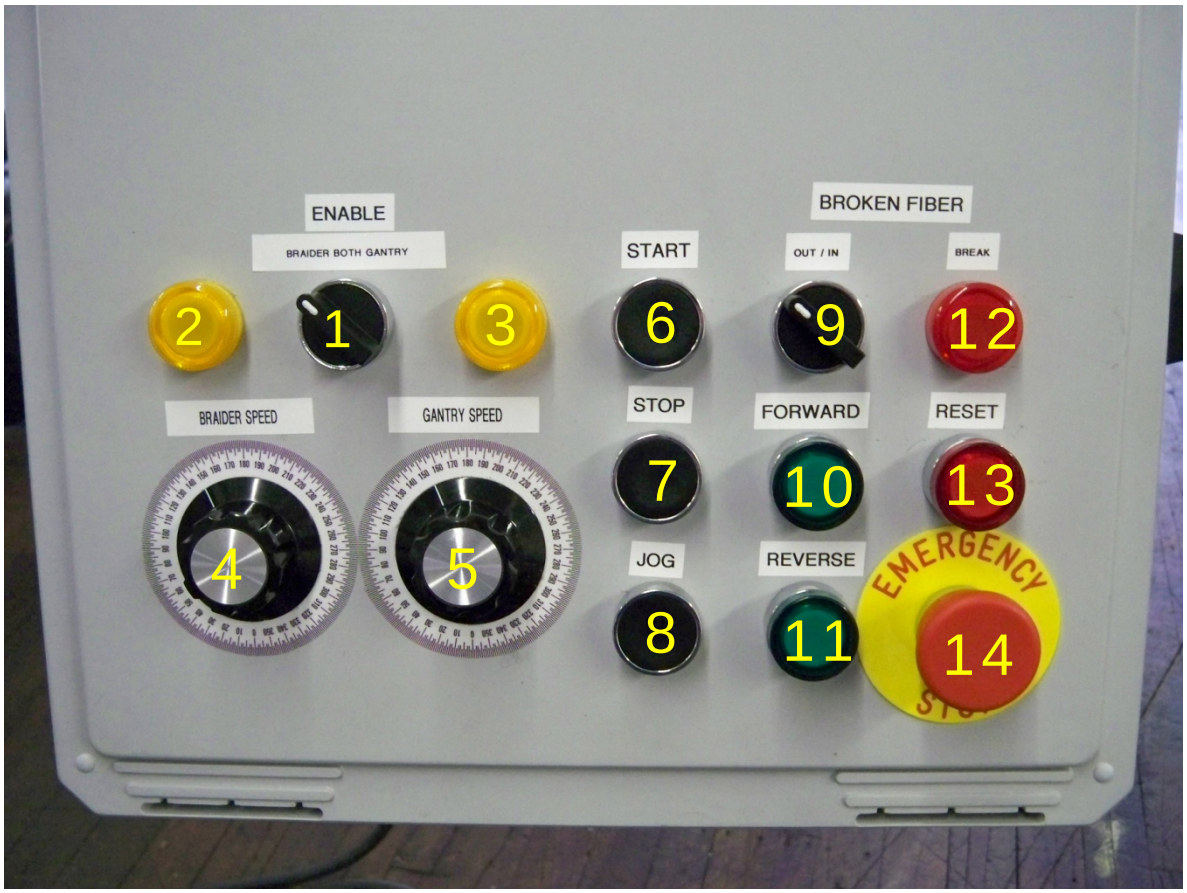

Figure 68

Description of controls: (figure 68)

6. Push Button for Start
    a. Gives power to braider, gantry, or both
7. Push Button for Stop
    a. Stops power to braider, gantry, or both
8. Push Button for jog
    a. Can only be used when control box is in stop position
    b. Allows braider, gantry, or both to be moved during none fabrication
9. Broken Fiber Control Knob (**this is an optional feature**)
    a. Turned to the left (out) indicates broken fiber option is **off**
    b. Turned to the right (in) indicates broken fiber option is **on**
10. Forward Push Button/Green Indicator Button
    a. Depress button to drive gantry in forward
    b. Button will illuminate green when forward is selected

Controls

Control Box /Usage

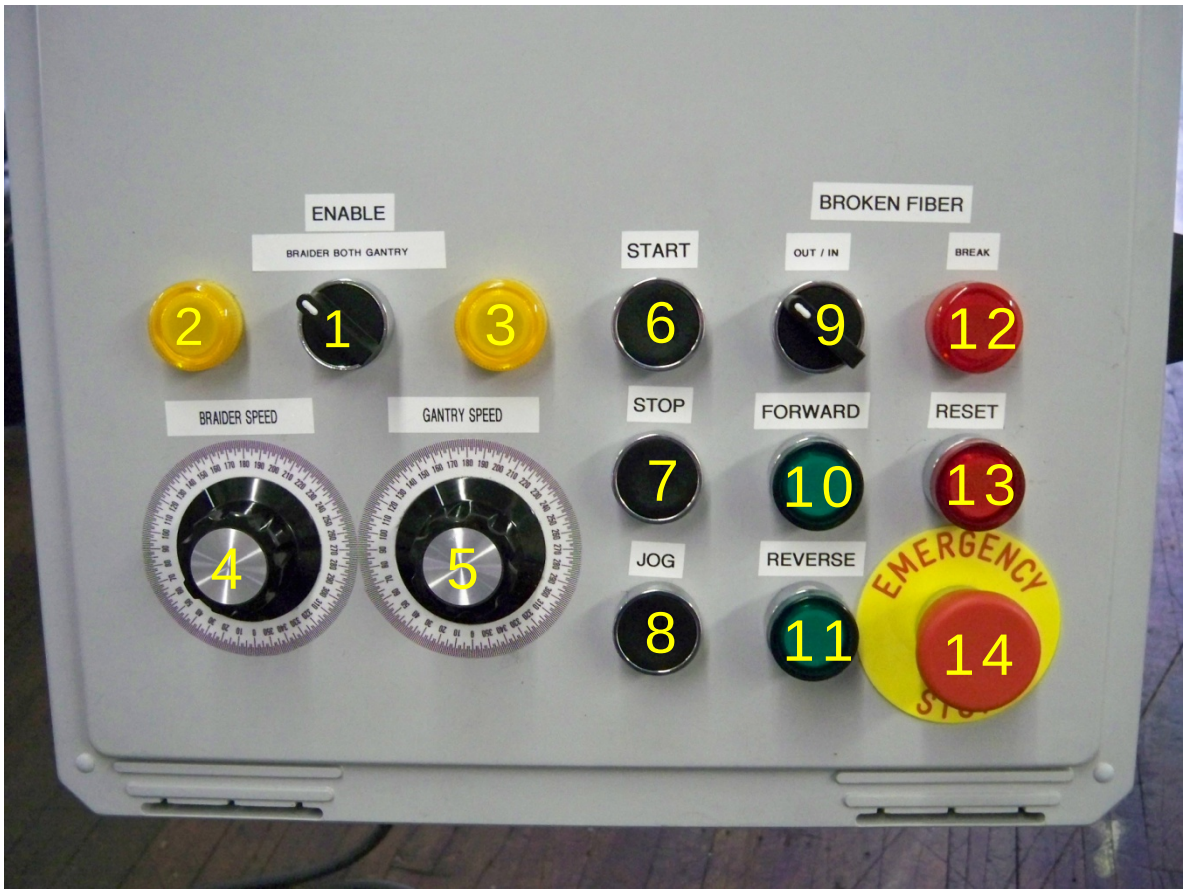

Figure 69

Description of controls: (figure 69)

11. Reverse Push button/Green Indicator Button
    a. Depress button to drive gantry in reverse
    b. Button will illuminate green when reverse is selected
12. Fiber Break Indicator Light (**this is an optional feature**)
    a. Light will illuminate when there is a fiber break if the fiber break switch is on the "in" position
13. Reset Push Button/Red Indicator Button
    a. Depress button to give control box power
    b. Button will illuminate red when reset is activated
    c. Reset is activated when main power has been turned on and/or when any emergency stop button has been used
14. Emergency Stop Button
    a. When depressed all power to machine will be stopped

Controls

Wiring Box /Usage external

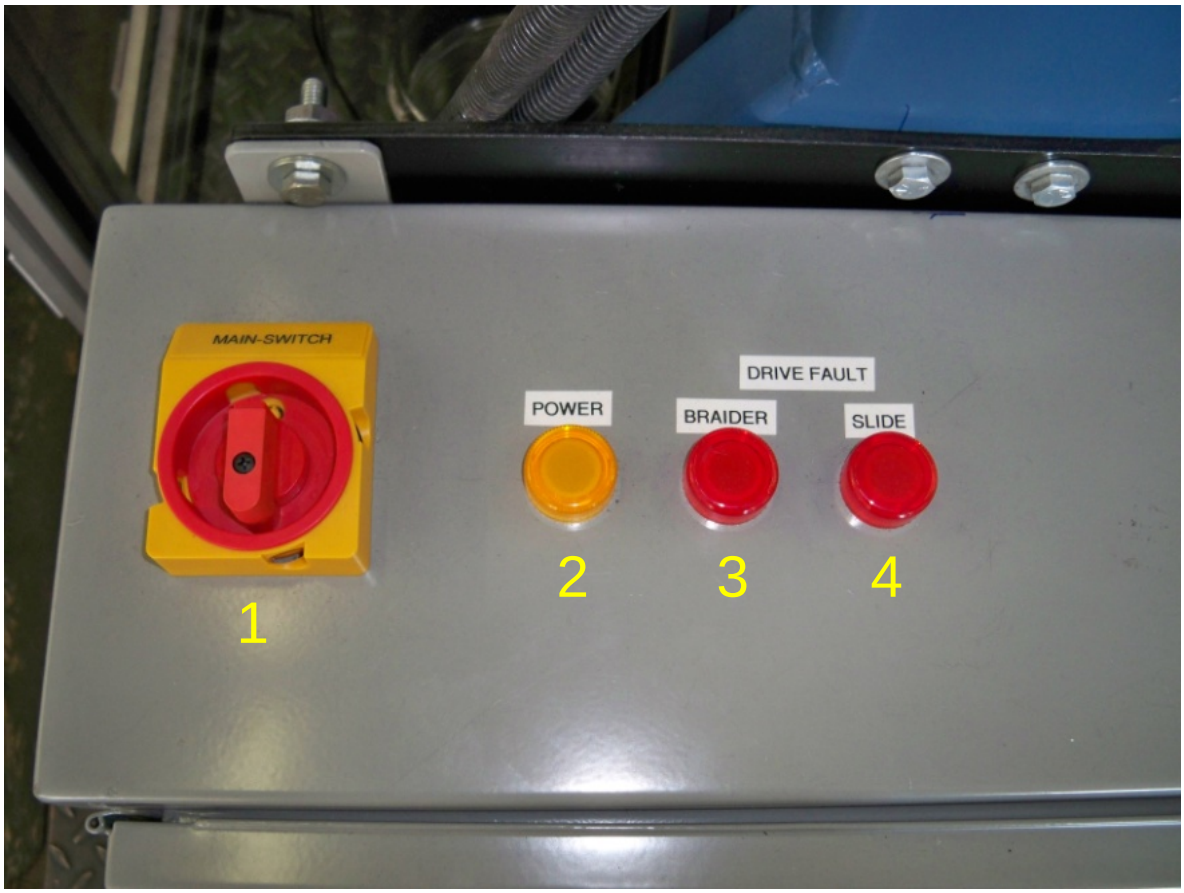

Figure 70

Description of controls: (figure 70)

1. Main power switch
    a. Two positions (On/Off)
2. Yellow Indicator Light
    a. Illuminates when main power is turned on
3. Red indicator Light
    a. Illuminates when the Automation Direct AC Drive for the braider goes into fault and needs to be reset inside the main wiring box
4. Red indicator Light
    a. Illuminates when the Automation Direct AC Drive for the gantry (slide) goes into fault and needs to be reset inside the main wiring box

Controls

Wiring Box /Usage internal

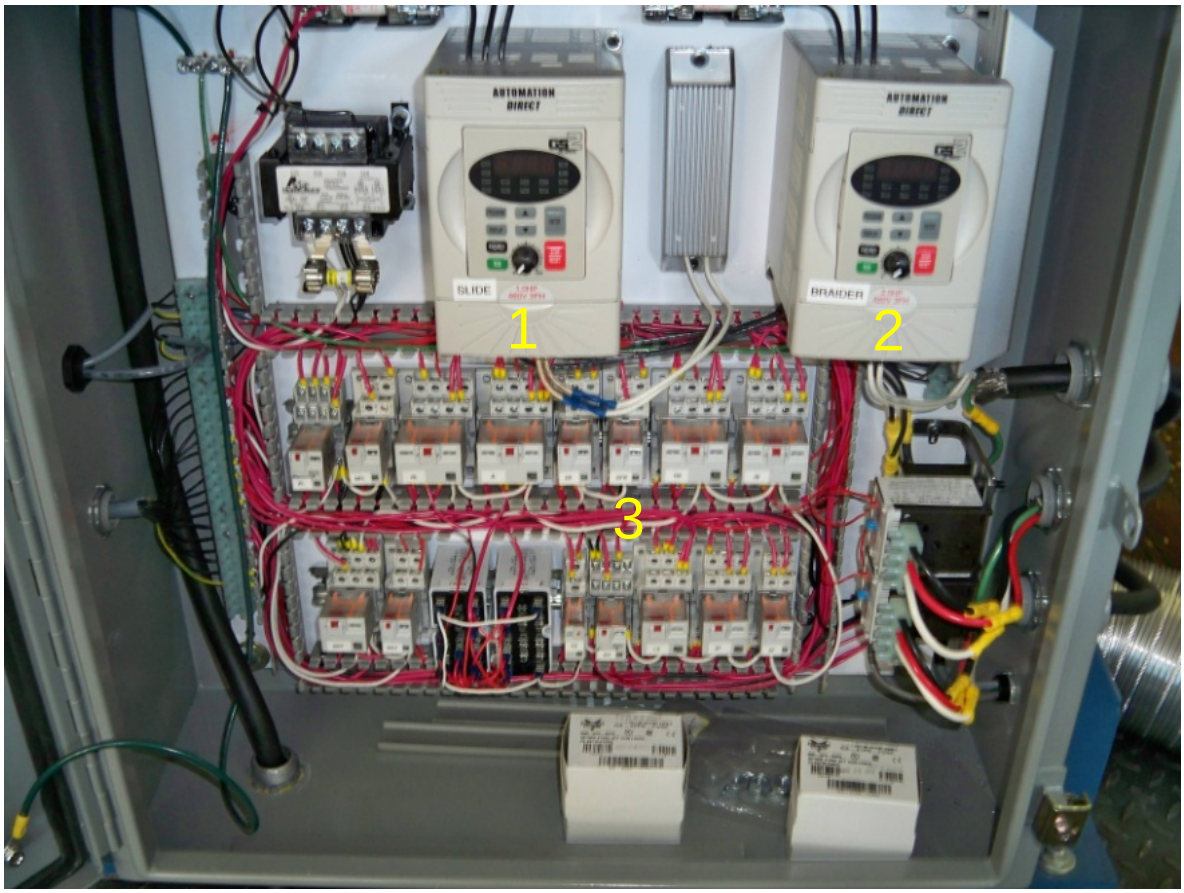

Figure 71

Description of controls: (figure 71)

1. Automation Direct AC Drive for the gantry (slide)
    a. If needed to be reset press red button
2. Automation Direct AC Drive for the braider
    a. If needed to be reset press red button
3. Complete Wiring Board
    a. Refer to wiring schematic

Enclosure

Diagram/Usage

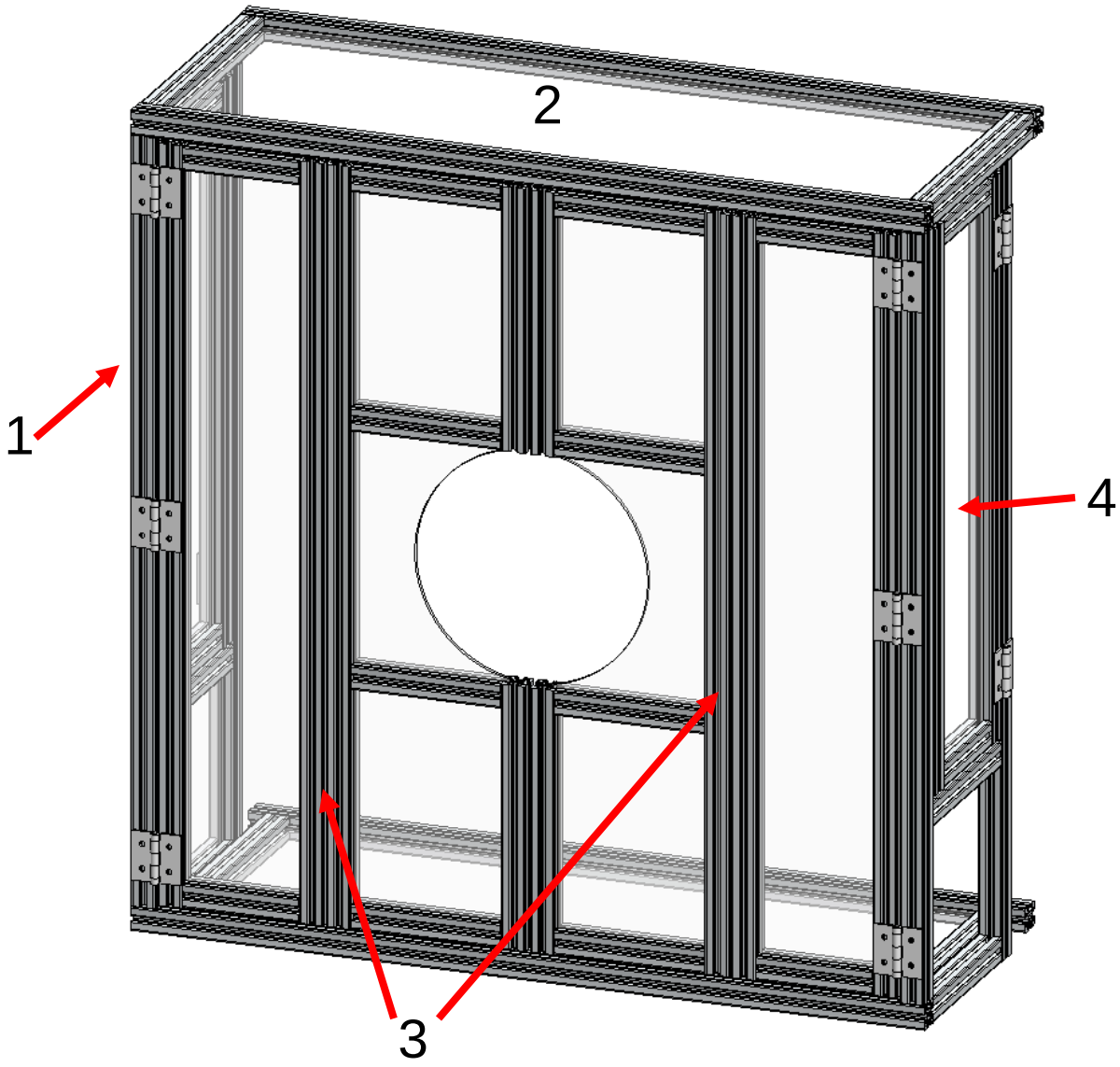

Figure 72

Description of enclosure: (figure 72)

1. Frame
2. Polycarbonate panels
3. Bi-fold doors
    a. Pull outwards to access front of braider
4. Side doors left and right
    a. Open to access side of braider

Attachment F

MENTIS SCIENCES, INC.

August 10, 2011 MSI 1032-032M

Memorandum

To: Chris Norfolk

From: Brad Mate, Chris Anderson

Cc: John J. Dignam

Subject: POMI Final Report – August 10th 2011

Task 1 – Co-Ordinate development activities with prosthetic socket designers
MSI will meet with the prosthetic socket designers to ensure the design and fabrication integration is seamless. In this task a detailed list of design information and format will be generated. The information that will be required includes but is not limited to a solid model of the composite socket and the specific material and fiber architecture required.

Task 1 – Progress Summary
Mentis Sciences worked closely with Georgia Tech University (GT) to be able to take information gathered from a MRI and then produce a solid model of a residual limb. GT was able to model tissue, bone, fat, etc. and then produce a solid model drawing of a residual limb. With the solid model Mentis used CAMWORKS software to transfer the solid model into a machining code to produce prosthetic molds without every actual meeting or having any interaction with the patient. Mentis received several of these solid models and prototypes were produced and sent back to GT for further evaluation.

Along with constructing a prosthetic mold from a MRI Mentis and GT were tasked to develop a laminate design for the prosthetic sockets being produced. Some discussion took place about adjusting stiffness in certain areas of the laminate but no other direction was given by team members in regards to a laminate design for the prosthetics that were to be produced. Mentis developed a 4 layer braid laminate design that worked for manufacturing purposes but there was no testing of the laminate to determine if all strength requirements were meet.

Mentis also worked closely with Walter Reed. Several Mentis engineers spent two days in the prosthetics lab learning current techniques and studying current manufacturing rates. The fabricators at Walter Reed demonstrated what the current state of the art was in fabrication of prosthetics and Mentis was able to take that information and try and advance the state of the art by implementing techniques developed under this program. Areas that Mentis believes improvements can be made are part to part consistency, and overall production rates. With implementing braider manufacturing techniques each part will have the same fiber placement and orientation from part to part and braid time for a four layer composite takes less than five minutes as opposed to traditional carbon sock lay ups that can take 10-15 minutes.

Task 2 – Male Mold Fabrication

In this task Mentis will select mold fabrication material, which includes the mold materials, CNC equipment and software for mold fabrication, and development of standard procedures and protocols for fabrication.

Task 2 – Progress Summary

Mentis looked into several different mold making materials under this program. One thing all materials had in common was they were all to be premade mold blanks in varying sizes. The reason for the premade mold blanks was to be ready for any size part that was sent to us by GT, and so that part could be machined immediately and then be shipped back to GT the next day.

The first material investigated was Aquacore; this material is a washout material which means that cold water can dissolve the material away after a part has been laid up over it. The Aquacore material was easy to machine and worked well in the braiding process. The only problem with the Aquacore material was the cost. The raw material price was expensive, over $100 in raw material on average per part and the parts were labor intensive to produce. Each mold blank needed to be hand packed and then cured overnight. Also after machining before a lay-up could be done on the mold; the part had to be coated with a type of silicone spray to seal the pours Aquacore material. The coating was required to prevent resin from infusing into the outer surface of the mold which would cause a thin layer of the mold to become bonded to the inside surface of the composite.

The second material that was looked at was plaster, which is the industry standard material. Mentis determined that plaster was the best material to use if the manufacturing process was beginning from a check socket or some other type of female mold. This material was not good when manufactured into mold blanks and then machined. The mold blanks were too heavy and the blank often cracked during machining. When compared to the Aquacore the plaster was not as good in machining but was substantial less expensive costing only around $10-15 in raw material costs on average per part.

The third material investigated under this program was machinable wax. The wax had many benefits when compared to the other materials. The wax was easy to cast into mold blanks, but the wax did have shrinkage and that needs to be taken into account when determining the size of the mold blanks. The wax was also great to machine and could be cut faster than both the Aquacore and the plaster, it also did not damage the cutting tools like the Aquacore and plaster so each tool could get a much longer usage life with the wax than with the Aquacore or plaster. De-molding with the wax was done by heating up the mold and composite, after fabrication was complete, and once the wax was properly heated the mold could be pulled out of the composite socket. The biggest benefit of the wax was its ability to be reused. All machined scrap and the molds could be re-melted and reused. This made the use of wax the least expensive and also did not produce the waste that the other Aquacore and plaster produce, making it a “green” method of mold fabrication. The average cost for raw material was under $10 per part and that included the 10% by weight of new material that was added after each re-melt, the addition of material is a manufactures recommendation to ensure material integrity after re-melt.

Task 3 – Computer Automated Braiding

Mentis will determine the best suited commercially available braider that meets the requirements for prosthetic socket fabrication. As well as integrated the braider with Mentis Sciences computer automated braiding system, MSCABS.

Integration will involve altering the MSCABS program for the specific use of braiding sockets. The alterations will include direct conversion of the solid model and fiber architecture into machine operation controls.

Task 3 – Progress Summary

Mentis chose a commercially available 64 carrier Wardwell braider to be used for this program. On receipt of the braider Mentis designed and fabricated a gantry system, which had several iterations on it during the life of the program. The final design was a large actuator, which was chosen for its compactness and to minimize pinch points from a safety stand point, which was bolted to the braider to ensure proper alignment and to give the system the smallest footprint possible. A protective shroud was also designed around the braider acting as a safety barrier from the braiders many moving parts. The shroud also acts as a containment area for the carbon dust that is produced in this process. The carbon dust is contained by installing an industrial vacuum into the shroud which produces a negative pressure in the shroud keeping the majority of carbon dust in the protective shroud and not on the technicians or any other nearby equipment.

The controls for the braiding system, like the gantry, went through several iterations before deciding on a final functional and easy to use control system. The programs original idea of having the braider be fully computer controlled was quickly determined to not be practical. The main reason for the impracticality of the computer control was every prosthetic is different and each mold would only have several parts made from it. Due to the low production demand of each part the time it would take to develop the automated path of the braided layers was determined to be cost prohibitive. Also the training and skill level required for fabrication technicians would have been higher than current technicians in the field and this also was determined to be cost prohibitive.

Due to the impracticality of the computer automated braiding system Mentis developed an easy to use manually controlled braider system. The manual controller are attached to the braider by a swing arm and has easy to use braider and gantry speed controls allowing a technician quick and easy to adjust controls. From Mentis's limited manufacturing experience with prosthetics, Mentis has determined that above and below the knee prosthetics generally have similar braiding techniques from beginning to end but no two prosthetic parts are exactly the same. So allowing the technician to adjust speeds of the braider and gantry based on braid coverage through merely visual observations makes it easier and faster than developing a computer controlled program for each part. In regards to repeatability from part to part, even when producing the same part, braider and gantry speeds can be recorded based on position through the braid plain and can be easily be repeated numerous times. The manual controls also make training quicker and easier and does not require as high skill level technician to operate. This was illustrated during training

sessions given by Mentis to current fabricators in industry; more detail of the training is discussed in Task 5 of this report.

Task 4 – Curing Procedures

The optimal curing procedure will be determined for the specific resin system that was determined during Task 1. The optimal curing conditions will be determined and suitable equipment will be selected or fabricated.

Task 4 – Progress Summary

The resin system to be used for prosthetic fabrication was to be determined by a collaborative effort form the team assembled for this program. Talk involving shape memory polymers and thermoplastic resin systems took place but no action was taken in either front. Mentis did not receive any resin from team members as was planned and Mentis moved forward without team collaboration and chose are resin system currently used in industry.

The resin chosen was an off-the-shelf Acrylic Epoxy. Mentis decided to use this resin system to allow focus to be placed on the new automated braiding manufacturing system and not a new resin process for laminating. Mentis followed the same laminating procedures that are currently considered to be industry standards.

Mentis was able to make to make one improvement in the laminating process; Mentis was able to reduce the amount of resin required by more than ½ per lamination. This improvement is a direct result of the new braiding manufacturing system. In traditional lay-up procedures, utilizing carbon socks being pulled over a mandrel the fabricator does not get a great deal of compaction from layer to layer and because of the lack of compaction the resin has more areas to fill, requiring more resin and subsequently adding more weight to the part. With the braiding process each layer is applied under tension, which automatically de-bulks the part as layers are applied. This compaction of the dry carbon layers reduces the void area that resin needs to fill requiring less resin and in turn producing a lighter part.

Task 5 – System Implementation

A detailed protocol will be developed for all features of the socket fabrication process. This documentation will be supplied along with a training session to the personnel at Walter Reed hospital.

Task 5 – Progress Summary

A comprehensive instruction manual has been developed and implemented in a training session. MSI developed the manual to train new technicians and to also be used as an easy to use reference guide. The training manual can be seen as an attached document to this report.

Training at Walter Reed hospital did not take place, it was determined that Walter Reed did not have the room in there facility for the braider system and would there for not be able to implement the braider into their fabrication process; because implementation was not able to take place at Walter Reed, a secondary facility was chosen to implement training. Training of the prosthetic braiding system took place with the Friddles, a prosthetic and orthotics supplier and manufacturer.

MSI's engineering lead on the POMI program; lead the training with included 8 individuals. The training session lasted three days. The first day focused on equipment set-up and maintenance. The second day was used to demonstrate braiding techniques and to illustrate the braiding process on a wide range of parts and sizes, in all over 30 prosthetic parts were braided in the training session. The third day focused on having all trainees actually braid parts for the entire day until all in attendance could start the braider, apply all required layers, stop the manufacturing process, and get the part ready for lamination. The training did not include lamination instruction because the process Mentis uses for lamination is already in practice and is considered an industry standard. Since the training session technicians form the Friddles organization have manufactured below and above the knee prosthetics without direct supervision from Mentis.

Attachment G

Socket Cooling Project
Concept / Feasibility Report
Revision B

SCRA / ARDI TO# 2012-534

Greg Patterson
Porticos Inc.
(919) 468-0033 x153

January 30, 2013

REVISION HISTORY

Date	Rev	Description
24Oct12	A	Original Release
30Jan13	B	Confidential material removed

TABLE OF CONTENTS

1. PURPOSE

This purpose of this report is to present the results from the concept and feasibility phases of the SCRA/ARDI Socket Cooling Project.

2. RESULTS SUMMARY

- In order to meet a request an aggressive delivery date for the prototype units, activities originally scheduled to occur separately during the concept, feasibility and/or prototype phases were combined or eliminated. Specifically:
  - New components deemed necessary during conceptualization and practical based on Porticos previous experience were moved directly to prototype design; circumventing the feasibility design and samples that were planned for the feasibility phase.
  - A custom test apparatus was designed and built to allow test and evaluation activities schedule for the feasibility phase to be completed on a component level without the need for the feasibility samples. Testing focused on characterization of the relationship between CO2 flow rate / cooling power and toward testing existing / alternate expansion solutions to obtain the low flow rates necessary.
  - Reviews planned for concept and feasibility are being replaced by a status review being schedule for some time prior to the receipt of the prototype units.
- Cooling target was established to be 5 to 7 Watts (17 to 23.8 BTU/hr).
- Prototype design was completed (and released to manufacturing) for the manifold, back pressure regulator, distribution module and tubing layout / integration (IE the top level assembly). Custom parts are scheduled to arrive for final assembly on or before Nov 9, 2012. All other components are off the shelf and have already been received.

3. ACTIVITY DETAILS

The following activities were identified in the original schedule as tasks that would be completed during the concept / ideation phase of the project. Each is discussed in detail below. A green ✓ in front of the activity indicates it was completed as planned. A red ✘ in front of the activity indicates that it was not completed or eliminated.

3.1. User Research

✓ Obtain Prosthetic Limb

Rob Kistenberg supplied the prosthetic limb along with several liners and socks.

✓ Evaluate Prosthetic Applications

During the kickoff meeting several configurations were discussed. The long term "ideal" solution focused on integrating the tank into the prosthetic limb structure, incorporating the high pressure tubing into the liner gel and developing custom liner pin / prosthetic socket interface that would provide the necessary connection between the liner and tank. This ideal configuration is outside of the scope (schedule and funding) of this specific project. Therefore it was decided that the prototypes delivered as part of this project would consist of an off the shelf tank (9 oz), an existing (though slightly modified) tank mounted control module and sewing the high pressure tubing directly onto the "sock".

✓ Develop Cooling Targets

After researching the topic, it became apparent that setting a conclusive cooling target was not practical. Rather we could establish a range of cooling targets based on different analytical approaches and settle on a cooling target somewhere in the median of that range for the initial prototypes. This would allow for user trials to determine if cooling should be more or less in future studies. As a result of the three approaches defined below, the cooing target was defined to be between 5 to 7 Watts (17 to 23.8 BTU/hr).

Approach 1: The first approach was to calculate what cooling would be required to account for the temperature rise experienced in the socket region. Based on the report "Residual Limb Skin Temperature in Transtibial Sockets" (See reference section for complete bibliography), the skin temperature increased by 0.8˚C after 15 minutes of donning the prosthetic and 1.7˚C after 10 minutes of walking. The region of maximum temperature increase was the posterior section while the anterior section had the least temperature increase as illustrated in Figure 3.1.a.

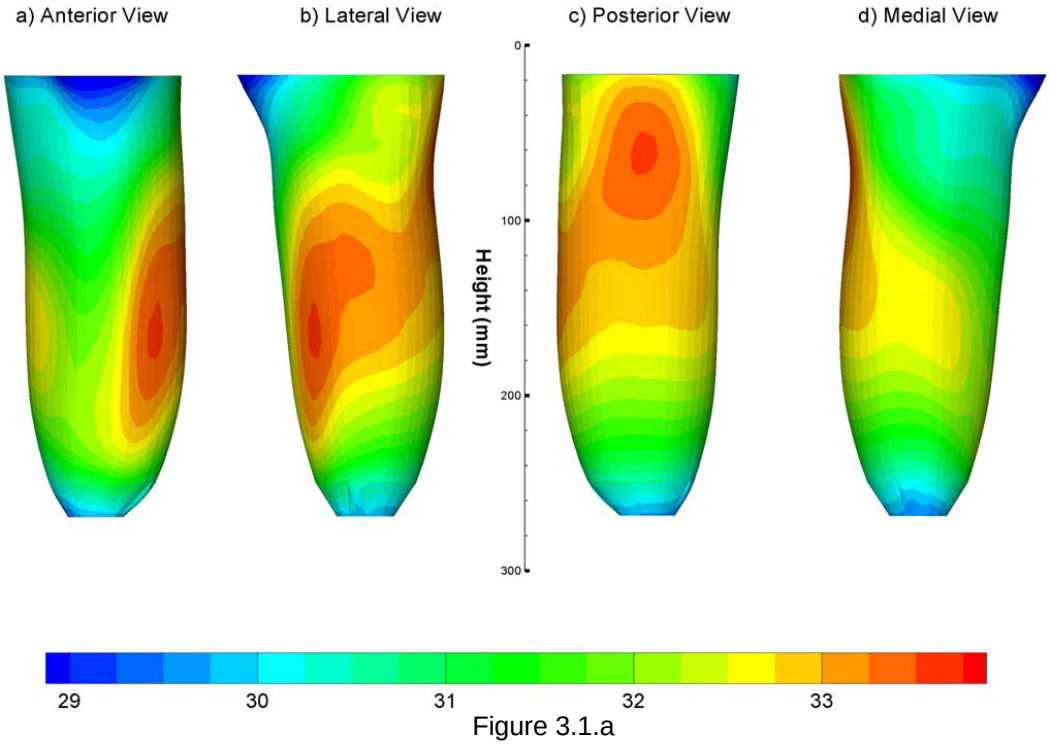

Figure 3.1.a

Assuming 1.7°C is the change in temperature, the rate of heat transfer of the residual limb may be used to develop the cooling target. In a study titled "Convective and Radiative Heat Transfer Coefficients for Individual Human Body Segments" (see references), the rate of heat transfer of the body was successfully compartmentalized such that individual sections may be analyzed. The heat transfer coefficients were broken up into 2 parts, convection and radiation. With the residual limb fully insulated, the convective portion is assumed to be zero. The following heat transfer law is used to calculate the cooling rate required:

$$Q = h_r \cdot A \cdot \Delta T$$

Where: Q is the heat rate of the system,

h_r is the heat transfer coefficient (5 W/m^2 K),

A is the area of the body transferring heat (0.16 m^2), and

ΔT is the change in temperature of the system (1.7°C).

The result from this approach is 4.64 BTU/hr or 1.36 Watts.

Approach 2: The second approach was to consider the metabolic rate of the human body during different activities and assume that the amount of heat that had to be dissipated in the residual limb region was related to the % area in that region. Based on the report "Steady State and Transient Temperature Distributions in the Human Thigh Covered with a Cooling Pad" (See reference section for complete bibliography), the metabolic rates were calculated to be 200 BTU/hr (sitting), 300 BTU/hr (standing), 600 BTU/hr (walking), 900 BTU/hr (moderate work) and 1800 BTU/hr (heavy work). To be consistent with approach 1 (10 minute walk), the 600 BTU/hr rate was selected. Referring to the "Convective and

Radiative Heat Transfer Coefficients for Individual Human Body Segments" report (see reference section for complete bibliography), for an average human body where the area is 1.471 m^2, the lower leg makes up 0.089 m^2 and the thigh makes up 0.16 m^2. Assuming that the amputation leaves 40% of the lower leg and the prosthetic encapsulates 30% of the thigh, the area would drop to 0.036 m^2 and 0.048 m^2 respectively. Those two regions combined would then make up 5.7% of the body. As a result, the amount of heat generated in the residual limb region would be 5.7% of 600 BTU/hr = 34 BTU/hr or approximately 10 Watts.

Approach 3: The third approach assumed the same metabolic rates and total body area that was used in approach 2 however the area for cooling was reduced to only include the region that the cooling lines were going to be distributed over. In this approach the area was 4" x 12" (48 in^2 = 0.031 m^2). That equates to 2.1% of the body area resulting in 12.6 BTU/hr (2.1% x 600 BTU/hr) or 3.7 Watts.

3.2. Product Requirement Definition

✓ Kickoff at SCRA/ARDI

The Kickoff meeting was held on June 21, 2012. Attendees were Chris Norfolk, Rob Kistenberg, Hunter Patterson and Greg Patterson

✘ Interview Amputee

It was decided that the expertise provided by Rob Kistenberg was adequate for establishing the requirements and user input necessary for this project.

✓ Develop Requirements Document

Requirements were defined during the kickoff meeting:

- Cooling Power was established during research phase at 5 to 7 Watts.
- Low or no noise generated
- Limit the contact between the cooling lines and the bone in the residual limb
- Tank should be 9oz and refillable
- Tank should be mounted to the user's belt
- Tubing to be sewn directly to the residual limb sock
- Distribution manifold should not create pressure on the residual limb
- Tubing must support radial and axial stretch directions
- Tubing must survive 1200 bend cycles
- Distribution manifold size should be the same or smaller than the current Porticool 2
- Garment should be hand washable
- Implementation should not impact the "vacuum" created between the residual limb and liner.

✓ Porticool Mockup

A Porticool 2 was taken to the kickoff meeting and demonstrated in conjunction with a presentation explaining the Porticool technology.

3.3. Concept Generation

✓ Smaller Expansion Device

The majority of work and testing to this point has been focused on reducing the Porticool 2 flow rate down to a level that will provide the small amount of cooling that is required in this application. Extensive testing was conducted to correlate flow rate reduction methods with resulting flow rate. Figure 3.1.c illustrates data obtained from one of the correlation tests.

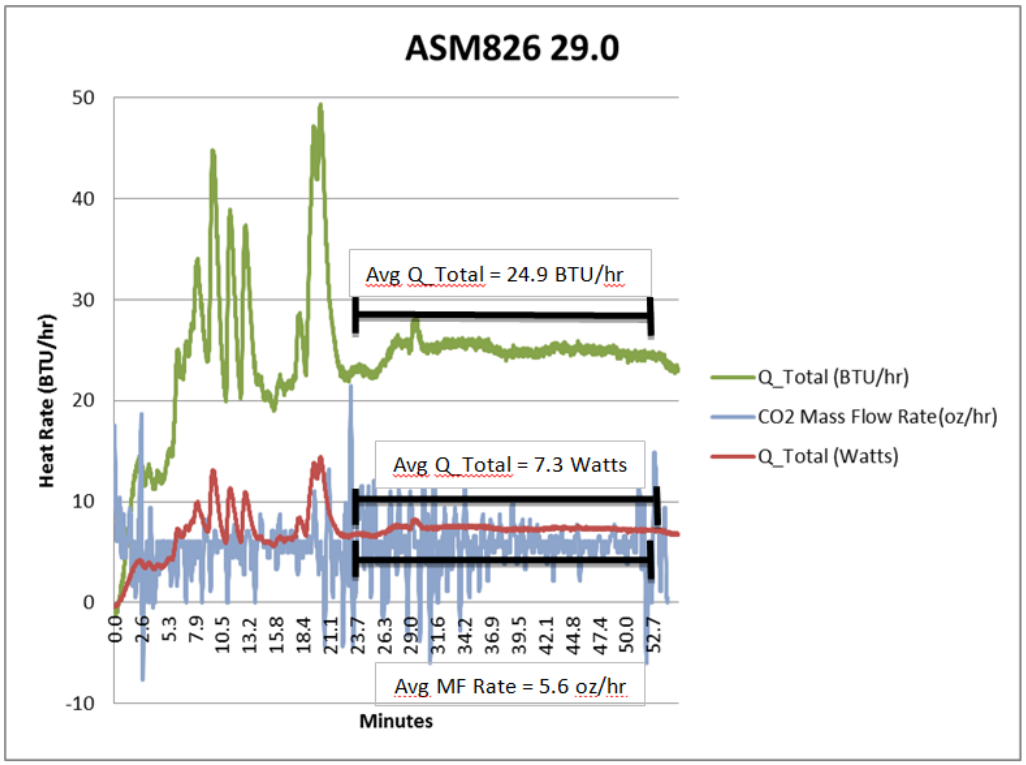

Figure 3.1.c

While the flow rate was restricted sufficiently to create a 7.3 Watt average cooling rate target additional investigation is required to improve the flow stability. Notice the wide fluctuation in the flow rate in the test illustrated in Figure 3.1.c; going to zero flow in many instances. The fluctuations were apparent audibly as well.

Testing continues in an attempt to identify a configuration that will reduce the flow rate to the desired level. If it is determined that the flow rate cannot be reduced strictly by mechanical restrictions, then future work could focus on using electronic controls to cycle the valve on/off. In this way a duty cycle can be defined to meet the cooling rate target.

✓ Smaller BPR

The back pressure regulator (BPR) is an integral component in the Porticool 2 liquid CO2 cooling technology. Without a BPR, the liquid CO2 would flash to gas (creating dry ice "snow") immediately upon exiting the tank and experiencing atmospheric pressure. The

BPR used in the Porticool 2 is based on a cartridge contained within a custom plastic housing that attaches and seals the cartridge to the downstream side of the manifold (see Figure 3.3.f).

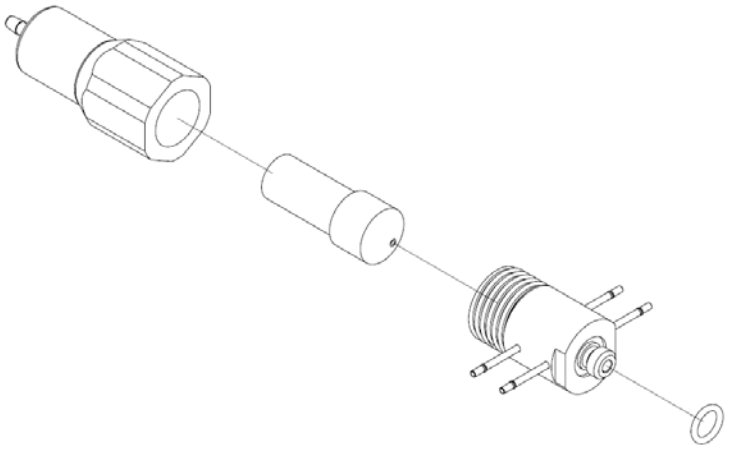

Figure 3.3.f

While this solution functions acceptably, it does so at the expense of size. For the socket cooling project, it was decided to design a custom BPR. Figure 3.3.g illustrates the internals of the IDEX BPR (this is typical of most BPR designs). The key elements are a plunger and a spring that forces the plunger to seat against a mating surface. Once the pressure reaches a level sufficient to overcome the spring force, the plunger moves to create an open path for the liquid or gas to escape. In the Porticool 2 system, the liquid CO2 has completely converted to a gas within the high pressure tubing sewn in the vest (or in this application in the residual limb sock) so only gaseous CO2 flows past the BPR.

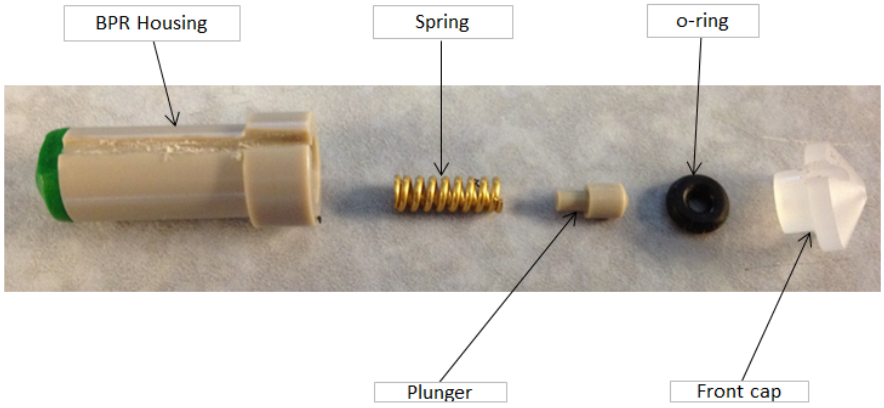

Figure 3.3.g

Figure 3.3.h illustrates the custom BPR designed for this socket cooling project. To reduce size as much as possible, a new manifold was designed which allowed integration of a custom plunger and spring. This greatly reduced the size of the overall package. Furthermore the new manifold allows attachment of an off the shelf muffler (item 4 in Figure 4.3.h), along with the capability to attach standard Beswick Sapphire Jeweled orifices in series prior to the manifold (IE in the liquid CO2 region) or after the manifold (IE in the gaseous CO2 region). This may prove useful when experimenting to reduce the CO2 flow rate.

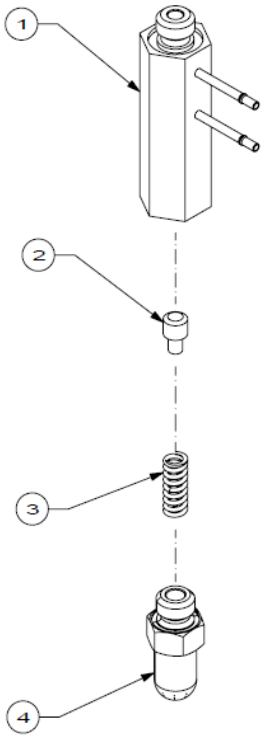

Figure 3.3.h

- Smaller ASA

While there is a slightly smaller ASA adapter available from the same manufacturer of the current Porticool 2 unit, the decision to go with a standard off the shelf 9oz tank and the realization that the expansion device for the socket cooling prototypes will most likely continue to utilize the current strategy of PEEK tubing eliminated any advantage that would have been associated with selecting a smaller ASA adapter. As a result, the existing Porticool 2 ASA adapter will be used for this project.

- New Tank

It was determined that the cost and schedule impact associated with designing a custom tank was beyond the scope of this project. As a result the decision was made to use an existing off the shelf 9oz refillable tank for this project.

✘ Control Module

As stated previously, the decision to go with a standard off the shelf 9oz tank and the realization that the expansion device for the socket cooling prototypes will most likely continue to utilize the current strategy eliminated any advantage that would have been associated with designing a custom control module. As a result, the existing Porticool 2 control module will be used for this project.

✓ Distribution Module

A new smaller distribution module was designed to take advantage of the smaller manifold and BPR. Figure 3.3.j shows the new design. The module consists of a single plastic part that will "clamshell" together via a living hinge and mounts to nylon webbing sewn onto the sock (see next section for details). A bulkhead mounted quick disconnect (Beswick part QDC-101-I-2PM) is attached to the housing and the new manifold screws directly onto the quick disconnect.

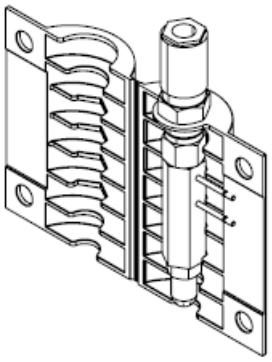

Figure 3.3.j

✓ Liner-Module Interface

A piece of nylon webbing is sewn onto the sock and extends beyond the seal created by the gel liner. The distribution module is attached to the end of the nylon webbing outside of the gel liner. The high pressure tubing will traverse from the sock to the manifold inside of the distribution module within this nylon webbing to protect it from wear and abuse. Figure 3.3.k and 3.3.L illustrate the design.

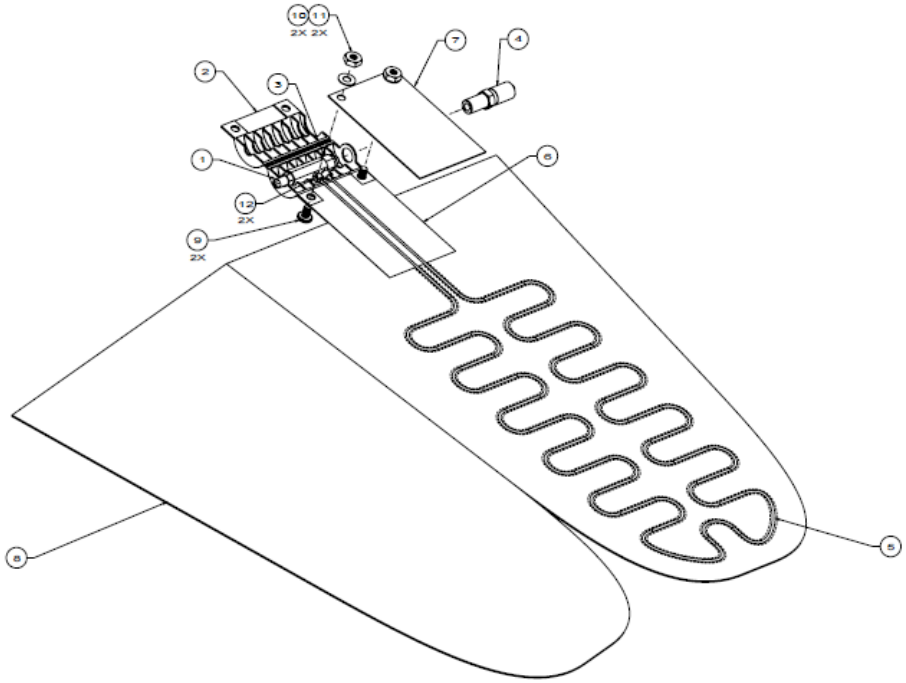

Figure 3.3.k

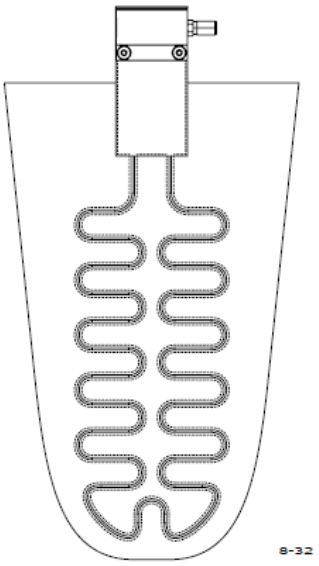

Figure 3.3.L

✓ Tubing Layout / Integration

High pressure “capillary” tubing will be sewn directly onto the sock using a stitching profile that crosses back and forth over the tubing. The pattern illustrated above in Figure 3.3.L focuses the cooling in the posterior region covering an area approximately 4” wide by 12” long. The geometry ensures that the tubing will not impede the ability of the sock to stretch along its length or circumference.

✘ Mounting Solutions

The decision to go with a standard off the shelf 9oz tank negated the need to define a custom mounting solution for the socket cooling prototype units. As a result the decision was made to use the holster currently available with the Porticool 2 system to secure the tank to the user’s belt.

✘ Leak Detection / Failsafe

Leak detection and the ability for the system to automatically shut down in the situation where a leak was detected is a stretch goal for the project. Several ideas were discussed by the Porticos team during the concept phase. The most promising concept required integration of a closed loop diaphragm style relief valve located in the control module that would shut off the flow based upon detecting a downstream pressure less than the level set by the BPR. Design and integration of this solution was outside of the scope of this project but can be considered in future phases.

✘ Concept Review

Due to scheduling issues a dedicated concept review was not conducted. It was decided that the concept review and feasibility review would be replaced with a single design review during the prototype phase.

3.4. Feasibility

✓ Design

In order to meet a request for an early delivery date for the prototype units, it was decided that the feasibility design would be combined with the prototype design. Therefore all custom parts were designed with the intent to support the prototype units. This activity has been completed as part of the prototype phase.

✘ Engineering Samples (2 arm or knee sleeves)

In order to meet a request for an early delivery date for the prototype units, activities originally scheduled to occur separately during the concept, feasibility and/or prototype phases were combined or eliminated. Creation of engineering samples in the feasibility phase was one of the items that was postponed until the prototype phase. The 2 arm sleeves will be built as part of the prototype build.

✓ Test and Evaluation

As discussed in great detail in section 3.3, sub-section heading “smaller expansion device”, the focus of testing conducted during the concept and feasibility phases was on trying to reduce the CO2 flow rate. System testing will be conducted in the prototype phase.

✓ Compliancy Document

The compliancy document was created. See reference section for document details.

✘ Feasibility Review

Due to scheduling issues a dedicated feasibility review was not conducted. It was decided that the concept review and feasibility review would be replaced with a single design review during the prototype phase.

4. REVISED SCHEDULE

The following schedule has been revised based and reflects the activities remaining in the prototype phase.

Task Name	Duration	Start	Finish
Prototype Phase	**54 days**	**Tue 9/4/12**	**Fri 11/16/12**
Design	8 wks	Tue 9/4/12	Mon 10/29/12
Flow Rate Tests Continued	2 wks	Mon 10/22/12	Fri 11/2/12
Design Review	0 days	Thu 11/1/12	Thu 11/1/12
Order / Receive Material	**41 days**	**Tue 9/11/12**	**Tue 11/6/12**
Lee Springs	6 days	Tue 9/11/12	Tue 9/18/12
Beswick Fittings	6 days	Thu 9/20/12	Thu 9/27/12
101 Machine (Manifold Body & Plunger)	11 days	Mon 10/8/12	Mon 10/22/12
NEST (Manifold Assy)	5 wks	Wed 10/3/12	Tue 11/6/12
CoolShirt (Control Mod, Hose & Holsters)	4 days	Tue 10/23/12	Fri 10/26/12
Adroit Medical (Sewn Socks)	12 days	Mon 10/22/12	Tue 11/6/12
Fineline (Distribution Hsg)	1 wk	Fri 10/26/12	Thu 11/1/12
Oetiker (Clamps)	1 wk	Wed 10/24/12	Tue 10/30/12
McMaster (Hardware)	3 days	Mon 10/29/12	Wed 10/31/12
Re-calibrate control modules	2 days	Mon 11/5/12	Tue 11/6/12
Assemble Units	3 days	Wed 11/7/12	Fri 11/9/12
Ship 1 Sample to Kistenberg	2 days	Thu 11/8/12	Fri 11/9/12
Functional Test	2 days	Mon 11/12/12	Tue 11/13/12
Refine Assemblies	1 day	Wed 11/14/12	Wed 11/14/12
Update Compliance Document	1 day	Thu 11/15/12	Thu 11/15/12
Prototype Review / Delivery	0 days	Fri 11/16/12	Fri 11/16/12

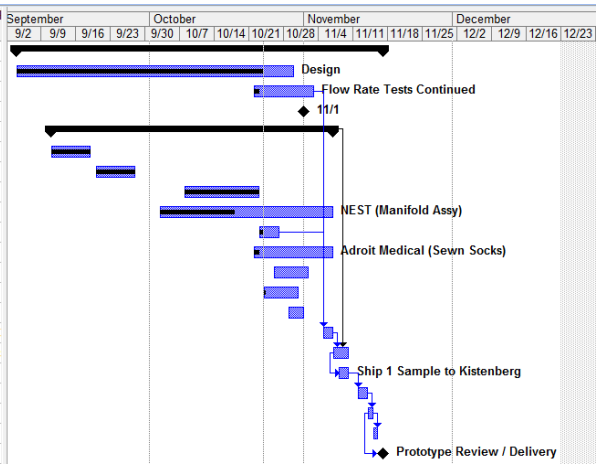

5. REFERENCES

5.1. Jeffrey T. Peery, MS; William R. Ledoux, PhD; Glenn K. Klute, PhD; “Residual Limb Skin Temperature in Transtibial Sockets”, Journal of Rehabilitation Research and Development, Volume 42, Number 2, Pages 147-154, March/April 2005

5.2. Richard J. de Dear; Edward A. Arens; Hui Zhang, PhD; Masayuki, Oguro; “Convective and Radiative Heat Transfer Coefficients for Individual Human Body Segments”, Center for the Built Environment, UC Berkeley, Nov 27, 1996.

5.3. R.J. Leo; A. Shitzer; J.C. Chato; B.A. Hertig; “Steady State and Transient Temperature Distributions in the Human Thigh Covered with a Cooling Pad”, Department of Mechanical and Industrial Engineering, Laboratory for Ergonomics Research, Engineering Experiment Station, University of Illinois at Urbana-Champaign, Technical Report ME-TR-286, June 1971.

5.4. G.S Patterson; “ARDI Socket Cooling Compliance Document”, Revision A Dated 10/22/12.